Stochastic Transport Models on Simple Networks: Phase Diagrams and Braess Paradox

Inaugural - Dissertation

zur

Erlangung des Doktorgrades

der Mathematisch-Naturwissenschaftlichen Fakultät

der Universität zu Köln

vorgelegt von

Stefan Alexander Bittihn

aus Bad Soden am Taunus

Köln, 2018

Berichterstatter: Prof. Dr. Andreas Schadschneider
Prof. Dr. Joachim Krug

Tag der letzten mündlichen Prüfung: 30.11.2018

Kurzzusammenfassung

Das Braess-Paradoxon ist ein kontraintuitives Phänomen, welches in Verkehrsnetzen mit egoistischen Nutzern auftreten kann. Es besagt, dass das Hinzufügen einer neuen Straße zu einem Verkehrsnetzwerk unter bestimmten Umständen zu längeren Reisezeiten für alle Nutzer führen kann. Dies kann wichtige Konsequenzen für die Planung neuer und den Ausbau bestehender Verkehrsnetzwerke haben, da die naive Annahme, dass zusätzliche Straßen immer zu einer besseren Verkehrssituation führen, nicht immer zutrifft. Um negative Folgen vom Bau neuer Straßen zu verhindern, ist ein detailliertes Verständnis des Paradoxons essenziell. Dies ist insbesondere wichtig, da die Kapazitäten der Straßennetzwerke vieler großer Städte schon lange erreicht und der Platz für den Bau neuer Straßen begrenzt ist.

Trotz vieler Beispiele, welche darauf hindeuten, dass das Paradoxon in echten Straßennetzwerken auftritt, fehlt ein fundiertes Verständnis dieses Effekts. Die meisten bisherigen Arbeiten zu diesem Thema basierten auf deterministischen mathematischen Modellen, deren Ergebnisse sich nicht direkt auf reale Verkehrsnetze übertragen lassen. Darin wurden einige stark vereinfachende Annahmen getroffen. Die Beschreibung des Verkehrsflusses wurde auf Reisezeitfunktionen beschränkt, welche linear mit der Anzahl der Autos auf den Straßen zunehmen. Weiterhin wurde angenommen, dass allen Nutzern fehlerfreie Verkehrsinformationen zur Verfügung stehen und dass sie ihre Routen auf dieser Basis komplett rational wählen.

In dieser Arbeit wird das Verständnis des Paradoxons auf eine realistischere Basis gehoben. Dazu werden Netzwerke aus total asymmetrischen Exklusionsprozessen („totally asymmetric exclusion process“, TASEP) in Bezug auf das Braess-Paradoxon untersucht. Der TASEP beschreibt Autos als Teilchen, welche auf einem eindimensionalen Gitter springen. Er ist ein einfaches stochastisches Transportmodell, welches mikroskopische Wechselwirkungen beinhaltet und eine nichtlineare Fluss-Dichte Relation aufweist. Auch Reisezeitfunktionen von TASEPs haben eine annähernd realistische Form, sie sind monoton wachsend und divergieren bei maximalen Dichten. Der TASEP kann nicht alle Phänomene von echtem Straßenverkehr beschreiben, bildet jedoch viele Effekte ab, welche in vorheriger Forschung oft vernachlässigt wurden.

Die Netzwerkstruktur, welche in Braess ursprünglicher Veröffentlichung benutzt wurde, wird in verschiedenen Varianten analysiert, wobei der Verkehrsfluss im Netzwerk durch TASEPs beschrieben wird. Verschiedene Randbedingungen, Routenwahlverfahren und Dynamiken werden betrachtet. Zunächst werden die Entscheidungen der Nutzer extern festgelegt. Dies bedeutet, dass die Nutzer nicht intelligent entscheiden, welche Routen sie wählen, sondern dass diese extern vorgegeben werden. Durch Vergleiche der Nutzeroptimumszustände („user optimum states“) der Netzwerke mit und ohne neue Straße wird gezeigt, dass das Paradoxon in solchen Netzwerken grundsätzlich auftreten kann.

Es wird gezeigt, dass das Braess-Paradoxon in großen Bereichen des Phasenraumes des Braess-Netzwerkes mit periodischen Randbedingungen und zufällig-sequentieller Dynamik auftritt. Verkehrsstillstände können in großen Bereichen des Phasenraumes gefunden wer-

den, falls fixe Anzahlen von Nutzern bestimmte Routen wählen. Wenn Nutzer hingegen mit festgelegten Wahrscheinlichkeiten auf die Routen verteilt werden, sind in großen Bereichen des Phasenraumes starke Fluktuationen in den Reisezeiten zu beobachten.

Unerwartete Phasen, in welchen das System potentiell zwischen nicht-stabilen Zuständen oszilliert können bei offenen Randbedingungen und zufällig-sequentieller Dynamik festgestellt werden. Das Braess-Paradoxon wird hier indirekt beobachtet, da eine resultierende Zunahme der Reisezeiten erwartet wird, falls dieses System von „intelligenten“ Teilchen genutzt wird.

Die Untersuchung der Netzwerke wird komplizierter, wenn parallele statt zufällig-sequentieller Dynamik verwendet wird. In diesem Fall werden Ampeln eingesetzt um potentielle Konflikte an Kreuzungen zu vermeiden. Das Braess-Paradoxon tritt auch in diesem Fall auf.

Zusätzlich zu der Erkenntnis, dass das Braess-Paradoxon in TASEP Netzwerken beobachtet werden kann, werden Phasendiagramme für alle untersuchten Varianten des Netzwerkes präsentiert, welche die Auswirkungen des Hinzufügens einer neuen Straße detaillierter beschreiben.

Das Braess-Paradoxon tritt auch auf, wenn Teilchen ihre Routen individuell intelligent wählen. Im zweiten Teil der Arbeit wird ein Routenwahlalgorithmus implementiert und am Beispiel des Braess-Netzwerkes mit periodischen Randbedingungen getestet. Verschiedene Arten von Verkehrsinformationen werden als Grundlage des Algorithmus genutzt und alle Teilchen wählen ihre Route individuell darauf basierend. Das Paradoxon tritt auf, wenn Teilchen Entscheidungen basierend auf ihren eigenen Erfahrungen treffen. Es tritt ebenfalls auf, wenn die Entscheidungen auf Abschätzungen zukünftiger Reisezeiten basieren, welche für alle Teilchen zugänglich sind. Diese Abschätzungen werden auf Basis der aktuellen Positionen aller Teilchen im System berechnet. Dies kann als Näherung von Verkehrsinformationen, wie sie von Smartphone-Apps zur Verfügung gestellt werden, verstanden werden. Es wird weiterhin gezeigt, dass das Paradoxon auftritt, wenn einige Nutzer ihre Entscheidungen auf Basis von persönlichen Erfahrungen und der Rest basierend auf öffentlich zur Verfügung stehenden Informationen treffen. Dies beschreibt die Situation von Pendlern im Berufsverkehr.

Die erzielten Ergebnisse unterstreichen die Bedeutung des Braess-Paradoxons für reale Verkehrsnetzwerke.

Abstract

The Braess paradox is a counterintuitive phenomenon that can occur in traffic networks, which are used by selfish users. It states that under certain circumstances the addition of a new road to a traffic network can result in increased travel times for all network users. This can have important consequences for the design of new traffic networks and for the extension of existing ones, since the naïve assumption that the traffic situation in a road network always improves when adding new roads does not always hold. A detailed understanding of this paradox is needed, since possible negative externalities resulting from the construction of new roads have to be understood in order to be avoided. This is especially true, since the capacity of the road networks of many cities has long been reached and space for the construction of new roads is limited.

Even though there have been numerous real world examples that indicate that the Braess paradox might occur in real world traffic networks, a deep understanding based on realistic traffic models is still missing. This thesis provides important stepping stones towards this much needed understanding. Most previous research on the topic focused on analysing deterministic mathematical models, the results of which are not directly transferable to real traffic networks. Often many oversimplifying assumptions were made: the description of traffic flow is reduced to unrealistic road travel time functions that increase linearly with the numbers of cars using the roads. Furthermore, perfect traffic information and perfectly rational decision makings of the network users were assumed.

This thesis is dedicated to the study of the Braess paradox in networks of totally asymmetric exclusion processes (TASEPs). The TASEP models drivers as particles hopping on a one dimensional lattice. It is a simple stochastic transport model that includes microscopic interactions and exhibits a nonlinear current-density relation. The travel time functions of TASEPs have close-to-realistic shapes: they increase monotonically and diverge when approaching the maximum possible density. TASEPs do not reproduce all phenomena of real road traffic, but many basic features which are not included in most previous research on the Braess paradox, can be described.

The network originally used by Braess is studied in several variants, but with the traffic flow described by TASEPs: various boundary conditions, route choice mechanisms and update types are considered. In a first step, it is shown that states realizing the paradox exist in TASEP networks. For this the decisions of the road users are tuned externally, i.e. users do not decide individually in an intelligent way, but are set to choose certain routes in the network. The user optimum states of the networks without and with the new roads are identified and their travel times are compared.

It is shown that Braess' paradox occurs in large regions of the phase space in the networks with added periodic boundary conditions and random-sequential dynamics. With fixed amounts of drivers assigned to individual routes, gridlock states are found in large parts of phase space. Assigning drivers to their routes according to turning probabilities results in

states with strong fluctuations in travel times that dominate large regions of the phase space. Unexpected phases in which the system is prone to oscillations between several unstable states are observed in the system with open boundary conditions and random-sequential dynamics: the Braess paradox is observed in an indirect way, since an increase of travel times is expected if this system was used by 'intelligent' particles. If parallel dynamics are employed instead of random-sequential dynamics, the treatment becomes more complicated. Traffic lights are implemented to avoid potential conflicts at junction sites. Braess' paradox is also observed in this case.

Beyond confirming that Braess' paradox can be observed in TASEP networks, phase diagrams which characterize the influences of the new road in more detail are presented for all analysed variants of the network.

Braess' paradox is also realized if intelligent particles, which individually choose their routes, use the network. In the second part of the thesis, a route choice algorithm is implemented and results of a performance test in the Braess network with periodic boundary conditions are presented. All particles choose their routes individually based on this algorithm. Several types of traffic information are used as input for the algorithm. The Braess paradox occurs if particles decide based on their own memories from previous travel experiences. It is also realized if all particles base their decisions on publicly available approximations of future travel times. These approximations are calculated based on the current positions of all particles in the system and are a type of information similar to that provided by smartphone apps in real traffic networks. It is also shown that the paradox occurs if some particles base their decisions on personal information and the others on public information. This situation is very similar to that of real commuters' scenarios. These results further stress the importance of Braess' paradox for real road networks.

Contents

1 Introduction

Many transport systems can be modelled by stochastic nonequilibrium processes. Some examples are car traffic on a freeway [1], thermoelectricity [2] and percolation processes [3]. In the real world, most transport processes take place on networks. These networks are comprised of various edges, connected to each other by nodes. The individual edges can be described by transport processes that retain a current in the system which keeps it out of equilibrium. An example from everyday life is that of car traffic on road networks [4]: a road network of a city is comprised of many roads, i.e. many transport processes, that form the edges of the network, which are connected through various junction sites. Some examples from various scientific disciplines, which can also be described by networks of transport processes, are the intracellular motor protein movement on a cytoskeleton [5], the dynamics of supply chains [6], data transfer in computer networks [7] and predator prey models describing population dynamics in ecosystems [8].

Many phenomena observed in such networks are consequences of the interplay of the individual transport processes and the network's structure. They can thus neither be explained by a reduction to just the individual transport processes that form the network's edges, nor by just the network's structure. Instead, the interaction of both has to be taken into account [9].

The Braess paradox, which was was first described by German mathematician Dietrich Braess in 1968 [10, 11], is an especially interesting network phenomenon: it describes the fact that under specific circumstances the addition of a new road to a congested road network can lead to increased travel times for all drivers. Vice versa, sometimes the closure of roads can lead to lower travel times on all other roads in a network. This specific paradox is one example of various network effects that also became known as "more-for-less" effects [9]. The paradox is genuinely surprising: naïvely one would expect that a new road, which increases the number of choices for the network users, would always lead to lower travel times, especially if the new road results in per-se faster connections between origins and destinations for the drivers.

A crucial prerequisite for the occurrence of the paradox is that network users are selfish (or noncooperative), i.e. that they want to minimize their own travel times and do not act altruistically. If certain prerequisites are met, it is generally agreed that the stable state of traffic networks of such users is given by the user optimum state: this state is reached if the drivers distribute themselves onto the routes, such that all used routes have the same travel times which are lower than those of any unused routes [12]. If the traffic was controlled by some external authority, which optimizes the traffic state, the paradox would not occur: in such cases a new road would always either improve traffic conditions or at least not worsen

them. In most modern day street networks no such authorities are at work. The Braess paradox is one of many examples of noncooperative games [13] in which selfish users drive the system into a state that is worse than the optimum state.

A detailed understanding of the Braess paradox and other phenomena of traffic flow is of great importance: the population of urban areas is increasing rapidly. Currently, 55% of the world's population lives in urban areas with a predicted increase to 68% in 2050 [14]. The efficient development of new traffic networks and the expansion of existing ones, an interplay of top-down planning and self-organizational processes [15], is just one important aspect to be considered very carefully as a consequence. Space is limited and the road capacities have long been reached in many cities around the world: in 2014, the average commuter in the USA spent 42 hours and wasted approximately 70 litres of fuel in congestion [16]. According to the TomTom traffic index [17], based on data gathered in 2016, Mexico City is the city with the highest congestion worldwide with travel times doubling during peak hours. Even in Cologne, which is only ranked 56^{th} worldwide, travel times go up by 50% during peak congestion periods, as compared to the free flow times.

Building new roads does not seem to be the right measure to tackle the problem of continuously increasing congestion. The so-called "Fundamental Law of Road Congestion" [18] states that newly built roads might only relieve traffic conditions in the short term, while more available roads result in an increased usage and thus in even stronger congestion in the long term. Braess' paradox is another indication that building new roads might not always be a good idea: since its model-based discovery, there have been numerous real world examples that indicate Braess' paradox might occur in real world traffic networks [19–25]. Indeed, research based on empirical road usage data identified major routes in cities such as New York City, the closure of which could reduce congestion [26]. If new roads may potentially have such adverse effects, city planners have to be considerably careful. A deeper understanding of the paradox is thus needed.

In his original paper, Braess demonstrated the paradox itself and sparked an ongoing interest in this phenomenon [27–34]. The original publication as well as many of the subsequent publications on the topic employ models which represent real traffic networks in an oversimplified manner. Many effects occurring in real road networks are only described in their most basic form while other effects are not included at all. Results obtained with these models can thus not be directly applied to real road networks. In particular, they can not be used to predict the occurrence of Braess' paradox in a reliable way.

The assumptions that limit the real world applications can be subdivided into the following two main categories.

a) A strongly simplified description of traffic flow.

b) Unrealistic assumptions regarding travel time information and decision makings of the drivers.

Regarding Category a), Braess' model uses deterministic, macroscopic mathematical models for the description of traffic flow on the individual roads of the network. Real traffic flow,

resulting from the interactions of all the individual decisions made by all the participants, is by its nature not a deterministic process. To be able to reproduce characteristic effects of real traffic, stochastic microscopic models have proven to be effective methods [35]. Additionally, the travel times of the roads are assumed to grow linearly with the number of cars using the roads, omitting some decisive characteristics of real road traffic. Real travel time functions are not linear, in particular they diverge for high densities as a consequence of traffic jams [36–42].

Some efforts have been made to analyse Braess' network with more realistic traffic descriptions: time-independent dynamics have been introduced into the study of the paradox, e.g. by considering queueing models for the description of traffic flow [27, 43, 44]. These models do not include microscopic dynamics and thus many important characteristics of real traffic are not represented in these models either. To my knowledge no demonstration of the paradox in models employing microscopic stochastic transport models has been published prior to our research.

Regarding Category b), Braess' model assumes that users have perfect information on all travel times in the network and that they decide which routes to take perfectly rationally based upon this information. User optimum states that potentially exist are assumed to always be reached, as a consequence of these assumptions. In most real road networks neither of these assumptions hold: network users have limited knowledge about travel times based upon their own experience or upon information from public sources, such as radio broadcasting or personal navigational systems like smartphone apps [45, 46]. While the accuracy of these predictions seems to grow, neither of them can be considered perfect. Furthermore, it was shown that road network users do not decide perfectly rationally and that travel time minimization is not the only aim underlying route choice processes [47–49]. The assumption that user optima are realized in real road networks is thus also a topic of ongoing discussion [33, 50]. Modifications of the original concept of the user optimum have been proposed as more realistic concepts for stable states in road networks of selfish users [51, 52]. However, more recent research indicates that the increasing use of smartphone routing apps could indeed realize user optima in traffic networks [53].

The aim of this thesis is to analyse and understand Braess' paradox in more realistic models. For this, I analysed networks of Totally Asymmetric Exclusion Processes (TASEPs) for the occurrence of the paradox. The TASEP is a simple particle hopping model which was first introduced to model protein translation [54]. Despite its simplicity it covers some basic features of road traffic [1] and exhibits interesting nonequilibrium properties such as boundary induced phase transitions [55]. It is nowadays considered one of the standard models of nonequilibrium statistical mechanics and became known as the "mother of all traffic models" [35], if the particles are interpreted as drivers on roads. While single TASEP segments are well understood and analytically solvable (see e.g. [35] for a review of many established facts on TASEP), networks of TASEPs are generally not analytically solvable [56]. In recent years, mean field approximation methods as well as Monte Carlo simulations have been applied to study some simple networks of TASEPs [56–62].

With the aim of understanding the paradox in a more realistic scenario and improving on

the two main categories of simplification, a) and b), two main questions were addressed:

1. Can the paradox occur in networks of TASEPs?
2. Given that the paradox may occur: is it reached by particles which base their route choices on realistic types of traffic information?

In the following, I describe how this thesis is structured and where these two questions are addressed throughout the thesis.

Thesis Outline

In Chapter 2 the scientific background of Braess' paradox is explained in more detail. After introducing some important definitions, the original example is recapitulated. Some additional results on the paradox in the context of traffic flow as well as some examples from other scientific areas are presented. The major limitations of the model, already hinted at in a) and b), are addressed in more detail by juxtaposing the simplifying assumptions of the model and observations from the real world. Important results on traffic flow, traffic information and decision makings as obtained in traffic science, the social sciences and related fields are presented. Based on this foundation, the scope of my research is then motivated more specifically.

Chapter 3 presents the most important models and methods which I used throughout my thesis. The TASEP is introduced in some detail, before presenting the basic model of the research in the following chapters: the Braess network of TASEPs. The results in all subsequent chapters are based on this model. Furthermore, Monte Carlo simulations as used in this thesis are explained.

Chapter 4 addresses Question 1, i.e. if the paradox can occur in networks of TASEPs. Braess' network of TASEPs with externally tuned global strategies is analysed. The term "externally tuned" refers to the fact that the particles do not make their own intelligent decisions. Instead, the decisions of all particles are set externally by fixing some model parameters. In doing so, the question if Braess' paradox is in principal accessible in networks of TASEPs is answered. This is repeated for various variations of the network.

Chapter 5 addresses Question 2, i.e. if the paradox is reached by particles that base their route choice decisions on realistic types of information. While in Chapter 4 the particles do not decide individually but are instead assigned to their routes, Chapter 5 examines what effect intelligent particles have onto the network's situation. For this purpose, a route choice mechanism was implemented. The particles make their decisions based upon various types of information, including a combination of personal and public information. This is a scenario occurring in many modern day commuter scenarios in which travellers have information based upon their own experiences and from modern personal navigational systems. The question, whether Braess' paradox is actually realized in these cases, is answered.

A short summary, concluding remarks and some suggestions for possible future research are given in Chapter 6.

2 Scientific Background of the Focus Topic

In the present chapter, the scientific background of the Braess paradox is summarized. First, some definitions which are needed to describe traffic networks and which will be used throughout the whole thesis, are introduced. Then, Braess' paradox is presented in detail: the original example by Braess and some significant results of the vast amount of research on the topic are recapitulated. Subsequently, it is worked out why the descriptions of traffic flow and decision makings in many models, used in the context of Braess' paradox, are unrealistic. This is followed by a summary of some results of research on traffic flow and route choice scenarios in real traffic networks, as obtained in various scientific fields. Based on this, the general idea of how this thesis adds to a better understanding of Braess' paradox is explained in some more detail.

2.1 Transport Networks: Important Definitions

For analysing transport networks certain definitions have proven useful. They are used to distinguish different types of networks and network users and help characterizing the performance of such networks, as measured e.g. by the travel times experienced by its users.

Transport networks have been analysed in various scientific fields such as traffic sciences, traffic engineering, mathematics, network sciences and physics. Therefore sometimes different terminologies are used to describe the same things. In the present chapter some important definitions are introduced as they will be used throughout this thesis. In this whole thesis the primary focus is on (car-) traffic networks. The presented definitions can nevertheless also be applied to most other transport networks.

2.1.1 Basic Definitions Used in All Kinds of Networks

The definitions presented in this subsection are used in the description of all networks in this thesis independent of the detailed natures of the networks.

Junctions, Roads and Routes. A connection between two "junctions" (or "points") [1] of a traffic network is called a "road"[2]. Roads have to be distinguished from "routes": in this thesis a route is always a connection from an origin to a destination. A route can be comprised of multiple roads. For clarification consider the example network shown in Figure 2.1. The nodes A to F of the network could e.g. be cities which are connected by several roads. If

[1] In network science terminology: "nodes".
[2] In network-science terminology: "edge".

"network users"[3] want to go from point A to point F, they can choose from two different routes which are marked in green and in blue in the figure.

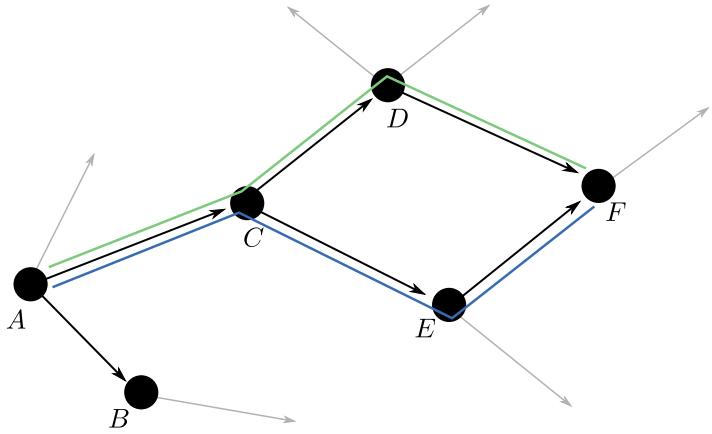

Figure 2.1. A sample (transport) network. The nodes A to F could e.g. represent cities in a road network. The grey arrows indicate that this network could be embedded into a larger network. If a certain amount of cars wants to go from A to F, they can choose between the green route, traversing points C and D and the blue route traversing points C and E.

Travel Times. The amount of time it takes to go from an origin to a destination using a specific route is called the "travel time" on that route.

Network States. A "state" of the network is given by the distribution of the network users onto the available routes. If in the network shown in Figure 2.1 a number of X network users want to go from point A to point F, one possible state would e.g. be $0.75 \cdot X$ users choosing the blue route and $0.25 \cdot X$ users choosing the green route. Different states can lead to different network performances as they may influence e.g. the travel times of the routes in the network.

Individual and Global Strategies. The route choices individual network users make to get from their origins to their desired destinations are also referred to as their "individual strategies". The set of all individual strategies is also called the "global strategy".

An individual strategy can be given by an individual user always choosing one specific route or by assigning probabilities for using various routes. These two variants are also called "pure and mixed strategies", respectively. For an example go back to the network in Figure 2.1: if a network user has to go from A to F repeatedly (A and F could be e.g. home and workplace of a commuter), a possible pure strategy would be him choosing the green route everyday. A possible mixed strategy would be choosing either the green or the blue route with equal probabilities.

[3] Depending on the context also referred to as "cars", "drivers", "particles" or "agents".

2.1.2 Different Types of Networks

Numerous types of traffic networks can be distinguished based on several characteristics. The types presented here can be distinguished by their travel time characteristics and by the types of agents using the network.

Uncongested and Congested Networks. When describing road traffic networks one has to differentiate between uncongested and congested networks. In "uncongested networks" the travel times of routes do not depend on the numbers of users on the routes while in a "congested network" the travel times increase with the number of agents on the routes [28]. All real road networks become congested from a certain number of users upwards.

Networks of Selfish Users. In a network of "selfish users" all agents can decide on their own upon which routes to take towards their destinations. In past- and present-day road networks this is mostly the case. Users may be influenced by navigational systems, radio traffic broadcasting or other things but ultimately they are free in their route choice decisions.

While factors like the length of the route, the road conditions or the scenery can also have an influence, the most important factor influencing these decisions seems to be the minimization of the expected travel time. This is especially true for traffic in cities and for commuters route choice scenarios (see e.g. [47, 48, 63] for reviews on which factors influence traveller's route choices). This topic will also be discussed in greater detail in Section 2.4.

Throughout this thesis it will be assumed that the only objective of selfish users is minimizing their own travel times and that they do not act altruistically in pursuing this goal.

Networks with Traffic Guidance Authorities. In some networks external[4] "traffic guidance authorities" can regulate the traffic. They can decide how the individual network users are distributed onto the roads and routes of the network. In a road traffic network this may e.g. be realized by the police assigning individual cars onto specific routes. Alternatively, traffic lights could be used not only for giving the right of way to specific roads at specific times, but also assigning route choices (e.g. if there are two routes leading to the same destination). Another possible example could be a situation in which all users have navigational systems which are coupled to each other, and to the infrastructure via the internet of things (also called car-to-car or car-to-X communication [64]). If all individual devices are coupled, a global strategy can be developed and the individual users can be assigned to their routes accordingly. If all users make their route choices (voluntarily or by obligation) according to this strategy, one could speak of a network with a guidance authority.

2.1.3 Characteristic States for Different Network Types

Two states are of major importance for characterizing road networks: the system optimum and the user optimum. The former is typically associated with networks with traffic guidance

[4]The term "external" means 'controlled by authorities external to the network users', i.e. not controlled by the users themselves.

authorities while the latter is associated with networks of selfish users. In most cases these states lead to different network performances. The performance differences can be quantified by the so-called price of anarchy which is defined subsequent to the two optima.

User Optimum. The "user optimum" (*uo*) is the stable state or equilibrium state of a network used by selfish users. This means that the distribution of drivers onto the routes will not change with time once the user optimum is reached.

In an uncongested network it is always given by all users choosing the shortest available routes. The problem of finding equilibrium states in congested transport networks used by selfish users goes back to Pigou in 1920 [65] and Knight in 1924 [66]. The notion of the user optimum was explicitly introduced by Wardrop in 1952 [12]. If a certain amount of agents wants to go from the same origin to the same destination and there are multiple possible routes to choose from, the following definition holds.

> The system is in its user optimum state if the users choose their individual strategies in such a way that all used routes have the same travel times which are lower than those of any unused routes [12].

This state is stable since there is no incentive for any user to change its strategy: since in congested networks travel time functions are always increasing with the number of users on the road [67], a change of routes would always lead to an increase of the switching user's travel time.

Throughout the literature on this topic the user optimum is often also referred to as "Wardrop equilibrium" or as "user equilibrium" (see e.g. [29]). It corresponds to the concept of a "Nash equilibrium" [68] in game theory.

The following two variants of user optima are distinguished in this thesis.

1. The "pure user optimum" is realized if each network user chooses one specific route. If applied e.g. to a commuter's scenario this means that individual users keep using the same routes over and over. The numbers of users on each route are fixed integer numbers. This corresponds to a "pure Nash equilibrium" if one considers the situation from a game theory perspective [68].

2. The "mixed user optimum" is in the context of game theory known as a "mixed Nash-equilibrium" [68]: it corresponds to the case that all network users keep their strategies, while here these strategies do not correspond to always choosing one specific route, but are fixed probabilities for choosing (various) routes. A mixed user equilibrium is reached if the *average values* of the travel times of used routes are equal and lower than those of unused routes.

In 1955, Beckmann et al. showed for deterministic macroscopic traffic models that if travel time functions are monotonically increasing with the number of cars, a unique user optimum always exists [69].

The two definitions presented above assume that network users have knowledge of travel times on all routes, that their perceptions of travel times are not in any way distorted and that they decide perfectly rationally. Thus if any route had a minimally lower travel time than the route used by a certain user, this user would switch routes. This is not always the case in real road networks, as can be explained from a simple example: imagine a person drives to work on the same route everyday and on this route the travel time is normally 30 minutes. If there is another route which, on one day, is expected to have a travel time of 29 minutes, this would not necessarily lead the person to switch routes. If the amount of potentially saved time is relatively small, factors like routine can be more important than saving a small amount of time. To account for some effects of this kind, the following two notions have been proposed.

a) The "stochastic user optimum" was introduced by Daganzo et al. in 1977 to account for the fact that real network users may not always perceive travel times perfectly [51]. Furthermore, network users may not choose their routes on a perfectly rational basis. To account for such effects the stochastic user optimum was defined as the state in which no user *believes* that he can improve his travel time by unilaterally changing routes. To account for this in mathematical models it was suggested that for each driver a small random number is added to the expected travel times.

b) The "boundedly rational user optimum", as introduced by Mahmassani et al. in 1987, accounts for the effects already mentioned above, namely that real drivers may not be induced to change to another route if travel times can only be decreased by a small amount [52]. It is achieved if all selfish users are satisfied with their current travel choices. In models it can e.g. be implemented such that users only switch routes if the potentially saved travel time is higher than a certain threshold.

Some of these concepts will be applied throughout this thesis. It is important to keep in mind that they all refer to the same general understanding of what a stable state is in a network with selfish users: a state in which there is no incentive for any user to change its strategy.

System Optimum. The "system optimum" (*so*) is the state which is *best for the system as a whole*. Different definitions of the system optimum are used depending on *how the system is defined*. Two of many possible definitions are the following: on the one hand, the system could be considered from an external viewpoint and it could then be optimized with regard to its performance as measured from that external perspective. On the other hand, the set of all network users could be considered to be the system. The system could then be optimized with regard to the set of all user experiences. Optimizing the system based on different definitions of what the system actually is, can lead to different states being considered optimal.

Applied to a city traffic network, an external viewpoint could e.g. be that of the city planning council. The council might want to optimize the performance of a part of the city's road network with regard to how this network part influences the surrounding network. From

this point of view there could be various possible definitions of the system optimum. One is the state which minimizes the total travel time of all users, as used e.g. in [70]. A second one would be the state which maximizes the flow through the network. This was e.g. used in [27]. These definitions do not necessarily optimize the network with regard to the convenience of its users.

If the system is considered to be described by the set of all the network users, among others, the following definitions of system optima were proposed. In Wardrop's original definition of the system optimum [12], often referred to as the "social Wardrop equilibrium", the system optimum is the state in which the weighted average (with regards to the number of users on the routes) of the travel times of all routes is minimized. This is the state which is *on average* best for all network users. It is not necessarily the best for *each individual user* since it could be a state in which a few users experience very high travel times while most users experience much lower travel times. This would imply a certain altruism of some network users who take the routes with longer travel times for 'the greater good'. Altruistic behaviour is in general not assumed for real road users.

A definition of the system optimum accounting for this problem was given by D. Braess in his original paper on his paradox and *will also be used throughout this thesis*.

> The system optimum is the state which minimizes the maximum travel time of all used routes [10].

While in Wardrop's definition of minimizing the average travel times individual users could be worse off than in the user optimum, this cannot be the case in Braess' definition: his definition implies that each network user faces a situation which is at least as good as in the user optimum.

All the above-mentioned definitions can, depending on the actual example, be coinciding in the same state but are generally fulfilled by different states. Oftentimes the system optimum, no matter the exact definition, does not coincide with the user optimum. In such cases the system optimum is not a stable state when dealing with selfish drivers, since individual routes may have lower travel times than other routes. Users would then tend to switch to the routes with lower travel times. The system optimum can generally only be achieved if the traffic is regulated by an external traffic guidance authority.

The Price of Anarchy. In an uncongested network the user optimum always equals the system optimum: it is always the state of all users choosing the shortest route, i.e. the route with the lowest travel time. As mentioned above, all real networks become congested from a certain density upwards. The performance of a congested network may be different depending on if it is used by selfish users or some traffic guidance authority is present. To quantify these differences the "price of anarchy" (PoA) has been defined.

When applied to travel times in road networks, the price of anarchy is given by the ratio of the travel times in the user optimum $T(uo)$ divided by the travel times in the system optimum

$T(so)$:

$$PoA = \frac{T(uo)}{T(so)}. \tag{2.1}$$

Upper bounds for the price of anarchy were derived for mathematical traffic models fulfilling certain conditions. If e.g. all roads are considered to have travel time functions linear in the number of cars, the price of anarchy cannot exceed a value of 4/3. If travel time functions are continuous and nondecreasing, the user optimum travel time cannot exceed the total travel time in the system optimum for twice as many users. [71]. These limits are valid for deterministic mathematical models.

2.2 The Braess Paradox

The Braess paradox was first formulated by Dietrich Braess, a german mathematician, in his 1968 paper "Über ein Paradoxon aus der Verkehrsplanung" [10] (an english translation was published in 2005 [11]). It describes, roughly speaking, the counterintuitive phenomenon that adding a road to a road network used by selfish users can result in equilibrium states with increased travel times for all users.

In the present section, first, Braess' original example will be recapitulated to convey a detailed understanding of the exact nature of the paradox. Subsequently, a short summary of some results of additional research on Braess' paradox in road networks is given. This is followed by some examples of occurrences in real road networks and of some analogues of the paradox from other scientific disciplines.

Subsequently, a detailed analysis of the simplifying assumptions, used in Braess' original model is presented by juxtaposing these simplifications with what is observed in real road networks. Building on this, the section ends by explaining how the research presented in this thesis works contributes to an understanding of the paradox in a more realistic manner.

2.2.1 Braess' Original Example

The present subsection summarizes Braess' example of the paradox [10, 11]. The original example is the network shown in Figure 2.2 which became to be known as "the Braess network" or "Braess' network". It is assumed that all network users want to go from the same origin to the same destination. For this purpose, they can choose one of three available routes: "route 14", "route 23" or "route 153"[5]. Road 5 is the road which is considered to be added to the network (or deleted from the network if one deals with the inverse situation), resulting in the newly available route 153. The network without road 5 will from now on also be called the "4link network", while the network with road 5 will also be called the "5link network".

[5]Routes 14, 23 and 153 consist of roads 1 and 4, 2 and 3, and 1, 3 and 5, respectively.

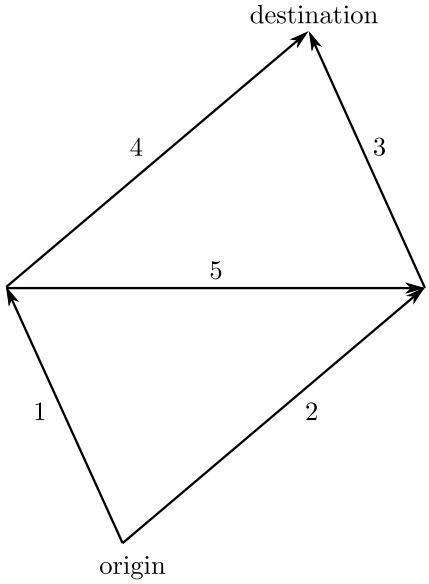

Figure 2.2. Braess' network as introduced in his original paper [10]. All cars want to go from the same origin to the same destination. There are five available roads, forming three possible routes: routes 14, 23 and 153.

The travel times T_i of all roads i were chosen to be linear functions of the number of cars n which use the roads,

$$T_i(n) = a_i + b_i n, \quad \text{with} \quad a_i, b_i \geq 0. \tag{2.2}$$

As will be discussed in detail in Section 2.2.5 this is an oversimplification of travel time functions of real roads. They do not cover, amongst other effects, neither the microscopic dynamics of road traffic nor fluctuations due to its stochastic nature.

Nevertheless, there are possible interpretations of the parameters in the linear travel time functions: the parameters a_i can be interpreted as the free flow travel time[6]. This is the time it takes for a single vehicle to traverse the road, if there are no other cars or only a sufficiently low number of cars, such that the cars do not influence each other. The parameters b_i indicate how strongly the travel time grows with the number of cars: they could be interpreted as a representation of the road conditions. A road which is in a good condition and has multiple lanes will have a lower b than a narrow road with many obstacles such as potholes.

For his network, Braess chose the following specific travel time functions:

$$T_1(n) = T_3(n) = 10n, \tag{2.3}$$

$$T_2(n) = T_4(n) = 50 + n, \tag{2.4}$$

$$T_5(n) = 10 + n. \tag{2.5}$$

Thus the 4link network is symmetric, as it its two routes 14 and 23 are comprised of two equal roads. Since there are no other roads in the 4link network it has no influence on the

[6] Indeed, the free flow travel times are $T_i(1) = a_i + b_i$, because these are the travel times that a single road user experiences if there are no other users on the road. However, throughout most literature on the topic, the a_i's are referred to as free flow times [30].

travel times that the equal roads are in reverse order on the two routes.

The total amount of cars that wants to go from the origin to the destination is denoted by N. The numbers of cars taking routes 14, 23 and 153 are denoted by n_{14}, n_{23} and n_{153}, respectively, with $N = n_{14} + n_{23} + n_{153}$. If a total amount of $N = 6$ cars wants to go from start to finish, the system optimum is given for

$$n_{14}^{so} = n_{23}^{so} = 3 \quad , \quad n_{153}^{so} = 0, \tag{2.6}$$

resulting in the following travel times:

$$T_{14}^{so} = T_{23}^{so} = 83 \quad , \quad T_{153}^{so} = 70. \tag{2.7}$$

In the system optimum, no car is using route 153 and the travel time on that route is lower than the travel times on both other routes. Thus, for selfish users, this state is not stable. Cars would tend to switch to route 153. The (pure) user optimum is found for

$$n_{14}^{uo} = n_{23}^{uo} = n_{153}^{uo} = 2, \tag{2.8}$$

resulting in the travel times

$$T_{14}^{uo} = T_{23}^{uo} = T_{153}^{uo} = 92. \tag{2.9}$$

Now all routes have equal travel times and there is no incentive for any driver to choose a different route.

The travel time in the user optimum is 92 on all routes and thus higher than that of the system optimum which is 83 on the used routes.

First, we note that the price of anarchy in the 5link network is $PoA = T^{\mathrm{uo}}/T^{\mathrm{so}}_{\mathrm{max}} = 92/83 \approx 1.1 > 1$: selfish users drive the system into a stable state which has a higher travel time than the best state of the whole system. The latter can only be achieved by externally regulating the traffic.

Second, we observe Braess' paradox in the following sense: if road 5 was taken out of the network, only routes 14 and 23 would be left. In the remaining symmetric network the system and user optima would coincide at $n_{14} = n_{23} = 3$. This means that for selfish users the 4link system would end up in its optimum state. Thus, while the elimination of road 5 leads to the vanishing of the fastest route (if used by only one car), it also leads to lower user optimum travel times. One can also imagine the inverse situation: if one starts with the network without road 5 and then adds this road, and thus a a shorter route, with the aim of decreasing travel times, one can end up in a worse situation as user optimum travel times go up.

The occurrence of the paradox is not limited to symmetric (4link) networks. As shown e.g. by Frank in 1981 [31] the paradox also occurs in networks with broken (4link) symmetry. In [31] the demand-regions[7] in which the paradox occurs in the Braess network were

[7]The "demand" refers to how many cars want to use a road network. In our it is thus given by N.

determined for travel time functions of the form of Equation (2.2) with arbitrary a_i and b_i.

Mixed User Equilibria. The Braess paradox is also observed if users choose their routes according to mixed strategies. Let p_{14}, p_{23} and p_{153} be the probabilities with which all users choose routes 14, 23 and 153, respectively. The probabilities are subject to $p_{14} + p_{23} = 1$ or $p_{14} + p_{23} + p_{153} = 1$ for the 4link and 5link systems, respectively.

In the 4link system, for mixed strategies the expectation values, denoted by $\langle T_i^{ms} \rangle$, of the travel times on the routes 14 and 23 are

$$\langle T_{14}^{ms} \rangle = 50 + (1 + p_{14} \cdot (N-1)) \cdot 11 \tag{2.10}$$

$$\langle T_{23}^{ms} \rangle = 50 + (1 + p_{23} \cdot (N-1)) \cdot 11 \tag{2.11}$$

for each car.

For $N = 6$ a mixed user optimum state (muo) is found for $p_{14} = p_{23} = 1/2$ with a travel time expectation value of $\langle T_{14}^{muo} \rangle = \langle T_{23}^{muo} \rangle = 88.5$.

In the system with the new road, the expectation values of the travel times on the three routes are

$$\langle T_{14}^{ms} \rangle = (1 + (p_{14} + p_{153})(N-1)) \cdot 10 + 50 + 1 + p_{14}(N-1) \tag{2.12}$$

$$\langle T_{23}^{ms} \rangle = (1 + (p_{23} + p_{153})(N-1)) \cdot 10 + 50 + 1 + p_{23}(N-1) \tag{2.13}$$

$$\langle T_{153}^{ms} \rangle = (2 + (p_{14} + p_{23} + 2p_{153})(N-1)) \cdot 10 + 10 + 1 + p_{153}(N-1). \tag{2.14}$$

Here a mixed user optimum is given for $p_{14} = p_{23} = 5/13$ and $p_{153} = 3/13$ with travel time values $\langle T_{14}^{muo} \rangle = \langle T_{23}^{muo} \rangle = \langle T_{153}^{muo} \rangle = 93.6923$.

For the case of mixed strategies the expected user optimum travel times are also higher in the 5link system than in the 4link system, i.e. the paradox occurs also with mixed strategies.

This example shows that the average number of cars on a specific route in the mixed user optimum does not have to correspond to the (integer) number of cars on that route in the pure user optimum: in the 5link system, the pure user optimum is for $N = 6$ given by distributing the users equally on the three routes. The mixed equilibrium is not achieved by all users choosing the routes with equal probability!

2.2.2 Braess' Paradox in Road Networks: Some Additional Results

The first description of the paradox in 1968 sparked an ongoing interest in the traffic science community as well as in network sciences, statistical physics and other related research areas.

A prerequisite for the occurrence was found to be the following: if a new road, and thus a new route with lower free flow travel time is constructed, user optimum travel times in the network can go up. This happens, if due to switching to the the new route more users switch to roads with high marginal travel costs[8] [70]. In Braess' original example this becomes

[8] The marginal travel cost of a route measures how much the travel time increases (for all users) if one more user decides to use that route. For linear travel time functions like Equation (2.2) a high marginal travel

clear: due to switching to the new route 153 more cars use roads 1 and 3. These roads have high marginal travel costs (high $b_1 = b_3 = 10$, cf. Equations (2.3) to (2.5)). One more user switching to one of these roads results in a large increase in travel time for all cars using them.

Since the occurrence of the paradox was in these terms understood as a consequence of network design and the choice of according travel time functions, with specific roads having high marginal costs, the paradox was not anymore considered paradoxical but as a pseudo-paradox [32].

In 1970, Murchland showed that the paradox also occurs for different choices of (linear) travel time functions in Braess' network [72] and the paradox was also demonstrated to occur in networks of different topologies by Steward in 1980 [70].

In the traffic sciences community the focus was primarily on pure user optima. Mixed user optima in the context of Braess' paradox were of higher interest in related research in the social sciences, e.g. [33].

A mathematical framework for predicting the occurrence of the paradox in networks of any topology with uncorrelated link travel time functions of the form (2.2), and also for nonlinear monotonically increasing travel time functions, was established in the research of Frank in 1981 [31] and Steinberg et al. in 1983 [28]. Steinberg et al. pointed out that "Braess' Paradox is about as likely to occur as not occur [in such general transportation networks]" [28]. Dafermos et al. introduced some correlation effects into the network by considering travel time functions which not only depend on the amount of cars on the individual roads, but also on the flow on all other roads in the network [29].

Some new insights on the paradox in the original Braess network were obtained in 1997 by Pas et al. [30]. In this publication it was worked out for which demands the paradox occurs for the original Braess example (Equations (2.3) to (2.5)). The results are summarized in the following.

Imagine the same network as presented in Braess' original example, but with more general travel time functions, all linear as in Equation (2.2) and subject to the conditions

$$a_1 = a_3 = 0, \tag{2.15}$$

$$a_2 = a_3 = \alpha_1, \tag{2.16}$$

$$b_1 = b_3 = \beta_1, \tag{2.17}$$

$$b_2 = b_4 = b_5 = \beta_2, \tag{2.18}$$

$$a_5 = \alpha_2. \tag{2.19}$$

The following conditions for the paradox to occur are valid for all choices constrained to (2.15) to (2.19).

In the 4link network, without road 5, the system is due to symmetry in its user optimum if half of the total number of cars N choose route 14 and the other half choose route 23. The

cost would correspond to large value of b_i.

travel times on both routes are then equal:

$$T_{uo}^{(4)} = \frac{N(\beta_1 + \beta_2)}{2} + \alpha_1. \tag{2.20}$$

In the 5link network, the user optimum can be derived from the condition that all used routes must have equal travel times which are lower than those of any unused routes. It turns out that for

$$N \leq \frac{\alpha_1 - \alpha_2}{\beta_1 + \beta_2} \tag{2.21}$$

the user optimum is given if all N cars use only route 153. Such a state will in the following be called an "all 153" state. In this state the user optimum travel time is

$$T_{uo}^{(5)} = \alpha_2 + N(2\beta_1 + \beta_2) \tag{2.22}$$

and this travel time is lower than that on the unused routes 14 and 23.

For the total numbers of cars obeying

$$\frac{\alpha_1 - \alpha_2}{\beta_1 + \beta_2} < N < \frac{2(\alpha_1 - \alpha_2)}{\beta_1 - \beta_2}, \tag{2.23}$$

all three routes are used and have the same travel times

$$T_{uo}^{(5)} = \alpha_1 + N\beta_1 + (\beta_2 - \beta_1)\left(\frac{\alpha_2 - \alpha_1 + N(\beta_1 + \beta_2)}{\beta_1 + 2\beta_2}\right). \tag{2.24}$$

For

$$N \geq \frac{2(\alpha_1 - \alpha_2)}{\beta_1 - \beta_2}, \tag{2.25}$$

only routes 14 and 23 are used and have equal travel times

$$T_{uo}^{(5)} = \frac{N(\beta_1 + \beta_2)}{2} + \alpha_1, \tag{2.26}$$

which is lower than that of the unused route 153.

Given this knowledge of the 4link and the 5link user optimum travel times, one can compare them for equal N. If the 5link travel time is higher, Braess' paradox occurs. If it is lower, the new road improves the system performance in the sense that it leads to lower travel times. It is important to observe that for total numbers of cars obeying (2.25) the new route will not be used at all in the user optimum. This regime is not considered "Braess", but the new road does not lead to any improvement either and is thus useless. This means that from the the lowest number of cars for which the 5link user optimum travel time is higher than the 4link user optimum travel time the new road first renders the situation worse, since Braess' paradox is observed. Then, at even higher densities, the paradox vanishes. Nevertheless, the road does still not improve the traffic situation since it is not used at all.

For the specific choice of Braess' original example, Equations (2.3) to (2.5) and $0 \leq N \leq 15$, the results are shown in Figure 2.3. One can see that the Braess region begins at $N = 2.58$,

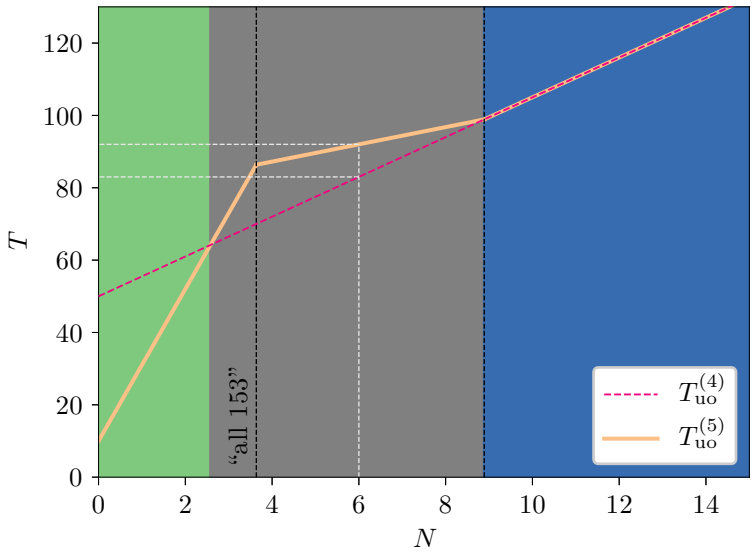

Figure 2.3. The travel times in the user optima of the 4link and 5link systems for Braess' original example against the total number of cars N. One can see that for $N < 2.58$ the new road leads to lower user optimum travel times (green region). For $2.58 \leq N \lesssim 8.89$ the system shows Braess behaviour: the 5link travel time is higher than the 4link travel time (grey region). For $N > 8.89$ the new route is not used in the 5link system. Thus the two systems have equal travel times (blue region). For $N \lesssim 3.64$ (black dotted line), in the 5link system's user optimum only the new route is used ("all 153" state). Braess' original example of $N = 6$ with $T_{uo}^{(5)} = 92$ and $T_{uo}^{(4)} = 83$ is also indicated by the dotted line in a bright grey color.

where $T_{uo}^{(5)}$ surpasses $T_{uo}^{(4)}$. One can also see that for $0 \leq N \lesssim 3.64$ the 5link user optimum is an "all 153" state. This means that for $N \lesssim 3.64$ only the new route is used - but from $N = 2.58$ upwards this leads to higher travel times than those reached in the system without the new road. For $N \gtrsim 8.89$ the new route is not used anymore. This is why from this N upwards, $T_{uo}^{(4)} = T_{uo}^{(5)}$. Summarizing one can say that for $N > 2.58$ the new road renders the situation worse and then for $N > 8.89$, it is not used at all[9].

In 2010, Nagurney showed for networks of arbitrary topologies, comprised of roads with monotonically increasing travel time functions: if Braess' paradox occurs at certain densities from a certain density upwards, the new route is not used anymore [34].

Thus city planners have to be careful when designing new roads since the effects of new roads are density dependent. The new road could lead to higher travel times or be ignored not only for specific fine-tuned densities but for large density regimes.

2.2.3 Real World Occurrences

The model proposed by Braess seems rather artificially constructed. In the following, first an example of how the Braess network could be realized in the real world is presented. Then some reports on actual realizations of the paradox in real, more complex road networks are

[9]Note that N does not have to refer to single cars per time unit but could be measured e.g. in $\frac{1000\text{cars}}{\text{h}}$. Thus non-integer values of N get a more realistic interpretation.

resented: it turns out that the phenomenon of the closure of roads leading to improved traffic situations is indeed observed.

Where Could Braess' Network Be Realized in the Real World? To make Braess' specific example a bit more applicable to a real world scenario, imagine a situation as depicted in Figure 2.4 which is based on [73]. One could imagine that there is one city at the origin and another city at the destination. The cities are separated by a mountain (or some other kind of obstacle which prevents the construction of a high-capacity road). To get from origin to

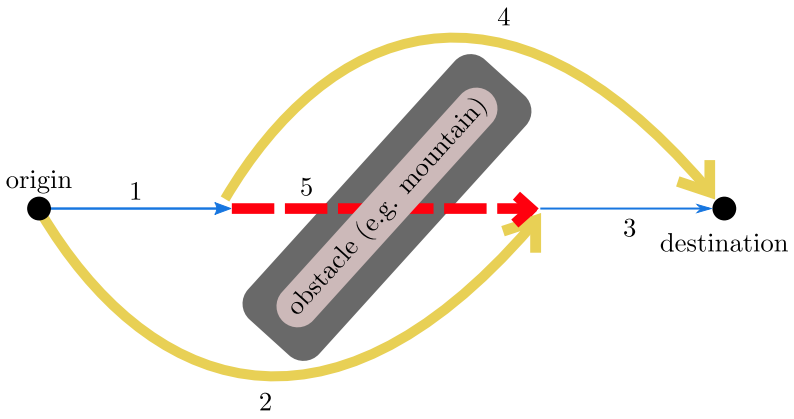

Figure 2.4. A more illustrative example of Braess' network. To justify the choice of the travel time functions of roads 1 to 5 (Equations (2.3) to (2.5)) one can imagine the origin and destination to be two cities separated by an obstacle like a mountain. There are two equivalent routes available to reach the destination. Both are made up of short narrow road (roads 1 and 3) and a long road with a high capacity (roads 2 and 4). Road 5 is a short wide new road which is a tunnel through the mountain. When this road is built it results in a per-se faster origin destination connection: route 153. This figure was inspired by [73].

destination, one can choose between route 14 which consists of a narrow rural road (road 1) and a relatively long but well-developed freeway (road 4) around the mountain. Alternatively one can choose route 23 which consists of equal parts, but in opposite order. Since a lot of cars use both routes, authorities decide to build a tunnel through the mountain to construct road 5 and thus enable route 153. Road 5 is slightly longer than roads 1 and 3 but wider. Equations (2.3) to (2.5) capture the main aspects of the roads in this scenario. The numbers of cars n_i using the roads of the network could be measured in units of $\frac{1000\,\text{cars}}{\text{h}}$ and the T_i (and the a_i) could be measured in minutes (min) and the b_i in $\frac{\text{min}\cdot\text{h}}{1000\,\text{cars}}$. If 6000 cars want to go from origin to destination each hour, the construction of the tunnel results in a travel time increase of 9 minutes for every car.

Examples of the Paradox in Real Road Networks Braess' paradox, as it is described in the original article and also in most further research that was recapitulated in the previous subsections, describes a phenomenon occurring in very specific models of traffic flow. Many aspects seem overly simplified and rather artificial.

First, the networks which are studied are very simple. Second, the modelling of the traffic is also a vast simplification (more details on travel time functions can be found in Section 2.3).

Finally, the assumptions that all cars want to go from the same origin to the same destination and that they all have perfect knowledge about travel times on all routes are generally not met in real road networks.

This leads to the question if the paradox actually occurs in the real world. Generally one speaks of an occurrence of the Braess paradox, if the closure of a road in a traffic network leads to better traffic situations, such as shorter travel times and less jams, in the surrounding road network. Inversely, one speaks of the (inverse) Braess paradox if a newly built road leads to worse traffic situations for the road's surrounding network. In real world scenarios this is without knowing all details like the origins and destinations of all individual network users.

Braess' paradox in this sense was observed in various real world situations. The first scientific reporting was made in 1969 by Knödel in an example in the city of Stuttgart [19]. Other examples include the closure of 42nd street in New York due to Earth Day celebrations in 1990 which lead to lower travel times in all surrounding streets [20]. In 2010, also in Downtown New York, some major traffic routes were decided to be closed permanently. Additionally to citizens and tourists enjoying pedestrian-only zones, traffic in the surrounding streets improved [21]. A similar situation was observed in Seoul in 2005, where a city motorway was closed in order to restore a river bed. The closure of this vast motorway lead to improvements in traffic flow [22–24]. A situation which could turn out to be a realization of Braess' paradox is at present taking place in front of our physics institute here in Cologne. Parts of the Zülpicher Straße are shut down for cars since April 2016 [25] and it seems like traffic in the surrounding streets did at least not get worse [74]. A final evaluation is still missing in this case.

In addition to these actual sightings of the paradox which were mainly by accident, i.e. a street was closed for different reasons and it turned out to be beneficial for surrounding traffic, some research was done into forecasting the paradox in city networks. In 2008, Youn et al. analysed the main roads of the street networks of Boston-Cambridge, London and New York City [26]. Traffic data was obtained from Google Maps and other sources. From this data about traffic demands, the price of anarchy under several circumstances was calculated. For this analysis more realistic travel time functions following the Bureau of Public Roads functions [75] (these functions will also be discussed in 2.3) were used. It was observed that in all three networks several routes exist which would improve the traffic situation if they were closed. This is still under some limiting assumptions as described in detail in the article [26] but hints strongly at the possibility of improving traffic conditions in existing city networks by closing already existing roads. Additionally, Roughgarden showed in 2006 that Braess' paradox occurs with high probability in natural random networks with a fixed origin destination pair [76].

It is really difficult to completely simulate road closures and predict their effects in actual real world scenarios since for detailed predictions one has to know all origins and destinations of all network users and also the exact travel time functions of all roads.

2.2.4 Analogues from Different Disciplines

Many analogues of the Braess paradox from disciplines other than traffic sciences have been found. Generally, when the addition of nodes and/or links to a network leads to a decrease of the network's performance (or if their removal leads to a performance increase) one refers to the system as showing Braess behaviour. Among other disciplines examples have been found in mechanical and electrical networks [77, 78], pedestrian dynamics [79], oscillator networks and power grids [80, 81] and thermodynamic systems [82]. A review of some examples from mechanical systems, biological networks, to power grids can be found in a 2018 article from Motter et al. [9]. Furthermore, on the official homepage of Dietrich Braess [83] numerous works on the paradox from various disciplines are collected.

Since this thesis focusses on Braess' paradox in road networks, only two examples are presented. Figure 2.5 **(a)** shows a mechanical analogue and Part **(b)** of that figure shows an example from power grids.

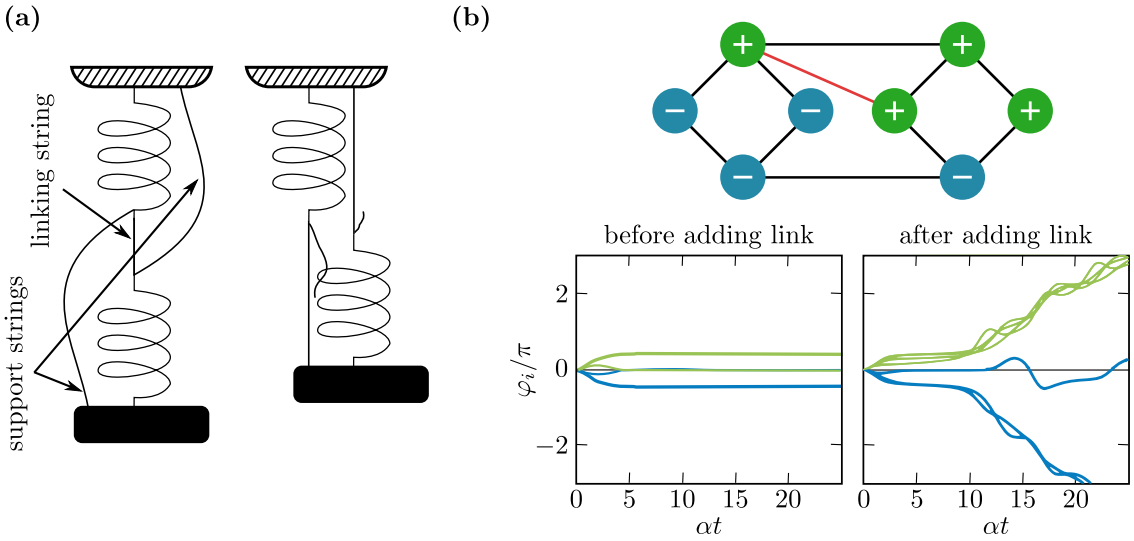

Figure 2.5. Two examples of analogues of Braess' paradox from other disciplines than traffic science. Part **(a)** shows a mechanical analogue: a weight is supported by two springs that are connected by a linking string. When this string is cut, the weight goes up. Part **(b)** shows an example of the paradox in power grids: the green nodes represent generators while the blue nodes are motor nodes. The graphs show that the grid looses synchronisation after the red link is added to the network. Part **(a)** is based on [77], Part **(b)** is based on [80].

Figure 2.5 **(a)** shows a weight subject to gravity. The weight is attached to the ceiling via two springs. There are two support strings in parallel to the two springs which are additionally connected to each other via the linking string. If the linking string is cut, the weight goes up instead of down. This paradoxical result can easily be explained if the force balance equation is written down explicitly. Effectively the system of springs and the strings is changed from a serial to a parallel system by cutting the linking string.

Figure 2.5 **(b)** shows an example in a power grid. The green nodes represent generators while the blue nodes represent motor nodes. In the system with just the black connections a stable synchronised state exists, i.e. the the sum of the angle differences is a multiple of 2π.

This stability criterion breaks down after adding the red connection.

2.2.5 What Can Be Improved in Braess' Model?

As already hinted at in Section 2.2.3 there are several aspects in Braess' original model, as well as in many subsequent works on the paradox, which are vast oversimplifications of real road traffic. These simplifications lead to the question, if the paradox really occurs in real traffic networks in the way it is described in the model. The real world observations cited in Section 2.2.3 have not been studied systematically and the traffic improvements after road closures could also be consequences of different origin. Due to the simplifications, the models cannot be used to predict the paradox in real road networks, either.

Obviously the structure of the network, put forward by Braess as a demonstrative example, is very simple and rather artificial. In real traffic networks such a small structure will normally be embedded into a larger, more complex road network. But even if the five roads are viewed just as a substructure of a larger network one would assume that there are more connections to the surrounding network.

If one takes the structure of the network for granted and neglects effects of a surrounding larger network, there are still many aspects of the model which are insufficient. They can be grouped into two main categories.

1. The description of traffic flow on the roads from a physical point of view.
    a) The description of traffic flow on the individual roads by linear travel time functions is an oversimplification.
    b) Correlations between the roads are neglected.
    c) Influences of a larger, surrounding network, which the Braess network is embedded into, are neglected completely: even if one decides to analyse just the network structure itself, its boundary conditions have to be addressed. The question about how cars enter and leave the system or if they stay inside the system is not addressed in Braess' model.
2. The assumed availability of accurate travel time information and the assumed perfectly rational decision making of the drivers.
    a) The assumption that accurate travel time information is available to all users at any time is unrealistic as well as
    b) the assumption that all users decide perfectly rational based on this information.
    c) Following from a) and b), the assumption that user optima are always reached is also unrealistic.

These two main points of criticism will be analysed in a more detailed manner in the following sections: in Section 2.3, I will summarize some established facts from empirical research on traffic flow on freeways. Subsequently, I will present some basic characteristics

which should be included in traffic models to reach a certain level of realism and juxtapose these characteristics to those inherent to the traffic description in Braess' model.

In Section 2.4, traffic information as it is available in real road networks is described. Some results of research regarding the question of how such information influences road users' decision makings are presented.

Based on this information about traffic in modern day road networks, in Section 2.5 I describe how I analysed the paradox in an improved, more realistic model and how this thesis adds to the understanding of Braess' paradox in realistic contexts.

2.3 The Description of Traffic Flow on Freeways

In the following the travel time characteristics of single roads are discussed. This discussion is limited to roads on which the interactions between the cars are the main influence on the state of the traffic flow. This kind of traffic is also called uninterrupted flow [84]. It can be found e.g. on freeways.

Traffic subject to other potential influences like obstacles on the road, such as potholes, accidents or traffic lights, on top of the interactions between the cars themselves is called interrupted flow [84]. Interrupted flow is not treated here.

Obtaining reliable experimental data of uninterrupted flow is a big challenge as detailed e.g. in [35, 85]. Furthermore, experimental data is best to be gathered in situations which are considered to be close to a stationary state. This is a prerequisite to capture characteristic behaviours not influenced by factors like changing traffic densities. Making sure that experiments are conducted under stationary state conditions poses further challenges which are summarized in [85].

From basic reasoning it is clear that on real roads in the uncongested regime, i.e. for low densities when individual cars do not influence each other, the travel time T should be proportional to the length L of the road divided by the maximum allowed speed[10] v: $T \propto L/v$. This means that on a road with a given maximum speed the travel time will be independent of the density in that regime. For really high densities the travel time should diverge since jams will form and when approaching the maximum density eventually the road will gridlock completely.

What happens exactly throughout all possible densities has been an active field of research for a long time. In the following, the main characteristics of freeway traffic as obtained in experiments are summarized. The characteristics which are of highest importance are determined and subsequently, these results are compared to the traffic description used in Braess' model.

[10] It is generally assumed that cars drive at approximately the maximum allowed speed.

2.3.1 Established Facts from Empirical Research

The first empirical research on the characteristics of traffic flow in the traffic science community dates back to Greenshield's work from 1935 [86], in which he used photographs to determine traffic states. Reviews on how these earliest studies on this topic were conducted can be found in [87] and [88] (in German). In more recent works on the topic data is generally gathered either by inductive-loop traffic detectors[11] or floating-car data. The latter are cars equipped with sensors, such as GPS, that are emerged in traffic and gather traffic data. The two mechanisms are different in the sense that the former gathers data at a static position while the latter is using a moving car [35].

By analysing data from freeways at different locations (e.g. Canada [36], Germany [37] and the Netherlands [38]) as well as from some controlled experiments in which cars were set up to drive in a circle without any obstacles [39], several shared general characteristics of freeway traffic were determined.

In the analysis of traffic flow the so-called fundamental diagram has proven to be the most important characteristic. The fundamental diagram can be given in three different forms. They are connected through the hydrodynamic equation

$$J = v\rho \tag{2.27}$$

with J being the flow[12] (generally given in units of $\frac{\text{no. of cars passing a certain position}}{\text{time unit}}$), v the velocity (generally given in units of $\frac{\text{length unit}}{\text{time unit}}$) and ρ the density (also called traffic volume, generally given in units of $\frac{\text{no. of cars}}{\text{length unit}}$) [35]. The three variants of the fundamental diagram are: the flow depending on the density, the speed depending on the density and the speed depending on the flow.

Since the fundamental diagram relates the velocity and the flux to the density there cannot be one unique fundamental diagram for all roads: the fundamental diagrams of different roads can vary due to different allowed maximum speeds, different overall behaviours of the road users and other influences. Even the fundamental diagram of a single road is not independent of measurement time since effects like the weather or the time of the day can influence the driver's behaviours [35].

Nevertheless a typical general form of a fundamental diagram describing how traffic on single roads behaves *generally* (or *on average*) has been found (see, among others, [35–39, 89]).

An example of a typical experimental dataset is shown in Figure 2.6. Part **(a)** of the figure shows the $J(\rho)$ version of the fundamental diagram, as obtained from measurements on a Canadian freeway. As most other data collected for fundamental diagrams it shows a characteristic linear increase of the flow for low densities[13]. After reaching a maximum it decreases linearly with further growing densities. In the decreasing branch the individual

[11] Insulated, electrically conducting loops that are installed in the pavement.
[12] Or current, or flux.
[13] In some road networks also nonlinear increases at low densities are observed while linear increases are most commonly found [89].

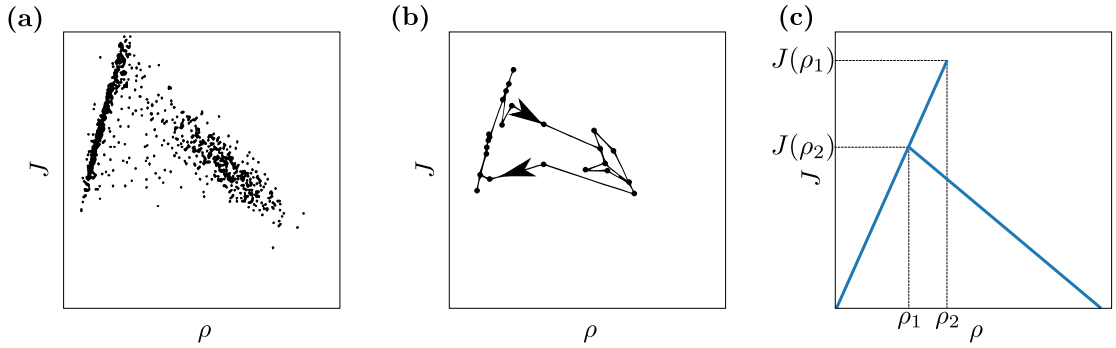

Figure 2.6. Part **(a)** shows a typical experimental dataset for the fundamental diagram connecting flow J to density ρ. The individual points show single measurements. Part **(b)** shows a time-evolution path observed in experiments (the arrow represents the direction of time), indicating the existence of hysteresis in freeway traffic. Part **(c)** shows a typical functional form of a fundamental diagram in the inverse lambda shape with a non-unique part for $\rho_1 < \rho < \rho_2$. Parts **(a)** and **(b)** show data from a Canadian freeway as published in [36]. Part **(c)** is taken from [35]. The visual appearances have been slightly modified from the original figures.

measurement points scatter more widely than in the increasing branch. Analysing the data in a more sophisticated manner revealed that, as shown in Part **(c)** of Figure 2.6, there exists a density regime in which the flow-density relation is not unique. The depicted shape of the fundamental diagram is known as the inverse lambda shape. For densities $\rho_1 < \rho < \rho_2$ there exist metastable high-flow states. If a road is in such a high-flow state, a distortion at a random position can lead to a drop in the flux down to a stable low-flow state[14].

It was shown that hysteresis effects can be observed in the fundamental digram. Figure 2.6 **(b)** shows a time typical evolution in the fundamental diagram suggesting that the high flow branch can typically only be directly reached if density increases from below ρ_1 but not if it decreases from densities above ρ_2.

A more detailed, highly successful theory describing three different traffic phases was suggested by Kerner [90] and is nowadays widely agreed upon [35]. The details of this theory are beyond the scope of this thesis and will not be treated here.

If details such as potential metastable high-flow states and other subtleties are neglected the main universal characteristics of freeway traffic can be summarized in the forms of the fundamental diagrams shown in Figures 2.7 **(a)** and **(b)**.

The travel time, which is the most important characteristic of a road in the context of Braess' paradox, has generally not been of major interest in most research in traffic science. Nevertheless, an expected average travel time can be extracted from the fundamental diagrams.

If one assumes that $v(\rho)$ is the average speed on the freeway, which is supposedly equal on the whole length L of the freeway, one can deduce the travel time T dependent on the density

[14] These metastable states are not found on all freeways [35]!

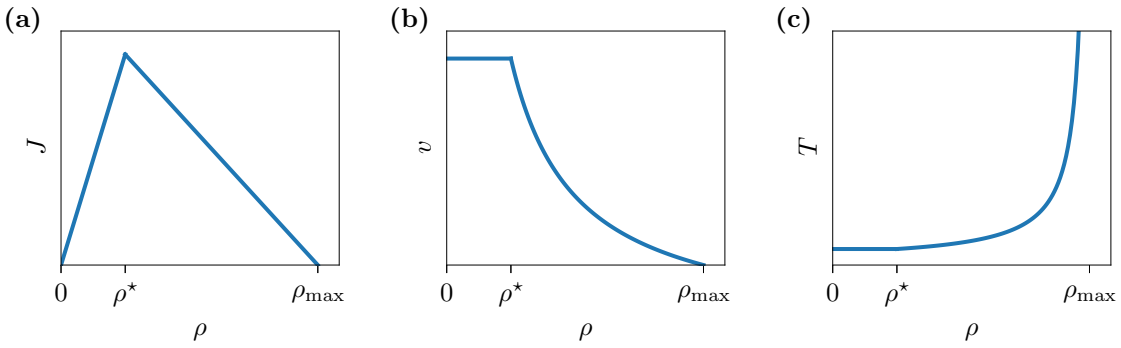

Figure 2.7. The typical forms of fundamental diagrams of freeway traffic if details are omitted. Part **(a)** shows the flow J dependent on the density ρ while Part **(b)** shows the velocity v depending on ρ. Part **(c)** shows the form of a travel time functions deduced from the shape of the fundamental diagrams as described by Equation (2.30). These figures are based on [35]. The visual appearances have been modified from the original figures.

ρ. From the form of the flow we deduce that it is given by

$$J(\rho) = \begin{cases} a\rho, & 0 \leq \rho < \rho^\star \\ b - c\rho, & \rho^\star < \rho < \rho_{\max} \end{cases} \tag{2.28}$$

while a, b, c have to be determined through experimental data and have to fulfill $(a+c)\rho^\star = b$. From this the velocity can be deduced to be

$$v(\rho) = \begin{cases} a, & 0 \leq \rho < \rho^\star \\ \frac{b}{\rho} - c, & \rho^\star < \rho < \rho_{\max} \end{cases}, \tag{2.29}$$

and from this the travel time:

$$T(\rho) = \begin{cases} \frac{L}{a}, & 0 \leq \rho < \rho^\star \\ \frac{L}{b/\rho - c} & \rho^\star < \rho < \rho_{\max} \end{cases}. \tag{2.30}$$

The resulting travel time function looks as shown in Figure 2.7 **(c)**. The travel time is constant for low densities $0 \leq \rho < \rho^\star$ and then diverges hyperbolically for ρ approaching $\rho_{\max}$. We assume this to be a reasonably realistic representation of the travel time in uninterrupted flow.

In the traffic engineering community different forms of travel time function were proposed. These functions are designed to mimic the main characteristics of the travel time while being suitable for usage in traffic assignment procedures [85]. Traffic assignment procedures are used e.g. to decide upon policies for city planning. To be applicable in these assignment procedures the travel time functions had (at least in the time they were developed) to meet certain prerequisites. One of them was that they do not diverge when approaching the maximum density (or the maximum capacity). This is why these functions purposely do not describe high density states correctly [85].

One of the most prominent of these functions was proposed by the U.S. Bureau of Public Roads (BPR) in 1964 [40] on the basis of experimental data. This function reads

$$T = T_0 \left(1 + \alpha \left(\frac{\rho}{J_{\max}} \right)^{\beta} \right), \tag{2.31}$$

with the free flow time T_0, the capacity (in this context: the maximum possible flow) $J_{\max}$ and α and β all being empirical constants specific to individual roads. Some other successful formulas, some based on models others on empirical data are e.g. the Davidson function [41] and the Akcelik function [42]. A review of these formulas is found e.g. in [67].

Since the functions from the traffic engineering community are designed for practical traffic assignment purposes rather than describing reality in the most precise way they will not be further considered.

Functions based on measurements of the fundamental diagrams shown in Figure 2.7 are instead used as a standard to compare models to.

2.3.2 The Traffic Description in Braess' Original Model

In Braess' model travel time functions are linear in the density. They are of the form of Equation (2.2), which can be rewritten as

$$T(\rho) = \frac{L}{v_{\max}} + a\rho, \tag{2.32}$$

with $v_{\max}$ being the maximum allowed speed. The first term is thus the free flow travel time. The function was rewritten here to fit the variable names used in the previous subsection. Braess did originally not use the density but the number of cars using a road. This number of cars can be translated into a density if the total length of a road is given. The conversion factor is assumed to be included in a.

Employing $T = L/v$ and $J = \rho v$ one arrives at the according velocity function

$$v = \frac{1}{\frac{1}{v_{\max}} + \frac{a}{L}\rho} \tag{2.33}$$

and the function of the flux:

$$J = \frac{1}{\frac{a}{L} + \frac{1}{v_{\max}\rho}}. \tag{2.34}$$

The forms of the travel time function and the resulting fundamental diagrams are shown in Figure 2.8. As one can see they differ strongly from the curves based on experimentally observed data, as shown in Figure 2.7. If the travel time is linearly increasing, there is effectively no free flow phase in which the travel time is independent of the density. Furthermore, the $J(\rho)$ diagram shows no peak flow, instead the flow is monotonically increasing, reaching an asymptotic limit. This is unrealistic since traffic jams cannot be modelled like this. This is

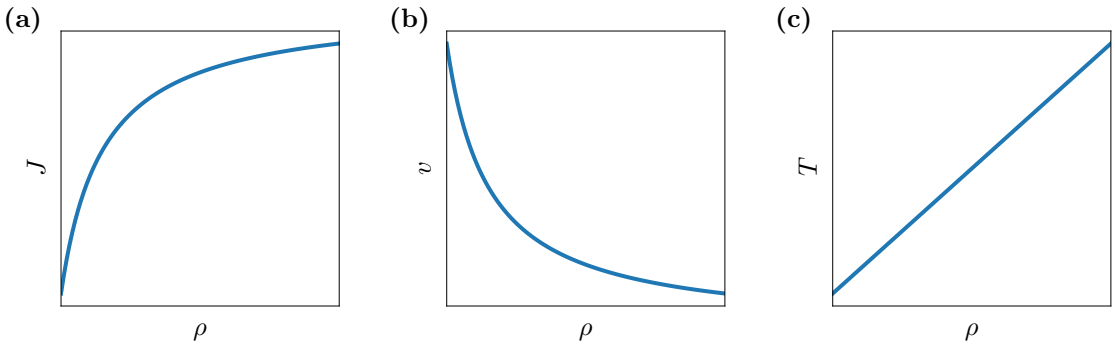

Figure 2.8. The forms of the travel time function (Part **(c)**) and the corresponding fundamental diagrams (Parts **(a)** and **(b)**) as used in Braess' original model. When comparing them to experimental observations as in Figure 2.7 one can see that many important features are missing.

a major argument why a more complex approach should be used to describe traffic efficiently. The velocity function has a similar shape as the experimental one except for a missing free flow regime.

Overall one can see that the traffic description on the individual roads using Equations of the form of (2.2) simplifies the traffic flow process too strongly to model traffic realistically. This is especially true at high densities since the travel times do not diverge. The linear travel times could be considered an appropriate approximation at low densities if the parameters are chosen appropriately.

Additionally to the traffic description on the individual roads, Braess' model also lacks correlations between them. A simple example is making this clear (see Figure 2.2). If road 3 was completely gridlocked, this would lead to diverging travel times on roads 2 and 5 as well. Such queuing effects and other spillback effects also occur in less extreme cases, not just for complete gridlocks. Such effects are not covered in the original model and most further research. Exceptions are found in Dafermos et al from 1984 [29] in which a model with some correlations is established. Furthermore, in Thunig et al, 2016 [27] considered Braess' paradox in a queuing network. These models consider the correlations in a basic way while the traffic flow description on the individual roads is again limited.

In addition to the fact that the travel time functions do not reproduce experimentally observed fundamental diagrams, modelling traffic flow in a deterministic way is generally unsuitable since deterministic models do not represent the stochastic nature of traffic that arises due to the individual decisions of all drivers.

2.4 Traffic Information and Decision Making Processes in Road Networks

In Braess' original text on the paradox, most further works on the topic and generally in most works dealing with selfish users and user optima, it is assumed that network users have perfect knowledge of current travel times[15] in the road network. Additionally it is assumed that all selfish network users decide rationally based only upon this knowledge to minimize their own travel times. *If* these two assumptions hold for all network users, the user optimum is the equilibrium state of the network. In the present section it is discussed why the assumption of perfect knowledge of current travel times does not hold in most real traffic networks. Different types of traffic information are defined and some specific types, available in present-day road networks are discussed. Subsequently, some results from research on decision making process, subject to various types of information, are presented.

2.4.1 Different Types of Traffic Information

Information on traffic conditions (here, I will focus specifically on travel time information) available to network users may be divided into the following two main categories.

1. "Public Information" is in principle accessible to everyone. It can be provided by various forms of advanced traffic information system (ATIS) [91], such as the radio or the internet. Information from personal navigation systems can also be considered public information since it is principally available to everyone with access to such a device.

2. "Personal Information" is information that is only available to specific individual network users. It could be information on traffic states which is built upon personal experiences made in the road network: e.g. a person commuting everyday will gain some knowledge about typical traffic patterns.

These two main categories can contain information from three different sub-categories [45].

a) "Historical Information" describes travel times measured in the network in previous time periods. This information may be comprised of personal and public information. The former refers to travel times, an individual user experienced in the past himself (this specific type is also called "experiential information" [92]). This could refer to the immediate past or also to long-time experiences. The latter refers to information on the network's performance in the past, which is publicly available.

b) "Current Information" refers to the most up-to-date information available. It can be given in the form of providing network users with the current state of the network, e.g.

[15] The term "current travel time" is in this context referring to the travel time, a driver will experience if he decides for a specific route and then starts the journey exactly in the current moment, i.e. the moment of the decision. The current travel time then refers to the time span (reaching into the future) from the journey's start right in the current moment until the journey's completion.

providing the current traffic densities or the currently measured (average) speeds on certain routes.

If one sticks strictly to this definition, in real traffic networks travel time information cannot be current information, due to the following problem: if e.g. a network user finishes a trip in a given moment and his experienced travel time information is immediately made available to the public, this information does not represent the travel time in the network right in that moment. It is instead the travel time of the used route at the current time minus the measured travel time. In the current moment the traffic situation might have changed and a user choosing the same route right now might experience a different travel time.

c) "Predictive Information" is e.g. given in the form of potentially to-be-expected travel times of routes. In contrast to the two other types of information which can be assumed to be accurate[16] since they rely on the past or the present, predictive information can by its nature not be guaranteed to be valid. If predictive information is given to network users in the context of route choices, a specific dilemma occurs: the information potentially influences the recipients, leading to take certain route choice decisions which then change the traffic state and thus falsify the information [93].

With the rise of personal navigation systems and *smartphone routing apps*, a special type of predictive information is getting very important: instead of just giving information of overall network states or potential travel times on specific routes, these systems often suggest a specific route to the user. If specific routes are suggested this is also called "prescriptive information" [92] as opposed to the other type being referred to as "descriptive information" [92].

Network users may have access to combinations of all these types of information and make their own individual route choice decisions based upon them.

2.4.2 Available Information in Present-Day Real Road Networks

Users of real road networks may combine their information sources and from them form a personal prediction of travel times on certain routes, and then choose the route which seems most attractive to them. Personal information is by definition not available for public studies, since it depends on the individual. While it may be possible to obtain some insights on personal information, e.g. by surveys, it still depends on various factors such as the specific road network. How public information is obtained and distributed can be studied. In the following the example of traffic information as provided by smartphone apps will be analysed.

Smartphone routing apps have become the most important source of 'public' traffic information (in 2018 approximately 70% of all americans owned at least one smartphone and

[16] Obviously historical and current information can also be false if they come from unreliable sources. This is not be dealt with here.

used it at least once per month [94] and 90% used their smartphones at least once for routing [95]). Among many alternatives Google Maps is the most popular routing app used in the US in 2018 [96]. While former ATIS systems, such as variable message signs, depended on information from public agencies and their infrastructure (e.g. induction loops or traffic cameras [46]), Google Maps relies on crowdsourcing [97]. In the given context this means that all people using Google Maps send their GPS location data to Google which then combines all the received data to provide the users with a fairly accurate depiction of the current traffic situation. Current data is combined with a large stock of historical data.

Google Maps can on the one hand just be used to see current traffic conditions and on the other hand also to suggest the fastest route to a desired destination, including step by step directions. For predicting the travel time, in a first step historical information is used. If there are enough active users on a route, the to-be-expected travel time takes the current traffic situation into consideration. One of the key components considered seems to be the average present speed on the roads (according to information provided officially by Google in 2009 [97]). How Googles algorithms work in detail is not known to the public [97, 98].

Next to positive implications the increased knowledge of travel times on all possible routes leads to many negative side effects for the infrastructure. The most prominent is that cut-through traffic[17] is observed to be rapidly increasing leading to many problems in city-parts formerly not subject to a lot of traffic (see e.g. [99] for one of many examples of reports on that topic in public media).

While travel time information provided by smartphone apps may be fairly reliable in networks with low congestion, prediction problems persist if networks are highly congested: one major problem is that, as already stated above, information from such sources as smartphone apps (or also radio broadcasting) can influence the decisions of many drivers. If there is e.g. an accident or some other kind of unexpected obstacle blocking a road, such ATISs suggest replacement routes. If many drivers follow these replacement routes, the whole traffic state changes and the replacement route itself can get so congested its travel times increase vastly. Thus the effects of such information can render the information itself wrong. This was demonstrated e.g. in a simulation example presented in [53].

Regarding the question discussed here – if user optima are actually reached – some research suggests that the usage of routing apps can lead traffic networks into user optima. This is in the sense that also smaller routes get used, which might not be known to many network users if it wasn't for apps. This seems to lead to travel time equilibration of such alternative routes and the main routes [53, 99].

Generally the impact of such routing apps is still under heavy discussion [100]. As will be explained in the following subsection, indeed the whole process of route choices is not well understood. Neither the human decision making is well agreed upon nor is there an agreement which information is best to be provided to network users [46].

It is important to keep in mind that reaching user optima is not necessarily desirable in

[17] The usage of smaller side roads with the aim to reduce travel times by avoiding congested high capacity roads

traffic networks.

2.4.3 Some Results of Research on Route Choices

Research on route choices based upon various types of traffic information can broadly be subdivided into three types: analyses of real world traffic data, research based on simulations and laboratory experiments. Some research results from these three areas are summarized in the following.

Analyses of Real World Traffic Data. Generally it is not possible to systematically control all the different factors at play in real road networks. Thus it is difficult to gain some objective, quantifiable information from observations of real road networks. There are of course a lot of anecdotal observations about what happens if a certain type of information is available to network users. An example are the many reports in the popular media about the effects of smartphone navigation apps, such as [99]. In a more systematic study conducted by Zhu et al. in 2015 [49] the cars of a large number of voluntary participants were equipped with GPS sensors and the routes of all their trips were recorded over a certain time interval. In accordance with previous, less structured approaches, it was found that on average only approximately one third of network users choose the fastest path available. A good review of previous studies on this topic is also found in [49]. Indeed it was shown that travel time is not the only factor influencing route choices (see e.g. [48] for some results obtained in Taipei city in 2001 and also a good review on previous research). Furthermore, travel times seem to be systematically misperceived [47]. It could be the case that if more and more people rely solely on predictions of the shortest travel time, as given by smartphone apps, the travel time becomes the most important factor influencing route choices in the future (at least for commuter scenarios in which other factors, such as scenery are supposedly neglected). It is generally not agreed upon, to which extend travel time expectations influence route choices. Since all users of real networks are individual humans, the route choices are also individual decisions and thus the process may never be completely understood.

Research Based on Simulations. There is a large quantity of research based on simulations of route choice scenarios. Some mathematical models were considered to get a detailed understanding of route choice scenarios [45, 101, 102], while it has proven most useful to implement models employing so-called "multi-agent techniques" [93, 103, 104]. These models combine traffic flow simulations, based on microscopic stochastic models, with algorithms for the individual network user's decision makings based on certain types of information. In such models, the description of the traffic flow is called the "tactical layer", while the algorithms for the information acquisition and decision making are called the "strategic layer" [103].

A simple, extensively studied, scenario that demonstrates potential negative effects of information is a simple two route model: image a single origin and a single destination connected by two equivalent routes which the network users can choose from (this is basically the 4link version of Braess' network, see Figure 2.2). The user optimum is in this situation given by

half the cars choosing one route and the other half the other route. All network users have to decide for one of the two routes with the aim of minimizing their origin-destination travel times. By studying this scenario in stochastic mathematical models, the following dilemma has been shown [45, 101]: if at the beginning of each trip the travel times of both routes in the previous round is made available to all drivers, the amounts of drivers using the two routes end up oscillating around the user optimum. If the travel time on the first route is much shorter in a given time period, more and more users will switch to this route, until the travel time on the second route is much shorter. The average travel times of both routes end up being higher than in the user optimum. The underlying cause of such oscillatory behaviours has been called "overreaction" [45]. It has since been reproduced in simulations employing queueing models [105] and microscopic stochastic traffic models [93]. They all show this behaviour if the most up to date travel times are made available to all network users, who then base their route choices on this information.

Studying microscopic stochastic models, especially those with the tactical layer being established by Nagel-Schreckenberg models [106] as suggested by Wahle et al. in 2000 [93] has been an active field of research for a long time. Important parameters in such models, next to the type of information provided to network users, are generally the fraction of users providing information (called floating cars, the fraction of floating cars being s_{FC}) and the fraction of cars reactive to this information (dynamical cars, the fraction denoted by s_{dyn}). It was already suggested by Hall in 1996 [105] that there may be a shift from positive to negative consequences of ATIS with a growing number of cars having access to information.

The observation of oscillations in the two route scenario lead to an ongoing search for 'better' types of current information to provide to network users. The motivation behind this research was to find types information which lead the two route system into its user optimum. Numerous suggestions were made, such as providing information based on average speeds [107], the so-called congestion coefficient [108] and several variants, time-flux feedback [109] and many others. Some suggested information methods lead to good results in the two route network. An extensive review is found in the paper of He et al. from 2014 [110]. In the same paper it is shown that most of the suggested feedback mechanisms fail to realize user optimum flow, when used in different scenarios then the symmetric two link network.

Recently, some studies were published in which information of the type provided by personal navigation systems is made available to the agents. A mathematical framework for analysing networks with this type of information was proposed by Thai et al. in 2016 [100] and large scale simulations were carried out by Cabannes et al. in 2018 [53]. The main results of this research indicate, that this type of information may lead to user optima, but has some negative externalities like the growing cut-through traffic.

Most models deal with (mainly two route-) networks with open boundary conditions. Users enter the network, are given access to a specific type of information and then perform their route choices. Like this the effects of this public information on the traffic states can be studied. To my knowledge not many studies examined the influences of personal historical information, such as the knowledge of travel times that day-to-day commuters build from

their own experiences. Levy et al. studied the influences of personal information in a paper released in 2016 [111]: they studied a microscopic two route traffic model with dynamics similar to TASEP dynamics[18]. Users route choice decisions were based on their own personal experiences of travel times in previous rounds. It was shown that this type of information can lead the system into its user optimum state.

To my knowledge no model was studied yet in which personal historical information and public historical, current or predictive information are combined.

Laboratory Experiments. Next to research based on simulations, which was mainly conducted in the traffic engineering and traffic science communities, many route choice experiments with real human subjects were performed in the field of social and economic sciences. Such experiments are usually designed as follows: a certain route choice scenario and a travel time model are implemented: most often traffic flow is modelled by deterministic travel time functions that are either linear or of the BPR-type (see Section 2.3). Human subjects are then asked to repeatedly perform route choices, while money is paid as an incentive for finding the route with the shortest travel time. These experiments are most often carried out in laboratories and are sometimes also app-based. Certain types of information may be provided to the participants throughout the experiments. Analysing the subjects behaviours, one can then deduce what drives human decision making and also what types of information have which consequences.

While these experiments yield quantitative results, which are generally not available from observations in the real world, the validity of these results are still to be considered carefully: generally, in such experiments, the networks or sets of routes to choose from are very simple; indeed much simpler than most real road networks. Furthermore, many influences on the route choice process are not covered in such studies. The travel time is by definition the only factor influencing the route choice processes. While this is still assumed to be one of the quantities of major importance, as already mentioned previously, in the real world it is by far not the only factor influencing route choices [47]. Nevertheless, these studies shine some light on the question if user optima are reached in traffic networks, under the *assumption that travel time is the only important factor*.

Some results from the vast amount of literature on this topic are summarized in the following. A good review of a large quantity of the literature is found in [46]. I focus on results for systems which are similar to, or directly on the topic of the Braess paradox.

In laboratory studies in which participants had to repeatedly perform route choices (in a short period of total time) Meneguzzer et al. in 2007 [92] analysed a scenario with three origin-destination connections with BPR-type travel time functions. In a similar study, Selten et al. in 2007 [50] analysed a scenario with two routes connecting origin to destination. In the latter stuy linear travel time functions were used. In both experiments participants depended on their personal historical information, i.e. they only knew the travel times of the routes they

[18]The Totally Asymmetric Exclusion Process (TASEP) is a stochastic transport model which is also used in this thesis. It will be introduced in Section 3.1

themselves chose in the past. In both cases user optima were reached *on average*: the mean number of users on the specific routes were close to the user optimum, while oscillations around this user optimum persisted. Selten et al. [50] also added a second round of the experiment in which the historical travel times of all routes were given to the participants. This also resulted in the user optimum on average, with slightly smaller fluctuations than without the public information.

A similar experiment was performed by Ye et al. in 2017 [112]: the analysed network corresponded to the 5link Braess network with the travel time functions of the roads being of BPR-type. The experiment was conducted using the smartphone app WeChat. Participants had to perform one round of route choices per day, while travel times of all routes on the previous day were provided. In this experiment the user optimum was approached and fluctuations decreased significantly after several rounds.

In some laboratory experiments, Braess' paradox was analysed directly: participants had to perform route choices in networks before and after the addition of a new road. Rapoport et al. in 2009 [33] considered Braess' original network and also an extended version. Travel time functions were linear in the number of users. Participants had to perform route choices in the network for several rounds before and after addition of the new road. Participants were provided information about travel times on their chosen routes as well as on the other routes, as realized in the previous rounds. Braess' paradox was observed in both networks. In the networks without the added road user optima were reached on average, while in the 5link version of Braess' original network a pure user optimum was approached after several rounds (i.e. fluctuations around the user optimum decreased significantly). It has to be noted that while the network was of the original Braess form, the travel time functions were varied such that in the 5link network, for the given amount of participants, the "all 153" state was the user optimum.

Mak et al. in 2018 [113] performed a route choice experiment on Braess' paradox in a slightly different form: the network was modified and a route with travel time decreasing with the number of users was introduced (this route was considered to be a type of public transportation instead of a road used by individual cars)[19]. Participants also had to perform route choices repeatedly and travel time information about all routes in the previous round was publicly available. In both networks Braess' paradox was observed. In this case the pure user optimum was directly reached (with almost no fluctuations) in the network without the new route while fluctuations around the user optimum were observed in the system with the new route.

Summarizing, in most laboratory experiments user optima were reached either directly, or on average with persisting fluctuations around pure user optima. In none of the experiments the participants drove the systems into states far from the user optima. While this hints at user optima being reached in real traffic networks, it is still no proof: various other factors

[19] The system optimum of the network with the new route was actually different (with lower travel time) from that of the system without the new route. The user optimum in the system with new route had higher travel times. This type of behaviour will be called "Braess 2" behaviour later in this thesis (see Section 3.2.4).

than just travel time optimization, which are neglected in such experiments, influence route choices. Furthermore, the examined networks are much simpler than real networks and in the presented experiments no realistic microscopic traffic flow models were used. Instead the employed models are deterministic which is, as worked out in Section 2.3, not a realistic description of traffic flow. Overall, due to the fact that these are laboratory experiments of scenarios which are much more complex in the real world, the results always have to be considered carefully.

2.5 How this Thesis Adds to a More Realistic Understanding of Braess' Paradox

During my doctoral studies I analysed the Braess paradox in networks of TASEPs[20]. As will be described in Section 3.1.2, TASEP covers important aspects of real traffic flow that are not represented in most preious research on the topic.

My research can be subdivided into the following two parts. Both parts analyse the Braess network shown in Figure 2.2, with the traffic described by TASEPs.

1. The first part of my research is presented in Chapter 4. In this part the question "Does the Braess paradox appear in this model with more realistic traffic dynamics?" is addressed by analysing several variants of the network. These variants are distinguished by different boundary conditions, different dynamics and different route choice scenarios. The analyses are carried out without modelling individual decisions: the network states (i.e. how many drivers choose which route) are tuned externally and no individual route choice behaviours are implemented. Pure and mixed user optima of the networks with and without the new road are determined and their corresponding travel times are compared. It is found that the paradox occurs rather generically in these networks. Furthermore, phase diagrams of the networks are obtained.

2. The second part of my research is presented in Chapter 5. The Braess network of TASEPs is implemented as a multi-agent model [104] with TASEP dynamics being the tactical layer and a route choice algorithm being the strategic layer of the multi-agent model. Building on the results from Chapter 4, i.e. that the paradox can occur in the Braess network with TASEP dynamics, the following question is addressed: "which type of information is needed and how do the individual drivers have to choose their routes such that user optima – and thus Braess' paradox – are realized?". To answer this question, a route choice mechanism for all drivers based on personal and public information is implemented. It is found that the paradox is realized for different combinations of those information types.

In the following chapter, the models and methods that I used are introduced.

[20]The Totally Asymmetric Exclusion Process (TASEP) will be introduced in Section 3.1

3 Models and Methods

In this chapter, the main models and methods that were used in the research presented in this theses are introduced. The Totally Asymmetric Exclusion Process (TASEP), the stochastic transport model that was employed to simulate traffic flow, is explained in the first section. The focus is on the defining properties of this model with random-sequential dynamics since this type of dynamics was used in most of my research projects. After summarizing the main characteristics of single TASEP segments, a general framework for analysing networks of TASEPs is presented.

In the next section the basic model system of my thesis is introduced: the Braess network of TASEPs. This is Braess' network as used in his original paper on his paradox, but with traffic flow on the edges based on TASEP dynamics. All results which are presented later on in this thesis will be based on variants of this system which are all explained and distinguished in this section.

The last section of the present chapter explains some Monte Carlo techniques which were used for analyses which are not accessible neither in exact nor in approximate mathematical ways.

3.1 The Totally Asymmetric Exclusion Process

The TASEP is a simple one-dimensional transport model. Originally it was introduced as a model for protein translation [54]. Due to its simple update rules and applicability to car traffic and many other transport processes it became to be known as the paradigmatic model for one-dimensional transport and is also called "the mother of all traffic models" [35]. A single TASEP segment consists of L cells or sites (L is also called the length of a TASEP), each of which can either be empty or occupied by a single particle. If a site is chosen to be updated and is occupied by a particle, this particle can jump to the next site with hopping rate[1] p iff this next site is empty. TASEPs can be realized with periodic boundary conditions (PBC) or open boundary conditions (OBC). In the periodic case, site $L+1$ is associated with site 1 and the TASEP effectively becomes a ring. In the open boundary case particles are fed onto site 1 from a reservoir which is occupied with the so-called entrance rate α and particles can leave the system by jumping out of site L into a reservoir which is empty with the so-called exit rate β. A schematic of an open boundary TASEP is shown in Figure 3.1.

[1] Depending on the specifically chosen update scheme, simulating either discrete or continuous time, the various parameters are either probabilities or rates. Since the main parts of this thesis consider dynamics which approximate continuous time (except for Section 4.5) I generally talk about rates.

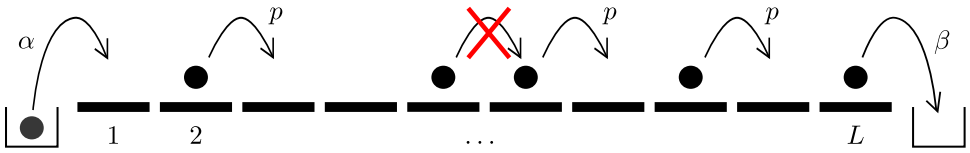

Figure 3.1. A TASEP segment consisting of L sites with open boundary conditions. Each site can either be empty or occupied by one particle. If a site is chosen to be updated and contains a particle, this particle can jump forward with hopping rate p iff the next site is empty. Particles can enter the segment on site 1 from an entrance reservoir which is occupied with probability α and can leave the system by jumping out of site L into the exit reservoir which is empty with probability β. In the case of periodic boundary conditions site $L+1$ is associated with site 1 and the system becomes a ring.

The dynamics in the system can be generated by different update procedures. Amongst other possibilities the two most important ones are the random-sequential and the parallel update procedures.

In the random-sequential update procedure for periodic boundary conditions, one of the L sites is chosen with uniform probability while in the open boundary case the entrance reservoir is to be included and thus one of the total $L+1$ sites has to be chosen with uniform probability. The chosen site is then updated with the hopping rate p. After L or $L+1$ (for PBC and OBC respectively) of such single site updates a time step is complete. If a TASEP system's dynamics is simulated employing a Monte Carlo simulation (see Section 3.3), a time step is also called a sweep.

In the parallel update procedure all L or $L+1$ sites are updated at the same time. One of those updates is a time step.

The random-sequential update approximates to continuous time while the parallel update corresponds to discrete time steps. The parameters α, β, p are thus rates in the random-sequential update scheme and probabilities in the parallel update scheme. While the latter is a more realistic model of car traffic, it is also more difficult to deal with, especially when networks of TASEPs are treated. In networks, conflict situations can arise if e.g. two TASEP segments merge into one: here it can happen that particles from two different sites want to jump onto the same target site at the same time. Such a conflict cannot happen in the random-sequential case.

Most research I conducted during my doctoral studies and thus most results presented in this thesis use TASEPs with random-sequential updates and $p = 1$. For random-sequential updates hopping rates $p < 1$ correspond to a rescaling of time which is why there is no loss of generality when limiting the discussion to $p = 1$. For parallel updates a hopping probability $p = 1$ corresponds to deterministic dynamics which is why it is important to consider values $p < 1$ in that case [35].

In addition to the results on random-sequential updates, some results obtained by Leonard Fischer during his Master's thesis [114] (which I supervised partly) in which parallel updates were employed, are shown in Section 4.5. In that section also the main differences of TASEPs with parallel updates compared to TASEPs with random-sequential updates are summarized.

A good overview over TASEP in general and also various extensions is found in [35].

In the following subsection the main characteristics of the TASEP with random-sequential updates are summarized.

3.1.1 Important Results for Random-Sequential Dynamics

In the steady state the average density profile ρ_i, with i denoting the cell number, of a TASEP segment does not change. The local current in the system is given by

$$J(i) = p \cdot \rho(i)[1 - \rho(i+1)]. \tag{3.1}$$

As a consequence of the continuity equation in the stationary state the current in a single TASEP segment has to be site independent, thus

$$J(i) = J. \tag{3.2}$$

3.1.1.1 Steady State for Periodic Boundary Conditions

For periodic boundary conditions the total number of particles in the system M is constant. Since the system is translationally invariant, the steady state density profile is given by a flat profile: the average density of each site is equal with $\rho(i) = \rho = M/L$ (see e.g. [115]).

3.1.1.2 Phase Diagram for Open Boundary Conditions

For open boundary conditions the situation changes. Here the phase of the system depends of the entrance and exit rates. This behaviour is known as boundary induced phase transitions [55]. The steady state properties of the open boundary TASEP are also known exactly, they can e.g. be derived using recursion relations [116, 117] or a matrix formulation [118].

If the entrance rate is smaller than the exit rate and smaller than 1/2 ($\alpha < 1/2$, $\alpha < \beta$) the system is in a low density (LD) phase. In this case the limiting rate is the entrance rate as particles are more likely to leave the system than to enter it. In this case the bulk density (i.e. the density at $i = L/2$) is equal to α. If the exit rate is lower than the entrance rate and smaller than 1/2 ($\beta < 1/2$, $\beta < \alpha$), the system is in a high density (HD) phase, since the system's limiting rate is the exit rate. Here the bulk density equals $1 - \beta$. If both rates are larger than 1/2 ($\alpha,\ \beta > 1/2$), the bulk current is limiting factor: the system is in the maximum current (MC) phase.

The phase diagram is shown in Figure 3.2. One can see that the LD and HD phases are both sub-divided into two sub-phases. They differ in the behaviour of the density profiles near the boundaries. A summary of the most important features of the phases LD-I, LD-II,HD-I, HD-II and MC is shown in Table 3.1. There is also a line in the phase diagram at $\alpha + \beta = 1$ at which the density profile becomes flat. Examples of how the density profiles look in the LD, HD and MC phases are shown in Figures 3.3 **(a)** to **(c)**. I do not go into details about all the special cases and the phase transitions here (a good summary of all of them is found e.g.

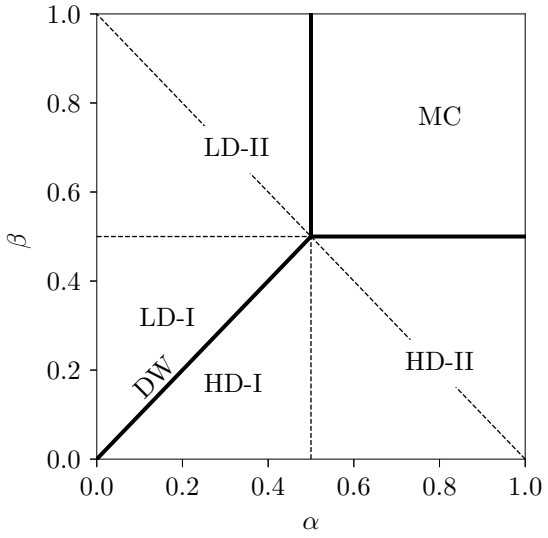

Figure 3.2. The phase diagram of the OBC TASEP. For ($\alpha < 1/2$, $\alpha < \beta$) the system is in a low density (LD) phase, while for ($\beta < 1/2$, $\beta < \alpha$) it is in a high density (HD) phase. These two can both be divided into two sub-phases (dotted lines at $\alpha = 1/2$, $\beta < 1/2$ and $\beta = 1/2$, $\alpha < 1/2$ respectively) which differ in their density profiles near the boundaries (c.f. Table 3.1). For (α, $\beta > 1/2$) the system is in a maximum current (MC) phase. At the phase boundary between LD and HD phases at ($\alpha = \beta < 1/2$) a domain wall (DW) performs a random walk through the system. Furthermore, on the dotted line at ($\alpha + \beta = 1$) the density profile becomes a straight line. Examples of density profiles are shown in Figure 3.3.

in [35]), but I do have a closer look at the LD/HD phase transition happening at $\alpha = \beta < 1/2$ in the following.

Domain Wall 'Phase'. At the LD/HD transition line ($\alpha = \beta < 1/2$) the average density profile becomes a straight line ascending from α at $i = 1$ to $1-\alpha = 1-\beta$ at $i = L$. The linear averaged density profile is a consequence of freely a *diffusing shock* or *domain wall* (DW) in the system [119]. The shock separates a high density region with density $1 - \alpha$ on the right from a low density region with density α on the left. The shock's position performs a random walk through the system. An example of this behaviour is shown in Figure 3.3 **(d)**. The density profile obtained in a Monte Carlo simulation of this system is shown. The thick orange line is the averaged density profile, measured over the whole measurement process of $3 \cdot 10^6$ sweeps. As one can see the line is not perfectly straight. It would become perfectly straight if measured over really long times. Additionally, as thinner lines in different shades of grey, several short-term density profiles are shown. They are measured over $2 \cdot 10^4$ sweeps each during the measurement process. One can clearly see that they correspond to system times in which the domain wall is at different positions in the system.

For a single TASEP in the hydrodynamic limit (a TASEP of inifinte length) this behaviour only occurs on the exact line $\alpha = \beta < 1/2$. For finite size TASEPs domain walls can also be observed in a small region around that line. To observe this behaviour in a single TASEP one needs to fine tune the parameters. It turns out that in some networks of TASEPs (e.g. in

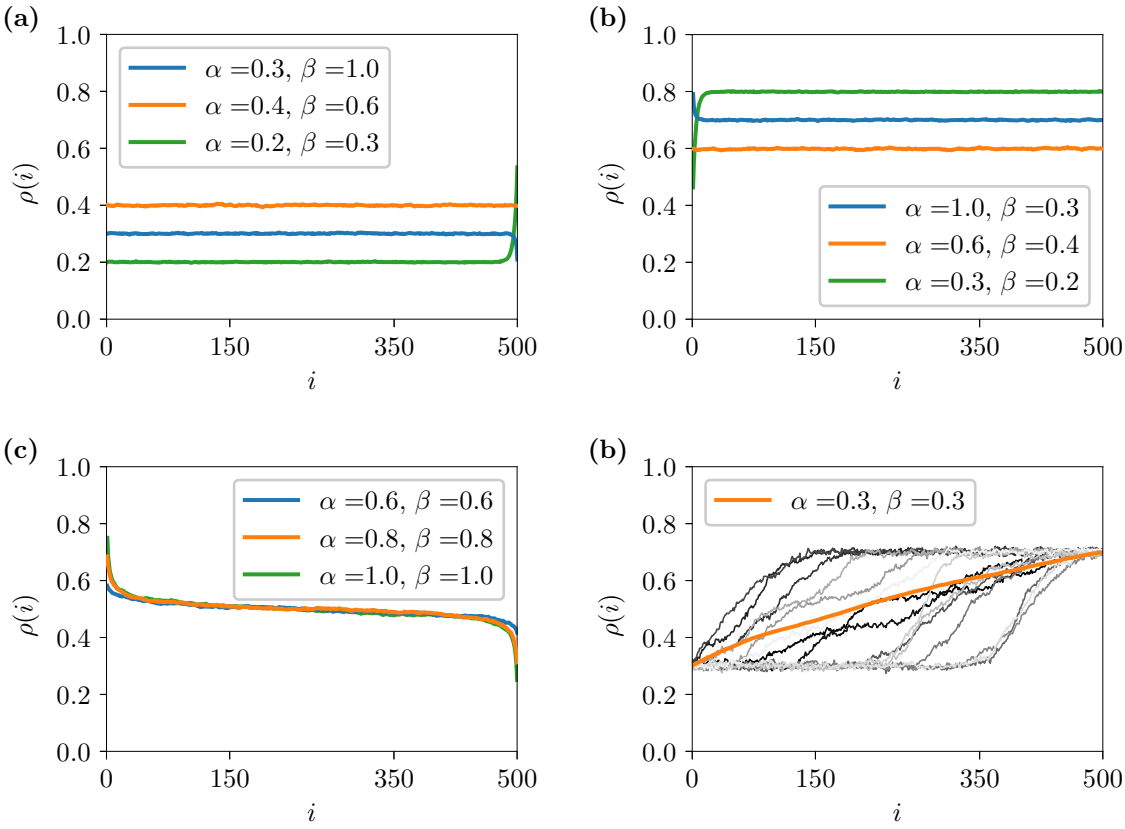

Figure 3.3. Examples of density profiles in the different phases of an OBC TASEP. The averaged density ρ is shown against position i for various entrance and exit rates. Part **(a)** shows profiles in the LD phase, Part **(b)** shows profiles in the HD phase, Part **(c)** shows profiles in the MC phase. In Part **(d)** a DW state which occurs at the LD/HD boundary at $\alpha = \beta < 1/2$ is shown. The (almost) linear orange line shows the averaged density profile while the grey lines show different instances during the measurement process. Data was obtained using Monte Carlo simulations.

the unbiased figure of eight network which is treated in Section 3.1.3.1) fluctuating domain walls occur for a large parameter region. In such circumstances one can talk about a domain wall phase. In the context of just a single TASEP there is no domain wall phase but domain walls just occur on the phase separation line between the LD and HD phases.

3.1.1.3 Travel Times

Since this thesis' main topic is Braess' paradox in networks of TASEPs, an observable which is not often addressed in the context of TASEPs is very important to be looked at in more detail: the (average) travel time of a TASEP segment. For a TASEP with open boundary conditions this is the time (i.e. the number of time steps) a particle needs to traverse the TASEP, i.e. the time from entering the TASEP on site 1 till jumping out of site L. In the case of periodic boundary conditions the travel time is the number of time steps a particle needs to complete one round, i.e. the time from jumping out of a specific site till jumping back into that site.

Table 3.1. Summary of the main features of the phases of a TASEP with OBC. For the LD-I, LD-II,HD-I, HD-II and the MC phase the current J, the density in the bulk $\rho_{L/2}$, at the first site ρ_1 and at the last site ρ_L are shown. Furthermore, the asymptotic decay of the density profile near the entrance (left end) and the exit (right end) and the parameter regions where each phase occurs are shown.

Phase	$J(\alpha,\ \beta)$	$\rho_{L/2}$	ρ_1	ρ_L	Left end	Right end	Parameter region
LD-I	$\alpha(1-\alpha)$	α	α	$\frac{\alpha(1-\alpha)}{\beta}$	α	$\mathrm{e}^{-j/\xi}$	$\alpha < \beta < 1/2$
LD-II	$\alpha(1-\alpha)$	α	α	$\frac{\alpha(1-\alpha)}{\beta}$	α	$j^{-3/2}\mathrm{e}^{-j/\xi_\alpha}$	$1/2 > \alpha < \beta > 1/2$
HD-I	$\beta(1-\beta)$	$1-\beta$	$1-\frac{\beta(1-\beta)}{\alpha}$	$1-\beta$	$\mathrm{e}^{-j/\xi}$	$1-\beta$	$\beta < \alpha < 1/2$
HD-II	$\beta(1-\beta)$	$1-\beta$	$1-\frac{\beta(1-\beta)}{\alpha}$	$1-\beta$	$\mathrm{e}^{-j/\xi}$	$1-\beta$	$1/2 > \beta < \alpha > 1/2$
MC	$1/4$	$1/2$	$1-\frac{1}{4\alpha}$	$\frac{1}{4\beta}$	$\frac{1}{2\sqrt{\pi j}}$	$-\frac{1}{2\sqrt{\pi}}j^{-1/2}$	$\alpha,\ \beta > 1/2$

Periodic Boundary Conditions. For periodic boundary conditions, the averaged density profile is flat. Thus the velocity

$$v(i) = J/\rho(i) \tag{3.3}$$

is site-independent: $v(i) = v$. The travel time is then simply given by dividing the length by the velocity. For $p = 1$ it is given by

$$T_{\mathrm{PBC}}(\rho) = \frac{L}{1-\rho}, \tag{3.4}$$

with $\rho = M/L$.

Open Boundary Conditions. For open boundary conditions for most entrance and exit rates the density profile is not flat throughout the whole length of the TASEP. Thus the average velocity also depends of the site. A good approximation for the travel time can here be obtained by substituting the density in Equation (3.4) by the bulk density $\rho_{L/2}$ (cf. Table 3.1) of the given OBC case:

$$T_{\mathrm{OBC}}(\alpha,\beta) \approx T_{\mathrm{PBC}}[\rho_{L/2}(\alpha,\beta)]. \tag{3.5}$$

From the exact boundary behaviours as given in Table 3.1 and shown in Figure 3.3 one can see that depending on the specific (sub-) phase, i.e. on α and β, the error of that approximation can be positive or negative.

In Figure 3.4 one can see that Equation (3.5) holds relatively well for most entrance and exit rates. The relative difference of Equation (3.5) to travel time measurements obtained by Monte Carlo simulations T_{MC} is shown. In the figure for each data point travel times where measured for 10^6 sweeps. One can see that in the LD, HD and MC phases the difference is well below 10 %. Only on the phase boundaries between LD/MC, HD/MC and especially between LD and HD – i.e. in the DW phase – the difference is significantly higher, taking values of up to 20 %.

The deviations of the measured travel times in the DW phase from Equation (3.5) is no sur-

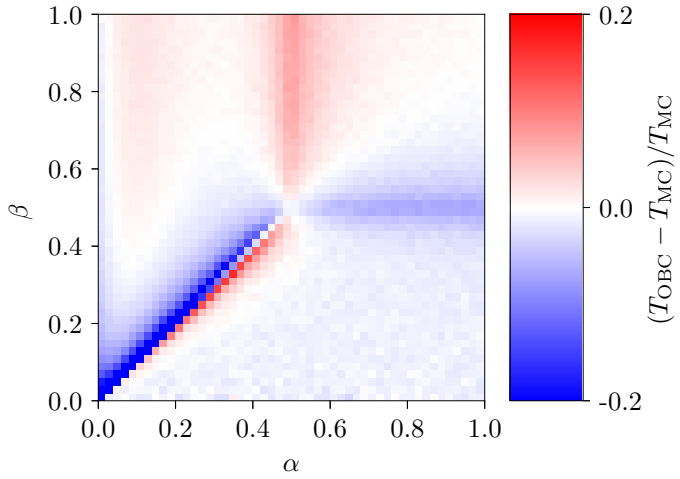

Figure 3.4. The relative difference of the travel times in the OBC TASEP approximated through Equation (3.5) and Monte Carlo data (see Section 3.3 for details on Monte Carlo simulations). As one can see the approximation is pretty good inside the LD, HD and MC phases but worse around the phase boundaries. Especially on the LD/HD boundary, i.e. in the DW phase, the approximation deviates strongly. This is due to the fluctuation of the domain wall position in this phase leading to unstable travel times. Travel times were measured for 10^6 sweeps for 2500 individual parameter sets.

prise: as explained previously, in the DW phase a domain wall separating a low density region on the left from a high density region on the right diffuses through the system. Depending on where the domain wall is when a particle enters the system, the particle will experience another travel time. The longer the high density region is at a given time, the higher the travel time. As the Monte Carlo data to which Equation (3.5) is compared was obtained by measuring the system for one million sweeps, one has to note that not all possible positions of the domain wall were covered in this measurement. If the travel times were measured over a really long time, the difference from Equation (3.5) would decrease. Nevertheless, even when measuring for a really long time generally not all DW positions would be achieved equally often.

For this thesis the behaviour for shorter measurement times is of higher importance than the limit of averaging over very long times: we will use TASEPs to simulate traffic on the edges of Braess' network. The traffic situation faced by each driver in the network is of importance here. It is thus important to note that for a TASEP in the DW phase, a driver entering at one time could face a totally different situation (and travel time) than a driver entering the system at another time, even if the system is in its stationary state at both times. This means that even if in the very long time limit the average of travel times will stabilize, the situation of a TASEP in a DW phase is changing all the time and thus no stable travel time predictions are possible (at least not for individual drivers entering the TASEP at individual times).

3.1.2 How Well Does TASEP Describe Road Traffic?

In Section 2.3 several characteristic aspects of traffic flow on freeways, as obtained in analyses of real world data, were discussed. Defining properties which should be represented in realistic traffic models were deduced: traffic models should be stochastic, include microscopic interactions and they should be able to reproduce typical traffic phenomena. Some of these phenomena can be reflected in the shapes of the fundamental diagrams and travel time functions of traffic models. Furthermore, it was worked out why the traffic description in Braess' original model is unrealistic. In the following I summarize how realistically traffic flow can be modelled by TASEP and explain why analysing TASEP networks is a good starting point to gain an understanding of Braess' paradox in a more realistic way.

First, one has to note that the TASEP is a stochastic transport process. By that nature it is better suited to model road traffic flow than deterministic descriptions. In the random-sequential update case the stochasticity is introduced by the random choices of sites to update.

Second, one can study the fundamental diagram and travel time functions of TASEPs. The fundamental diagram, i.e. the flow-density relation (Equation (3.1)), and the travel time (Equation (3.4)) dependend on the density of a TASEP with periodic boundary conditions are shown in Figures 3.5 **(a)** and **(b)**. The flow is increasing with the density until a single

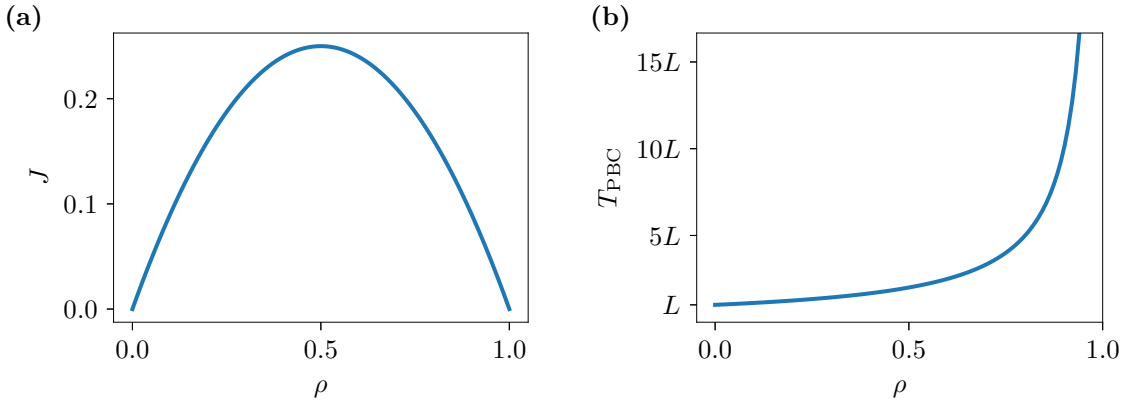

Figure 3.5. The flow J dependent of the density ρ (Part **(a)**) and the travel time T_{PBC} dependent on the density ρ (Part **(b)**) for a TASEP with periodic boundary conditions. The travel time was obtained for a segment of length $L = 600$. Comparing this to experimental observations of traffic flow on real freeways as shwon in Figure 2.7 one can see that major aspects like the single-maximum in the flow and a diverging travel time are covered. Still TASEP is a vast oversimplification of real road traffic.

maximum is reached at $\rho = 0.5$. For $\rho > 0.5$ the flow decreases with the density, reaching $J = 0$ at $\rho = 1$. Comparing Figure 3.5 **(a)** to a fundamental diagram based on empirical research, as shown in Figure 2.7 **(a)**, one can conclude: the basic shape is recovered in the sense that the flow increases from zero up to a single maximum and then decreases back to zero at the maximum density. The exact shape is different, as the increasing and decreasing parts are not linear.

The travel time function (Figure 3.5 **(b)**) has a similar shape to that obtained from the

fundamental diagram based on empirical data (Figure 2.7 **(c)**): the free flow travel time is given for $\rho = 0$ and the travel time diverges as $\rho \to 1$. Nevertheless, there is an important difference. The travel time of the TASEP is strictly monotonically increasing, i.e. there is no regime $0 < \rho < \rho^\star$, in which the free flow travel time persists.

In spite of these discrepancies between experimental fundamental diagrams and travel time functions and those of TASEPs, one can conclude that relevant features are included in TASEP dynamics which are not included in the traffic description used in Braess' model (compare to Figure 2.8): the flow decreases with the density after reaching a maximum and accordingly the travel time diverges for high densities. Neither of those effects are included in the mathematical description used by Braess.

TASEP dynamics is still an oversimplification of real road traffic: 'imperfect behaviour', inevitably found in road traffic due to human decisions, such as a finite reaction times or overreaction, is not modelled in TASEP. Phenomena like spontaneous formations of traffic jams are thus not covered. Furthermore, cars either drive or do not drive – there is just one velocity. Networks of more sophisticated traffic models, such as the Nagel-Schreckenberg model [106] or the velocity-dependent randomization model [120], should be studied in the future to obtain even more realistic understandings about phenomena like the Braess paradox.

Nevertheless, TASEP is a good starting point for an analysis of Braess' paradox since major characteristics are roughly covered while the model is still relatively simple to handle. As will be explained in the following subsection, networks of TASEPs quickly become relatively complicated and are not analytically tractable despite the simplicity of single TASEP segments.

3.1.3 Networks of TASEPs

Most other real world traffic phenomena are not limited to single roads. This is particularly true to the focus topic of this thesis: the Braess paradox is by nature a network phenomenon. Nevertheless, before being able to analyse what happens in a road network it is important to understand the traffic dynamics on the individual roads. The same principle is applied to networks of TASEPs. In the previous subsections it was established that TASEP segments cover some important aspects of traffic on real roads and the most important characteristics of single TASEP segments were introduced.

Several TASEP segments can easily be connected to form networks of TASEPs. While single TASEP segments can be analytically solved, networks of TASEPs are generally not exactly solvable. Mean field theory (MFT) with several extensions, domain wall theories and Monte Carlo simulations have proven to be useful tools to tackle TASEP networks (Monte Carlo simulations for TASEP dynamics will be introduced in Section 3.3).

Over the years, different simple network topologies have been studied. For the case of random-sequential updates, among others, the cases of one TASEP splitting into two lanes, then merging into one again [57], two TASEPs feeding into one [58] and all different variations of four TASEPs [59] (i.e. 3 on 1, 2 on 2, 1 on 3) were studied.

Most of these studies focused on open boundary conditions (one exception is found in [59]). Furthermore, three general network classes (Bethe networks, Poissonian networks and strongly correlated networks) have been examined [56]. By studying Bethe networks, it was shown that closed regular networks[2] are in large density regions dominated by domain walls [56].

Networks with parallel update schemes instead of the random-sequential updates were studied in [60–62]. Summaries of these findings are found in [5, 121].

In the following, the general mechanism of a MFT for analysing a network of TASEPs is exemplified based on the example network shown in Figure 3.6. This network was studied first in [57] but with a slightly modified update scheme. In [58] it was first treated in the way presented here. In the following the main steps of analysing this (or any other) network in a MFT are summarized. Also some results are presented, while the reader is referred to the article for all results on this network.

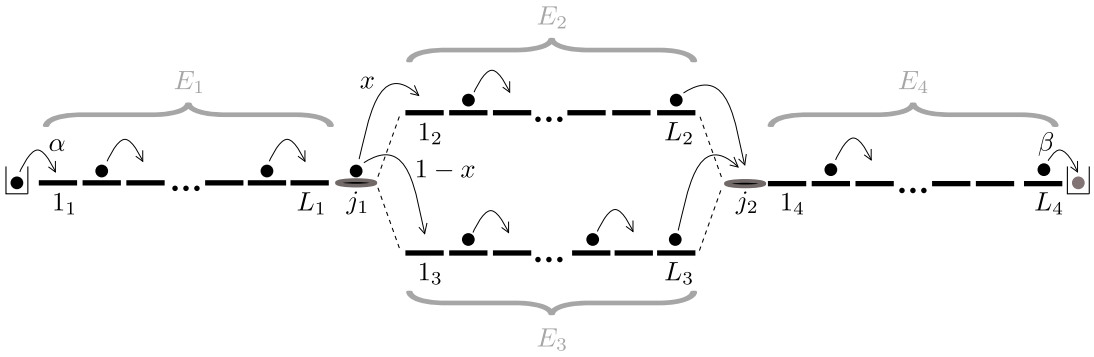

Figure 3.6. The network for which the main steps of a mean field analysis are repeated here. It consists of four edges $E_1, \ldots, E_4$ which are all TASEPs of lengths L_i. The network has open boundary conditions: edge E_1 is on the left coupled to the entrance reservoir which is occupied with entrance rate α. Edge E_4 exits on its right into the exit reservoir with exit rate β. Particles jump out of E_1 onto junction j_1 and form there with probability x onto edge E_2 or to edge E_3 with probability $1 - x$. Particles jump from the last sites of E_2 and E_3 onto junction j_2 and from there onto edge E_4.

The network consists of four coupled TASEPs, or network edges $E_i,\ i \in [1, 2, 3, 4]$. The TASEPs are connected by so-called junction sites j_1 and j_2. The junction sites are essentially just normal TASEP sites that can take up one particle at a time while they can be reached by more than just one site and can be left to various cells. While e.g. j_1 could just be treated as the last site of E_1, as was done in the earliest works on TASEP networks [57], the concept of introducing explicit junction sites has proven to be useful [59] in an MFT framework. This is nevertheless just a conceptual difference: j_1 can also regarded as the last site of E_1 and j_2 as the first site of E_4.

Particles are fed into E_1 from a reservoir with entrance rate α. From the last site of E_1 they jump onto j_1 from which particles jump onto E_2 with probability x and onto E_3 with probability $1 - x$. Particles on the last sites of E_2/E_3 jump onto j_2 and from there to E_4. Particles can then leave the network by jumping out of E_4 into an exit reservoir which is

[2]Networks with periodic boundary conditions, in which all nodes have the same connectivity, i.e. same number of incoming and outgoing edges.

empty with exit rate β.

The networks dynamics is generated by random-sequential updates. In the case of networks this means that one of all cells is chosen randomly with uniform probability. Here these are the $\sum_{i=1}^{4} L_i + 3$ total sites (the sites of the four edges plus the two junction sites and the entrance reservoir). After as many of such single site updates as sites in the system one sweep/time step is complete.

A first step in analysing such a network is to explicitly write down the current conservation in the system, from which possible phases of the individual TASEP segments can be deduced. Here the current conservation reads:

$$J_{\text{tot}} = J_1(\alpha, \beta, x) = J_2(\alpha, \beta, x) + J_3(\alpha, \beta, x) = J_4(\alpha, \beta, x). \tag{3.6}$$

The currents can then be expressed as follows

$$\begin{aligned} J_{\text{tot}} \quad &= \alpha(1 - \rho_{1_1}) = \rho_{L_1}(1 - \rho_{j_1}) = x \cdot \rho_{j_1}(1 - \rho_{1_2}) + (1 - x) \cdot \rho_{j_1}(1 - \rho_{1_3}) \\ &= (\rho_{L_2} + \rho_{L_3})(1 - \rho_{j_2}) = \rho_{j_2}(1 - \rho_{1_4}) = \beta \rho_{L_4}, \end{aligned} \tag{3.7}$$

since inside the individual edges the currents are independent of position (which is a consequence of the continuity equation). Until here no simplifying assumptions were made.

To be able to draw some conclusions about the possible stationary states of the network, a first assumption is that all individual TASEP segments will be in one of the possible phases of the single OBC TASEP (see Figure 3.2). For this assumption to be reasonably valid all edges have to be sufficiently long. It is assumed that in the bulk of each segment, as in the thermodynamic limit for a single OBC TASEP, the pair correlations between neighbouring sites vanish which leads to the current through a segment being

$$J = \rho_{L/2}(1 - \rho_{L/2+1}) \tag{3.8}$$

with $\rho_{L/2}$ in the specific phases taking up values as in Table 3.1. Also, $\rho_{L/2+1} \approx \rho_{L/2}$ is assumed as the density in the bulk is assumed to be constant. The differentiation between the LD and HD sub-phases is neglected in this analysis. It turns out that the DW-phase occurs very frequently in networks whereas in a single TASEP segment it only occurs for fine-tuned parameters on the LD/HD transition line. Following this reasoning, each TASEP segment can be in one of the four possible states LD, HD, MC, DW. This leads to $4^4 = 256$ different possible states of the network depending on α, β and x.

Using Equation (3.6) combined with the assumption that all segments have to take one of the possible states of single OBC TASEPs, it becomes clear that some of the 256 combinations are not accessible: using $J_1(\alpha, \beta, x) = \rho_{L/2_1}(1 - \rho_{L/2_1}) = J_4(\alpha, \beta, x) = \rho_{L/2_4}(1 - \rho_{L/2_4})$, it follows that either $\rho_{L/2_1} = \rho_{L/2_4}$ or $\rho_{L/2_1} = (1 - \rho_{L/2_4})$. Thus if segment 1 is in an LD phase, segment 4 has to be in an LD or HD phase, it cannot be in an MC phase. In the case of $x = 1/2$ also the two middle segments have to be in the same state for symmetry reasons.

Several other phase combinations can be ruled out exploiting the current conservation.

This will not be done in detail here, since this section is just presenting the idea of analysing TASEP networks.

By neglecting the correlations between the junction sites and its neighbouring sites one treats the individual network edges as independent open boundary TASEPs with effective entrance and exit rates which then depend on the average densities of the junction sites. These densities then become the physical control parameters of the network [59][3].

If correlations between junctions and its neighbouring sites are neglected, the individual TASEP segments have the following (effective) entrance and exit rates:

$$\alpha_1 = \alpha, \qquad \beta_1^{\text{eff}} = 1 - \rho_{j_1} \tag{3.9}$$

$$\alpha_2^{\text{eff}} = x\rho_{j_1}, \qquad \beta_2^{\text{eff}} = 1 - \rho_{j_2} \tag{3.10}$$

$$\alpha_3^{\text{eff}} = (1-x)\rho_{j_1}, \qquad \beta_3^{\text{eff}} = 1 - \rho_{j_2} \tag{3.11}$$

$$\alpha_4^{\text{eff}} = \rho_{j_2}, \qquad \beta_4 = \beta. \tag{3.12}$$

The current of each segment is then given by the piecewise functions given in Table 3.1, depending on the (effective) entrance and exit rates of the segment. This, combined with the current conservation (Equation (3.6)) then gives two equations which can be used to deduce ρ_{j_1} and ρ_{j_2} depending on α, β (and x). This process is sometimes called current matching [59]. From the obtained ρ_{j_1} and ρ_{j_2}, using Table 3.1 one can then deduce the state of each segment given a combination of α, β (and x).

This is the general strategy when analysing TASEP networks using a MFT. It turns out that it produces correct predictions of the general behaviour of TASEP networks, at least for simple topologies, as can be tested employing Monte Carlo simulations (see e.g. [5, 121] for summaries of previous work done in this fashion).

The MFT approach has some limitations. While it predicts the general phases of networks fairly well, especially in predicting density profiles it breaks down. This is a consequence of neglecting the correlations between the segments which are relevant for many parameter sets. Several extensions to the simple MFT model addressing these limitations (see e.g. [125]) were studied.

3.1.3.1 The Unbiased Figure of Eight Network

Here the main properties of a special network, the so-called unbiased figure-of-eight network, are summarized. They are presented since this network is very similar to Braess' 4link network (Figure 2.2 without edge 5) with added periodic boundary conditions. The results give some insight into how Braess' 4link network with TASEPs as edges behaves as will be seen in Section 4.2.2. The presented results are reproduced from [59] where more details can be

[3] Before this concept was first applied to networks of TASEPs it has proven to be useful in single TASEP segments with defects [122]. In this context the site with reduced hopping probability corresponds to a junction site in the context of networks. The general behaviour of systems with defects was predicted correctly by this MFT treatment. Limitations of this MFT study were examined and an extended in [123]. Indeed networks of TASEPs with junction sites and TASEPs with defects behave very similarly [124].

found.

The unbiased figure of eight network is shown in Figure 3.7. It consists of two TASEPs E_A and E_B, which feed and are – unbiasedly, i.e. with equal probability – fed by junction j. Due to the symmetry, both edges are always in the same state: either an LD, HD or domain

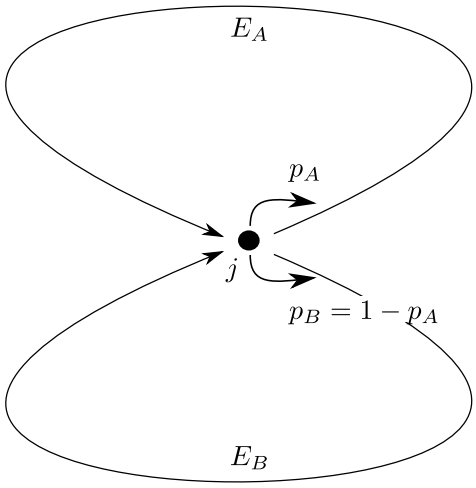

Figure 3.7. The figure of eight network consists of two symmetric TASEPs E_A and E_B which feed onto and are, with probabilities p_A and $p_B = 1 - p_A$, fed by junction j. In the unbiased case the probabilities are equal, $p_A = p_B = 0.5$.

wall state. A MC phase can not be reached since the effective entrance rates are always smaller than 1/2 due to the unbiased feeding. Using this symmetry, in a mean-field picture the particle density of the junction ρ_j depends on the global density ρ_{global} as

$$\rho_j = \begin{cases} 2\rho_{\text{global}} & (\rho_{\text{global}} < 1/3) \\ 2/3 & (1/3 < \rho_{\text{global}} < 2/3) \\ \rho_{\text{global}} & (\rho_{\text{global}} > 2/3) \end{cases} \tag{3.13}$$

and the current through the junction is given by

$$J = \begin{cases} 2\rho_{\text{global}}(1 - \rho_{\text{global}}) & (\rho_{\text{global}} < 1/3) \\ 2 \cdot 2/9 & (1/3 < \rho_{\text{global}} < 2/3) \\ 2\rho_{\text{global}}(1 - \rho_{\text{global}}) & (\rho_{\text{global}} > 2/3) \end{cases} \tag{3.14}$$

as shown in Fig. 3.8. This has an easily understandable interpretation. For low global densities ($\rho_{\text{global}} < 1/3$), both segments are in an LD phase, while the density increases with the global density. At $\rho_{\text{global}} = 1/3$, the effective rates of the edges become equal $\alpha^{\text{eff}}_{A/B} = \beta^{\text{eff}}_{A/B} = 1/3$ which leads to diffusing domain walls between LD and HD segments in both links. The junction occupation saturates at $\rho_j = 2/3$, while the lengths of the HD regions grow with growing global density. At $\rho_{\text{global}} = 2/3$, the HD regions fill the whole edges. This behaviour is very different to single TASEPs. In single TASEPs with open boundary conditions domain walls only appear for fine-tuned parameters $\alpha = \beta < 1/2$, while in this network, they dominate

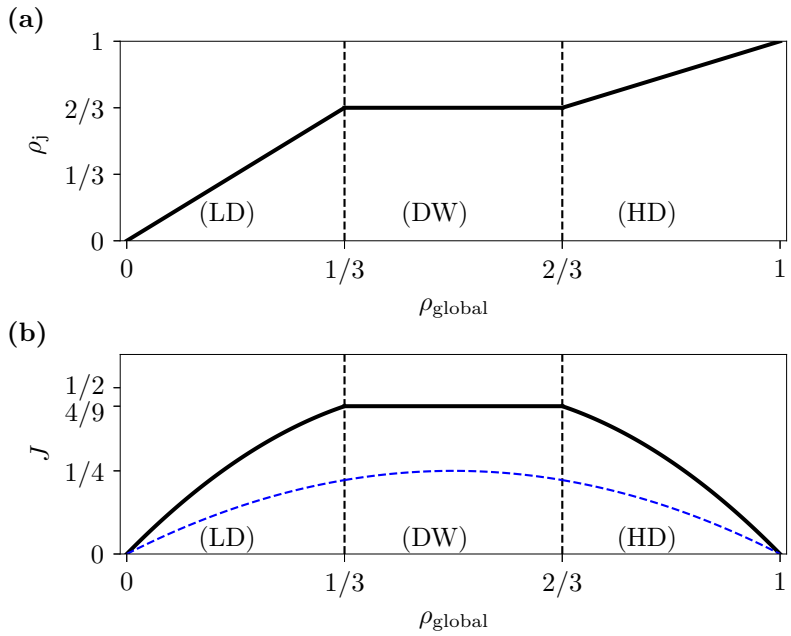

Figure 3.8. The unbiased figure of eight network shows a domain wall phase in a large intermediate density regime $1/3 < \rho_{\text{global}} < 2/3$. This can be seen in **(a)** the junction occupation ρ_j which takes a constant value of $2/3$ in that regime according to Eq. (3.13). As seen in **(b)** the current density relation shows that behaviour aswell, as the parabola for a single periodic TASEP $J = \rho(1-\rho)$ is truncated with constant value $2/9$ in the DW regime according to Eq. (3.14). The current for a single TASEP is shown for comparison (blue dotted line).

the system over a large density regime ($1/3 < \rho_{\text{global}} < 2/3$) and are thus far more important for its analysis.

The main part of the remainder of this thesis focusses on the question if and when Braess' paradox appears in networks of TASEPs. As Braess in his original work, I addressed the Braess network with a symmetric 4link sub-network. The system and user optima of the symmetric 4link networks are expectedly given by a symmetric distribution of the particles onto both routes. Thus, for the sake of applicability, the discussion of the figure of eight network is limited to unbiased feeding.

The biased version of the figure of eight network in which the probabilities for jumps from the junction to the edges are not equal shows two plateaus in the fundamental diagram. They correspond to domain wall phases, for two distinct global density regimes. For more details, see [59]. This study has also been extended to symmetric junctions feeding onto more than two edges [56, 125].

3.2 The Basic Model of This Thesis: The Braess Network of TASEPs

The Braess network of TASEPs serves as the basic model for most results of my research. In this section the network is introduced: first, the general structure, its variants of boundary conditions and possible route choice strategies are elucidated. Second, two observables for the determination of system optima and user optima strategies are defined. Then, the possible phases which can be observed when comparing the 4link and 5link versions of the network for the same demand are worked out. By analysing these different phases, the influence of the added road can be studied beyond the question about the occurrence of Braess' paradox. In the last subsection, a method for finding system and user optima by Monte Carlo simulations is explained.

3.2.1 Network's Structure

The Braess network of TASEPs is realized with periodic and with open boundary conditions. Both versions of the network are shown in Figure 3.9 (Part **(a)** shows the periodic boundary version and Part **(b)** the open boundary version). The networks have the same structure

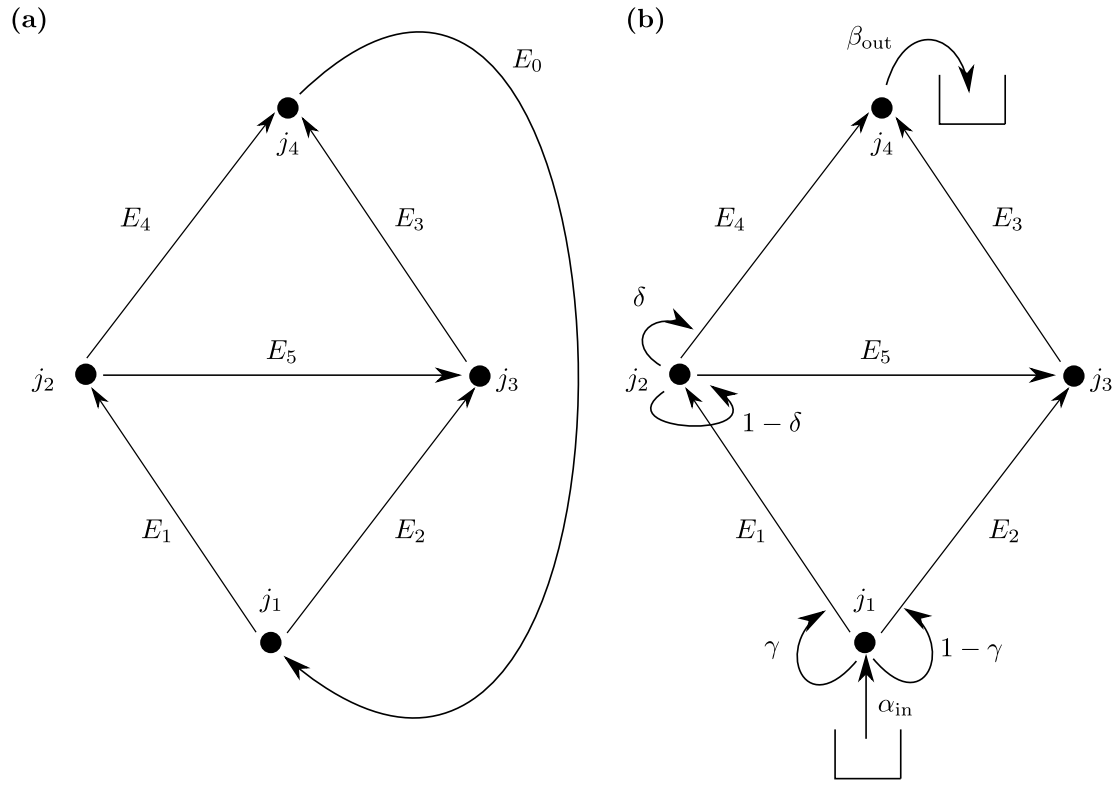

Figure 3.9. The Braess network with the edges made of TASEPs. The edges E_i are TASEPs of lengths L_i. They are connected through junction sites j_k. Part **(a)** shows the version with added periodic boundary conditions, achieved through E_0 which is set to have length $L_0 = 1$ throughout this thesis. Part **(b)** shows the open boundary version. Here junction j_1 is fed from the entrance reservoir which is occupied with probability α_{in} and junction j_4 exits into the exit reservoir which is empty with probability β_{out}.

as the network in Braess' original publication (see Figure 2.2). Each network edge E_i, with $i \in [0, 1, 2, 3, 4, 5]$ is made up of a TASEP segment with L_i discrete cells (or of the length L_i). The TASEPs are joined through junction sites j_k, with $k \in [1, 2, 3, 4]$, which behave as ordinary TASEP cells, as explained in Section 3.1.3. Junction j_1 is considered the origin of network users and junction j_4 is the destination (j_1 and j_4 are also called start and finish points, respectively). The influence of the new edge E_5 will thus, as in Braess' original work, be examined under the assumption that all particles want to go from j_1 to j_4. One complete trip from j_1 to j_4 will also be referred to as one *round*.

As in Braess' original work the network is always chosen to be symmetric. The individual roads have the lengths

$$L_1 = L_3 \qquad \text{and} \qquad L_2 = L_4\,. \tag{3.15}$$

We consider the case $L_1 \leq L_2$. Thus, for

$$L_5 \leq L_2 - L_1 - 1 \tag{3.16}$$

the addition of E_5 results in a new possible route through the system, which is of shorter or equal length as the routes without the new link:

$$\begin{aligned} \hat{L}_{153} &= 4 + L_1 + L_3 + L_5 + (L_0) && (3.17)\\ &\leq 3 + L_1 + L_2 + (L_0) && (3.18)\\ &= \hat{L}_{14} = \hat{L}_{23}, && (3.19) \end{aligned}$$

with $\hat{L}_i$ denoting lengths of routes. Routes are in this context paths to go from j_1 to j_4 as opposed to individual edges, also called roads, which go from one junction, also called nodes, to the neighbouring one. The length L_0 is put into brackets to indicate that it is only added in the case of periodic boundary conditions since it does not exist in the open boundary case.

There are then three routes from j_1 to j_4: route 14 goes from j_1 to j_4 via E_1, j_2 and E_4. Route 23 goes from j_1 to j_4 via E_2, j_3, E_3 and route 153, the new route which is the result of the new road E_5 goes from j_1 to j_4 via E_1, j_2, E_5, j_3, E_3.

In the analysis, the 4link and 5link systems, i.e. the networks without and with the new edge E_5, will be compared. Corresponding variables are denoted with a superscript (4) or (5) respectively. Most parts of the analyses will deal with travel time measurements.

A travel time in the context of our network is given by the number of time steps a particle needs to traverse the system, i.e. the number of time steps the particle needs from jumping onto j_1 till jumping out of j_4.

The travel times of the different routes are denoted by T_{14}, T_{23} and T_{153}.

3.2.1.1 Boundary Conditions

The two parts of Figure 3.9 shows the Braess network of TASEPs with two different boundary conditions. Their individual characteristics are explained in the following.

Periodic Boundary Conditions. In the periodic boundary case (Figure 3.9 **(a)**) there is an additional edge E_0 which is always chosen to have length $L_0 = 1$ which couples j_4 back to j_1. Particles that finish one round are fed back to the starting point via E_0. The number of particles M and thus the global density ρ_{global} in the system are constant. We will use the global densities of the system with E_5 ($\rho^{(5)}_{\text{global}} = M/(4 + \sum_{i=0}^{5} L_i)$) and without E_5 ($\rho^{(4)}_{\text{global}} = M/(4 + \sum_{i=0}^{4} L_i)$) when comparing the two systems. Both densities are related as follows:

$$\begin{aligned} \rho^{(5)}_{\text{global}} &= \rho^{(4)}_{\text{global}} \frac{5 + 2L_1 + 2L_2}{5 + 2L_1 + 2L_2 + L_5} \\ &= \rho^{(4)}_{\text{global}} \frac{5 + 2L_1 + 2L_2}{2L_2 + \frac{\hat{L}_{153}}{\hat{L}_{14}}(4 + L_1 + L_2)}. \end{aligned} \tag{3.20}$$

The latter Equation (3.20) is used in the resulting phase diagram of the system. It allows to compare the performance of the 4link and 5link systems through their defining properties given the same total number of particels M. These defining properties are the global densities $\rho^{(4/5)}_{\text{global}}$ and the length ratio $\frac{\hat{L}_{153}}{\hat{L}_{14}}$ of the new route and the old routes.

Open Boundary Conditions. In the open boundary case (see Figure 3.9 **(b)**) particles are fed onto junction j_1 from a reservoir which is occupied with entrance probability α_{in}. Particles leave the system, jumping out of junction j_4, into a reservoir which is empty with exit probability β_{out}. Since the individual particles do not stay in the system, other than in the periodic boundary case, one cannot define a global density.

3.2.2 Route Choice Strategies

Two different route choice mechanisms were examined. In the present context the term "route choice" refers to how particles are distributed onto the three possible routes. Both mechanisms are sketched in Figure 3.10 and explained in the following. These strategies are variables which are tuned externally, i.e. the particles do not decide intelligently for themselves[4].

3.2.2.1 Fixed Route Choices

The first possible route choice mechanism, as depicted in Figure 3.10 **(a)**, can only be employed in the system with periodic boundary conditions since it requires that the same fixed set of particles stay in the system. It works as follows: all particles have a fixed 'personal' route choice. N_{14} particles take route 14, N_{23} particles take route 23 and N_{153} particles take route 153 respectively. These numbers are subject to

$$N_{14} + N_{23} + N_{153} = M. \tag{3.21}$$

[4]Results obtained for these strategies presented here will be shown in Chapter 4. In Chapter 5 results obtained by intelligently deciding particles, as implemented through route choice algorithms are shown.

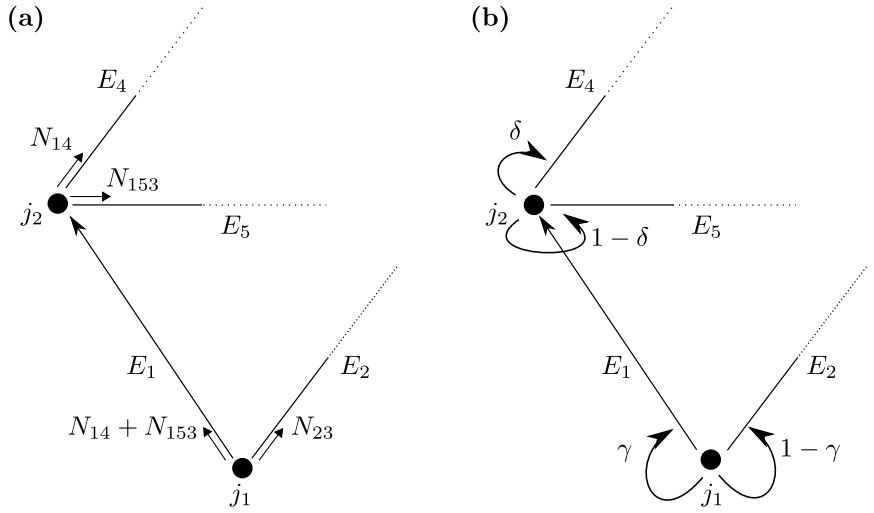

Figure 3.10. The route choices in the periodic boundary case of Braess' network were realized in two different ways. Part **(a)** shows the fixed route choices case: here the individual particles stick to their own 'personal' route choices. Part **(b)** shows the case of turning probabilities in which routes are assigned to the particles by the probabilities γ and δ of turning left on junctions j_1 and j_2 respectively.

All particles stick to their route choices. Even if a particle on j_1 or j_2 cannot jump for multiple attempts due to its target site being occupied it will stick to its route choice. A user optimum found in the network with fixed route choices is a pure user optimum (see Section 2.1).

Useful quantities are

$$n_1^{(j_1)} = 1 - \tfrac{N_{23}}{M}, \tag{3.22}$$

$$n_1^{(j_2)} = \tfrac{N_{14}}{N_{14}+N_{153}}, \tag{3.23}$$

i.e. the fraction of particles which turn 'left' on junctions j_1 and j_2, respectively.

3.2.2.2 Turning Probabilities

The second route choice mechanism shown in Figure 3.10 **(b)** can be employed with periodic and open boundary conditions. Here the particles are assigned to the routes via turning probabilities γ and δ. These probabilities determine the probability of jumping to the left for particles sitting on junction j_1 or j_2: if a particle on j_1 is updated, it will jump onto E_1 with probability γ and onto E_2 with probability $1-\gamma$. A particle on j_2 will jump onto E_4 with probability δ and onto E_5 with probability $1-\delta$. If the particle cannot jump due to the first site on its target edge being occupied, the next time it is updated its target site will be chosen anew according to γ or δ. All particles are equal and are subject to the same turning probabilities. User optima in the network with this route choice mechanism are thus mixed user equilibria (see Section 2.1).

For this type of route choices, there are $\gamma \cdot \delta \cdot M$ particles on route 14, $(1-\gamma) \cdot M$ particles on route 14 and $\gamma \cdot (1-\delta) \cdot M$ particles on route 153 *on average*.

3.2.2.3 Comparison of the Strategies

The tunable parameters for a given set of (L_5, M) are $(n_1^{(j_1)}, n_1^{(j_2)})$ (or $(N_{14}, N_{23}, N_{153})$) and (γ, δ) for the two route choice mechanisms. A set of $(n_1^{(j_1)}, n_1^{(j_2)})$ or (γ, δ) is called a (global) strategy. By varying $(n_1^{(j_1)}, n_1^{(j_2)})$ or (γ, δ) from 0 to 1, all possible strategies, i.e. states with all particles using route 14, route 23 or route 153 and all states in between, can be accessed. Specific choices of these strategies correspond e.g. to the user optimum or system optimum states of the system. All possible global strategies and corresponding values of observables can be visualized in $2d$ heat maps.

The turning probabilities in the second route choice case are an additional source of stochasticity. As will be seen in Sections 4.1 to 4.3 this difference leads to different characteristics in the system – in our context especially in the stability of measured travel time values as explained in detail for the 4link systems in Section 4.2.2.

Both the model with turning probabilities and the model with fixed strategies can be regarded as realistic models of a commuter's route choice scenario: as already discussed in greater detail in Section 2.4, laboratory experiments with real human participants performing route choices suggest that both fixed route choices or turning probabilities could be realistic. Some important results which are of importance to the question, if the two chosen route choice strategies are realistic are the following: in [33, 50] a network similar to our network without E_5 and in [33] also the network with E_5 was examined. It turned out that in their aim to minimize their individual travel times, in the network without E_5 users kept varying their individual strategies while on average the strategies stayed the same. This is an indication that mixed user optima are approached in road networks and thus that the model with turning probabilities is realistic. In the network with E_5, strategy changes of individual users seemed to vanish after some time rather indicating that pure user optima are realized and thus the fixed-strategy model of the present paper is realistic.

Therefore, both models seem to have some validity and a mixture of both could be at play in reality. Before addressing the more complex scenario of a mixture of both, it is interesting to analyse if pure user optima and and mixed user optima can be found in their 'pure' forms. Knowledge about these optima also serves as prior information for analysing systems with intelligent particles.

3.2.3 Observables

To analyse the influence of the new road E_5 on the system, the performances of the 4link and the 5link systems have to be compared for the same number of total particles M in the periodic boundary condition case and for the same entrance and exit rates α_{in} and β_{out} in the open boundary condition case. According to Section 2.1, a network state is defined by the distribution of cars onto the available routes. Depending on the route choice mechanism, in our context a state is thus given by a pair of turning probabilities (γ, δ) (which determines the *average* number of cars per route) or a certain combination of fixed route choices $(n_1^{(j_1)}, n_1^{(j_2)})$.

To test the system for the occurrence of Braess' paradox one has to compare the travel times

in the user optima of the two systems. If the travel time in the 5link's user optimum is higher than in that of the 4link's, Braess' paradox occurs (see Section 2.2). To get more information about the influence of the new road on the system (beyond the question if the paradox occurs), also the two systems' system optima were compared. As explained in Section 2.1, in our analysis the system optimum is defined as the state which minimizes the maximum travel time of all used routes and the user optimum is defined as the state in which all used roads have the same travel time which is lower than that of any unused routes.

Two observables are defined, the values of which determine for which strategy (or in some cases various strategies) the system is in its user or system optimum:

$$\Delta T = |T_{14} - T_{23}| + |T_{14} - T_{153}| + |T_{23} - T_{153}| \tag{3.24}$$

$$T_{\max} = \max[T_i, i \in \{14, 23, 153\}]. \tag{3.25}$$

The T_i denote the travel times on routes i. The user optima and system optima are given by the strategies which minimize ΔT and $T_{\max}$, respectively. Such strategies are denoted as *so* and *uo*.

A true user optimum is characterized by $\Delta T = 0$ since then all routes have the same travel times. If there are any unused routes and the travel times of these unused routes are higher than that of the used ones, ΔT is reduced to only the absolute values of the travel time difference of the used routes. Also when analysing the 4link network, ΔT reduces to $\Delta T = |T_{14} - T_{23}|$.

The system optimum is given by the strategy which minimizes $T_{\max}$ according to the definition of the system optimum. For the 4link system it reduces to $T_{\max} = \max[T_i, i \in \{14, 23\}]$.

In the following analyses of Braess' network, the strategies which minimize ΔT are considered user optima, if their value of ΔT is below a certain threshold. This threshold is chosen to be $\Delta T \leq 100$ in most cases. The case for ΔT going to zero is often not found since firstly travel times are stochastic variables and secondly the strategies are generally examined with a finite resolution. In a state with $\Delta T \leq 100$ the travel times of the roads are sufficiently close to each other for considering such a state a user optimum. According to the definitions of different types of user optima, those states are thus boundedly rational user optima (see Section 2.1). For cases in which no strategy leading to a ΔT value below the threshold exits, the strategy minimizing ΔT is called the *closest candidate for a user optimum*.

3.2.4 Possible Network Phases

Depending the exact parameters of the networks, such as edge-lengths or the total number of users, the new road can have different influences onto travel times in the road network and the network's overall performance. By comparing the user optima and system optima of the networks before and after the addition of E_5, the new edge's influence can be quantified both for selfish users and for networks with traffic guidance authorities. The Braess paradox applies to the selfish users case. The specific relations of travel times of the user and system

optima of 4link and 5link systems for a given parameter set define what phase the two systems are in.

For a fixed set of $L_1 = L_3$ and $L_2 = L_4$ like this a so-called phase diagram can be constructed. The phase diagram then contains information about the relations of travel times in user and system optima of the 4link and 5link networks depending of the length of the new road (denoted by the routelength ratio $\hat{L}_{153}/\hat{L}_{14}$) and the global density (PBC) or entrance and exit rates/probabilities (OBC). In our publications on this topic [126, 127] and in the following a "phase", i.e. a comparison of the 4link and the 5link system for a given parameter set, is sometimes also called a "state". It is not to be confused with the state of an individual network (e.g. the user optimum state of a specific 5link network). It should always be clear form the context what definition of the terms "state" or "phase" is meant. The possible

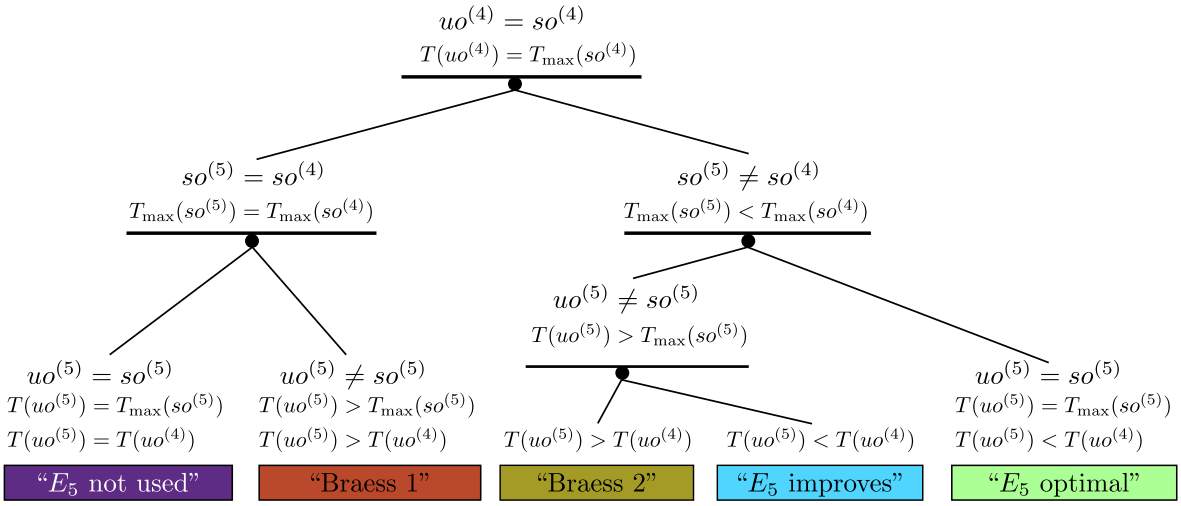

Figure 3.11. The tree of possible phases (when comparing the 4link and 5link systems) the Braess network can be in. Since the 4link system is symmetric user and system optimum coincide. If 4link and 5link system optima are the same the system's travel times cannot be lowered due to E_5. Either the new road will not be used if the 5link's user and system optima coincide ("E_5 not used") or the user optimum travel times are higher in the 5link ("Braess 1"). The latter is Braess' paradox in its original sense. If the 5link's system optima is not equal to the 4link's, the system can be improved due to the addition of E_5. Nevertheless, in the 5link user optimum travel times can be higher than in the 4link user optimum ("Braess 2"). If user optimum travel times are lower in the 5link system, the system is improved ("E_5 improved" and "E_5 optimal").

phases, i.e. the possible influences of E_5 onto the network, are shown in Figure 3.11.

The following analysis of the possible phases of the system is based on the assumption that in both the 4link and the 5link system user and system optima exist and are unique for every parameter set. This is true for linear mathematical models of traffic flow [69] as in Braess' original work and is, as a starting point for our analyses, also assumed to be true in our network of TASEPs. It turns out that this assumption does not hold in some cases in the sense that e.g. no stable travel times can be measured (see Section 4.2.2), no user optima exist (see Section 4.1.3) or that user optima exist but are not unique (see Section 4.1.3.1).

If the aforementioned assumptions hold, the tree of possible phases can be built as follows: since the 4link system is symmetric, it is expected that its user and system optima always

coincide in the state with turning probability $\gamma = 0.5$ or fixed route choices such that $N_{14} = N_{23} = M/2$. The coinciding user and system optima of the 4link, $uo^{(4)} = so^{(4)}$, build the root of the tree. If the system optima of the 4link and the 5link are the same ($so^{(5)} = so^{(4)}$, left branch of the tree in Fig. 3.11), the system cannot be improved, even for the case of non-selfish drivers or with traffic guidance systems. If selfish drivers lead the 5link system into its optimum ($uo^{(5)} = so^{(5)}$) the new road will not be used at all ("E_5 not used"). If selfish drivers in the 5link do not reach the system optimum, the new road will be used but the travel times will increase ("Braess 1"). This state is the Braess paradox in the classical sense as described by Braess.

If the system optima of the 4link and the 5link are not the same ($so^{(5)} \neq so^{(4)}$, right branch of the tree in Fig. 3.11), the travel times of network users can potentially be improved due to E_5. Since the 4link system is included in the 5link system, the maximum travel time of the system optimum in the 5link system can only be smaller than that of the 4link system ($T_{\max}(so^{(5)}) < T_{\max}(so^{(4)})$).

If traffic is controlled by an external authority driving the system into its system optimum, the system can always always be improved in this case. If the 5link's system and user optima coincide ($uo^{(5)} = so^{(5)}$) the system of selfish drivers will be in the "E_5 optimal" state.

If the 5link's system and user optima do not coincide ($uo^{(5)} \neq so^{(5)}$), two different phases can occur. If the 5link travel times in the 5link user optimum are lower than those in the 4link user optimum, the system is in the "E_5 improves" state. If they are higher, the system is in the "Braess 2" state. In the latter, selfish network users will experience higher travel times in the network after the addition of E_5. It is thus a Braess state. It differs from Braess' original example in the fact that by guiding the traffic to the system optimum externally, E_5 would reduce the travel times of network users. This is not possible in Braess' original example since in that case the 4link's and 5link's system optima coincide.

The "E_5 improves" and "E_5 optimal" states are the only cases in which the new route is useful (in the sense of leading to lower travel times) for the case of selfish drivers.

A further possible state that could occur would be described by $so^{(5)} \neq so^{(4)}$, $uo^{(5)} \neq so^{(5)}$ and $T(uo^{(5)}) = T(uo^{(4)})$. Such a state could be considered a special version of an "E_5 improves" state and was never found in my analyses. Thus it is not explicitly included in the tree of possible phases.

For the presented distinction between the possible states (or phases) it is essential to define the system optimum as the state that minimizes the maximum travel time. For different definitions, as e.g. the state maximizing the flow or the state minimizing the total travel time, this classification scheme does not necessarily hold.

3.2.4.1 Approximate Phase Border of the "E_5 optimal / all 153" Phase

The phase border of a special case of the "E_5 optimal" phase, the "E_5 optimal / all 153" phase, can be approximated analytically. The system is in the "E_5 optimal / all 153" phase if the state in which all particles use route 153 is the system and user optimum at the same

time. This means that if all particles use route 153 the two following conditions have to hold:

1. The travel time on route 153 is lower than that of the unused routes 14 and 23.

2. The travel time on route 153 is lower than that of the system and user optimum of the 4link system given by half the particles using route 14 and the other half route 23.

This phase is naturally expected to be present if the new route is much shorter than the old routes and if there is only a small number of particles is the system.

Periodic Boundary Conditions. For periodic boundary conditions (Figure 3.9 **(a)**) the upper border of that phase, i.e. the total number of particles in the system M or the global density up to which is phase is present for a given route length ratio $\hat{L}_{153}/\hat{L}_{14}$, can be approximated as follows.

If only route 153 is used, this route corresponds to a single TASEP with periodic boundary conditions and length $\hat{L}_{153}$. The stationary state of a single periodic boundary TASEP is given by a flat density profile and the exact travel time is given by Equation (3.4): $T_{\mathrm{PBC}}(\rho) = \frac{L}{1-\rho}$. The travel times of route 14 is in this state given by the fraction of the route 153 travel time which corresponds to j_4, E_0, j_1, E_1 and j_2 and the free flow travel time of E_4 which is just L_4. The travel time of route 23 in this state is given by the fraction of the route 153 travel time which corresponds to j_3, E_3, j_4, E_0 and j_1 and the free flow travel time of E_2 which is just L_2. The first condition requires the travel time on route 153 to be lower than on the other two routes:

$$\begin{aligned} & T_{153}\left(uo^{(5)}\right) < T_{14}\left(uo^{(5)}\right) = T_{23}\left(uo^{(5)}\right) \\ \Leftrightarrow \quad & \frac{\hat{L}_{153}}{1-\frac{M}{\hat{L}_{153}}} < \frac{L_1+4}{1-\frac{M}{\hat{L}_{153}}} + L_2. \end{aligned} \tag{3.26}$$

The second condition can be approximated if one assumes that the two routes 14 and 23 are independent and their stationary states were given by flat density profiles in the 4link's system and user optimum. This is a mean field assumption which is not exact but turns out to be a valid approximation for small global densities. If the 4link user/system optimum travel times are approximated like this and are required to be higher than the travel time on route 153 if the latter is used by all particles, one arrives at the second condition:

$$\begin{aligned} & T_{153}\left(uo^{(5)}\right) < T_{14}\left(uo^{(4)}\right) = T_{23}\left(uo^{(4)}\right) \\ \Leftrightarrow \quad & \frac{\hat{L}_{153}}{1-\frac{M}{\hat{L}_{153}}} \lesssim \frac{\hat{L}_{14}}{1-\frac{M}{2\hat{L}_{14}}}. \end{aligned} \tag{3.27}$$

For the 5link user optimum to be the state with all particles choosing route 153, Equation (3.26) has to be valid. For the system (when comparing the 4link to the 5link) to be in an "E_5 optimal / all 153" phase, both Equations (3.26) and (3.27) have to hold.

Open Boundary Conditions. In the open boundary case (Figure 3.9 **(b)**) the same two conditions have to hold. Opposed to the periodic case, if only route 153 is used the travel time on this route is not easily obtainable in an analytically exact way. It can nevertheless be approximated well by Equation (3.5) with the bulk density given by the appropriate value for the given entrance and exit rates α_{in} and β_{out} as given in Table 3.1. In the 5link system the travel time on route 153 has to be shorter than those of the two unused routes. This condition now reads like this:

$$\begin{aligned} & T_{153}\left(uo^{(5)}\right) < T_{14}\left(uo^{(5)}\right) = T_{23}\left(uo^{(5)}\right) \\ \Leftrightarrow \quad & \frac{\hat{L}_{153}}{1-\rho_{L/2,153}} < \frac{L_1+3}{1-\rho_{L/2,153}} + L_2. \end{aligned} \tag{3.28}$$

One has to keep in mind that the travel time of route 153 is only approximated in this case. Also the travel times of the other routes are approximated with an even bigger error since the density profile will not be completely flat throughout the whole route 153 for open boundary conditions (see Figure 3.3).

The second requirement for the "E_5 optimal / all 153" phase is that the travel time on route 153 in the 5link is lower than that of the 4link's user optimum:

$$\begin{aligned} & T_{153}\left(uo^{(5)}\right) < T_{14}\left(uo^{(4)}\right) = T_{23}\left(uo^{(4)}\right) \\ \Leftrightarrow \quad & \frac{\hat{L}_{153}}{1-\rho_{L/2,153}} < T_{14}\left(uo^{(4)}\right) = T_{23}\left(uo^{(4)}\right). \end{aligned} \tag{3.29}$$

For the 4link open boundary system a mean field theory was derived as will be explained in Section 4.4.1. This is why the equation for $T_{14/23}\left(uo^{(4)}\right)$ will be given in that section.

3.2.4.2 How to Identify the System's Phase from the Strategy-landscapes of the Observables

In the present subsection the question of how the phase of a system is identified by analysing the values of the two observables $T_{\max}$ (Equation (3.25)) and ΔT (Equation (3.24)) depending on the strategy ($(n_1^{(j_1)}, n_1^{(j_2)})$ or (γ, δ)) is addressed.

Figures 3.12 to 3.16 show example observable-landscapes of 5link networks. They are artificially constructed landscapes and do not correspond to real measurements. They show what the values of $T_{\max}$ and ΔT could be for all possible strategies, i.e. $(n_1^{(j_1)}, n_1^{(j_2)})$ or (γ, δ) taking all possible values ($[0,1]\times[0,1]$). The overall landscapes could be completely different for real measurements, only the position of the minima of the two observables and the travel times at these minima (and the travel time's relation to the travel times in the 4link's user and system optima) decide upon the system's phase.

The shown landscapes correspond to the possible 5link-strategies. Due to symmetry, the 4link's system and user optima are both the same strategies, given by half the particles choosing route 14 and the other half route 23. This state is also included in the shown 5link

observable landscapes at $(\gamma/n_1^{(j_1)},\ \delta/n_1^{(j_2)}) = (0.5, 1.0)$. Thus the 4link's user and system optimum can also be seen in the 5link landscapes.

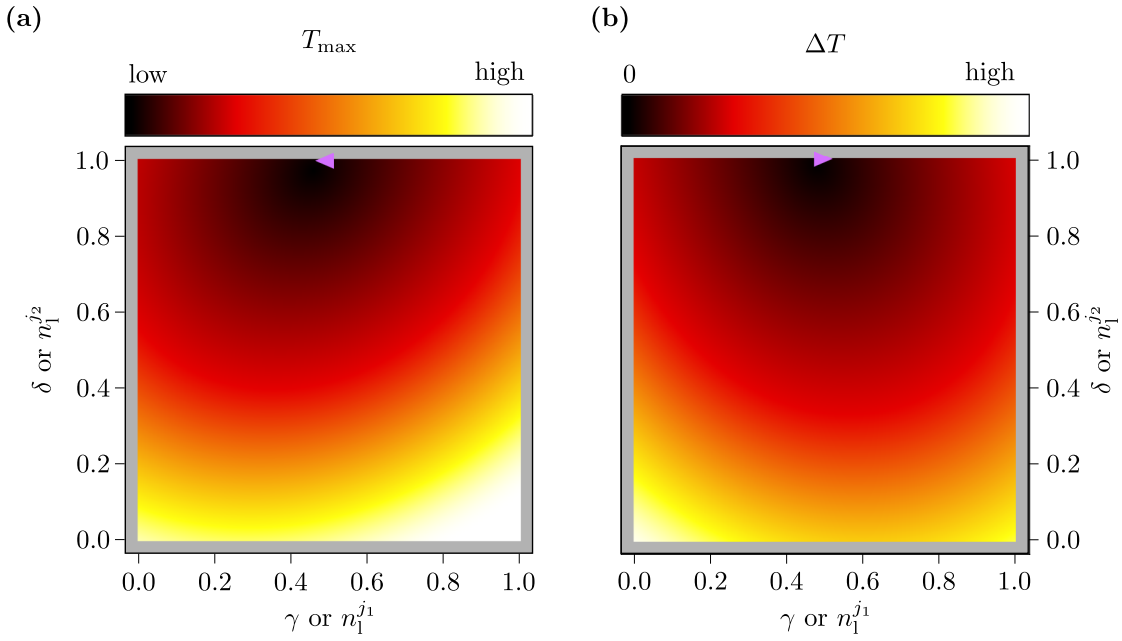

Figure 3.12. An example of what the $T_{\max}$ (Part **(a)**) and ΔT (Part **(b)**) landscapes could look like in an "E_5 not used" state. The minima of both observables are at $(\gamma/n_1^{(j_1)},\ \delta/n_1^{(j_2)})$=(0.5,1.0) which means that the new route will be ignored and particles distribute themselves in equal amounts onto the old routes. The minima of $T_{\max}$ and ΔT are marked by the pink ◀ and ▶, respectively.

Figure 3.12 is an example of what an "E_5 not used" state could look like. The minima of both $T_{\max}$ and ΔT are at $(\gamma/n_1^{(j_1)},\ \delta/n_1^{(j_2)})$=(0.5,1.0). This means that the new route is neither used in the system optimum nor in the user optimum. Particles distribute themselves (on average for turning probabilities) equally onto the two old routes. This distribution corresponds to user and system optima of the 4link system.

Figure 3.13 shows an example of a "Braess 1" state. The minimum of $T_{\max}$, corresponding to the system optimum, is at (0.5,1.0). This is the 4link's optimum in which the new route is ignored. The minimum of ΔT is found at another strategy, here at $(\gamma/n_1^{(j_1)},\ \delta/n_1^{(j_2)})\approx (0.7, 0.7)$. The user and system optima do not coincide. Furthermore, from looking at the value of $T_{\max}$ at $(\gamma/n_1^{(j_1)},\ \delta/n_1^{(j_2)}) \approx (0.7, 0.7)$ one can see that the maximum travel time in this strategy is higher than in the system optimum. The 5link system has a user optimum which has higher travel times and is different from the 5link's system optimum which coincides with the 4link's system optimum.

Figure 3.14 is an example of a "Braess 2" state. The system optimum is at $(\gamma/n_1^{(j_1)},\ \delta/n_1^{(j_2)}) \approx (0.7, 0.9)$. This is a state different from the 4link's system optimum, $(\gamma/n_1^{(j_1)},\ \delta/n_1^{(j_2)}) = (0.5, 1.0)$, which also has a lower maximum travel time than the 4link system optimum. The user optimum is found at $(\gamma/n_1^{(j_1)},\ \delta/n_1^{(j_2)}) \approx (0.2, 0.1)$. When looking at the maximum travel time of this strategy one can see that $T_{\max}(uo^{(5)}) > T_{\max}(so^{(4)}) > T_{\max}(so^{(5)})$.

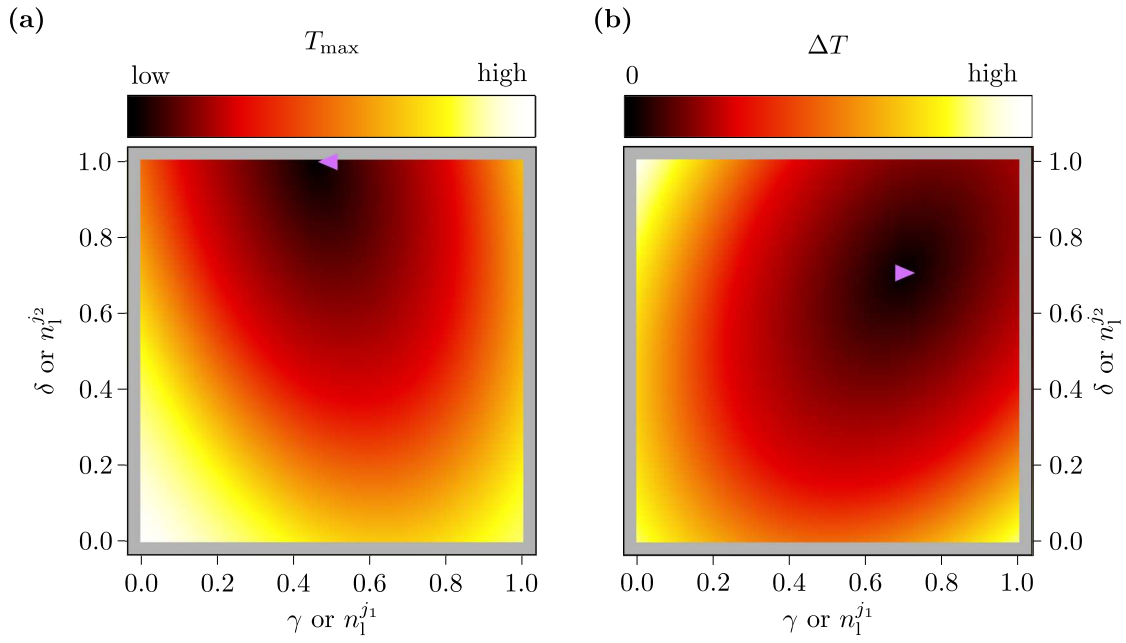

Figure 3.13. An example of what the $T_{\max}$ (Part **(a)**) and ΔT (Part **(b)**) landscapes could look like in an "Braess 1" state. The system optimum is at $(\gamma/n_1^{(j_1)}, \delta/n_1^{(j_2)}) = (0.5, 1.0)$, i.e. the 4link's system optimum. The user optimum is at $(\gamma/n_1^{(j_1)}, \delta/n_1^{(j_2)}) \approx (0.7, 0.7)$, a state which has higher travel times. The minima of $T_{\max}$ and ΔT are marked by the pink ◀ and ▶, respectively.

Figure 3.15 is an example of an "E_5 improves" state. As in the "Braess 2" state both the system optimum and the user optimum differ from the 4link's optima. The 5link's system optimum also has a lower travel time than the 4link's system optimum. The 5link's user optimum in this case has also a higher travel time than the 5link's system optimum but a lower travel time than the 4link's system optimum $T_{\max}(so^{(4)}) > T_{\max}(uo^{(5)}) > T_{\max}(so^{(5)})$.

Figure 3.16 is an example of an "E_5 optimal" state. Here, the 5link's user and system optima coincide at $(\gamma/n_1^{(j_1)}, \delta/n_1^{(j_2)}) \approx (0.8, 0.2)$. Thus the 5link's system will be in its optimal state also when used by selfish drivers. The travel times in the system / user optimum are lower than in the 4link's optima.

There can be special cases of the described states. Examples of special cases would be that e.g. several routes are not used at all. This is also the case in the "E_5 not used" state in which only the two old routes are used and the new one is ignored in the system optimum *and* in the user optimum. In the other observable-landscapes presented in Figures 3.13 to 3.16 the user optima are given by states in which all three routes are used. This is not necessarily always the case. One special case which is present especially at low global densities and if the new route is really short compared to the old routes is the "all 153" state. This is a special case of an "E_5 optimal" state in that only the new route is being used and the travel time on this route being shorter than on the two unused older routes. This special case is given if $T_{\max}$ and ΔT both have their minima at $(\gamma/n_1^{(j_1)}, \delta/n_1^{(j_2)}) \approx (1.0, 0.0)$.

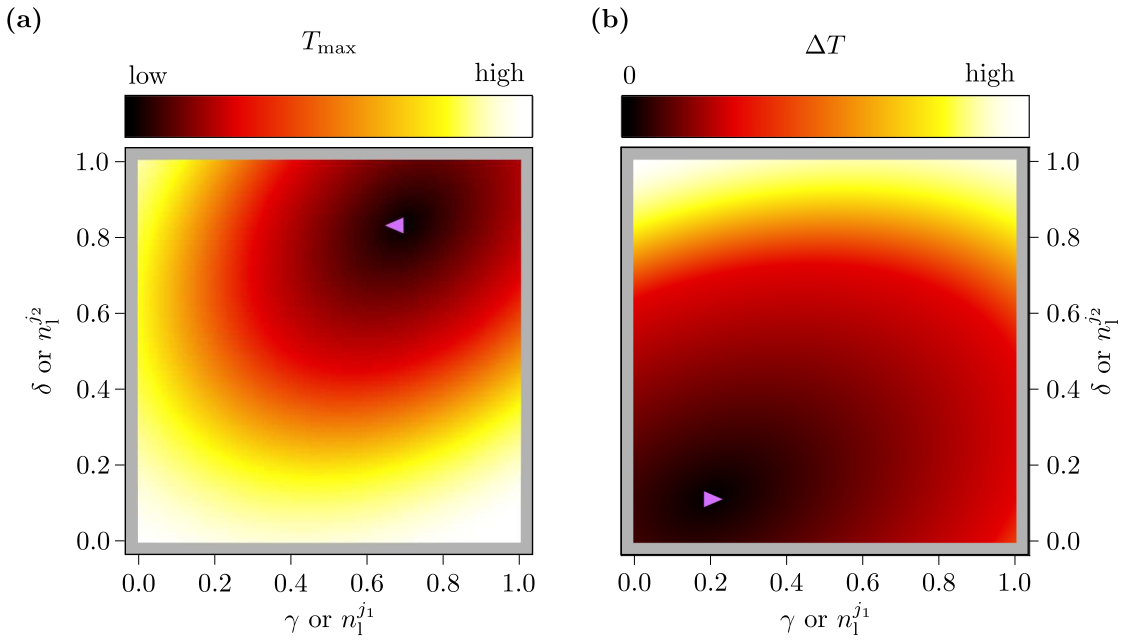

Figure 3.14. An example of what the $T_{\max}$ (Part **(a)**) and ΔT (Part **(b)**) landscapes could look like in an "Braess 2" state. The system optimum differns from the 4link's system optimum. The user optimum also differs from both, and $T_{\max}(uo^{(5)}) > T_{\max}(so^{(4)}) > T_{\max}(so^{(5)})$ holds. The minima of $T_{\max}$ and ΔT are marked by the pink ◀ and ▶.

3.2.5 How to Find System Optima and User Optima

The former section explained how the observable-landscapes of the possible phases of the system look like. For this, artificial $T_{\max}$ and ΔT landscapes with values for all possible strategies were shown. The positions of the minima and the relations of the corresponding travel time values then determine the state of the system. When describing real instances of the systems, the travel times are not known for all possible strategies. As explained in Section 3.1.3 networks of TASEPs are generally not analytically tractable. This is why the tool of choice to attain travel time values and with them to deduce the system phases are Monte Carlo simulations. Since finite sized systems are examined, for the fixed route choice case the $(n_1^{(j_1)}, n_1^{(j_2)})$-landscape is, other than indicated in Figures 3.12 to 3.16, not a continuous landscape. The (γ, δ) landscapes in the turning probabilities case are in principal continuous. When employing Monte Carlo simulations to analyse the systems, the landscapes have to be discretized with a finite resolution since otherwise infinite computational time would be required. In the following a strategy which was employed for finding user and system optima is presented.

3.2.5.1 Sweeping the Observable-landscapes to Find User and System Optima

The straight forward method for finding system and user optima is, as already hinted at, to discretize the $(\gamma/n_1^{(j_1)}, \delta/n_1^{(j_2)})$-landscape, measure travel times of the three routes for all discrete strategies, calculate $T_{\max}$ and ΔT from those measurements and then find the

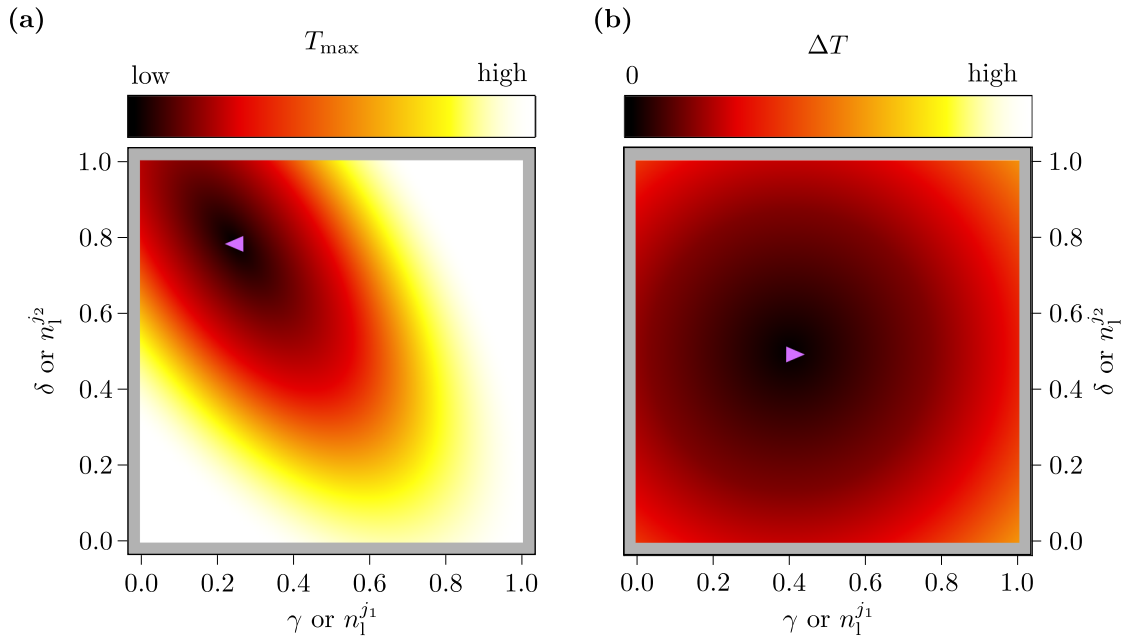

Figure 3.15. An example of what the $T_{\max}$ (Part **(a)**) and ΔT (Part **(b)**) landscapes could look like in an "E_5 improves" state. The 5link's user and system optima differ from each other and from the 4link's optima. $T_{\max}(so^{(4)}) > T_{\max}(uo^{(5)}) > T_{\max}(so^{(5)})$ holds. The minima of $T_{\max}$ and ΔT are marked by the pink ◀ and ▶.

strategies which minimize $T_{\max}$ and ΔT. Those strategies are then the system and user optima. This method is good to obtain a general 'feeling' for how the landscapes look like. Furthermore, one can be sure that, at least inside resolution of the discretization, all strategies have been examined. An example of the results of this method is given in Figure 3.17. It shows an example of an "E_5 optimal" state for the fixed route choices case and periodic boundary conditions. The landscape was sweeped in steps of 0.1.

There are some downsides to the method of sweeping the observable-landscape in a discretized way: the grid resolution sets a limit on how precisely the optima can be found. It can be the case that the actual optima lie in between the discrete grid points. In this case one way of improving the measurement is rescanning a smaller region around the minimum of the observables in the current grid resolution with a finer grid resolution. Like this one can 'zoom in' until the real optimum is found. This procedure is exemplified in Figure 3.18.

Another downside is the fact that a lot of measurements are performed on strategies which are very far away from the optima. The results of these measurements will not be used afterwards and are thus a useless use of CPU time. This is why another technique was developed which is presented in Section 3.3.2.

3.3 Monte Carlo Simulation Methods

Oftentimes one is interested in the stationary state expectation value of an observable of a stochastic process. This could e.g. be the average density profile of a TASEP segment or the

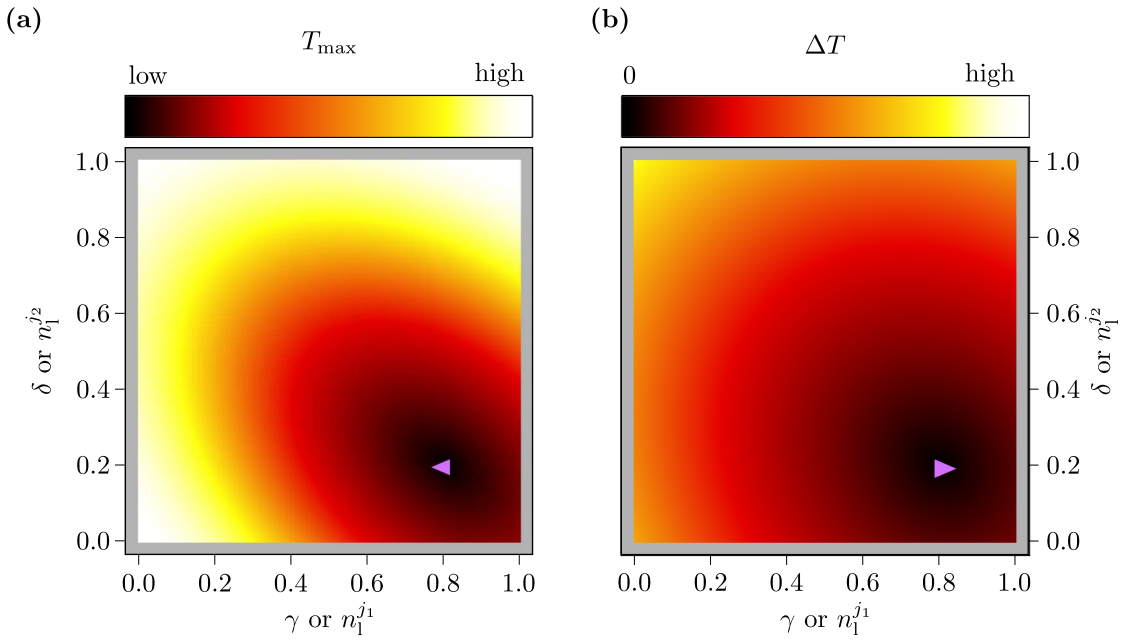

Figure 3.16. An example of what the $T_{\max}$ (Part **(a)**) and ΔT (Part **(b)**) landscapes could look like in an "E_5 optimal" state. The 5link's user and system optima coincide at $(\gamma/n_1^{(j_1)}, \delta/n_1^{(j_2)}) \approx (0.8, 0.2)$, a strategy with lower travel times than the 4link's user /system optimum. The minima of $T_{\max}$ and ΔT are marked by the pink ◀ and ▶.

travel time of a TASEP segment. Such expectation values are given by the ensemble averages of the given observables. In the stationary state the probabilities of each microstate do not change with time. The ensemble average $\langle O \rangle_{\mathrm{E}}$ of an observable O is then given by

$$\langle O \rangle_{\mathrm{E}} = \sum_{i=1}^{N} p(s_i) O(s_i), \tag{3.30}$$

with s_i being a microstate of the system, $p(s_i)$ the stationary-state probability of microstate s_i, N the total number of microstates and $O(s_i)$ the value of O in microstate s_i.

For systems that are not analytically tractable the $p(s_i)$ are not known. Monte Carlo methods use pseudo random numbers to simulate the time evolution of the stochastic process of interest. From the ergodic hypothesis we know that in ergodic systems the temporal average (over infinitely long times) $\langle O \rangle_{\mathrm{T}}$ of an observable O equals the ensemble average of that observable, i.e.:

$$\lim_{t\to\infty} \langle O(t) \rangle_{\mathrm{T}} = \lim_{t\to\infty} \frac{1}{t \cdot \tau} \sum_{i=1}^{t} O(i \cdot \tau) = \langle O \rangle_{\mathrm{E}}, \tag{3.31}$$

with t being the number of time steps, τ the length of one time step and $O(i \cdot \tau)$ the value of O at time $i \cdot \tau$.

Using this knowledge, stationary state expectation values can be approximated by averaging over the time evolutions of given observables for sufficiently long times (as infinitely long

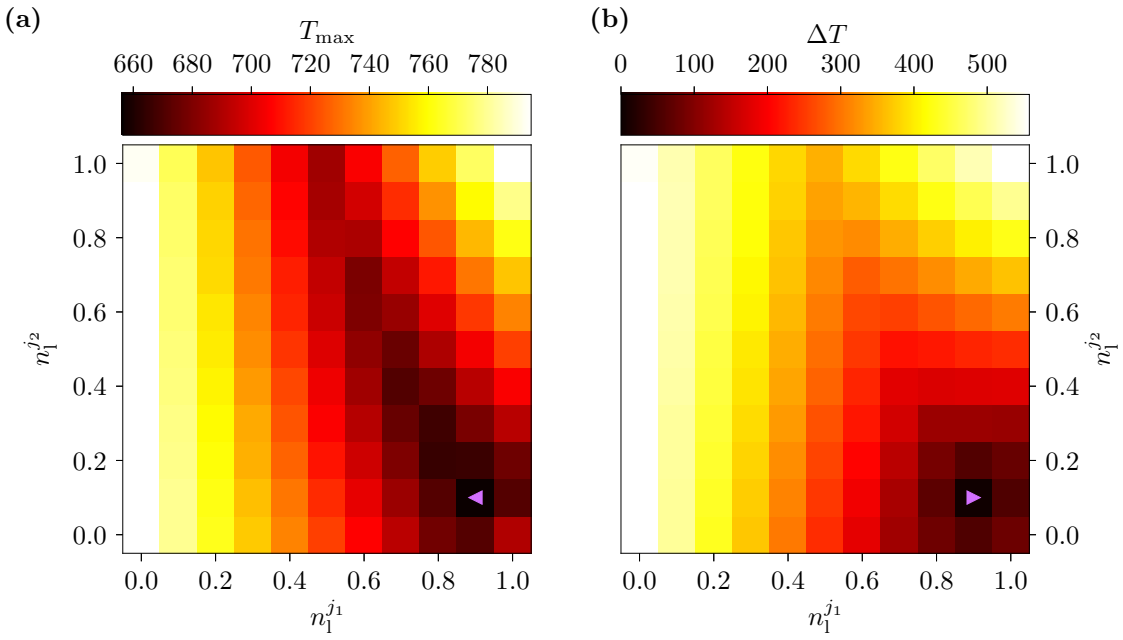

Figure 3.17. The $T_{\max}$ (Part **(a)** and ΔT (Part **(b)**) landscapes of the 5link system for periodic boundary conditions, fixed route choices and $L_1 = L_3 = 100$, $L_2 = L_4 = 500$, $L_5 = 278$ and $M = 148$ depending on the $n_1^{(j_1)}$ and $n_1^{(j_2)}$. As can be seen, this is an "E_5 optimal" state, since the minima of ΔT and $T_{\max}$ coincide at $n_1^{(j_1)} = 0.9$ and $n_1^{(j_2)} = 0.1$ and the corresponding strategy has a lower maximum travel time than the 4link's system optimum which is found at $n_1^{(j_1)} = 0.5$ and $n_1^{(j_2)} = 1.0$. The minima of $T_{\max}$ and ΔT are marked by the pink ◀ and ▶.

measurements are not possible by definition). To obtain valid results one has to let the system *relax* into the stationary state before starting the measurement. This means that one has to make sure that, when measurement begins, the system is in a state which is likely to occur in the stationary state.

In all Monte Carlo simulations performed for this thesis the Mersenne Twister algorithm [128] was used to generate pseudo random numbers.

3.3.1 Measurements of Observables in TASEP Networks

As mentioned previously, TASEP networks are oftentimes not analytically tractable. In some cases mean field theory can provide valuable insights and good approximations to quantities of interest. For most results presented in the following chapters of this thesis no such approximations could be obtained, which is why Monte Carlo methods were used.

The TASEP networks addressed in this thesis contained up to approximately 1500 sites. Before measurement was started the system always relaxed for at least $5 \cdot 10^5$ sweeps/time steps[5]

If not indicated otherwise, whenever values of observables, e.g. O, determined through

[5]When random-sequantial dynamics are simulated one sweep corresponds to N single site updates, with N being the total number of sites in the system. If parallel dynamics are simulated one time step corresponds to all sites being simultaneously updated once.

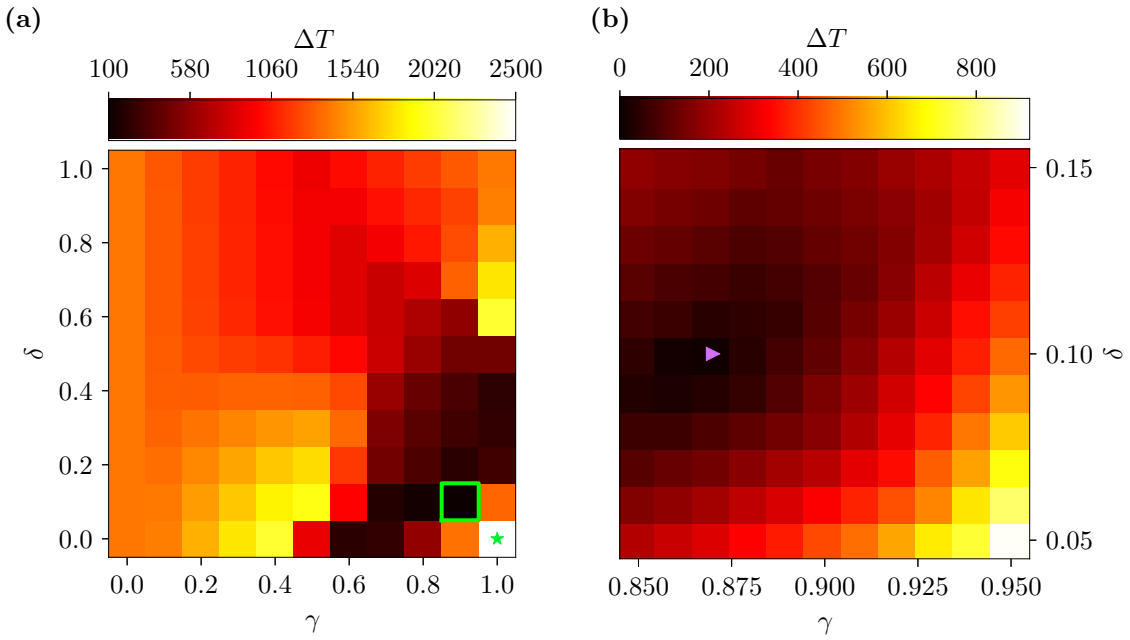

Figure 3.18. The ΔT landscape of the 5link system for periodic boundary conditions, turning probabilities and $L_1 = L_3 = 100$, $L_2 = L_4 = 500$, $L_5 = 37$ and $M = 248$ depending on γ and δ. Part **(a)** shows a discretization with a coarse grid resolution of 0.1 for the whole parameter spectrum. It has its minimum at $(\gamma, \delta) = (0.9, 0.1)$ with $\Delta T \approx 118$. The strategy marked with a green $\star$ leads to a gridlock of the system as will be explained in Section 4.2.1. Part **(b)** shows a zoom with finer grid resolution of 0.01 into the area around the minimum of Part **(a)** (marked therein by the green square). The minimum is here found at $(\gamma, \delta) = (0.87, 0.10)$ with $\Delta T \approx 10$. This is pretty close to the actual user optimum. The minimum of ΔT is marked by the pink ▶.

Monte Carlo simulations are presented. The presented values are the mean values

$$\bar{O} = O = \frac{1}{t\tau} \sum_{i=1}^{t} O(i\tau) \tag{3.32}$$

of measurements instances of the observable measured over a sufficiently long time. To gain some more insights into the statistical distribution of the observable, sometimes the standard deviation

$$\sigma(O) = \left(\frac{1}{t\tau} \sum_{i=1}^{t} (O(i\tau) - \bar{O})^2 \right)^{1/2} \tag{3.33}$$

which measures how far the individual measurements on average deviate from their mean value is also given.

The method to approximate expectation values, Equation (3.32) with τ being the length of one sweep or time step, can be directly applied to measure observables such as density profiles or currents. For these observables one can get a data point every sweep/time step and average over all data points after a sufficiently long time.

The measurement of travel times is a bit more complicated as the travel time itself is an observable which measures time spans of multiple sweeps/time steps – it is not possible

to measure a single travel time data point at every sweep/time step. For travel times T a specific number n of data points is gathered and the approximation of the expectation value is calculated as

$$\bar{T} = T = \frac{1}{n} \sum_{i=1}^{n} T_i, \tag{3.34}$$

while each data point corresponds to a specific time span.

Travel times in TASEP networks are the most prominent observables in this thesis. The measurement of travel times was implemented in two different ways for the results presented in the following sections. The two types were implemented at different times during my research, they were not specifically designed to tackle specific tasks.

Consider as the simplest example a single TASEP with periodic boundary conditions and length L, used by M particles. The travel time can be defined as the time a particle sitting on site 1 needs from jumping out of site 1 until it re-enters site 1 by jumping out of site L. The first way travel times were measured was by tagging one specific particle at a time and keeping track of its position. The travel time is then given by the number of sweeps (or time steps for parallel updates) for completing one round. After this one round the measurement starts again for a second round etc. Like this the desired number of measurements for the travel time can be obtained and from the average of those individual values an approximation of the expectation value of the travel time is found. The second way is to keep track of the positions of all particles in the system. Every time any particle jumps out of site 1, the current system time will be recorded as its starting time. Once this particle jumps back into site 1, the travel time measured by this particle can be calculated. Then after a sufficient amount of measurements again the expectation value can be approximated by averaging over all individual measurements.

It is important to note that with the second method it is possible to gather many individual measurements much faster, i.e. with way less system sweeps/time steps. This is very important to keep in mind if travel times are measured – especially in domain wall phases: since in these phases the short-term density profile changes with the fluctuating domain walls, so do the individual travel time measurements depending on the current position of the domain wall. This is why e.g. a specific number of measurements gathered with the first method will grant a travel time value much closer to its long term average than the same number of measurements gathered with the second method. In the second method much less system time (thus less potential positions of the domain wall) is covered. Gathering the same amount of data points with the first method will take more time but will also cover 'more of the system's dynamics'.

For measuring travel times in TASEP networks and with the route choice governed by turning probabilities the first version was modified as follows: a single particle is tracked and then forced to traverse the system on a specific route, the travel time of which is measured. During this measurement the rest of the system keeps evolving according to the turning probabilities. If the desired amount of data points for the travel time of one route is gathered, a particle will be tracked and forced to traverse the system following the next route for which

the travel time is about to be measured and so on.

Figure 3.19 shows how the measured mean value of the travel times on route 14 and 23 (with $\gamma = 0.5$) evolves with the system for the first and second measurement methods (Figures 3.19 **(a)** and **(b)**). In both instances $3 \cdot 10^4$ sweeps are shown. Furthermore, on the second y-axis

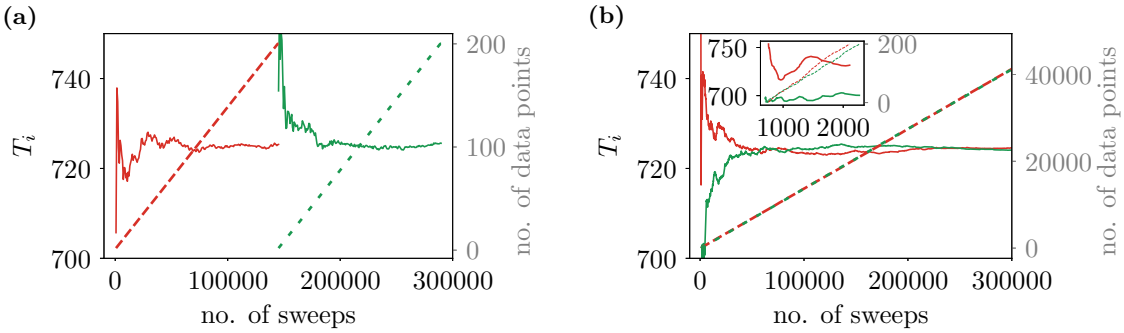

Figure 3.19. The evolution of the mean values of the travel times T_i against the number of performed sweeps in the 4link Braess network with $L_1 = L_3 = 100$, $L_2 = L_4 = 500$, $\gamma = 0.5$ and $M = 200$. The travel time on route 14 T_{14} is shown in red, that of route 23, T_{23} in green. Both plots show a second y-axis denoting how often the travel times where measured / how many data points were collected. The dotted lines correspond to this second y-axis. Part **(a)** was generated by the first measurement method, i.e. by tagging specific particles. Part **(b)** was generated with the second method, i.e. by keeping track of all particles. The inlet plot in Part **(b)** shows that for the second method 200 data points are already gathered after appr. 2200 sweeps. At that point of time in the measurement process the two mean values are still far from their actual values.

the number of gathered data points is shown. In the first method a single particle was tagged and then forced to use route 14 for 200 rounds. Then a particle was tagged and forced to use route 23 for 200 rounds. That means that after the $3 \cdot 10^4$ sweeps 200 data points for each travel time were gathered. In the second method all particles were tracked all the time. After the $3 \cdot 10^4$ sweeps approximately 40000 data points for each travel time are gathered. The inlet in Figure 3.19 **(b)** shows that 200 data pints are already gathered after approximately 2200 sweeps. At this point the measured mean values are still differing very much from the actual mean values.

This is shown to illustrate that the same amount of data point gathered by the second method does not account for the same system time and is thus not as precise. If the second method is used, the covered system time is more relevant than the number of data points.

If a route is not supposed to be used at all according to a given set of turning probabilities or fixed route choices, the travel time on that unused route is also of interest. To obtain travel time values whenever a route is not used at all a single particle was artificially forced to use that route and the travel times of that particle were measured. This results in small errors since one particle is forced to traverse routes which are not supposed to be used at all. Since in most simulations there were at least 100 particles in the systems, the effects of a single particle using a route which is technically not to be used does not result in large errors.

3.3.2 Metropolis Algorithm for Finding User Optima

Another way to find system or user optima, different from that presented in Section 3.2.5.1, is realized by walking through the landscape in a more directed manner. To be able to do that a Metropolis Monte Carlo [129] method was developed. It works as follows.

1. Set maximum step width sw and 'temperature' τ.
2. Set start values $(\gamma/n_1^{(j_1)}, \delta/n_1^{(j_2)})$. In the fixed route choices case from this
   - $N_{14} = M \cdot n_1^{(j_1)} \cdot n_1^{(j_2)}$
   - $N_{23} = M \cdot (1 - n_1^{(j_1)})$
   - $N_{153} = M \cdot n_1^{(j_1)} \cdot (1 - n_1^{(j_2)})$.
3. Let the system thermalize with strategy according to $(\gamma/n_1^{(j_1)}, \delta/n_1^{(j_2)})$.
4. Measure travel times T_{14}, T_{23}, T_{153} and calculate ΔT.
5. Suggest new $(\gamma_{\text{new}}/n_{1,\text{ new}}^{(j_1)}, \delta_{\text{new}}/n_{1,\text{new}}^{(j_2)})$ by drawing a random number z between 0 and 2π and setting $(\gamma_{\text{new}}/n_{1,\text{ new}}^{(j_1)}, \delta_{\text{new}}/n_{1,\text{ new}}^{(j_2)}) = (\gamma/n_1^{(j_1)} + sw \cdot \cos(z), \delta/n_1^{(j_2)} + sw \cdot \sin(z))$ (and for the fixed route choices case calculate N_{14}^{new}, N_{23}^{new}, N_{153}^{new} as in step 2).
6. Let the system thermalize with strategy according to $(\gamma_{\text{new}}/n_{1,\text{ new}}^{(j_1)}, \delta_{\text{new}}/n_{1,\text{new}}^{(j_2)})$.
7. Measure travel times T_{14}^{new}, T_{23}^{new}, T_{153}^{new} and calculate ΔT^{new}.
8. Accept the new strategy with probability $p = \min\left(1, \exp\left(-\frac{\Delta T - \Delta T^{\text{new}}}{\tau}\right)\right)$.
9. Repeat steps 5 to 8 as long as $\Delta T^{\text{new}} > \epsilon$, with tolerance ϵ.

In this algorithm, the maximum step width sw is the maximum possible value, $\gamma/n_1^{(j_1)}$ and $\delta/n_1^{(j_2)}$ can be changed by. The temperature τ is a measure for the probability with which a strategy with higher ΔT might be accepted and ϵ is the tolerance: if $\Delta T \leq \epsilon$ the strategy is accepted as the user optimum. The 'real' user optimum is reached, if ϵ is exactly zero. An additional tenth step could be added to the algorithm, in which sw would be reduced, if newly suggested probabilities get rejected a certain amount of times. Fig. 3.20 **(a)** shows the search path of the algorithm for periodic boundary conditions, fexed route choices, $L_1 = L_3 = 100$, $L_2 = L_4 = 500$, $L_5 = 278$ and $M = 148$ for 10 different start values $(n_1^{(j_1)}, n_1^{(j_2)})$. The observable-landscape with 0.1 step width as described in the previous subsection is underlayed for visualization purposes. Furthermore, in Fig. 3.20 **(b)** the ΔT values against the Metropolis step number (i.e. how often steps 5 to 8 of the algorithm were performed) is shown. From both pictures it can be deduced that the algorithm works really well for this case. Depending on the start values, the algorithm will not converge and has to be restarted with different start values. The algorithm can also be used to find system optima if after each step $T_{\max}$ is calculated and the newly suggested strategy is accepted if $T_{\max}$ got lower. The problem in this case is that there is no real termination condition as there is no a priori known lower bound to $T_{\max}$.

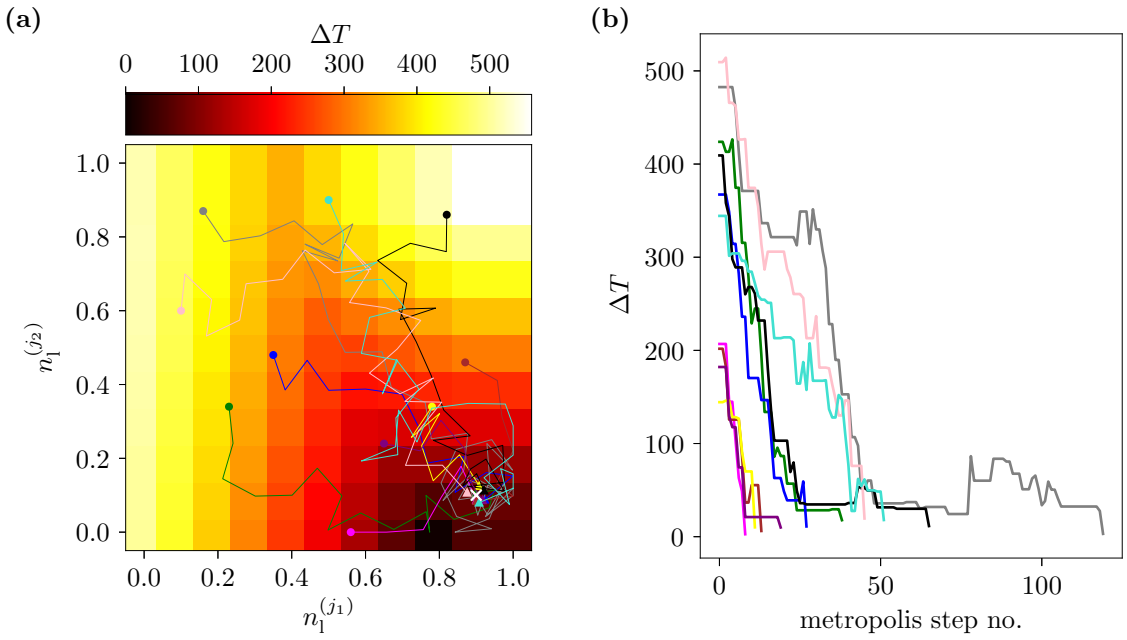

Figure 3.20. An example of the performance of the Metropolis algorithm for periodic boundary conditions, fexed route choices, $L_1 = L_3 = 100$, $L_2 = L_4 = 500$, $L_5 = 278$ and $M = 148$ and ten different start values. In **(a)** the search paths are shown with underlayed values of ΔT which were obtained by sweeping the $(n_1^{(j_1)}, n_1^{(j_2)})$-landscape as described in the previous section. The beginnings of all paths are marked by a $\circ$ and the endings by a $\triangle$. Also the user optimum is marked by a white $\times$. In **(b)** the corresponding ΔT values against the number of Metropolis steps are shown. One can see, that the algorithm converges pretty fast for all 10 start values.

For sweeping the whole strategies with a 0.1 resolution 121 measurements have to be done. If the actual optima lie in between the grid points of the level of discretization, even more measurements have to be performed. The Metropolis algorithm needs less measurements to find the optima with a finer resolution in most cases.

4 The Braess Network of TASEPs with Externally Tuned Global Strategies

The present chapter presents the part of my research devoted to the Braess network of TASEPs with externally tuned strategies. The term "externally tuned strategies" refers to the fact that the individual particles do not choose their strategies intelligently, but all strategies are set to specific values. Thus, here the first of the two major issues about what can be improved in Braess' model, which were worked out in Section 2.2.5, is addressed (the second issue will be addressed in Chapter 5): Braess' network is studied by employing a more realistic model of traffic flow and the question whether Braess' paradox is also observed under these circumstances is answered under the assumption that potential user optima are always realized. Furthermore, the influence of the new road on the network is analysed beyond the question about the paradox' occurrence. Phase diagrams according to the phase classifications presented in Section 3.2.4 are presented, and for some specific networks the new road's influence is further quantified.

Braess' network is studied for various combinations of boundary conditions and route choice strategies. The variants of the network addressed in Sections 4.1 to 4.4 focus on random-sequential dynamics, while in Section 4.5 some results on parallel dynamics are summarized.

4.1 Periodic Boundary Conditions and Fixed Strategies

In this section some results on the Braess network of TASEPs with periodic boundary conditions, random-sequential updates and the drivers following fixed strategies are presented. The results have partially been published in [127, 130]

The network and the fixed route choices mechanism have been described in Sections 3.2.1 and 3.2.2 respectively. The network is depicted in Figure 3.9 **(a)** and Equations (3.15) to (3.20) hold. Furthermore, Equations (3.21) and (3.23) hold: the number of particles following route 14, 23 and 153 are given by N_{14}, N_{23} and N_{153}, respectively, and are subject to $N_{14} + N_{23} + N_{153} = M$. The user optima which are found in this section are pure user optima since the individual users keep their explicit route choices fixed and do not decide based on probabilities. The term "pure" is in the following omitted for readability reasons.

4.1.1 Gridlocks in the 5link Network

As explained in Section 3.2.2.1 in the case of fixed route choices each particle has a permanent 'personal' strategy. This is also the case for e.g. a particle on junction j_1 that was already

updated several times but could not jump due to its target site, i.e. the first site of either E_1 or E_2. Real drivers might be tempted to decide for another route if the preferred route is completely blocked but in the present scenario such 'smart' decisions are not included. This can lead to complete gridlocks of the whole system if all sites of one route (or several routes) are occupied. If one route is gridlocked the whole system is gridlocked since all routes share the sites j_1, j_4 and E_0.

Since gridlocks cannot dissolve, once they are formed they are the (absorbing) stationary state of the system. In an ergodic system (with finite edge lengths L_i) each accessible state will be reached at some point of the time evolution. Thus if a gridlock state is possible, it will always be reached at some point of the time evolution. Note that, depending on the initial state, the time to reach the gridlock state can be extremely long, as will be seen in Sec. 4.1.1.1. In the present section the requirements for gridlocks to be possible are determined.

If the system is analysed by Monte Carlo simulations it is important to initialize the system in a way that excludes gridlocks that could occur if the system was initialized into a state that could not occur according to the given strategy. In our simulations the system was always initialized such that particles were placed randomly but already on routes according to their strategies. This means that e.g. a particle following strategy 14 could not be placed on E_2. If the system was instead e.g. initialized completely randomly, i.e. particles are placed anywhere irrespective of the strategy, gridlocks which are generally not possible for the given global strategy could occur. A simple example for this are initial states where all sites on a specific route are occupied by the random initialization even if this is not possible according to the global strategy. For the following arguments to be valid in Monte Carlo simulations, our chosen initialization strategy has to be applied.

Gridlock on Route 14. For the occurrence of a gridlock on route 14 the following three conditions must be met:

$$(N_{14} \geq L_4 + 1) \quad \wedge \quad (N_{14} + N_{153} \geq L_1 + L_4 + 2) \quad \wedge \quad (M \geq \hat{L}_{14} = L_1 + L_4 + 4). \quad (4.1)$$

The first condition $N_{14} \geq L_4 + 1$ is necessary since all sites on E_4 can only be occupied by particles of strategy 14. Additionally to all sites on E_4, also junction j_2 must be occupied by a particle of the same strategy (a particle that intends to jump to E_4). As well as all sites of E_4 and j_2, also all sites on E_1 must be occupied at the same time either by particles of strategies 14 or 153. Also junction j_1 must be occupied by a particle that wants to turn left, thus one of strategy 14 or 153. This is represented in the second condition $N_{14} + N_{153} \geq L_1 + L_4 + 2$. For a complete gridlock of route 14, also sites j_4 and E_0 must be occupied. They can be be occupied by particles of any strategy 14, 153 or 23, which is represented in the third condition $M \geq \hat{L}_{14}$.

Gridlock on Route 23. For the occurrence of a gridlock on route 23 the following three conditions must be met:

$$(N_{23} \geq L_2 + 1) \quad \wedge \quad (N_{23} + N_{153} \geq L_3 + L_2 + 2) \quad \wedge \quad (M \geq \hat{L}_{23} = L_3 + L_2 + 4). \quad (4.2)$$

The first condition $N_{23} \geq L_2 + 1$ is necessary since all sites on E_2 can only be occupied by particles of strategy 23. Additionally to all sites on E_2, also junction j_1 must be occupied by a particle intending to turn right, thus of the same strategy 23. As well as all sites of E_2 and j_1, also all sites on E_3 must be occupied at the same time either by particles of strategies 23 or 153. Also junction j_3 must be occupied by one of those particles. This is represented in the second condition $N_{23} + N_{153} \geq L_3 + L_2 + 2$. For a complete gridlock of route 23, also sites j_4 and E_0 must be occupied. They can be be occupied by particles of any strategy 14, 153 or 23, which is represented in the third condition $M \geq \hat{L}_{23}$.

Gridlock on Route 153. The conditions for the occurrence of a gridlock on route 153 are a bit more complicated since there is edge E_5 which can only be used by particles of strategy 153 and there are the edges E_1 and E_3 which can be used by particles of strategies 153 and 14 and 153 and 23, respectively. The first condition which has to be met is

$$N_{153} \geq L_5 + 1. \quad (4.3)$$

This represents all sites of E_5 and junction j_2 being occupied by particles of strategy 153. Then one has to consider the remaining particles of strategy 153 which we denote by $r_{153} = N_{153} - L_5 - 1$. They can now be distributed onto edges E_1 and E_3. As the second condition for a gridlock to be possible on route 153, there has to exist an integer number $a \in \mathbb{N}$ with $0 \leq a \leq r_{153}$ such that

$$(r_{153} - a + N_{14} \geq L_1 + 1) \quad \wedge \quad (a + N_{23} \geq L_3 + 1). \quad (4.4)$$

The first part means that all sites on E_1 and also junction j_1 must be occupied by particles of strategies 14 or 153. The second one means that junction j_3 and all sites on E_3 must be occupied by particles of strategies 153 or 23. The third condition is

$$M \geq \hat{L}_{153} = L_1 + L_5 + L_3 + 5. \quad (4.5)$$

This ensures that sites j_4 and E_0 are occupied (by particles of any strategy 14, 23 or 153). Summarzing, for a gridlock on route 153 to be possible the conditions in (4.3) and (4.5) have to be met and an integer number $a \in [0, r_{153}]$ has to exist such that the two conditions in (4.4) can be fulfilled.

Figure 4.1 shows for which points in the strategy landscape (the $\left(n_1^{(j_1)},\ n_1^{(j_2)}\right)$ - landscape

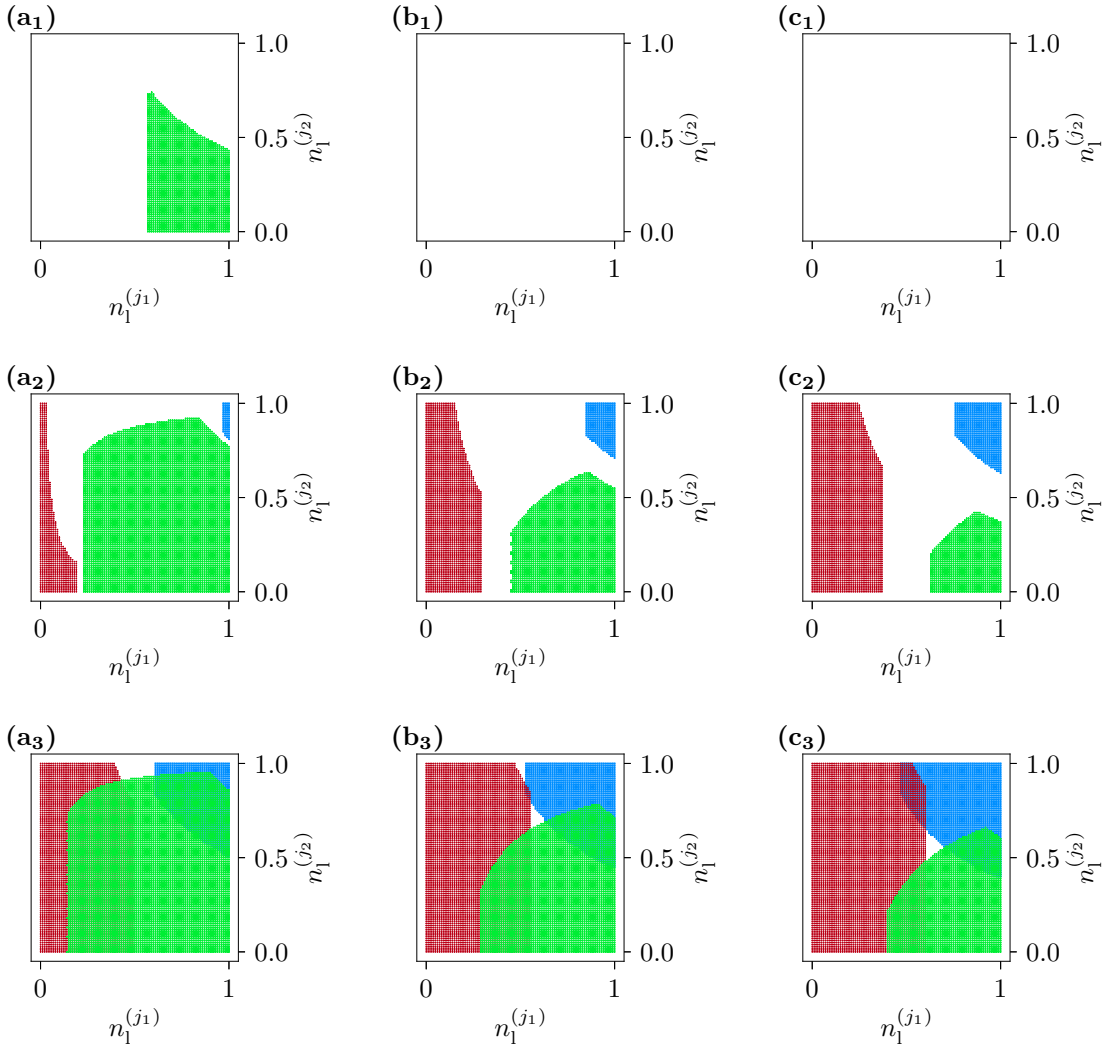

Figure 4.1. The $\left(n_1^{(j_1)},\ n_1^{(j_2)}\right)$ - landscapes for $L_1 = 100$, $L_2 = 500$ and **(a1)** $\hat{L}_{153}/\hat{L}_{14} = 0.4$ and $\rho^{(5)}_{\text{global}} = 0.2$, **(a2)** $\hat{L}_{153}/\hat{L}_{14} = 0.4$ and $\rho^{(5)}_{\text{global}} = 0.5$, **(a3)** $\hat{L}_{153}/\hat{L}_{14} = 0.4$ and $\rho^{(5)}_{\text{global}} = 0.8$, **(b1)** $\hat{L}_{153}/\hat{L}_{14} = 0.7$ and $\rho^{(5)}_{\text{global}} = 0.2$, **(b2)** $\hat{L}_{153}/\hat{L}_{14} = 0.7$ and $\rho^{(5)}_{\text{global}} = 0.5$, **(b3)** $\hat{L}_{153}/\hat{L}_{14} = 0.7$ and $\rho^{(5)}_{\text{global}} = 0.8$, **(c1)** $\hat{L}_{153}/\hat{L}_{14} = 1.0$ and $\rho^{(5)}_{\text{global}} = 0.2$, **(c2)** $\hat{L}_{153}/\hat{L}_{14} = 1.0$ and $\rho^{(5)}_{\text{global}} = 0.5$, **(c3)** $\hat{L}_{153}/\hat{L}_{14} = 1.0$ and $\rho^{(5)}_{\text{global}} = 0.8$. The landscapes were discretized in steps of 0.01. Strategies with potential gridlocks on routes 14, 23 and 153 are marked with blue $\times$'s, red $+$'s and green $\star$'s, respectively.

i.e. the phase space of a 5link system for a given (M, L_5)) gridlocks on the routes are possible for several combinations of $\hat{L}_{153}/\hat{L}_{14}$ and $\rho^{(5)}_{\text{global}}$. One can see that with growing global density and thus more particles in the system, more and more strategies can lead to gridlocks. Depending on the length ratio between the new route and the old routes, different strategies can lead to gridlocks. For low values of $\hat{L}_{153}/\hat{L}_{14}$ more strategies with high $n_1^{(j_1)}$ and low $n_1^{(j_2)}$ lead to a gridlock on route 153, which makes sense since the new route is much shorter compared to the old ones. A shorter route can naturally be gridlocked at lower global densities for certain strategies. For longer L_5, thus higher $\hat{L}_{153}/\hat{L}_{14}$, routes 14 and 23 are becoming

more and more likely to be gridlocked as well.

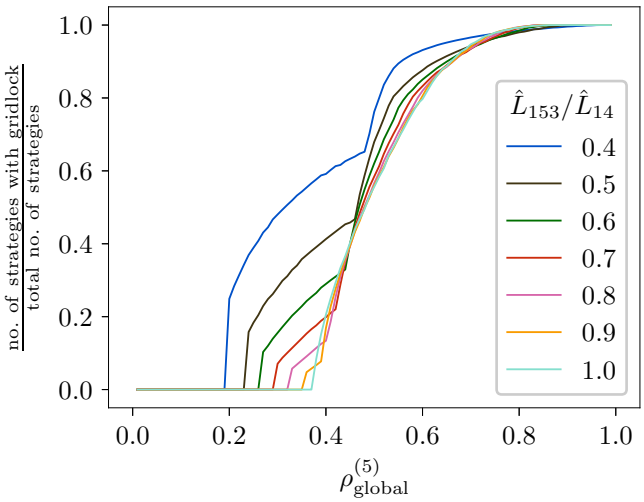

Figure 4.2. The number of strategies with potential gridlock over the total number of strategies against the global density $\rho^{(5)}_{\text{global}}$ for different values of $\hat{L}_{153}/\hat{L}_{14}$. To calculate the ratio the $\left(n_1^{(j_1)},\ n_1^{(j_2)}\right)$ - landscapes were discretized in steps of 0.01 and the number of strategies with possible gridlocks were counted and then divided by the total number of strategies.

In Figure 4.2 the ratio of the number of strategies in which gridlocks are possible and the total number of strategies is shown against the global density for various routelength ratios for $L_1 = 100$ and $L_2 = 500$. This plot was obtained by discretizing the $\left(n_1^{(j_1)},\ n_1^{(j_2)}\right)$ - landscapes in steps of 0.01. Then the number of strategies with potential gridlocks were counted and this number was divided by the total number of strategies. Since in our case $\hat{L}_{153}$ is always smaller than $\hat{L}_{14} = \hat{L}_{23}$, the lowest density for which gridlock can occur is always the density with $M = \hat{L}_{153}$ (cf. Eq. (4.5)).

For low values of L_5 large regions of the $\left(n_1^{(j_1)},\ n_1^{(j_2)}\right)$ - landscape are comprised of strategies with possible gridlocks even for low densities (e.g. over 60% of strategies can lead to gridlocks at densities of $\rho^{(5)}_{\text{global}} \approx 0.4$ for $\hat{L}_{153}/\hat{L}_{14} = 0.4$). For longer E_5 less strategies lead to gridlocks. The shape of the curves in Figure 4.2 depends on how fine the discretization of space is chosen and also on how phase space is described. It might look different if the phase space is chosen to be three-dimensional and described by $(N_{14},\ N_{23},\ N_{153})$ instead of $\left(n_1^{(j_1)},\ n_1^{(j_2)}\right)$. The time required for gridlock formation depends on the individual realization of the stochastic process. A closer look at when gridlocked states occur is given in the following.

4.1.1.1 When Do Gridlocks Form?

Here we address the question about when during the time evolution of the system gridlocks form by analysing an exemplary parameter set for which gridlocks are possible. We look at the parameter set $\hat{L}_{153}/\hat{L}_{14} = 0.5$ and $\rho^{(5)}_{\text{global}} = 0.49$. In Figure 4.3 we show the $n_1^{(j_1/j_2)}$ - landscapes and the corresponding $T_{\max}$ (Part **(a)**) and ΔT (Part **(b)**) values. Strategies with

gridlocked steady states are marked by coloured ×'s, +'s and ⋆'s, while for strategies in which gridlocks are not possible the values of MC data for $T_{\max}$ and ΔT are shown. Four strategies are marked and the corresponding travel time values of the three routes and the $T_{\max}$ and ΔT values for these points are shown in Table 4.1.

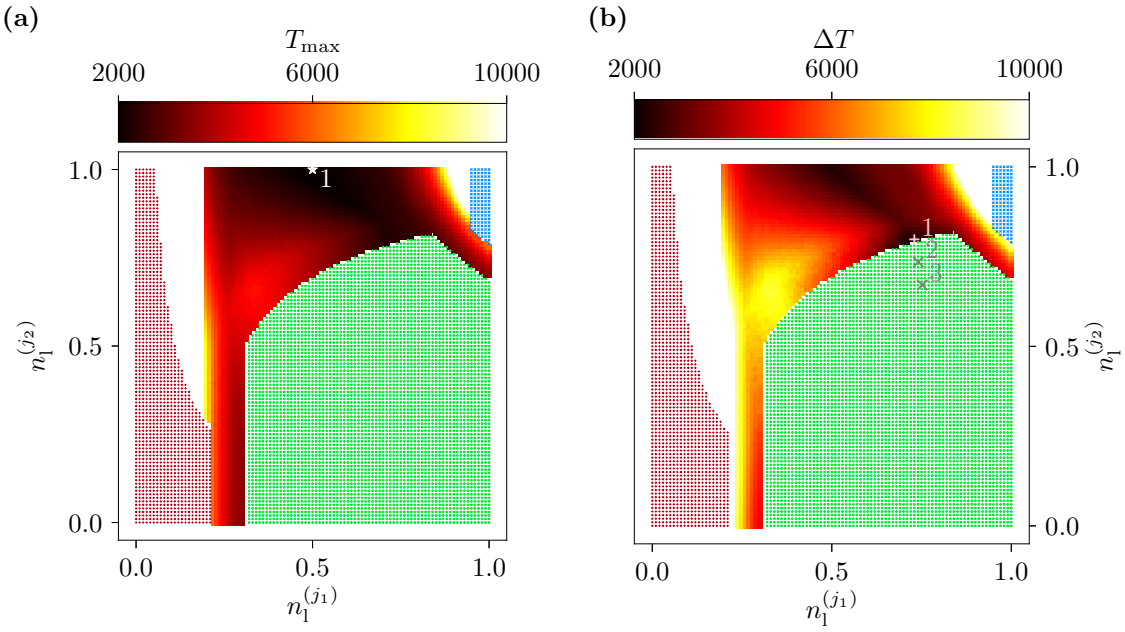

Figure 4.3. The $n_1^{(j_1/j_2)}$ - landscapes of **(a)** the $T_{\max}$ and **(b)** the ΔT-values for $L_5 = 97$ and $M = 638$, which means $\hat{L}_{153}/\hat{L}_{14} = 0.5$ and $\rho^{(5)}_{\text{global}} = 0.49$. States with possible gridlocks on routes 14, 23 and 153 are marked with blue ×'s, red +'s and green ⋆'s, respectively. Simulations were performed for regions where no gridlock is possible and $n_1^{(j_1/j_2)}$ was sweeped in steps of 0.01. The white point ⋆1 has the lowest value of $T_{\max}$ and is thus the system optimum. The pink point +1 is the point with the lowest value of ΔT of all strategies without gridlock. Thus this is the point which is used for the phase diagram. The grey points +2 and +3 have smaller values of ΔT but route 153 can gridlock.

In Part **(a)** of Figure 4.3 the point ⋆1 represents the system optimum of this parameter set. It is given by half the particles choosing route 14 and the other half route 23. This point has the lowest value of $T_{\max} = 1789$. It is not the user optimum as it has a high value of $\Delta T = 2230$ since the travel time on route 153 is much lower than on the other routes. Strategy +1 in Part **(b)** of the figure is the point with the lowest value of $\Delta T = 2215$ of all the strategies without gridlock. From Table 4.1 we see that at this point route 153 still has a much lower travel time than the routes 14 and 23. In a system with real selfish drivers, more and more drivers would thus switch onto route 153. From the markings in Figure 4.3 **(b)** we know that if more particles choose route 153, a gridlock on that route becomes possible. We marked two more points (point ×2 and ×3) in this figure. From Table 4.1 we see that the value of ΔT decreases for those two points. The travel time values of points ×2 and ×3 given in this table were measured before the system gridlocked. From the reasoning in the previous subsection we know that if a gridlock is possible it will in an ergodic system with finite edge lengths definitely be reached at some point of the time evolution. In Figure 4.4 we see how

Table 4.1. The $n_1^{(j_1/j_2)}$ values, travel time values of all three routes and the $T_{\max}$ and ΔT values of the the four points which are marked in Figure 4.3 **(a)** and **(b)**. Point $\star 1$ is the system optimum. Point $+1$ is the point with the lowest value for ΔT without potential for a gridlock. Thus this is the point we chose for construction of the phase diagram. The points $\times 2$ and $\times 3$ are states with gridlocked stationary states on route 153. The measured travel time values are marked with a star because they were measured before the system gridlocked and are not stationary state values.

Point	$n_1^{(j_1)}$	$n_1^{(j_2)}$	T_{14}	T_{23}	T_{153}	$T_{\max}$	ΔT
$\star 1$	0.5	1.0	1789	1789	674	1789	2230
$+1$	0.730	0.798	2270	2047	1162	2270	2215
$\times 2$	0.741	0.735	$2113^\star$	$2015^\star$	$1539^\star$	$2133^\star$	$1148^\star$
$\times 3$	0.752	0.671	$2797^\star$	$2744^\star$	$2748^\star$	$2797^\star$	$106^\star$

travel times of the individual routes and the value of ΔT develop during the measurement process at point $\times 3$. For this figure six instances of the system with different seed values for the random number generator were generated and the travel times were measured during the evolution of the system. The system was not relaxed before measurements begun. The relaxation was skipped here since otherwise the system may have already gridlocked during the relaxation process. One can see that in the beginning of the time evolution the state $\times 3$ seems to be actually a good candidate for a user optimum since the value of ΔT is very low since all three routes have similar travel times (also compare Table 4.1 for the numbers). Nevertheless, as expected, all six instances of the system gridlock at some point of the time evolution. The earliest gridlock occurs after 130000 sweeps (blue line) and the latest after 1470000 sweeps (grey line).

In a system with real drivers or intelligent particles which choose the route with the lowest potential travel time judging from their assumed knowledge of travel times on all routes gridlocks are very likely to develop. If a system is e.g. in a state like the $+1$ state in Figure 4.3 **(b)**, more and more drivers would switch to route 153 with the aim of reducing their travel time. This would in the end lead the system to gridlock.

The described observations about gridlock states are why strategies with gridlocks are not considered as candidates for user optima (or system optima) in the following analyses. This also means that for various parameter sets there are no real user optima as exemplified by the parameter set shown in Figure 4.3.

4.1.2 Results for the 4link Network

To analyse the impact of the new edge E_5 on the network and its performance in the sense of travel times, the user optima (and system optima) of the 4link and 5link systems have to be compared. Since the 4link system, our reference system, is symmetric one expects the user optimum and the system optimum to be given by half the particles taking route 14 and the other half taking route 23 ($N_{14} = N_{23} = M/2$) for all possible global densities $\rho_{\text{global}}^{(4)}$. Figure 4.5 shows that this is indeed the case for the case of drivers with fixed route choices.

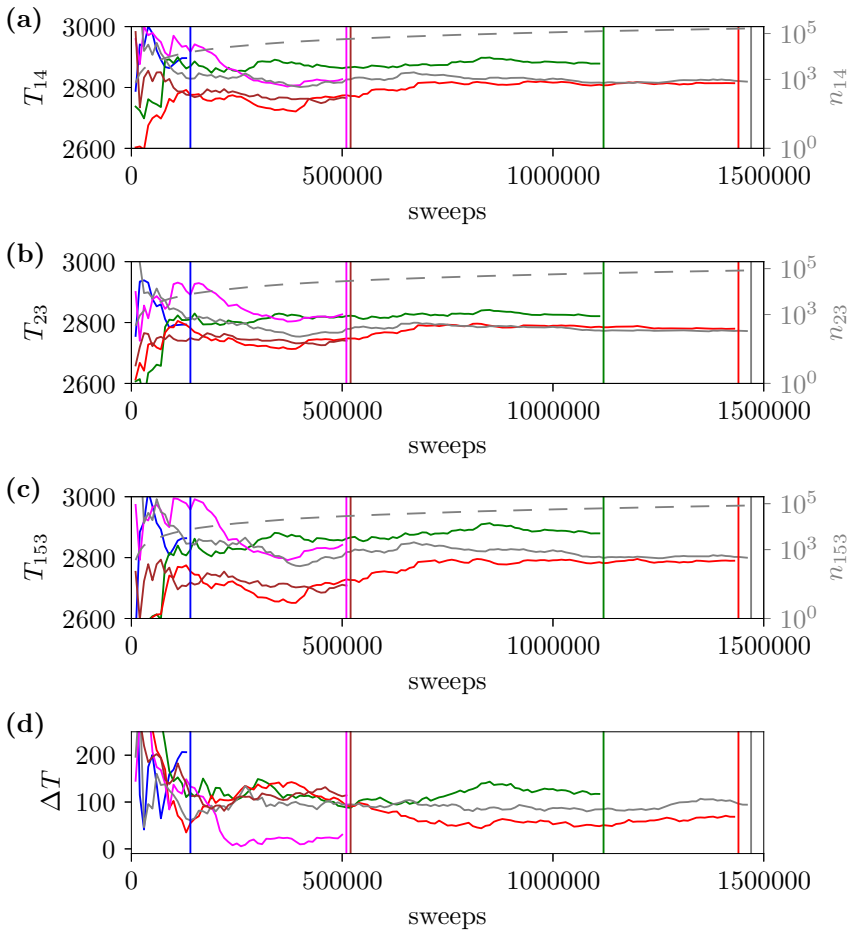

Figure 4.4. The time evolution of **(a)** - **(c)** the measured mean values of the travel times of the three routes and **(d)** the value of ΔT for the state $\times 3$ shown in Figure 4.3. The different coloured curves show six different instances of the system realized with six different seed values for the random number generator. The second y-axes on the right sides of the first three figures show how many times n_i the values of T_i were measured, represented by the dotted grey line. The vertical lines show the points in time when the individual systems gridlocked on route 153.

When particles are distributed in equal parts onto the two symmetric routes, gridlocks are automatically avoided since as long as there are less particles than the total number of sites minus two in the system gridlocks are not possible on either of the two routes (compare to Equations (4.3) and (4.4) with noting that $N_{153} = 0$ and $L_5 = 0$ for the 4link system). This means that user optima exist in the system up until global densities of almost 1.

In Figure 4.5 **(a)** we see the value of ΔT plotted against the global density in the 4link system. The value is close to zero for all global densities which means that the travel times are (almost) equal on both routes and this symmetric distribution of the particles is indeed the user optimum. Since the network is symmetric, this symmetric strategy is also the system optimum, as any unequal distribution of the particles would lead to a higher travel time on the route with more particles.

In Figure 4.5 **(b)** the average of the travel times measured on routes 14 and 23 ($T_{av} =$

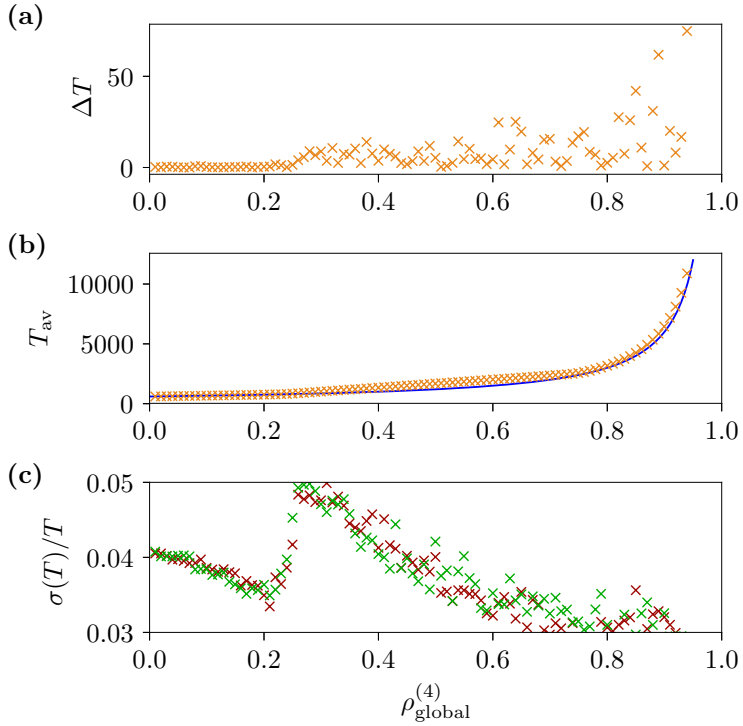

Figure 4.5. Results of MC simulations of the 4link system for 50% of the particles choosing route 14 and 50% choosing route 23 ($N_{14} = N_{23} = M/2$) for the whole density regime $0 \leq \rho^{(4)}_{\text{global}} \leq 1$ and $L_1 = L_3 = 100$ and $L_2 = L_4 = 500$. Part **(a)** shows, that throughout all densities, the travel times on routes 14 and 23 are almost equal. Part **(b)** shows the average travel times on these routes (orange ×'s) and for comparison the travel time of a single TASEP with $M/2$ particles according to Equation (3.4) (blue line). One can see, that jamming at j_4 plays an important role for densities $\rho^{(4)}_{\text{global}} \gtrsim 0.2$. As can be seen in part **(c)**, the relative standard deviations of the travel times on both routes are below 5% for all densities (values for route 14/23 in red/green).

$(T_{14} + T_{23})/2)$ is shown. For comparison also the travel time of a single TASEP used by $M/2$ particles (obeying Equation (3.4)) is shown by the blue line. One can see that for densities $\rho^{(4)}_{\text{global}} \gtrsim 0.2$ the travel times on the routes in the 4link system are higher than those in the single TASEP. This means that jamming in front of j_4, which forms a bottleneck since the two routes join at this site, leads to higher travel times from this density upwards.

In Figure 4.5 **(c)** we can see the relative standard deviation of the travel time measurements of both routes (see Equation (3.33)). One can see that it stays below 5% for all densities. This means that no matter the point of the time evolution, particles starting a new round at j_1 will experience similar travel times. This is a big difference to the system with route choices governed by turning probabilities (see Section 4.2.2).

Figure 4.6 shows the density profiles of the two routes for the half-half strategy for the four different global densities $\rho^{(4)}_{\text{global}} \in \{0.1, 0.2, 0.5, 0.75\}$. One can see that the density profiles on both routes look almost exactly equal reflecting the symmetry of the scenario. For the two lowest densities both routes are in LD phases. At the intermediate density there is a domain wall on both routes separating an HD region on the right from an LD region on the

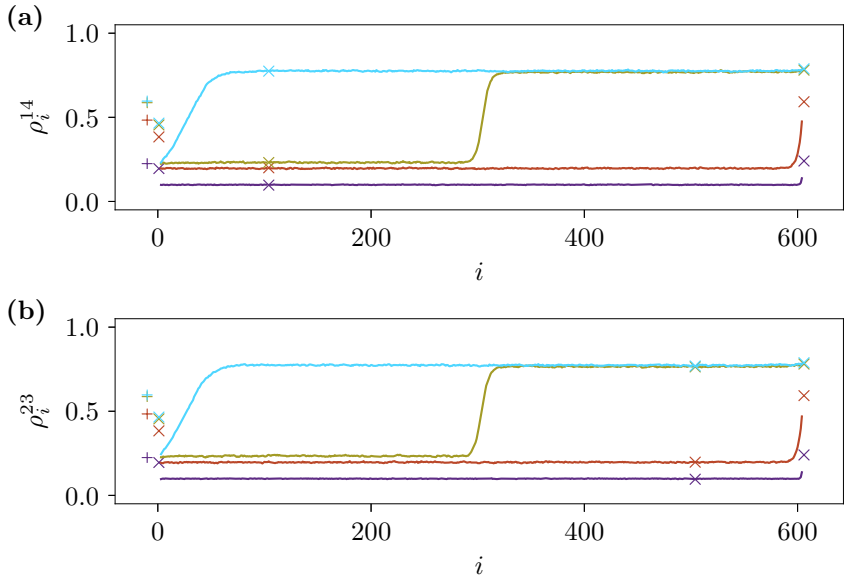

Figure 4.6. Density profiles of the routes 14 (Part **(a)**) and 23 (Part **(b)**) in the 4link system with $L_1 = L_3 = 100$ and $L_2 = L_4 = 500$ for the four different global densities $\rho^{(4)}_{\text{global}} \in \{0.1, 0.2, 0.5, 0.75\}$ printed in {purple,orange,brown,blue}. The local densities $\rho_i^{14/23}$ on the two routes are shown against the position i. The denisity on E_0 is given by a +, the density of junction sites on the roads by ×'s. One can see that in all cases the density profiles are almost equal on both routes. Domains walls form at the same fixed positions on both routes.

left. This domain wall is at a fixed position: it appears as a sharp domain wall in the density profile which was averaged over the whole measurement process. It is thus not to be confused with a fluctuating domain wall which appears in single OBC TASEPs for $\alpha = \beta < 1/2$ (see Section 3.1.1.2). For higher densities the HD parts (averaged density higher than 1/2) of the routes get longer. This behaviour is a big difference to the system with route choices governed by turning probabilities (see Sections 4.2.2 and 4.3).

4.1.3 Comparison of the 4link and 5link Networks

We used Monte Carlo simulations to obtain the user optima and system optima of the 5link system for different combinations of L_5 and M. Our methods for finding user and system optima are described in Sections 3.2.5 and 3.3.2. For the reasons described in Section 4.1.1 states with potential gridlock formation were not considered as candidates for user or system optima.

4.1.3.1 Strategies with Multiple User Optima in the 5link Network

For some configurations we could find more than one user optimum. Here we present the example of $\hat{L}_{153}/\hat{L}_{14} = 0.4$ and $\rho^{(5)}_{\text{global}} = 0.18$. In Figure 4.7 the $T_{\max}$ and ΔT landscapes for this parameter set are shown. In the figure, the values of a sweep of the landscapes in steps of 0.1 is underlayed. The travel time and ΔT and $T_{\max}$ values for the four marked points are

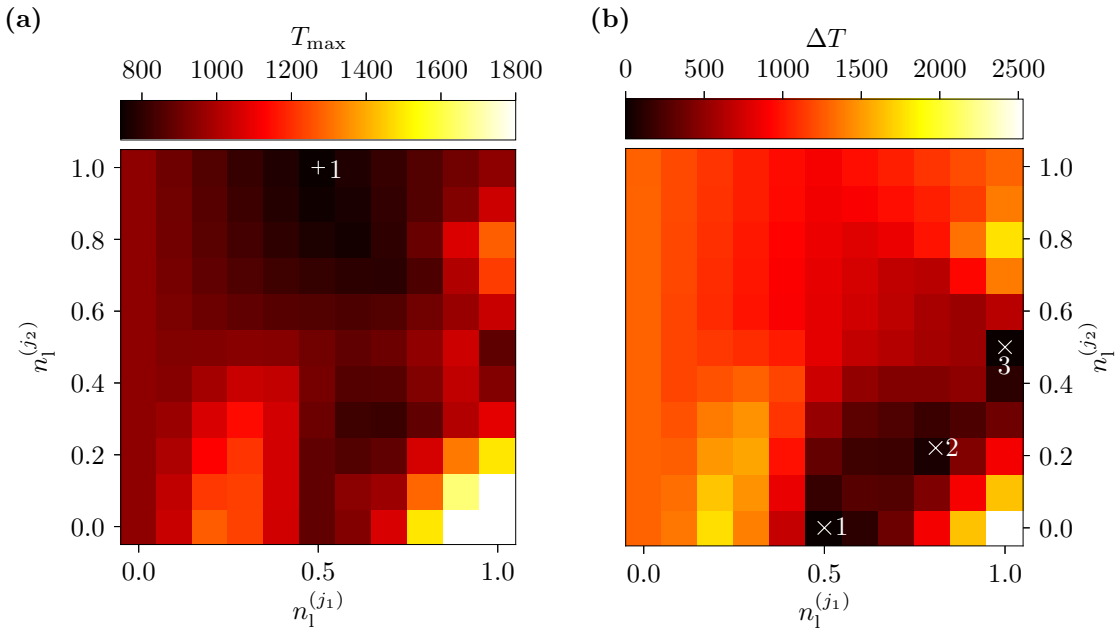

Figure 4.7. The $T_{\max}$ (Part **(a)**) and ΔT (Part **(b)**) landscapes of the 5link system with $L_1 = L_3 = 100$, $L_2 = L_4 = 500$, $L_5 = 37$, $M = 224$, $\rho^{(5)}_{\text{global}} = 0.18$. In Part **(a)**, the system optimum is marked by +1. In Part **(b)** one can see that there are three different user optima, ×1 to ×3, the values of which are given in Table 4.2.

given in Table 4.2. In Part **(a)** of the picture one can see that the system optimum is given by $n_1^{(j_1)} = 0.5$ and $n_1^{(j_2)} = 1.0$. This means that here $so^{(5)} = so^{(4)}$ since this is the state where half of the particles use route 14 and the other half route 23.

In Part **(b)** of Figure 4.7 one can see that there are three different user optima. The two user optima ×1 and ×3 were found by sweeping the $n_1^{j_1/j_2}$ landscapes (Section 3.2.5.1) and are special cases of user optima which were already mentioned in Section 3.2.3. The user optimum ×2 was found by our Metropolis (Section 3.3.2) algorithm. The optimum ×1 is a special case since only route 23 and 153 are used. Since both their travel times are almost equal and smaller than that of the unused route 14 this state is a user optimum. For calculating ΔT, only the difference between T_{23} and T_{153} is used. It would in this case not make sense for any particle to switch to route 14 which has a higher travel time. The same happens in the user optimum ×3, but here routes 14 and 153 are used and route 23 is not. The other user optimum ×2 is an 'ordinary' user optimum in which all three routes are used and have (almost) the same travel time. The (maximum) travel times in all three user optima are higher than that of the system optimum (which is the same as the 4link system optimum) which leads to the conclusion that no matter in which user optimum the system ends up, a "Braess 1" state is present.

The fact that we found multiple user optima with different travel times (and different $T_{\max}$ values and also different total travel time values) for the same parameter set is a difference to what is observed in mathematical models of road traffic. In these models it was shown that "[the user optimum] is unique whenever the shortest routes between all pairs of locations are

Table 4.2. The $n_1^{(j_1/j_2)}$ values, travel time values of all three routes and the $T_{\max}$ and ΔT values for the four points which are marked in Figure 4.7. The point +1 is the system optimum while points ×1 to ×3 are three user optima of the system.

Point	$n_1^{(j_1)}$	$n_1^{(j_2)}$	T_{14}	T_{23}	T_{153}	$T_{\max}$	ΔT
+1	0.5	1.0	743	742	294	743	898
×1	0.5	0.0	926	880	876	880	4
×2	0.808	0.221	970	975	975	975	10
×3	1.0	0.5	878	1136	875	878	3

unique and cost is strictly increasing with increasing flow" [69].

For most parameter sets which were analysed, only one user optimum was found. Also, when multiple user optima were found, they all lead to the same system phases as in the example presented in this section where all three different user optima result in a "Braess 1" phase. Nevertheless, I cannot guarantee that all existing user optima were found for all parameter sets. This is why the obtained phase diagram presented in the following section may not be totally accurate. Furthermore, from the example presented here, one can see that in the case of multiple user optima those optima can have different travel time values (Table 4.2). In Section 4.1.3.3 the influences of the new edge are quantified. For this quantification it has to be kept in mind that for each parameter set only one user optimum was taken into account and consequently the resulting quantifications are not to be taken as exact numbers but rather as tendencies.

4.1.3.2 Phase Diagram

By comparing the global strategies and their travel times of the found 5link user and system optima to those of the 4link system's user and system optima for the same M the phase diagram of the system according to the classification shown in Figure 3.11 was constructed. The phase diagram (Figure 4.8) and the following Figure 4.9 show the influence of the control parameters L_5 and M: the x-axis is always given by $\hat{L}_{153}/\hat{L}_{14}$ which is the ratio of the lengths of the new route 153 and the two old routes 14 and 23 (see Equations (3.17) - (3.19)). There are always two y-axes which decode the number of particles M via the global densities in the 4link/5link systems $\rho_{\text{global}}^{(4)/(5)}$ (see Equation (3.20)).

The phase diagram shown in Figure 4.8 can be divided into two super-phases which can then be subdivided into the individual phases. The first super-phase is that in which real user optima exist in the 5link system (there are real user optima in the 4link system for all densities as discussed before). This is in the sense that global strategies exist which lead to almost equal travel times on all three routes without the possibility of gridlock formation. This super-phase is comprised of the phases A_1, A_2 and B and C.

The second super-phase of the phase diagram is the part in which, due to gridlocks, no real user optima exist in the 5link system. This super-phase is marked by a hatching. It consists of

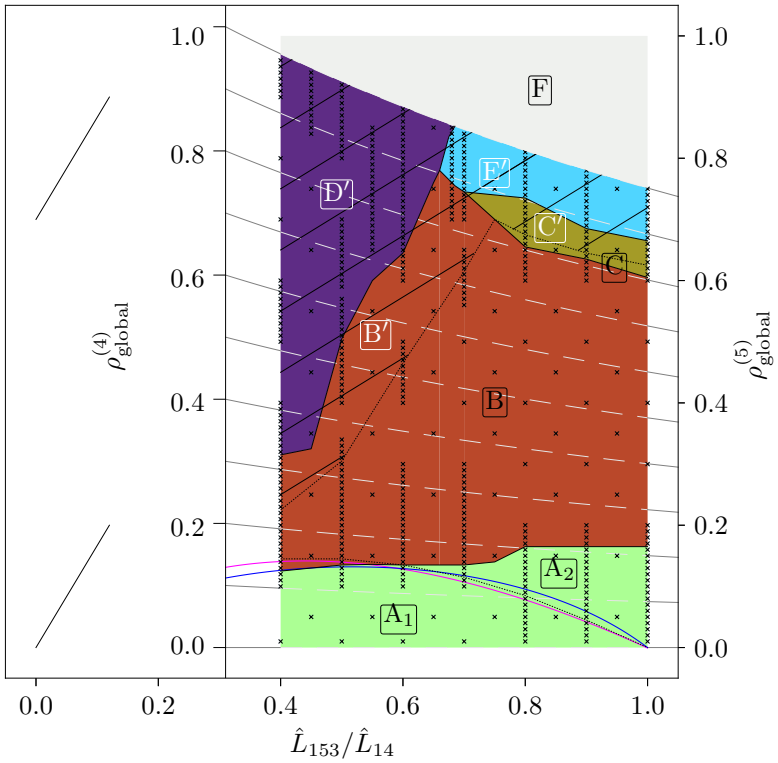

Figure 4.8. The phase diagram for the Braess network with periodic boundary conditions, random-sequential updates and fixed route choices according to the classification scheme given in Figure 3.11. The shown results were obtained for $L_1 = L_3 = 100$, $L_2 = L_4 = 500$ and varying lengths of E_5 (resulting in the x-axis $\hat{L}_{153}/\hat{L}_{14}$) and M (resulting in the two y-axes $\rho^{(4)/(5)}_{\text{global}}$). The $\times$'s show where simulations were performed. The phase boundaries are drawn according to those simulations and are thus, due to this limited number of simulations, only a rough estimate of the phase boundaries. In phases A, B and C real user optima could by found: phase A_1 is an "E_5 optimal - all 153" phase, phase A_2 is an "E_5 optimal" phase, phase B a "Braess 1" phase, phase C a "Braess 2" phase. In the area marked by a hatching (phases B′, C′, D′, E′) no real user optima could be found. Phase B′ is "Braess 1 - like", phase C′ is "Braess 2 - like", phase D′ is "E_5 not used - like", phase E′ is "E_5 improves -like". In phase F the 4link system is full. The magenta and blue lines denote the mean field phase boundary for the "E_5 optimal - all 153" phase, as given by Equations (3.26) and (3.27).

the primed phases B′, C′, D′, E′. For classifying these phases according to the scheme shown in Figure 3.11 the states with the lowest value of ΔT that cannot lead to gridlocks where used (compare Section 4.1.1.1 for an example) as the closest candidates for a user optimum: the maximum travel time of that state (since unlike in a real user optimum all three routes do *not* have equal travel times) was compared to the 4link user optimum travel time. One has to always keep in mind that no stable states exist in the 5link systems in these phases and if the system was used by real drivers, the system would at some point gridlock completely as described in Section 4.1.1.1.

In a large part of the phase diagram, there are more particles in the 5link system than sites in the 4link system. This part is called phase F. In this part of the phase diagram the two systems cannot be compared. Obviously, if that many particles were in the system, the new

road would improve the system's performance, but only in the sense that that many particles could not even fit into the network without the new road.

The two super-phases can also be identified in Figure 4.9 **(a)** which shows the value of ΔT in the states with the lowest value of ΔT in the 5link systems for selected parameter sets of $\hat{L}_{153}/\hat{L}_{14}$ and $\rho^{(5)}_{\text{global}}$. One can see that in the first super-phase, where real user optima exist, it stays below 100. In the phase A_1 it is actually zero while in the two other phases it takes values of the order of 10. If one sticks strictly to the definitions of user optima given in Section 2.1, all user optima in which ΔT is not zero are actually boundedly rational user optima.

In the second super-phase the value grow highly above 100, up to 10^5 and more, indicating that the closest candidates for user optima are actually very far from real user optima.

The First Super-phase / the Region with Real User Optima. Phases A_1 and A_2 which are found at $\rho^{(5)}_{\text{global}} \lesssim 0.2$ are "E_5 optimal" phases. The 5link system optima differ from those of the corresponding 4link systems and the 5link user optima coincide with the 5link system optima. This means that due to the new road, also for selfish users, in the 5link system users will align themselves in the optimal way and this will lead to lower travel times than in the user optimum of the system without the new road. Phase A_1 which is found at low global densities and low values of the route length ratio $\hat{L}_{153}/\hat{L}_{14}$ is a special case in the sense that it is an "all 153" phase. This means that the 5link user optimum actually corresponds to all particles using the new route 153 and the travel time on this route being lower than that on the two unused routes. This is also the reason for the value of ΔT being zero in that phase. The analytical approximation of the phase boundary of the "E_5 optimal / all 153" phase, given by Equations (3.26) and (3.26) is also shown in the phase diagram (magenta and blue lines). The correspondence is very good. The region in which both Equations (3.26) and (3.27) are valid (below both the magenta and the blue line) corresponds to the "E_5 optimal / all 153" phase. This is also very well represented in the A_1 phase border obtained by Monte Carlo simulations.

In phase A_2, which is present at higher route length ratios and low global densities, all three routes are used in the 5link user optimum leading to equal travel times on all three routes which are lower than the travel times in the 4link user optima.

Phase B which is the largest phase dominating most of the phase diagram from densities $\rho^{(5)}_{\text{global}} \gtrsim 0.2$ and for high route length ratios up to $\rho^{(5)}_{\text{global}} \lesssim 0.6$ is a "Braess 1" phase. In this phase the 5link system optimum is equal to that of the 4link system – an equal distribution of all particles onto routes 14 and 23. The 5link user optima are, however, given by different distributions of the particles onto the three routes. This leads to equal travel times on the three routes which are higher than those in the corresponding 4link user optima. In this large phase the Braess paradox in its original form occurs. The new road leads to a worse performance of the road network. This indicates strongly that the paradox is not only found but of major importance in networks of exclusion processes (i.e. more realistic traffic descriptions than mathematical models).

Phase C which is only found in a really small part of the phase diagram at densities of $\rho^{(5)}_{\text{global}} \approx 0.6$ and $\hat{L}_{153}/\hat{L}_{14} \gtrsim 0.7$ is a "Braess 2" phase. This means that the system optima of the 4link and 5link system are not the same: travel times in the 5link system optima are lower than those in the corresponding 4link user optima. If the 5link system was forced into its system optimum state, the new road would lead to lower travel times for all network users. For selfish users the 5link system will be in a user optimum state with travel times higher than those of the 4link user optimum though. Thus the new road worsens the network's performance in this phase if selfish users use the network.

The Second Super-phase / the Region Without Real User Optima. Phase B′ is a "Braess 1 - like" phase. It occurs at route length ratios $\hat{L}_{153}/\hat{L}_{14} \lesssim 0.7$ and medium global densities This means the 5link system optimum coincides with the corresponding 4link system's system optimum and statesthat the maximum travel time in the state which is the closest candidate for a user optimum (state with lowest value for ΔT without gridlock) is higher than that of the 4link user optimum.

The C′ phase is a "Braess 2 - like" phase. It is present at $\hat{L}_{153}/\hat{L}_{14} \gtrsim 0.7$ and at densities $0.8 \lesssim \rho^{(4)}_{\text{global}} \lesssim 0.9$ In that phase the 5link system optimum differs from that of the 4link and has lower travel times. The closest candidate for a user optimum has higher travel times than those in the 4link user optimum.

In phase D′ which is found at low route length ratios $\hat{L}_{153}/\hat{L}_{14} \lesssim 0.7$ and high global densities, the 5link system optimum coincides with the 4link system optimum and the 5link closest candidate for a user optimum also coincides with this state: it is thus an "E_5 not used - like" state. The new road will actually be completely ignored.

Phase E′ which is found at route length ratios $\hat{L}_{153}/\hat{L}_{14} \gtrsim 0.6$ and densities $\rho^{(4)}_{\text{global}} \approx 0.9$ is an "E_5 improves - like" phase. The system optimum of the 5link systems has lower travel times than that of the corresponding 4link systems. The closest candidate for a user optimum in the 5link does not coincide with the system optimum while it would still lead to lower travel times than the 4link user optimum.

All primed phases are in the region in which no real user optima exist and in a system with real selfish drivers, those would lead the system to gridlock. From this standpoint one could argue that in all primed phases, the new road has a negative impact on the system's performance. If some travel guidance authority was there to force traffic into its system optimum, in the D′ and E' phases the new road would reduce travel times. This means only at high routelength ratios (i.e. long lengths of E_5) $\hat{L}_{153}/\hat{L}_{14} \gtrsim 0.6$ and $\rho^{(4)}_{\text{global}} \gtrsim 0.8$ the new road would lead to decreased travel times. For selfish drivers, only for small global densities $\rho^{(5)}_{\text{global}} \lesssim 0.2$ the construction of the new road would lead to stable user optima with lower travel times.

Overall one could say that if it cannot be guaranteed that the network is only used by a small amount of drivers the construction of the new road is very risky from a network performance perspective.

Examples of what the observable-landscapes and densiy profiles on the routes look like in

the described phases can be found in A.1.1.

4.1.3.3 A Closer Look at the Influence of the New Edge

Additionally to just comparing the system and user optima of the 4link and 5link systems with respect to travel times and constructing the phase diagram on this basis, one can also take a more quantitative look at the new road's influence on the system. The corresponding results are shown in Figure 4.9 together with the values of ΔT of some points in the phase diagram. The ΔT values are shown in Part **(a)** of that Figure and were already discussed. In Part **(b)** the ratio of the maximum travel times of the 4link and 5link systems $T_{\max}(so^{(5)})/T_{\max}(so^{(4)})$ is shown. This measure quantifies how much the new road reduces system optimum travel times. If the 5link system was always in its system optimum, e.g. due to traffic guidance by some authority, travel times would be reduced in phases $A_{1/2}$, C, C′ and E′. As can be seen in the Figure the benefits would be highest for really low densities and really small values of L_5 (thus in phase A_1) and also for really high densities. The former makes sense since if there are only a few particles and they can all use a much shorter route then the travel times on this route will be much smaller than on the longer (old) routes. We know that travel times diverge if the density on a periodic TASEP approaches $\rho = 1$ (Equation 3.4). Thus the latter case makes sense too: at really high densities in the 4link system, the system optimum travel times diverge and thus the travel times in the system optimum of the 5link, where there is another, relatively long route available, are shorter.

Part **(c)** of Figure 4.9 shows the price of anarchy in the 5link system given by the ratio $T_{\max}(uo^{(5)})/T_{\max}(so^{(5)})$: how much does the 5link network suffer from selfish users opposed to controlled traffic. In the $A_{1/2}$ phase and in the D′ phases user and system optima coincide which is why the value of $T_{\max}(uo^{(5)})/T_{\max}(so^{(5)})$ equals 1. In the other phases the 5link user optima are not equal to the system optima. In the biggest phase, the B phase or "Braess 1" phase, the price of anarchy has values around 1.1 to 1.3. Selfish users do not increase travel times by a large factor here. The price of anarchy is highest in the C′ phase in which it reaches values above 1.5.

In Figure 4.9 **(d)** the ratio of the 4link and 5link travel times $T_{\max}(uo^{(5)})/T_{\max}(uo^{(4)})$ is shown. If it is larger than 1 the new road leads to higher user optimum travel times and Braess' paradox is present. If it is lower the road leads to lower user optimum travel times. The positive effects are highest in the A_1 and E′ phases while the negative consequences are dominant in most parts of phase space.

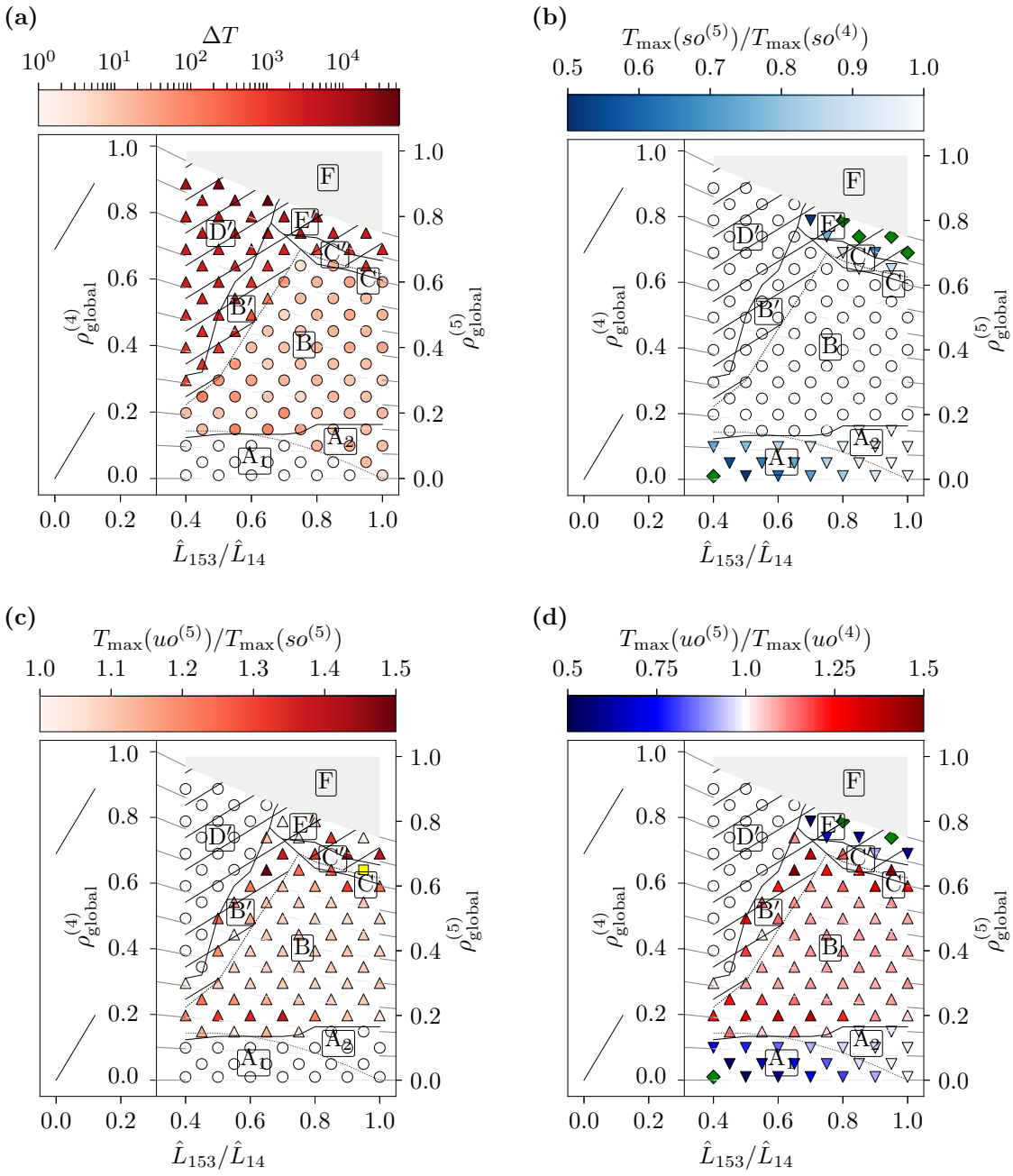

Figure 4.9. Quantifications of the influence of E_5 on the network. Part **(a)** shows the value of ΔT for selected measurement points. One can see that it is below 100 (indicated by coloured ∘) in the unhatched area and above 100 (indicated by coloured △) in the hatched area. In all three Parts **(b)** to **(d)**, white ∘ indicate values equal to 1, coloured △ indicate values between 1 and 1.5, coloured ▽ indicate values between 0.5 and 1, green ♢ indicate values below 0.5 and yellow □ indicate values above 1.5. Part **(b)** shows how the new road could improve the system if it was always in its system optimum, measured by $T_{\max}(so^{(5)})/T_{\max}(so^{(4)})$. Part **(c)** measures the so-called price of anarchy given by $T_{\max}(uo^{(5)})/T_{\max}(so^{(5)})$. This measure explains how much the travel times go up in the 5link, if users are selfish and not guided by external measures. Part **(d)** shows how much the travel times go up/down due to E_5 compared to the 4link system if the network is used by selfish drivers, measured by $T_{\max}(uo^{(5)})/T_{\max}(uo^{(4)})$.

4.2 Periodic Boundary Conditions and Turning Probabilities

In the present section some results on Braess' network of TASEPs with periodic boundary conditions, random-sequential updates and the route choice process governed by turning probabilities (as described in more detail in Section 3.2.2.2) are presented. Most presented results have been published in [126, 130]

The network is shown in Figure 3.9 **(a)** and the route choice process is sketched in Figure 3.10 **(b)**. Equations (3.15) to (3.20) hold. If site j_1 is updated and there is a particle on this junction, the particle will jump onto E_1 with probability γ and to E_2 with probability $1-\gamma$. If, in the 5link network, site j_2 is updated and there is a particle on this junction site, it will jump to E_4 with probability δ and to E_5 with probability $1-\delta$. Note that if the particle cannot jump due to its target site being occupied, the next time it is updated it will again choose a target site according to the turning probabilities.

All particles are equal and choose their routes according to the same turning probabilities. Thus user optima in this scenario are more precisely speaking mixed user equilibria. It turns out that the turning probability route choice process leads to some major differences in the travel time behaviour when compared to the model with fixed strategies.

4.2.1 Gridlocks in the 5link Network

Each time a particle on a junctions site is updated it chooses its route afresh according to the turning probabilities. Due to this, almost no strategies can lead to permanent gridlocks – often not even strategies leading to *on average* as many particles on a route as sites of the route. Only if γ or δ become deterministic, in the sense of γ or δ being equal to 0 or 1, permanent gridlocks can form if there are sufficiently many particles in the system. This is the case since for a permanent gridlock not only all sites on the edges of a route have to be permanently occupied, but also the three sites which are shared by every route: sites j_4, E_0 and j_1. If the system is not completely full and γ is unequal to 0 or 1, at some point in time, a particle on j_1 will be able to jump to its target site. Like this all particles will be able to move at some point, even though travel times may be really high.

Due to all routes sharing the three aforementioned sites, a gridlock on one route will lead to the whole network being gridlocked. In the following we show under which circumstances the three routes can gridlock, leading to a whole network gridlock:

- Gridlocks on route 23 are the stationary state for

$$M \geq \hat{L}_{23} = L_2 + L_3 + 4 \qquad \wedge \qquad \gamma = 0 \qquad \wedge \qquad \delta = \text{arbitrary}. \tag{4.6}$$

- Gridlocks on route 14 are the stationary state for

$$M \geq \hat{L}_{14} = L_1 + L_4 + 4 \qquad \wedge \qquad \gamma = 1 \qquad \wedge \qquad \delta = 1. \tag{4.7}$$

- Gridlocks on route 153 are the stationary state for

$$M \geq \hat{L}_{153} = 2L_1 + L_5 + 5 \qquad \wedge \qquad \gamma = 1 \qquad \wedge \qquad \delta = 0. \tag{4.8}$$

- Gridlocks on route both route 14 and route 153 are the stationary state for

$$M \geq L_1 + L_3 + L_4 + L_5 + 5 \qquad \wedge \qquad \gamma = 1 \qquad \wedge \qquad \delta = \text{arbitrary}. \tag{4.9}$$

- Gridlocks on route both route 23 and route 153 are the stationary state for

$$M \geq L_1 + L_2 + L_3 + L_5 + 5 \qquad \wedge \qquad \gamma = \text{arbitrary} \qquad \wedge \qquad \delta = 0. \tag{4.10}$$

- Gridlocks on route both route 14 and route 23 are the stationary state for

$$M \geq L_1 + L_2 + L_3 + L_4 + 5 \qquad \wedge \qquad \gamma = \text{arbitrary} \qquad \wedge \qquad \delta = 1. \tag{4.11}$$

One can see that there are significantly less states leading to gridlocks than in the network with fixed strategies (gridlocks in that system where treated in Section 4.1.1). As can be seen in Figure 4.1, for fixed strategies at high global densities almost all strategies become gridlocked. In the present case of turning probabilities, permanent gridlocks are only possible if either γ or δ is 0 or 1.

4.2.2 Results for the 4link Network

The network without E_5 is symmetric. Thus one would naturally assume that the user optimum and the system optimum is, for any number of particles M, given by the symmetric strategy $\gamma = 0.5$ distributing on average half the particles on route 14 and the other half on route 23. It turns out that in a large intermediate density region this is, at least for short-term measurements, which are relevant for individual particles, not the case. This is a consequence of domain walls whose positions are fluctuating in a coupled manner on both routes.

Figure 4.10 shows the 4link network visualized in two different, but equivalent, ways. The right side of the figure reveals that the 4link network is very similar to the symmetric figure of eight network, the properties of which were analysed in [59] and summarized in Section 3.1.3.1. The difference of the 4link network to the figure of eight network is that in the latter there is only one junction site connecting the two edges. The two edges are fed from the junction site and exit onto the junction site. In the 4link case, there are two separate sites: site j_1 from which the edges are fed and site j_4, the site the edges feed onto. They are connected by the periodic boundary site E_0. While the mean field arguments presented in Section 3.1.3.1 do not hold anymore, the system still behaves similarly.

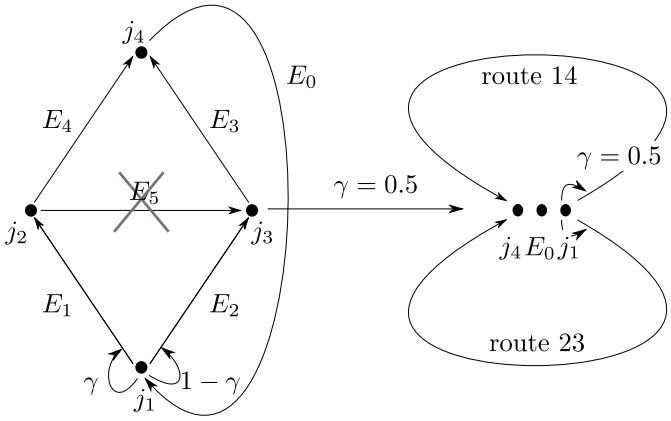

Figure 4.10. Two possible visualizations of the 4link network with $\gamma = 0.5$. In the 4link system E_5 does not exist. Furthermore, throughout the whole thesis $L_0 = 1$. Thus the 4link system with $\gamma = 0.5$ as shown on the left side can also be visualized as shown on the right side. The visualisation on the right side shows the network's similarity to the figure-of-eight network, the properties of which were summarized in Section 3.1.3.1. The difference is that in the figure-of-eight network there is only one junction site which the two routes feed onto and are fed by. In the present case there are three sites: j_4, E_0 and j_1.

In Figure 4.11 the effective entrance and exit rates of routes 14 and 23,

$$\alpha^{\text{eff}} = \tfrac{1}{2}\rho(j_1) \tag{4.12}$$

$$\beta^{\text{eff}} = 1 - \rho(j_4), \tag{4.13}$$

are shown. The values were obtained from Monte Carlo simulations. One can see that the effective rates are almost equal in the density region $0.29 \lesssim \rho^{(4)}_{\text{global}} \lesssim 0.75$. For densities below 0.29 the effective entrance rate is lower than the exit rate, thus the two routes are in LD states. For densities above 0.75 the opposite is the case and both routes are in HD states. For the large intermediate density region, both routes are in DW states.

In the DW phase there are no short-term stable travel times since the positions of the domain walls separating the LD and HD regions on both routes change constantly. Particles queue behind the beginning of the bottleneck (junction j_4). Due to the stochastic feeding (with turning probability γ) the number of particles per route is not fixed as in the fixed route choices model. Only on average there is the same amount of particles on both routes. In the DW phase the densities of the LD and HD regions are given by

$$\rho_{\text{LD}} \approx \alpha^{\text{eff}} \tag{4.14}$$

$$\rho_{\text{HD}} \approx 1 - \alpha^{\text{eff}}. \tag{4.15}$$

From the measurements shown in Fig. 4.11 we deduce that in the whole domain wall phase, $\alpha^{\text{eff}} \approx \beta^{\text{eff}} \approx 0.22$.

It turns out that the DWs on both routes perform a coupled random walk. The shorter the HD region in front of j_4 gets on one route, the longer it gets on the other route. This is also a consequence of the particle number conservation due to the periodic boundary conditions.

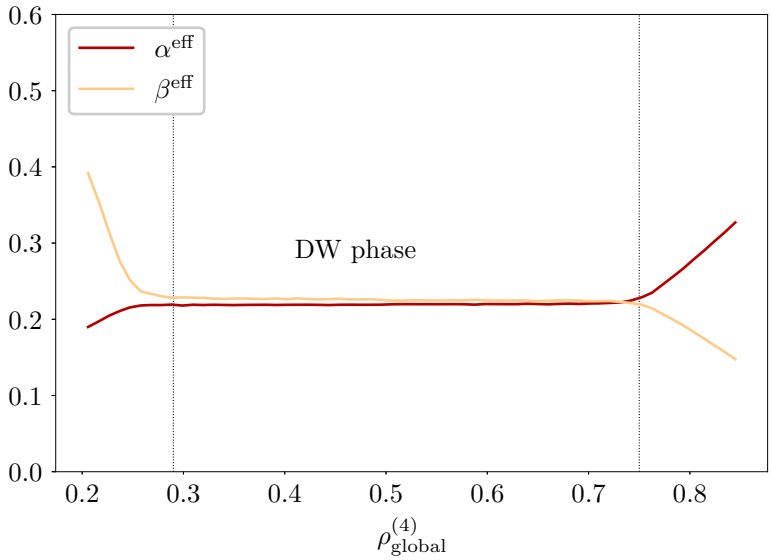

Figure 4.11. The effective entrance and exit rates α^{eff} and β^{eff} of both routes 14 and 23 for the 4link system with $\gamma = 0.5$ against the global density $\rho^{(4)}_{\text{global}}$ as obtained from Monte Carlo simulations. One can see that they are almost equal for $0.29 \lesssim \rho^{(4)}_{\text{global}} \lesssim 0.75$. In this whole density region both routes are in DW phases. Keep in mind that in this whole thesis $L_0 = 1$.

All possible distributions of the HD and LD regions onto the two routes are possible. From equally long HD regions on both routes to (depending on the global density) one route being in an HD state completely while the other route is completely in an LD state.

Using the densities of the LD and HD regions (Equations (4.14) and (4.15)) one can approximate the maximum and minimum travel times which can be measured on both routes. To do this, first note that the following two equations have to be valid:

$$M = \rho^{(4)}_{\text{global}} L^{(4)}_{\text{tot}} \approx \rho_{\text{HD}} L_{\text{HD}} + \rho_{\text{LD}} L_{\text{LD}}\,, \tag{4.16}$$

$$L^{(4)}_{\text{tot}} \approx L_{\text{HD}} + L_{\text{LD}}, \tag{4.17}$$

with $L_{\text{LD/HD}}$ denoting the total length of the LD/HD regions. These are not exact equalities but approximations since sharp discontinous domain walls separating the LD and HD regions were assumed. Furthermore, the junction sites and the site of E_0 were neglected to approximate the total number of sites in the system as $L^{(4)}_{\text{tot}} = 2L_1 + 2L_2 + 5 \approx 2L_1 + 2L_2$. Using $\rho_{\text{LD}} \approx 1 - \rho_{\text{HD}}$ from Eqs. (4.14) and (4.15), the system of Eqs. (4.16) and (4.17) can be solved:

$$L_{\text{HD}} = \frac{\rho^{(4)}_{\text{global}} L^{(4)}_{\text{tot}}}{\rho_{\text{HD}} - \rho_{\text{LD}}} - \frac{\rho_{\text{LD}} L^{(4)}_{\text{tot}}}{\rho_{\text{HD}} - \rho_{\text{LD}}}. \tag{4.18}$$

This equation tells us how long the HD region is depending on the global density. If we now make a further approximation and assume that the LD and HD regions themselves have flat density profiles with a sharp domain wall separating them, we can assume that Equation (3.5), $T_{\text{OBC}} \approx L/(1 - \rho_{\text{bulk}}(\alpha, \beta))$, holds approximately for the description of the travel time on the

LD and HD parts of the routes. Using these assumptions we can then deduce the minimum and maximum possible travel times of routes 14 and 23 in the DW phase:

$$T_{\max} \approx \begin{cases} \frac{L_{\mathrm{HD}}}{1-\rho_{\mathrm{HD}}} + \frac{\hat{L}_{14}-L_{\mathrm{HD}}}{1-\rho_{\mathrm{LD}}} & L_{\mathrm{HD}} < \hat{L}_{14} \\ \frac{\hat{L}_{14}}{1-\rho_{\mathrm{HD}}} & L_{\mathrm{HD}} > \hat{L}_{14} \end{cases}, \tag{4.19}$$

$$T_{\min} \approx \begin{cases} \frac{\hat{L}_{14}}{1-\rho_{\mathrm{LD}}} & L_{\mathrm{HD}} < \hat{L}_{14} \\ \frac{L_{\mathrm{HD}}-\hat{L}_{14}}{1-\rho_{\mathrm{HD}}} + \frac{L_{\mathrm{LD}}}{1-\rho_{\mathrm{LD}}} & L_{\mathrm{HD}} > \hat{L}_{14} \end{cases}. \tag{4.20}$$

For the case in which the whole HD segment is shorter than a route ($L_{\mathrm{HD}} < \hat{L}_{14}$), the maximum travel time is always given if the whole HD segment is inside one route only. This leads to the minimal travel time on the other route since the other route is completely in an LD phase. The situation changes as the HD region gets longer than a whole route, $L_{\mathrm{HD}} > \hat{L}_{14}$. Then the maximum travel time is realized if a whole route is in a HD state which realizes the minimum travel time the other route where the 'remnant' of the HD segment is. These two different situations are shown in Fig. 4.12.

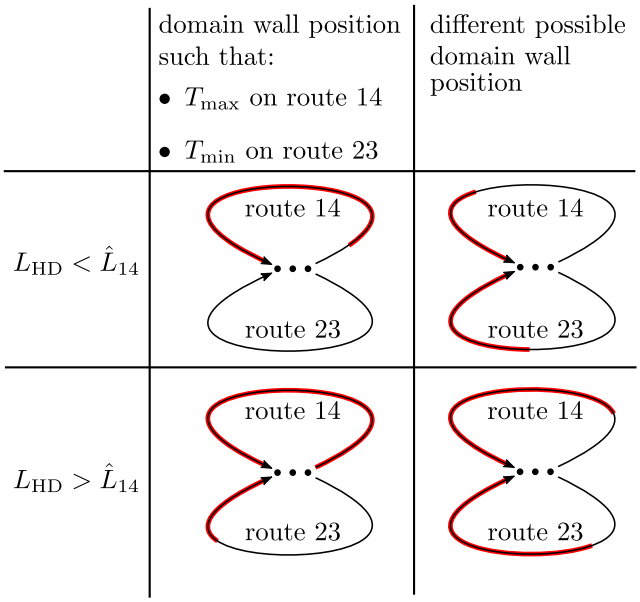

Figure 4.12. Schematic of the possible domain wall positions. For $L_{\mathrm{HD}} < \hat{L}_{14}$ (upper row), the maximum/minimum travel times can be measured on route 14/23 if the whole HD region (marked red) is on route 14 (left column). For $L_{\mathrm{HD}} > \hat{L}_{14}$ (lower row), the maximum/minimum travel times can be measured on route 14/23 if a whole route is in the HD phase, while the remnant of the HD region is in the other route (left column). The right column shows two possible different domain wall positions for the same L_{HD} that occur at different measurement times.

The validity of the predicted behaviour of Equations (4.19) and (4.20) are confirmed by Monte Carlo simulations as shown in Figure 4.13 (red and green lines). Outside the DW region, i.e. for densities $\rho^{(4)}_{\mathrm{global}} < 0.29$ and $\rho^{(4)}_{\mathrm{global}} > 0.75$, the travel time is assumed to be well-represented by a stable value according to Equation (3.5) (blue line). For each global density 400 individual measurements for the travel times of routes 14 and 23 were performed.

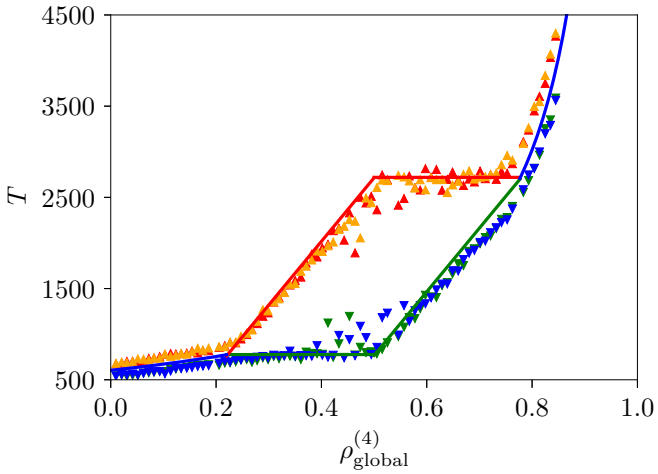

Figure 4.13. The minimum and maximum travel times of the system without E_5 for $L_1 = 100$, $L_2 = 500$ and $\gamma = 0.5$. In the large intermediate DW phase, Eq. (4.19) and (4.20) are good approximations for the maximum (red line) and minimum (green line) travel times. Outside of the DW phase, Eq. (3.5) (blue lines) is a good approximation for the travel times. The equations show a good agreement with MC data (red/orange $\triangle$ for $T_{\text{max},14/23}$, green/blue $\triangledown$ for $T_{\text{min},14/23}$). For each global density $\rho^{(4)}_{\text{global}}$ the travel times of each route were measured 400 times and the minimum and maximum values are plotted.

The obtained minimum and maximum values are then plotted for each density. The expected behaviour of a stable travel time value in the LD and HD regime as well as the approximate expressions (4.20) and (4.19) in the DW regime are confirmed very well.

To further clarify the effects of the fluctuating domain wall in the DW region, the travel times of 400 individual measurements of the travel times of routes 14 and 23 (travel times for route 153 are included for completeness) were collected and binned. The histograms are shown in Fig. 4.14 for three different global densities, $\rho^{(4)}_{\text{global}} \in \{0.2, 0.5, 0.85\}$. One can see that the measured travel times in the LD and HD regions form a distribution with a sharp peak while the distribution is almost flat in the DW region ($\rho^{(4)}_{\text{global}} = 0.5$). Here all the accessible travel times between $T_{\min}$ and $T_{\max}$ are observed with approximately the same frequency of occurrence.

The findings of these combined MF and MC arguments show that (for finite measurement intervals) in the large intermediate density regime $0.29 < \rho^{(4)}_{\text{global}} < 0.75$ there are no stable short-term values for the travel times of the routes in the system, even though the system is in a nonequilibrium stationary state. The long term expectation value is stable though as the DW performs an unbiased random walk. Nevertheless, in the context of Braess' paradox one is interested in the situations of individual drivers using the network. The fact that *in the same state* individuals could, depending on where the domain walls presently are, face *completely different* situations with completely different travel times leads to the conclusion that travel times are not 'stable' or 'constant' in this density region. The word stable is here to be understood in the short-term sense. Due to there not being stable travel time values, it is not possible to identify the system and user optima in this density region in

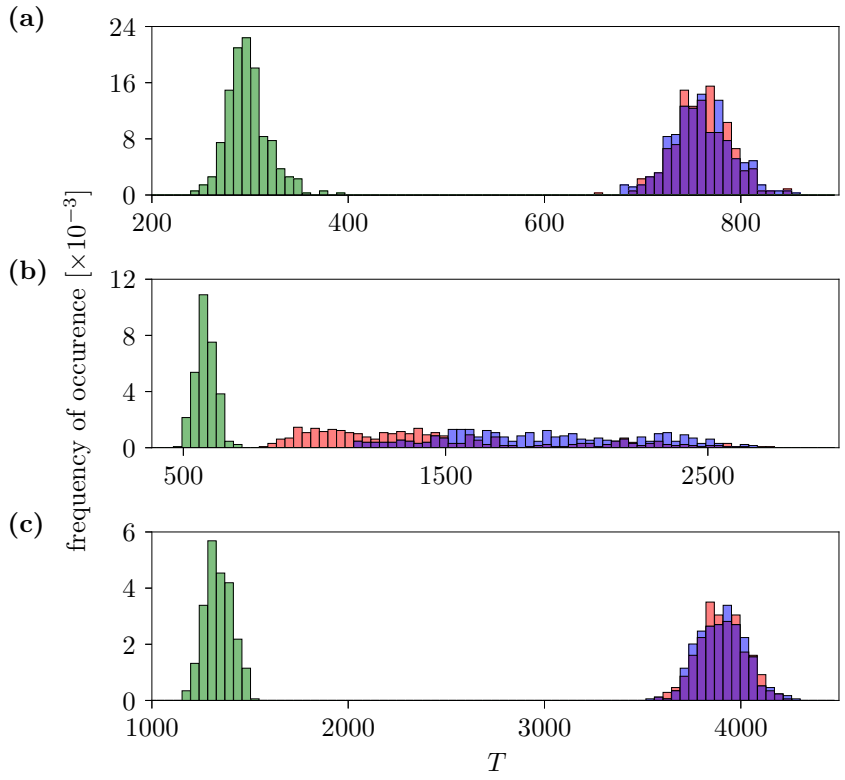

Figure 4.14. Histograms of the travel time measurements in the system of size $L_0 = 1$, $L_1 = 100$, $L_2 = 500$, $L_5 = 37$ for $\gamma = 0.5$ and $\delta = 1.0$ and **(a)** $\rho^{(4)}_{\text{global}} = 0.2$, **(b)** $\rho^{(4)}_{\text{global}} = 0.5$, **(c)** $\rho^{(4)}_{\text{global}} = 0.85$. The red bars represent the travel times on route 14, the blue bars those of route 23 and the green bars those of route 153. One can see that for the intermediate density, i.e. in the DW phase, the travel time distributions of routes 14 and 23 are almost flat. For each route 400 measurements were performed and binned.

the straightforward way described in Sec. 3.2.4.2. It turns out that the system with E_5 is also dominated by domain walls in an even larger density regime. Thus, with the means of travel time measurements, we can only identify the user and system optima of the system for densities outside of the DW region.

4.2.3 Phase Diagram

From the results of the previous section one can see that there are no stable travel time values in the assumed user and system optima of the 4link system for the large intermediate density region $0.29 < \rho^{(4)}_{\text{global}} < 0.75$. For densities outside of this region the system and user optima of the 4link are given by $\gamma = 0.5$: the *on average* equal distribution of the particles onto the two routes 14 and 23. If for these low and high global densities system and user optima of the corresponding 5link systems can be found, one is able to construct the phase diagram of the system according to the classification given in Figure 3.11. To find the system and user optima the observable-landscapes were sweeped in steps of 0.1 according to Section 3.2.5.1[1]

[1]Please note that the results presented here were generated and published in 2016 [126]. This was before the Metropolis Monte Carlo method (see Section 3.3.2) for identifying user and system optima was developed.

The resulting phase diagram is shown in Figure 4.15.

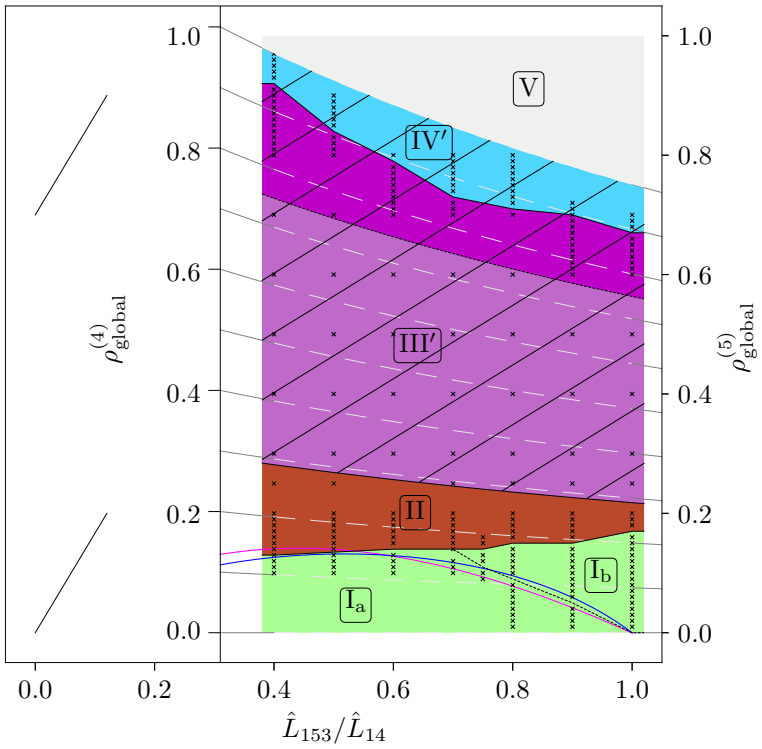

Figure 4.15. The phase diagram for the Braess network with periodic boundary conditions, random-sequential updates and turning probabilities. The shown results were obtained for $L_1 = L_3 = 100$, $L_2 = L_4 = 500$ and varying lengths of E_5 (resulting in the x-axis $\hat{L}_{153}/\hat{L}_{14}$) and M (resulting in the two y-axes $\rho^{(4)/(5)}_{\text{global}}$). The $\times$'s show where simulations were performed. The phase boundaries are drawn according to those simulations and are thus, due to this limited number of simulations, only a rough estimate of the phase boundaries. Phase I_a is an "E_5 optimal - all 153" phase. Phase I_b is an "E_5 optimal" phase. Phase II is a "Braess 1" phase. In the phases marked by a hatching no user optima could be found: phase III′ is an "E_5 not used - like" phase and phase IV′ is an "E_5 improves - like" phase. The part of phase III with a brighter color marks the density regime in which the 4link system is in the DW phase. In phase V the 4link system is full. The magenta and blue lines denote the mean field phase boundary for the "E_5 optimal - all 153" phase, as given by Equations (3.26) and (3.27).

The phase diagram consists of five phases. Phase I is found for low global densities $\rho^{(5)}_{\text{global}} \lesssim 0.2$ and consists of the two sub-phases I_a and $\text{I}_\text{b}b$. Both of them are "E_5 optimal" phases. Sub-phase I_a is an "all 153" phase which means that the system and user optima of the 5link are given by all particles choosing the new route. The higher the ratio $\hat{L}_{153}/\hat{L}_{14}$ gets, the lower gets the density of the I_a phase border. This is to be expected and also confirmed by Equations (3.26) and (3.27) which are represented by the magenta and blue lines in the phase diagram. The "all 153" phase is expected to be present in the region below both lines. The agreement between prediction and Monte Carlo simulations is good, while not as good as in the case of fixed strategies. Sub-phase I_b is also an "E_5 optimal" state but with the user and system optimum being given by states in which all routes are used. It only occurs for

$\hat{L}_{153}/\hat{L}_{14} \gtrsim 0.7$.

For slightly higher densities $\rho^{(5)}_{\text{global}} \gtrsim 0.15 - 0.2$ and $\rho^{(4)}_{\text{global}} \lesssim 0.29$ phase II, the "Braess 1", phase is found. Here the 5link's user optimum travel times are higher than the 4link's user and system optima travel times, while the 5link's system optimum coincides with the 4link's. The paradox occurs in this phase which is relatively large; it does not require fine tuning to find the paradox in the network with turning probabilities. The phase is smaller than in the fixed route choices case.

For all densities $\rho^{(4)}_{\text{global}} > 0.29$ no user optima could be found in the 5link's system. This is indicated by the hatching in the phase diagram. This large region can be divided into two phases.

In phase III, which is called the "domain wall phase" or the "fluctuation-dominated phase", fluctuating domain walls dominate the 5link system. The region in which domain walls dominate the 4link system $0.29 < \rho^{(4)}_{\text{global}} < 0.75$ is marked in the phase diagram with a slightly brighter purple coloration than the rest of phase III. Inside this region there are no stable short-term travel times in the 4link and the 5link system. For densities $0.75 \lesssim \rho^{(4)}_{\text{global}} \lesssim 0.9$ there are stable user and system optimum travel times in the 4link system but not in the 5link. The term *not stable* is always used in the short-term sense, since we are interested in the situation that individual network users face, which can even in the stationary state be very different for different individuals. If measured over a really long time, there will obviously be an average travel time value. In this whole region short-term measuring did not show stable travel times but the minimum of ΔT was in the whole region III found to be at $(\gamma, \delta) = (0.5, 1.0)$ which hints at the assumption that E_5 would not be of any good for the system's travel times here. Phase III is not predicted by the straightforward identification of possible phases which resulted in Figure 3.11. This is because in the reasoning behind the figure it was assumed that unique user and system optima exit both in the 4link and corresponding 5link systems. This is in the short-term sense not the case in phase III, which is why it is a 'new' phase which is accordingly coloured differently than all phases in Figure 3.11.

In phase IV, an "E_5 improves - like" phase, no user optima could be identified with $\Delta T \approx 0$ even though the travel times seem to be short-term stable. The minima of $T_{\max}$ are not at the 4link's system optimum but at different strategies in which all routes are used and have lower travel times than in the 4link' system optimum. The identified minima of ΔT, which are not real user optima since ΔT does not approach zero, are yet different strategies with higher travel times than the 5link system optima but lower travel times than the 4link system optima.

In phase V the 4link system is full. There are less sites in the 4link system than particles in the corresponding 5link systems. This is why the two systems cannot be compared in this whole region. The "Braess 2" phase is not found in the system with turning probabilities.

Examples of what the observable-landscapes and density profiles on the routes look like in the described phases can be found in A.1.2.

4.3 Periodic Boundary Conditions - Comparison of the Results

In Sections 4.1 and 4.2 it was shown that the Braess paradox occurs in the network with periodic boundary conditions both for fixed route choices and turning probabilities. Large parts of the two phase diagrams (Figures 4.8 and 4.15) share a similar structure. For all route length ratios and low global densities $\rho^{(5)}_{\text{global}} \lesssim 0.15$ the added road leads to decreased user optimum travel times. The systems are in "E_5 optimal" phases in this region of the phase space. When global densities grow above $\rho^{(5)}_{\text{global}} \approx 0.15$, the system enters a "Braess 1" phase for all route length ratios. The size of the parameter region in which this phase is observed is different for both route choice mechanisms. In neither of the cases fine tuning is required to observe the paradox. The paradox occurs in a significantly large phase space region for both route choice types, while the phase space region is smaller in the case of turning probabilities. The first question posed in the Introduction of this thesis, whether Braess' paradox can occur in TASEP networks, is thus affirmed.

The phase diagrams show significant differences for global densities $\rho^{(5)}_{\text{global}} \gtrsim 0.2$. From this density upwards, no user optima could be found in the system with turning probabilities. In the system with fixed route choices, the "Braess 1" phase extends up to densities $\rho^{(5)}_{\text{global}} \approx 0.6$ for route length ratios $\hat{L}_{153}/\hat{L}_{14} \gtrsim 0.7$, making this phase the one that occupies the largest part of phase space. The fact that no user optima can be found for densities $\rho^{(5)}_{\text{global}} \gtrsim 0.2$ in the system with turning probabilities is a consequence of fluctuating domain walls. Those domain walls do not occur in the system with fixed route choices. The different behaviours are visualized in Figure 4.16 on an example of the 4link networks for both strategy types. The figure shows the density profiles on the two routes 14 and 23 at approximately half filling of the systems. Part **(a)** of the figure shows the density profiles obtained in the system with fixed route choices by half of the particles choosing route 14 and the other half choosing route 23. Part **(b)** of the figure shows the density profiles in the corresponding 4link network with turning probabilities for the case of all particles choosing one of the two routes with equal probabilities. A localized domain wall is observed at position $i \approx \hat{L}_{14}/2$ for the case of fixed route choices. For this strategy type, each particle traversing either of the routes will experience a similar travel time. Independent of the point of the time evolution of the whole system, particles will face a similar situation on both routes. Thus we concluded that a stable user optimum exists in this system. This is indeed the case throughout the whole density regime $0 < \rho^{(4)}_{\text{global}} \lesssim 1$, as also indicated in Figure 4.5, which provides information about the standard deviations of travel time measurements on both routes.

The density profiles shown in Part **(b)** of Figure 4.16 can be interpreted as follows. In the system with turning probabilities, particles starting their journeys on junction j_1 at different times during the system's time evolution, can face completely different situations on the two routes. Even though the system is in a stationary state, the short-term density profile fluctuates strongly. At a point in time, at which the density profiles, which are printed in lighter shades of grey in the figure, are observed, a particle choosing route 14 will experience a significantly higher travel time than a particle choosing route 23. The situation keeps changing

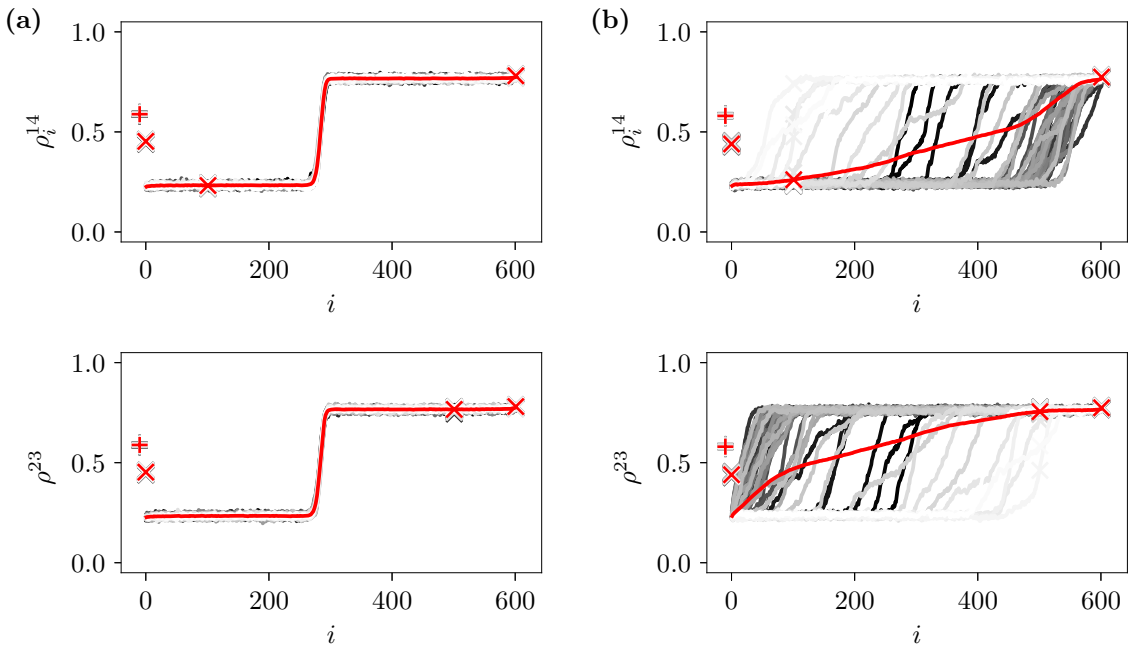

Figure 4.16. The average densities ρ^{14} and ρ^{23} on routes 14 and 23 depending on the position i in the 4link network, as obtained by Monte Carlo simulations. The parameters in both parts of the figure are $L_1 = L_3 = 100$, $L_2 = L_4 = 500$, $M = 622$, $\rho^{(4)}_{\text{global}} \approx 0.52$. Part **(a)** shows the densities measured in the system with fixed route choices and $N_{14} = N_{23} = M/2 = 311$. Part **(b)** shows the densities measured in the system with turning probabilities and $\gamma = 0.5$. In both figures the red line marks the density profiles averaged over the whole measurement process of $1 \cdot 10^6$ sweeps. The lines in different shades of grey show short-term density profiles, averaged over $1 \cdot 10^4$ sweeps each, obtained during the measurement process. This figure was published in [127].

during the time evolution. Thus we concluded that no short-term stable user optimum can be found.

At really high global densities $\rho^{(5)}_{\text{global}} \gtrsim 0.6$, no user optima could be found for either type of route choices. In the system with fixed route choices, for low path length ratios no user optima are found for $\rho^{(5)}_{\text{global}} \gtrsim 0.25$. This is since in this case potential candidates for user optima result in gridlocks. Such gridlocks do not occur at such low densities in the system with turning probabilities, since particles keep re-deciding their routes according to the turning probabilities if they cannot jump to their desired target sites.

The "Braess 2" phase is only observed in the system with fixed route choices, while a phase similar to the "E_5 improves" phase occurs in both systems for large route length ratios and high global densities.

Summarizing, first one can observe that the Braess paradox is very prominent in both types of networks. The "Braess 1" phase is the largest phase in the network with fixed route choices and also occupies a large part of phase space in the system with turning probabilities. The "Braess 2" phase is also observed in the system with fixed route choices. Furthermore, both systems behave very similarly at low densities. The different route choices lead to different behaviours at intermediate densities. The differences are mainly due to the fact that

fluctuating domain walls dominate the system with turning probabilities while fixed domain walls are observed in the case of fixed route choices. With regards to the general influence of the new road on the system, it is important to note that it does not reduce user optimum travel times in either of the systems for $0.2 \gtrsim \rho^{(5)}_{\text{global}} \gtrsim 0.7$.

4.4 Open Boundary Conditions and Turning Probabilities

The present section addresses Braess' network of TASEPs with random-sequential updates and open periodic boundary conditions. The network is shown in Figure 3.9 **(b)**. Since there are new particles fed into the network while others leave the network constantly, the individual particles do not remain in the network and thus the fixed strategies case cannot be examined. This is why only the case of turning probabilities is studied. All user optima that were found are thus mixed user optima.

Particles are fed onto junction j_1 from a reservoir which is occupied with the entrance probability α_{in}. From there they jump onto edge E_1 with probability γ or to edge E_2 with probability $1-\gamma$. At junction j_2, particles jump onto edges E_4 or E_5 with probabilities δ and $1-\delta$ respectively. Particles leave the system when jumping out of junction j_4 into the exit reservoir which is empty with probability β_{out}.

The total number of particles in the system is not conserved in the present case. If the system reaches a stationary state in which none of the links is in a DW phase, the *average* number of particles is constant. Nevertheless, also in these cases there will be temporal fluctuations of the number of particles in the system. This is a significant difference from the Braess paradox in its original sense. In the original model the road network's performances before and after adding the new road were compared for the same demand, i.e. the same number of particles. The model examined in the present section is thus innately different. It is nevertheless interesting to ask the question if Braess' paradox occurs in the system with open boundaries. In the present case Braess' paradox corresponds to a situation in which the user optimum travel times increase after adding a new link while the inflow and outflow rates (entrance and exit rates) are kept constant.

4.4.1 The 4link Network

Due to symmetry one expects the 4link's system and user optima to coincide at $\gamma = 0.5$. In the periodic boundary conditions case this is true for all densities if the route choice process is governed by fixed strategies (see Section 4.1.2). In the periodic boundary case with turning probabilities we saw that in a large area of intermediate densities this is only true if longterm averages are considered since there are (coupled) fluctuating domain walls on both routes which lead to short-term unstable travel times on both routes (see Section 4.2.2). Here we examine the travel times on both routes of the 4link network for open boundary conditions with $\gamma = 0.5$ depending on α_{in} and β_{out} in a MFT. The effective rates of both routes 14 and 23 are given by

$$\alpha^{\text{eff}}_{14/23} = \tfrac{1}{2}\rho_{j_1}, \tag{4.21}$$

$$\beta^{\text{eff}}_{14/23} = 1 - \rho_{j_4}. \tag{4.22}$$

The subscripts 14/23 are dropped in the following for readability. Both routes 14 and 23 are expected to be in the same phase due to the unbiased feeding. Since the occupation number

on junction j_1 can only be 0 or 1 and also the longterm average lies between 0 and 1, the effective entrance rate has to smaller or equal to 1/2: $0 \leq \alpha_{14/23}^{\text{eff}} \leq \frac{1}{2}$. Thus neither of the two routes can be in a maximum current phase. Both routes have thus to be in either low density, high density or domain wall phases. The phase diagram of the symmetrically fed 4link system depending on α_{in} and β_{out} can be derived (with some approximating assumptions) as follows:

The current conservation in the network reads

$$J_{\text{tot}} = \alpha_{\text{in}}(1 - \rho_{j_1}) = 2 \cdot J_{14/23} = \beta_{\text{out}}\rho_{j_4}. \tag{4.23}$$

Both routes 14 and 23 are assumed to be in either an LD, HD or DW state: the bulk densities are assumed to behave according to Table 3.1.

If both routes are in an LD phase, i.e. if $\alpha^{\text{eff}} < \beta^{\text{eff}}$, the bulk densities on both routes will be equal to α^{eff}. Plugging this assumption and the mean field assumptions of Equations (4.21) and (4.22) into Equation (4.23) leads to:

$$\alpha_{\text{in}}(1 - 2\alpha_{\text{eff}}) = 2\alpha^{\text{eff}}(1 - \alpha^{\text{eff}}) = \beta_{\text{out}}(1 - \beta^{\text{eff}}). \tag{4.24}$$

The left part of Equation (4.24) leads to

$$\alpha^{\text{eff}} = \frac{1 + \alpha_{\text{in}}}{2} \pm \frac{\sqrt{1 + \alpha_{\text{in}}^2}}{2}, \tag{4.25}$$

while only the "-"-part makes sense physically since it yields values of α^{eff} between 0 and 1, while the "+"-part yields values above 1. The "-"-solution (which can be approximated as $\alpha^{\text{eff}} \approx \frac{\alpha_{\text{in}}}{2} - \frac{\alpha_{\text{in}}^2}{4} + \mathcal{O}(\alpha_{\text{in}}^3)$) is actually smaller than $\frac{\alpha_{\text{in}}}{2}$ on the interval $[0, 1]$. The effective entrance rate is smaller than half the entrance rate of the boundary conditions. Naively one could have expected it to be equal to half the external boundary entrance rate since two edges are fed.

Plugging this solution for α^{eff} into the right part of Equation (4.24) leads to

$$\beta^{\text{eff}} = \frac{\alpha_{\text{in}}^2 - \alpha_{\text{in}}\sqrt{1 + \alpha_{\text{in}}^2} + \beta_{\text{out}}}{\beta_{\text{out}}}. \tag{4.26}$$

For this to really be an LD phase, $\alpha^{\text{eff}} < \beta^{\text{eff}}$ has to hold. Applying this condition to Equations (4.25) and (4.26) yields the phase border of the LD phase:

$$\beta_{\text{out}} < 1 + \alpha_{\text{in}} - \sqrt{1 + \alpha_{\text{in}}^2}. \tag{4.27}$$

If both routes are in HD phases, i.e. if $\alpha^{\text{eff}} > \beta^{\text{eff}}$, the bulk densities on both routes will be equal to $(1 - \beta^{\text{eff}})$. Plugging this assumption and the mean field assumptions of Equations (4.21) and (4.22) into Equation (4.23) leads to:

$$\alpha_{\text{in}}(1 - 2\alpha_{\text{eff}}) = 2\beta^{\text{eff}}(1 - \beta^{\text{eff}}) = \beta_{\text{out}}(1 - \beta^{\text{eff}}). \tag{4.28}$$

The right part of Equation (4.28) leads to

$$\beta^{\text{eff}} = \frac{\beta_{\text{out}}}{2} \quad \vee \quad \beta^{\text{eff}} = 1, \tag{4.29}$$

where only the first solution makes sense, since the other would imply that $\rho_{j_4} = 0$ independent of α_{in} and β_{out} (Equation (4.22)) which does not make sense and additionally the requirement for an HD phase, $\alpha^{\text{eff}} > \beta^{\text{eff}}$, would not be fulfilled. We see that in this case the effective exit rates are actually half the boundary exit rate.

Plugging the first part of Equation (4.29) into the left side of Equation (4.28) yields

$$\alpha^{\text{eff}} = \frac{1}{4}\left(2 + \frac{(\beta_{\text{out}} - 2)\beta_{\text{out}}}{\alpha_{\text{in}}}\right). \tag{4.30}$$

For both routes to be in HD phases $\alpha^{\text{eff}} > \beta^{\text{eff}}$ has to hold. Applying this to Equations (4.29) and (4.30) yields, as expected, the same phase border as already found for the LD phases in Equation (4.27):

$$\beta_{\text{out}} > 1 + \alpha_{\text{in}} - \sqrt{1 + \alpha_{\text{in}}^2}. \tag{4.31}$$

On the line

$$\beta_{\text{out}} = 1 + \alpha_{\text{in}} - \sqrt{1 + \alpha_{\text{in}}^2} \tag{4.32}$$

both routes are expected to be in DW phases.

Employing these approximative results, also the travel times on both routes, i.e. the user and system optimum travel times of the 4link system, can be approximated employing the approximate travel time for open TASEP segments (Equation (3.5)). In the LD phase the bulk density will be equal to α^{eff} and in the HD it will equal $1 - \beta^{\text{eff}}$. In the DW phase it will be 1/2. Note that in the DW there will be, as in the periodic boundary turning probabilities case (Section 4.2.2), no short-term stable travel times.

The travel times in the LD phases (obeying Equation (4.27)) will be

$$T_{\text{LD}} = \frac{\hat{L}_{14}}{1 - \alpha^{\text{eff}}} = \frac{2\hat{L}_{14}}{\sqrt{\alpha_{\text{in}}^2 + 1} - \alpha_{\text{in}} + 1}. \tag{4.33}$$

The travel times in the HD phases (obeying Equation (4.31)) will be

$$T_{\text{HD}} = \frac{\hat{L}_{14}}{\beta^{\text{eff}}} = \frac{2\hat{L}_{14}}{\beta_{\text{out}}}. \tag{4.34}$$

The longterm average of the travel times in the DW phases (obeying Equation (4.32)) will be

$$T_{\text{DW}} = \frac{\hat{L}_{14}}{0.5} = 2\hat{L}_{14}, \tag{4.35}$$

while at specific points in time the travel time could lie anywhere inside the region

$$\frac{\hat{L}_{14}}{1-\alpha^{\text{eff}}} = \frac{2\hat{L}_{14}}{\sqrt{\alpha^{\text{eff}^2}+1}-\alpha^{\text{eff}}+1} \leq T_{\text{DW}} \leq \frac{\hat{L}_{14}}{\beta^{\text{eff}}} = \frac{2\hat{L}_{14}}{\alpha^{\text{eff}}+1-\sqrt{\alpha^{\text{eff}^2}+1}} \tag{4.36}$$

The results are shown in Figure 4.17. Figure 4.17 **(a)** shows the the mean field prediction

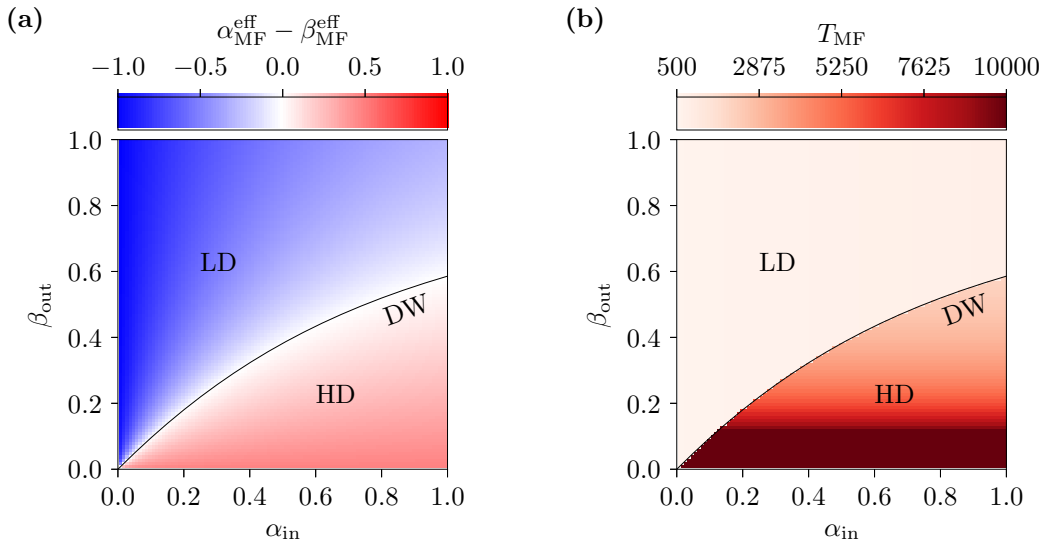

Figure 4.17. Part **(a)** shows the difference of the mean field (MF) preditions of $\alpha^{\text{eff}} - \beta^{\text{eff}}$ and Part **(b)** shows the mean field prediction of the travel time on route 14 and 23 in the 4link's user and system optimum. In both pictures the derived phase structure is underlayed while the phase borader between the HD and LD phases on which a domain wall phase arises is given by Equation (4.32).

of $\alpha^{\text{eff}} - \beta^{\text{eff}}$ and the phase diagram as predicted by the mean field considerations. Part **(b)** of Figure 4.17 show the expected 4link user/system optimum travel times inside the phase diagram. One can observe that the travel times are relatively constant in all the LD phase and grow rapidly in the HD phase, especially for low values of β_{out} which is as expected.

Comparisons of Monte Carlo and mean field data for the effective entrance and exit rates and the travel times can be found in Appendix A.2.1. It can be seen that the mean field predictions represent the system's behaviour well. There it is also shown that the phase boundary, i.e. the line on which DW phases can be observed according to the mean field theory, given by Equation (4.32) is not to be seen as an exact line but that DWs can be observed also in a small region around that line. Overall we can nevertheless conclude that in the open boundary 4link system domain walls do not play an important role as compared to the periodic boundary case with turning rates (Section 4.2.2). The parameters have to be fine tuned to observe domain walls.

Summarizing we can say that the 4link system is really well understood in terms of the mean field theory. For the context of Braess' paradox we saw that the user and system optima can be found at the point of $\gamma = 0.5$ throughout almost the whole parameter region. On a small line fluctuating domain walls occur and on this line the travel times fluctuate on short

time scales. Nevertheless in all the other areas of the phase space stable user and system optimum travel times can be found and can be compared to the 5link system, which is done in the following.

4.4.2 Comparing The 4link and the 5link Networks

In the present subsection, first, some phases which are observed in the 5link system that are not expected from the straight forward reasoning in Section 3.2.4 are described. Second, phase diagrams for the open boundary Braess network of TASEPs are presented for various route length ratios $\hat{L}_{153}/\hat{L}_{14}$.

4.4.2.1 'Unexpected' Phases Observed in the 5link Network

Comparing the user optima of the 5link open boundary system to its 4link counterpart one can determine the influence of the new edge E_5 onto the system. By assuming that distinct user optima exist in both the 4link and the 5link systems, in Section 3.2.4 (especially Figure 3.11) we derived the possible phases of the system. Several of these phases were found in the open boundary system as will be shown in the next subsection.

Additionally to these phases, predicted on the assumption of the existence of user optima in both the 4link and 5link system, two different phases were found. In both of these phases no user optima exist in the 5link system: in the strategies where the value of ΔT is the lowest, it is still highly above zero. What distinguishes the two phases are the strategies which lead to the lowest values of ΔT.

The first phase is called the "all 153 - unstable" phase. This phase is present for small exit rates $\beta_{\text{out}} < \alpha_{\text{in}} \leq 0.3$. Figure 4.18 shows the landscapes of the observables ΔT (Figure 4.18 **(a)**), $T_{\max}$ (Figure 4.18 **(b)**) and the total number of particles in the system (Figure 4.18 **(c)**) depending on the turning probabilities γ and δ. From the $T_{\max}$ landscape we can see that the system optimum is found at $(\gamma, \delta) = (1, 0)$, i.e. the strategy at which all particles use route 153. The ΔT landscape reveals that $(\gamma, \delta) = (1, 0)$ is also the strategy with the lowest value of ΔT. But one can see that the value of is actually pretty large for that strategy: $\Delta T \approx 1687$. The travel time on route 153, $T_{153} \approx 2379$, is higher than on both other routes: $T_{14} \approx 1544$, $T_{23} \approx 1535$. Still, this is the strategy in which the travel time values are closest to each other. As soon as the turning probabilities change such that more than one or even all three routes are used, the travel time differences increase. Strategies with only one of the other routes used, $\gamma = 0$ and δ arbitrary or $\gamma = 1$ and $\delta = 1$, are the strategies with the second lowest $T_{\max}$ and ΔT after $(\gamma, \delta) = (1, 0)$.

This behaviour is specific to the system with open boundary conditions. This phase is observed for $\beta_{\text{out}} < \alpha_{\text{in}}$ and $\beta_{\text{out}} \leq 0.3$. It turns out that due to the outer exit rate being smaller than the outer entrance rate, whenever more than one route is used all used routes are in HD phases. This is also represented in Part **(c)** of Figure 4.18. One can see that the total number of particles in the system is much lower for strategies in which only one or only two routes are used than if all routes are used. In the specific example of Figure 4.18 the

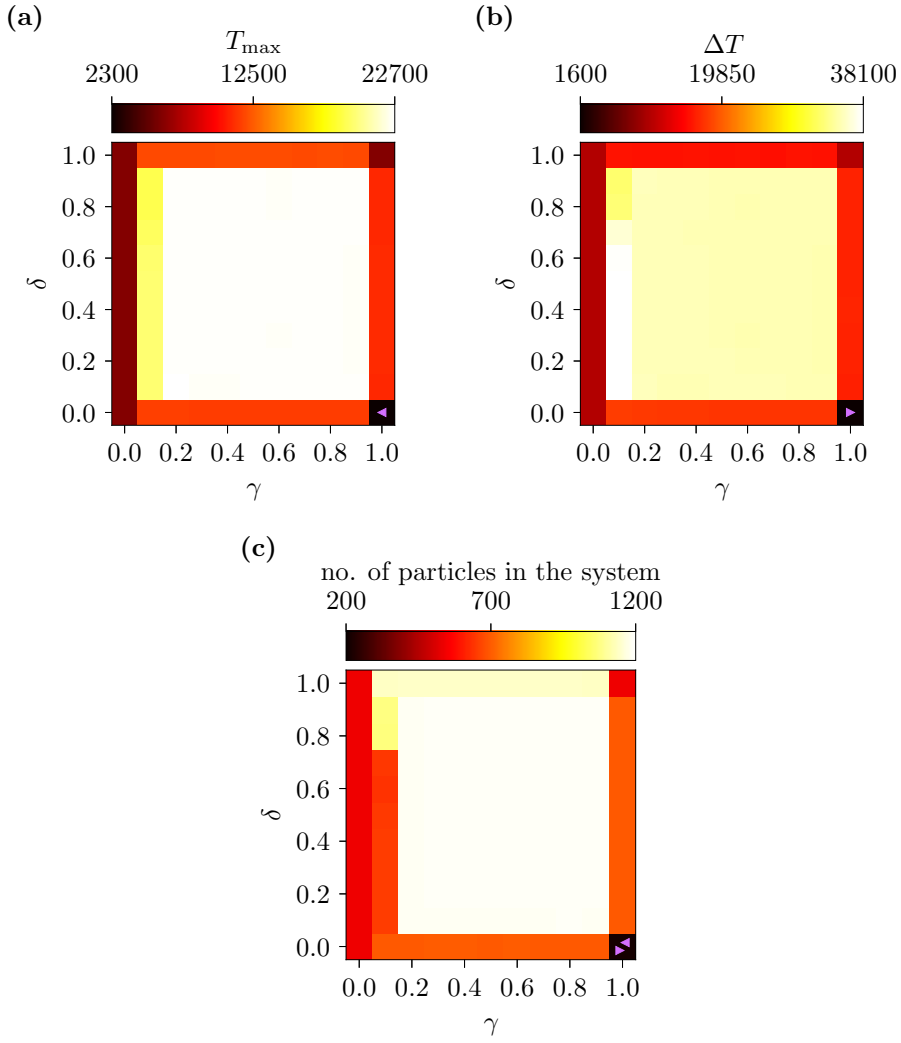

Figure 4.18. The observable landscapes of an "all 153 - unstable" state for **(a)** $T_{\max}$, **(b)** ΔT and **(c)** the total number of particles in the system, each depending on the turning probabilities γ and δ. The specific data is from measurements of a system with edge lengths $L_1 = L_3 = 100$, $L_2 = L_4 = 500$, $L_5 = 37$, i.e. $\hat{L}_{153}/\hat{L}_{14} = 0.4$ and $\alpha_{\text{in}} = 0.3$ and $\beta_{\text{out}} = 0.1$.
The system optimum (minimum of $T_{\max}$) is marked by a pink ◀ and the closest candidate for the user optimum (minimum of ΔT) is marked by a pink ▶. They both coincide at $(\gamma, \delta) = (1, 0)$. At this particular strategy the travel times are $T_{14} \approx 1544$, $T_{23} \approx 1535$, $T_{153} \approx 2379$ and $\Delta T \approx 1687$ with approximately 215 particles in the system.

total number of sites in the system is $\sum_{i=1}^{5} L_i + 4 = 1241$. For most strategies in which all routes are used, there are close to 1200 particles in the system indicating that most of the sites are permanently occupied and thus all routes are in HD states.

Since route 153 is the shortest, $T_{\max}$ will be lowest for the strategy of all particles using that route. Still the travel time on this route is then higher than that of unused routes. But as soon as particles start to use the other routes, HD states will develop on these routes and their travel times will be higher than that of route 153.

This behaviour is a consequence of the open boundaries and the infinite supply of particles entering the system – opposed to the fixed total particle number in the periodic boundary

case. Such a situation could be associated with the following: imagine an accident happening in rush hour traffic, leading to a significant slowing down of traffic of a major city route (the major route being route 153 in our example). Modern navigational systems may then suggest alternative routes. Since there is an almost 'infinite supply of cars', the traffic densities on the alternative routes will rise, until high density states, and thus long travel times, persist on all routes. Such a behaviour was demonstrated employing large scale simulations by Cabannes et al. in 2018 [53].

Coming back to the direct context of Braess' paradox, one could argue that in a system with real drivers, in the "all 153 - unstable" phase, drivers would tend to switch to other routes than route 153 and the system would end up in a state with higher travel times than in the 4link user optimum (all states with $\gamma \neq 1$ or 0 and $\delta \neq 1$ or 0 have higher $T_{\max}$ than $(\gamma, \delta) = (1.0, 0.5)$). Accordingly one could argue that the system shows Braess - like behaviour in this phase. For our non-intelligent driver / fixed turning probabilities scenario we just conclude that no user optimum exists.

There is another state which occurs at slightly higher exit rates that shows similar behaviour but with the minimum of ΔT at other strategies $\gamma = 1$ and $\delta \neq 0$ (with $\min(\Delta T) \gg 0$ like in the "all 153 - unstable" state). This state is called "E_5 optimal -unstable" state. See Appendix A.1.3 for the observable landscapes of that state.

4.4.2.2 Phase Diagrams

In this section the phase diagrams of the open boundary system are presented. The phase of the system depends on $\hat{L}_{153}/\hat{L}_{14}$ and α_{in} and β_{out}. Phase diagrams are shown for $L_1 = L_3 = 100$, $L_2 = L_4 = 500$ and for seven different lengths of the new road L_5, leading to the seven different route length ratios. Figure 4.19 shows the phase diagrams for route length ratios $\hat{L}_{153}/\hat{L}_{14} = 0.4$ to $\hat{L}_{153}/\hat{L}_{14} = 0.7$, Figure 4.20 shows the phase diagrams for route length ratios $\hat{L}_{153}/\hat{L}_{14} = 0.8$ to $\hat{L}_{153}/\hat{L}_{14} = 1.0$.

In each phase diagram the phase border line (Equation (4.32)) of the 4link system is shown (dotted black line). On this line and in a small region around it (see Section A.2.1 for details) the travel times of the 4link system are unstable and no short-term-stable user optimum exists. Since this is just a line of fine tuned parameters (opposed to the domain wall region in the periodic boundary case with turning probabilities, Section 4.2.2), a special in depth analysis of the behaviour on this line was dropped here.

The regions in which the "E_5 optimal - all 153" phase is predicted to be present by the mean field theory are marked in green. See Section 3.2.4.1 and also Appendix A.2.2 for details on the mean field predictions. The simulation data (orange □'s) agrees with the MFT predictions.

Apart from the "E_5 optimal - all 153" phase, no phase regions are marked in the phase diagrams but only the phases on the individual measurement points are shown. This is because measurements were only performed on an $\alpha_{\text{in}}/\beta_{\text{out}}$ grid with 0.1 resolution. In contrary to the periodic boundary conditions phase diagrams no finer measurements to determine the exact

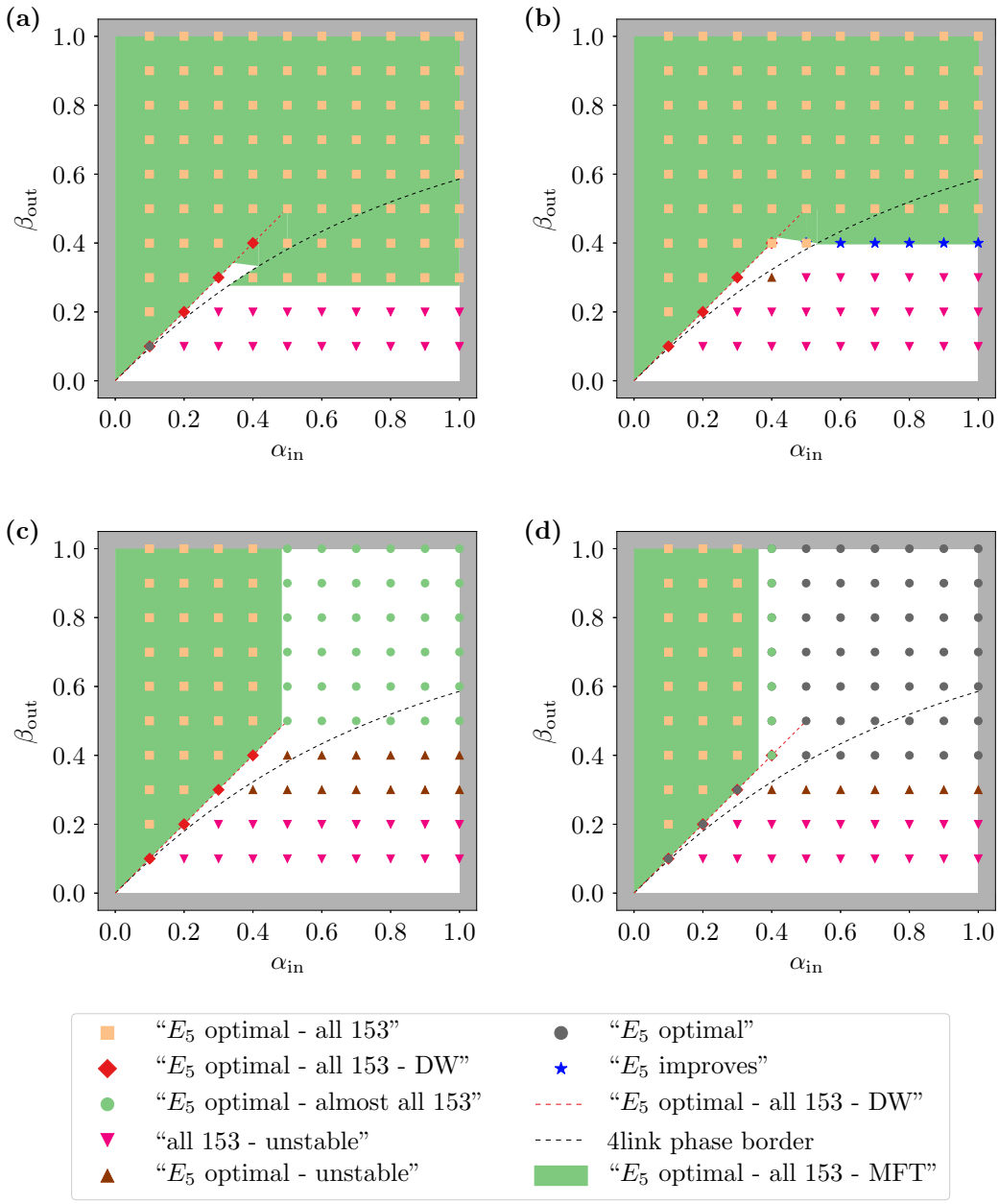

Figure 4.19. Phase diagrams of Braess' network with open boundary conditions, random-sequential updates and turning probabilities and edge lengths $L_1 = L_3 = 100$, $L_2 = L_4 = 500$ and **(a)** $L_5 = 37$, i.e. $\hat{L}_{153}/\hat{L}_{14} = 0.4$, **(b)** $L_5 = 97$, i.e. $\hat{L}_{153}/\hat{L}_{14} = 0.5$, **(c)** $L_5 = 157$, i.e. $\hat{L}_{153}/\hat{L}_{14} = 0.6$, **(d)** $L_5 = 218$, i.e. $\hat{L}_{153}/\hat{L}_{14} = 0.7$. The phases depend on the outer entrance and exit rates α_{in} and β_{out}. Monte Carlo simulations were performed on a 0.1 grid of the rates-landscape. The phases that were found are denoted by the symbols as given in the legend below. Along the dotted red line an "all 153" phase with domain walls on that route is possible. The black dotted line represents the 4link phase boundary as given by Equation (4.32) while the green area shows the region in which MFT predicts the system to be in an "E_5 optimal - all 153" phase.

phase borders were performed. Nevertheless, an intuition about which phase the system will be in depending on the outer entrance and exit rates can be obtained.

The "E_5 optimal - all 153" phase dominates the largest parts of the phase diagrams for

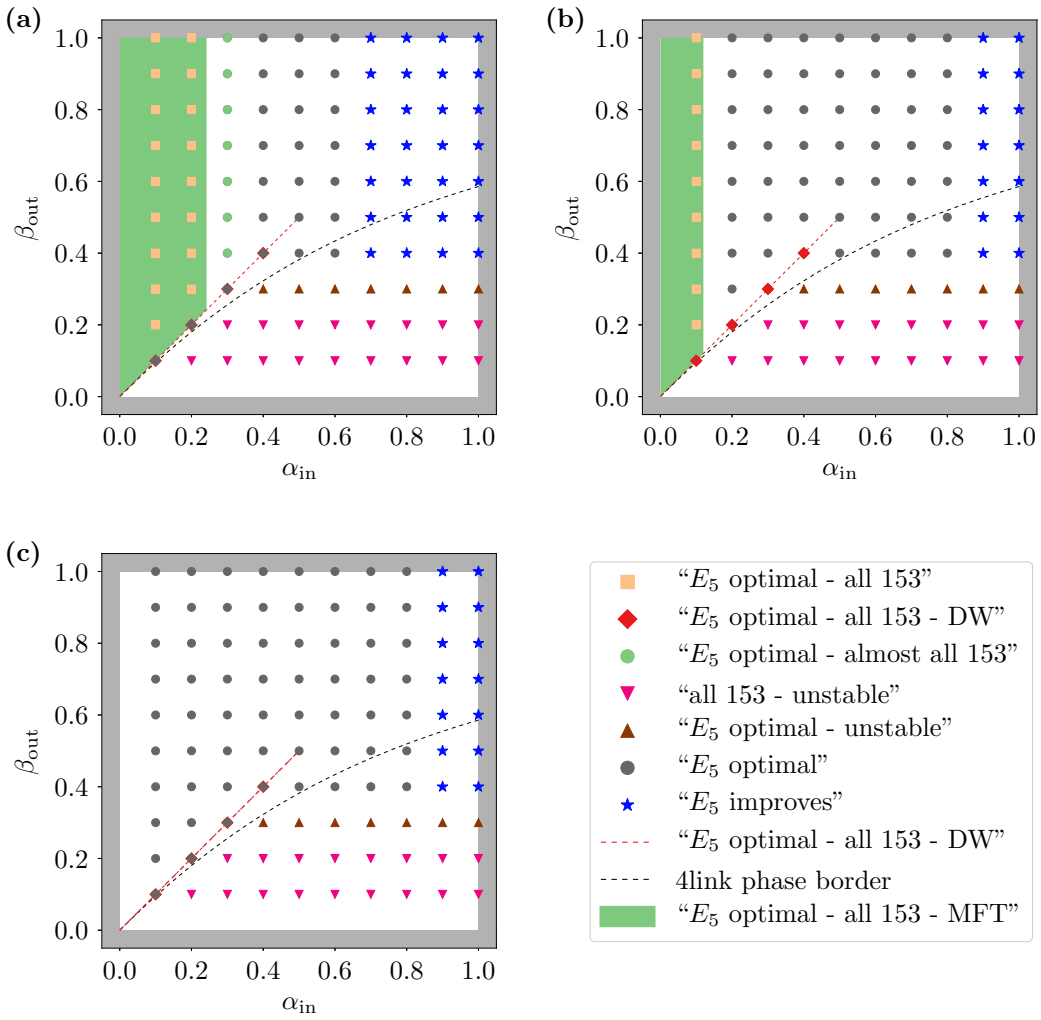

Figure 4.20. Phase diagrams of Braess' network with open boundary conditions, random-sequential updates and turning probabilities and edge lengths $L_1 = L_3 = 100$, $L_2 = L_4 = 500$ and **(a)** $L_5 = 278$, i.e. $\hat{L}_{153}/\hat{L}_{14} = 0.8$, **(b)** $L_5 = 339$, i.e. $\hat{L}_{153}/\hat{L}_{14} = 0.9$, **(c)** $L_5 = 399$, i.e. $\hat{L}_{153}/\hat{L}_{14} = 1$. The phases depend on the outer entrance and exit rates α_{in} and β_{out}. Monte Carlo simulations were performed on a 0.1 grid of the rates-landscape. The phases that were found are denoted by the symbols as given in the legend in the lower right part of the figure. Along the dotted red line an "all 153" phase with domain walls on that route is possible. The black dotted line represents the 4link phase boundary as given by Equation (4.32) while the green area shows the region in which MFT predicts the system to be in an "E_5 optimal - all 153" phase.

small $\hat{L}_{153}/\hat{L}_{14}$. This is not surprising: it is predicted by MFT and is also intuitively very easy to understand. If route 153 is much shorter than the other two (old) routes and the exit rate is not very small, i.e. not forcing all routes into HD states, the travel time on route 153 will be shorter than on the other routes. As the route length ratio $\hat{L}_{153}/\hat{L}_{14}$ gets higher, the regions of the "E_5 optimal - all 153" phase get smaller and are restricted to low entrance rates. As the new route becomes as long as the old ones, $\hat{L}_{153}/\hat{L}_{14} = 1$, the phase is not present anymore.

On the line $\alpha_{\text{in}} = \beta_{\text{out}} < 0.5$ (marked as a red dotted line in the phase diagrams) the "all

153" strategy, and also strategies where only route 14 or 23 are used, lead to domain walls on this route. This is since only one route is used and the situation corresponds to a single TASEP segment with the rates such that it is on the phase transition or domain wall line (see Section 3.1.1.2). On this line a strategy with only one route used can be the user optimum and system optimum at the same time, i.e. be an "E_5 optimal (all 153 or all 14 or all 23)" state, but only on short time scales. If the domain wall position changes such that the HD region becomes too large, the travel time on the used route can actually become too large for this to be the optimum strategy. It turns out that in many instances on this line also different strategies leading to an "E_5 optimal" state were found.

In the case of $\hat{L}_{153}/\hat{L}_{14} = 0.6$ for $\alpha_{\text{in}} \geq 0.5$ and $\beta_{\text{out}} \geq 0.5$ the system is in an "E_5 optimal" phase. Still the user optimum strategy is very close to the all 153 strategy: $\gamma > 0.95$ and $\delta < 0.05$. This is why in that region the phase was marked specifically to be "E_5 optimal (almost all 153)", marked by green •'s.

Independent of the route length ratio, the "all 153 - unstable" phase is present for small exit rates $\beta_{\text{out}} < \alpha_{\text{in}}$ and $\beta_{\text{out}} \leq 0.3$ (marked by purple ▼'s). This phase and the reasons for its occurrence were described in some detail in the previous subsection.

For route length ratios $\hat{L}_{153}/\hat{L}_{14} \geq 0.5$ also the "E_5 optimal -unstable" state is found (marked by brown ▲'s). As the "all 153 - unstable" it is also found for exit rates $\beta_{\text{out}} < \alpha_{\text{in}}$ and for $\beta_{\text{out}} = 0.3$ or $\beta_{\text{out}} = 0.4$.

In the regions of the phase diagram with $\beta_{\text{out}} > \alpha_{\text{in}}$ or $\beta_{\text{out}} > 0.4$ the phase diagram is either dominated by the "E_5 optimal - all 153" phase as described above or by the "E_5 optimal" (marked by gray •'s) phase. Only for $\hat{L}_{153}/\hat{L}_{14} \geq 0.9$ and $\alpha_{\text{in}} > 0.6$ the "E_5 improves" (marked by blue ⋆'s) phase is also found. In the found "E_5 improves" phases the maximum travel time in the system optimum is most times only slightly lower than that of the user optimum. The "E_5 improves" phases are thus all very close to "E_5 optimal" phases.

Summarizing one can see that no Braess phase, neither the "Braess 1" nor the "Braess 2" phase, is found in the open boundary system for the given route lengths. As explained in the previous Section one could argue that in a system with intelligent drivers the "all 153 - unstable" and the "E_5 optimal -unstable" phases could lead to Braess like behaviour. Still no 'pure' Braess phases are present (pure in the sense of a single strategy with fixed turning probabilities).

One has to note that the open boundary conditions lead to a different behaviour than what was first described by Braess. In the original Braess model the user optimum performances of networks before and after addition of a network edge were compared for the same demand (i.e. same total number of particles in the system). With open boundaries, for the same outer entrance and exit rates, different strategies lead to different numbers of particles in the system. This is shown in Figure 4.18 and also in Appendix A.1.3. Thus one cannot really compare the open and periodic boundary conditions. Nevertheless the open boundary system was analysed to check whether the Braess paradox in the sense that user optimum travel times can go up after adding a new road – independent of the total number of network users – can be found. This was not the case, except in the "all 153 - unstable" and the "E_5

optimal -unstable" phases, in which no user optima exist and one could argue that real selfish drivers would drive the system with the new road into states with higher travel times than in the system without the new road. In all other phases the new road always influences the system positively with respect to travel times.

Example landscapes and density profiles of all observed states are presented in Appendix A.1.3.

4.5 Parallel Updates and Periodic Boundary Conditions

In this section some important characteristics of Braess' network of TASEPs with parallel dynamics are presented. The presented results were obtained by Leonard Fischer during his Master's thesis [114] which he conducted under A. Schadschneider's and my supervision.

Before briefly summarizing some of the main results which are of interest for this thesis, the main characteristics of single TASEP segments employing parallel update schemes and their differences to TASEPs with random-sequential updates are recapitulated.

4.5.1 Main Characteristics of TASEPs with Parallel Dynamics

As already hinted in Section 3.1 there are many different update schemes for TASEPs while the two most widely used are the random-sequential and the parallel update schemes. In the random-sequential update scheme one of all available sites is picked randomly and then this site is updated. After as many of those single site updates as there are sites in the system a time step is complete. Aside from the present Section, all results in connection to TASEP in this thesis refer to TASEPs employing random-sequential dynamics.

In the parallel update procedure all sites of the TASEP are updated at the same time: if a site is occupied and the next site is empty a particle can jump forward with probability p. One of these update steps is then one *discrete* time step. The hopping rate p was set to be 1 in all results presented on random-sequential updates, since in that update procedure a $p < 1$ just corresponds to rescaling the time steps. In the parallel case, p is more important in the sense that for $p = 1$ the dynamics inside a TASEP segment becomes deterministic. This is a big difference to the random-sequential update case in which the system is always stochastic. To introduce stochasticity into the analysis of the system with parallel updates, cases with $p < 1$ have to be implemented. Variables corresponding to the parallel update procedure will be marked with a "par."-superscript from here on.

In the following some important characteristics of TASEPs with parallel updates are summarized. For a more comprehensive description of TASEPs with parallel updates the reader is e.g. referred to [35].

4.5.1.1 Periodic Boundary Conditions

In a single TASEP segment with parallel updates and periodic boundary conditions the stationary state density profile is flat with the density of all sites i being equal to the global density:

$$\rho^{\text{par.}}_{\text{PBC}}(i) = \rho^{\text{par.}}_{\text{PBC}} = \rho^{\text{par.}}_{\text{PBC,global}} = \frac{M}{L}, \tag{4.37}$$

with M being the total number of particles in the system and L the total number of sites of the TASEP segment. The flat density profile is also observed in TASEPs with periodic boundary conditions and random-sequential updates.

Due to additional correlations, the local current takes a different form when employing

parallel updates,

$$J^{\text{par.}}_{\text{PBC}}(i) = \frac{1}{2}\left(1 - \sqrt{1 - 4p\rho^{\text{par.}}_{\text{PBC}}(1-\rho^{\text{par.}}_{\text{PBC}})}\right), \tag{4.38}$$

which is slightly more complicated than the local current with random-sequential updates (Equation (3.1) in connection with Equation (3.2)).

The travel time of a periodic boundary TASEP with parallel update thus is

$$T^{\text{par.}}_{\text{PBC}}(\rho^{\text{par.}}_{\text{PBC}}) = \frac{\rho^{\text{par.}}_{\text{PBC}} L}{J^{\text{par.}}_{\text{PBC}}} = \frac{2\rho^{\text{par.}}_{\text{PBC}} L}{1 - \sqrt{1 - 4p\rho^{\text{par.}}_{\text{PBC}}(1-\rho^{\text{par.}}_{\text{PBC}})}}. \tag{4.39}$$

A comparison of the fundamental diagrams and the travel time functions for the random-sequential (for $p = 1$) and parallel updates for various values of p are shown in Figure 4.21.

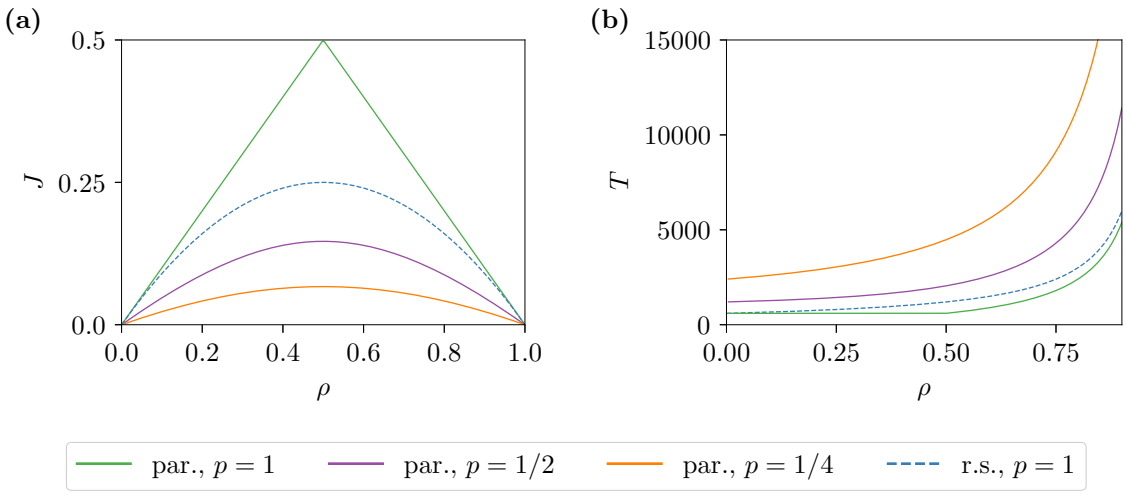

Figure 4.21. A comparison of fundamental diagrams (Part **(a)**) and travel time functions (Part **(b)**) for random-sequential (r.s.) and parallel update for various values of hopping probability p. The travel times T are shown for a TASEP of length $L = 600$. One can clearly see that the deterministic case, i.e. parallel updates with $p = 1$, leads to different genral behaviours as the fundamental diagram takes a triangular shape and the travel time is constant for densities $0 < \rho < 1/2$.

The general shapes of the fundamental diagrams and the travel time functions for the case of parallel updates are similar to those in the random-sequential update case. The different nature of the deterministic case (parallel updates, $p = 1$) can be seen in both parts of Figure 4.21.

4.5.1.2 Open Boundary Conditions

As for random-sequential updates, a TASEP segment with open boundary conditions and parallel update procedure can also be solved analytically [131, 132]. The first site of an open boundary TASEP is on its left connected to an entrance reservoir which feeds onto site 1 with the entrance probability α. The last site, site L, is on its right connected to an exit reservoir which is empty with exit probability β. As in the random-sequential case, three

distinct phases can develop in the parallely updated TASEP, depending on the entrance and exit rates. The main features, i.e. the bulk densities $\rho_{L/2}$ and the currents J, of these three phases are summarized in Table 4.3. In this table also the corresponding values for random-sequential dynamics are shown for comparison.

Table 4.3. Some important characteristics of the phases occurring in the open boundary TASEP. The values of the currents J, the bulk densities $\rho_{L/2}$ and the critical rates α_c, β_c in the low density (LD), high density (HD) and maximum current (MC) phases are given both for random-sequential and parallel updates.

Phase	rand.-seq. update	parallel update
LD-phases	$J = \alpha(1-\alpha/p)$ $\rho_{L/2} = \alpha$	$J = \frac{\alpha(p-\alpha)}{p-\alpha^2}$ $\rho_{L/2} = \frac{\alpha(1-\alpha)}{p-\alpha^2}$
HD-phases	$J = \beta(1-\beta/p)$ $\rho_{L/2} = 1-\beta$	$J = \frac{\beta(p-\beta)}{p-\beta^2}$ $\rho_{L/2} = \frac{p-\beta}{p-\beta^2}$
MC-phase	$J = \frac{p}{4}$ $\rho_{L/2} = \frac{1}{2}$	$J = \frac{1-\sqrt{1-p}}{2}$ $\rho_{L/2} = \frac{1}{2}$
Critical Rates	$\alpha_c = \beta_c = \frac{p}{2}$	$\alpha_c = \beta_c = 1-\sqrt{1-p}$

The phase diagram of an open boundary TASEP with parallel update scheme is shown in Figure 4.22. The three main phases (LD, HD and MC) meet at the critical point which is located at $\alpha_c = \beta_c = 1-\sqrt{1-p}$. For ($\alpha < \beta,\ \beta < \alpha_c$) the system is an LD phase, for ($\beta < \alpha,\ \alpha < \beta_c$) the system is in an HD phase and for $\alpha,\ \beta < \alpha_c$ it is in an MC phase. The two main phases LD and HD are subdivided into two subphases which differ in the behaviour of their density profiles near the boundaries, the details of which are not of importance here.

On the phase border line between the LD and HD phases, $\alpha = \beta < \alpha_c$, domain walls separating a low density region on the left and a high density region on the right form – as in the random-sequential update case. This leads to the (long-term) average density profile being a straight line ascending from α to $1-\alpha$, while on short term the position of the sock diffuses to the system.

On the line

$$(1-\alpha)(1-\beta) = 1-p \tag{4.40}$$

flat density profiles form.

An important difference to the random-sequential update case is the fact that the MC phase disappers for $p = 1$.

The travel time in an open boundary condition TASEP with parallel update can as in the random-sequential update case be approximated by the formula for the travel time in a TASEP with periodic boundary conditions but with the density replaced by the bulk density according to Table 4.3:

$$T^{\text{par.}}_{\text{OBC}}(\alpha,\beta) = T^{\text{par.}}_{\text{PBC}}(\rho_{L/2}(\alpha,\beta)). \tag{4.41}$$

On the LD-HD phase border line there exist no short-term stable travel times as the travel time

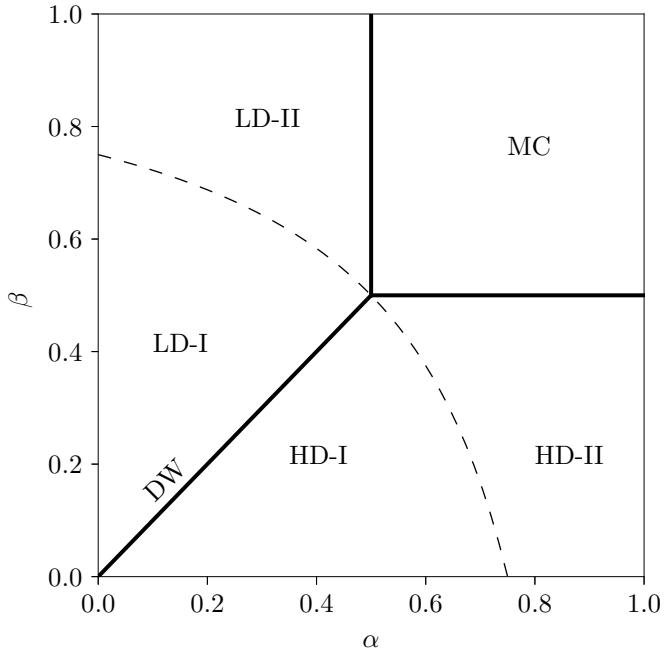

Figure 4.22. The phase diagram of a TASEP with open boundary conditions, parallel updates and hopping probability $p = 3/4$. Depending on entrance probability α and exit probability β the TASEP can be in distinct phases. The phase boundaries are marked by a solid black line. The two phases LD-I and LD-II are low density phases, phases HD-I and HD-II are high density phases. They all meet at the critical rate $\alpha_c = \beta_c = 1 - \sqrt{1-p}$. On the phase boundary between the LD and HD phases fluctuating domain walls (DW) form. On the dotted line given by Equation (4.40) the density profile becomes flat.

depends on the location of the domain wall for each particle entering the system. Averaged over long times, on this phase border line a bulk density of 1/2 can be assumed to approximate the travel time.

4.5.2 Braess' Network of TASEPs with Parallel Dynamics

When TASEPs with parallel update schemes are put together to form networks, conflict situations which do not exist for random-sequential updates can occur. Such conflicts occur if more than one TASEP segment feed onto one junction site.

Figure 4.23 shows Braess' network with periodic boundary conditions and the edges made of TASEPs. The two points with conflicts are marked by red ellipses. The conflict is sketched in Figure 4.24 **(a)** for two TASEP segments feeding onto junction j: if the last sites of both TASEPs are occupied and are then – as always in the parallel update scheme – to be updated at the same time, they cannot both jump onto j. This conflict has to be resolved by some rule determining the right of way. In [114], the main results of which are summarized here, traffic lights were employed

As sketched in Figure 4.24 **(b)** the right of way is given to the path which sees a green light. Which incoming route is given the right of way changes periodically.

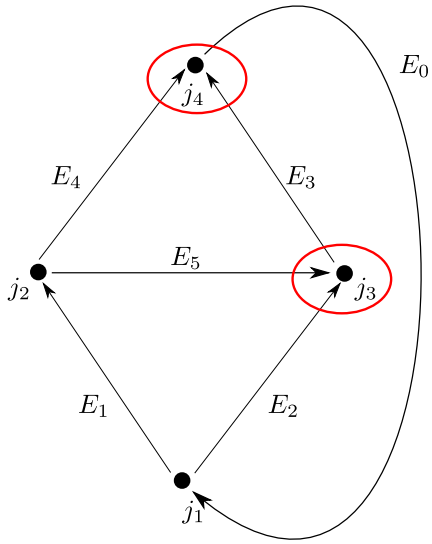

Figure 4.23. In Braess' network with the edges being TASEPs with parallel update scheme conflicts can occur on junctions j_3 and j_4 since they are fed by two TASEP segments.

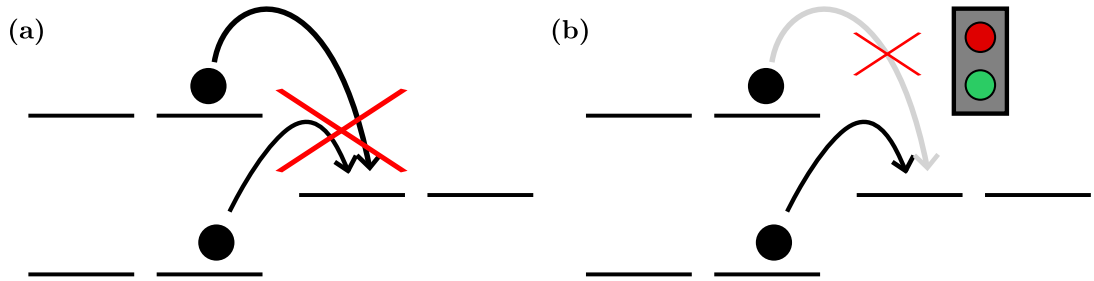

Figure 4.24. Part **(a)** shows how a conflict can arise in networks of TASEPs with parallel updates. If a (junction-) site is fed by more than one TASEP segment the situation in which multiple particles want to jump onto the same site can occur. Part **(b)** shows one possible way to resolve such a conflict: traffic lights give way to only one segment at a time. For the results presented here traffic light which switch the right of way between two incoming edges in an unbiased way periodically were employed.

In [114], in the 5link system on both junctions j_3 and j_4 traffic lights were employed with the green light periods of

$$f_{TL,j_3} = 50 \tag{4.42}$$

$$f_{TL,j_4} = 100. \tag{4.43}$$

This means that on j_3 the incoming edge E_2 has the right of way for 50 time steps, then the other incoming edge, edge E_5, has the right of way for 50 time steps. On j_4 the right of way switches between edges E_3 and E_4 every 100 time steps. In the 4link system the traffic light on j_3 is not present since due to E_5 not being there, there can be no more conflicts.

The edge lengths which were studied are the same as those that were studied employing

random-sequential updates:

$$L_1 = L_3 = 100 \tag{4.44}$$

$$L_2 = L_4 = 500, \tag{4.45}$$

and varying lengths of L_5 such that the route length ratio $\hat{L}_{153}/\hat{L}_{14}$ varies betwenn 0.4 and 1.0.

The network was studied for both route choice mechanisms, fixed route choices and turning probabilities (c.f. Section 3.2.1.1), with $p = 1$ and $p = 1/2$ for each case.

4.5.2.1 Possible Network Phases

Due to the traffic light at j_3, which is added together with E_5, the 4link system is not embedded in the 5link system. This is different to the random-sequential update case. In the latter there are no conflicts and thus no traffic lights are needed. The tree of possible states of the network (Figure 3.11) could be build from the starting point that $uo^{(4)} = so^{(4)}$ due to the symmetry of the 4link system. This symmetry still exists in the 4link system with parallel updates. With random-sequential updates one could then build the two branches $so^{(5)} = so^{(4)}$ with $T_{\max}(so^{(5)}) = T_{\max}(so^{(4)})$ and $so^{(5)} \neq so^{(4)}$ with $T_{\max}(so^{(5)}) < T_{\max}(so^{(4)})$.

The new traffic light for the parallel update version breaks the symmetry between routes 14 and 23 in the 5link system, even if road E_5 is not used. Thus there are now more than the two possible branches that emerge from the starting point. Figure 4.25 shows the possible phases that can arise in the system.

Without going into details about every phase, the phases can be divided into two groups: the first group consists of phases that exhibit Braess behaviour, i.e.

$$T_{\max}(uo^{(5)}) > T_{\max}(uo^{(4)}), \tag{4.46}$$

meaning that the user optimum travel time in the 5link system is higher than that of the 4link's user optimum. The names of those phases are given inside hexagonal boxes in Figure 4.25.

The other group consists of phases in which the user optimum travel times in the 5link are lower than in the 4ink:

$$T_{\max}(uo^{(5)}) < T_{\max}(uo^{(4)}). \tag{4.47}$$

The names of those phases are given inside boxes with rounded edges in Figure 4.25.

In the presented phase diagrams (Figures 4.27 and 4.30) the phases will also have differently shaped symbols to visualize if the user optimum travel times go up or down due to the addition of E_5.

The user optimum travel times can also be equal in both the 4link and 5link systems. This case was not found to occur very often.

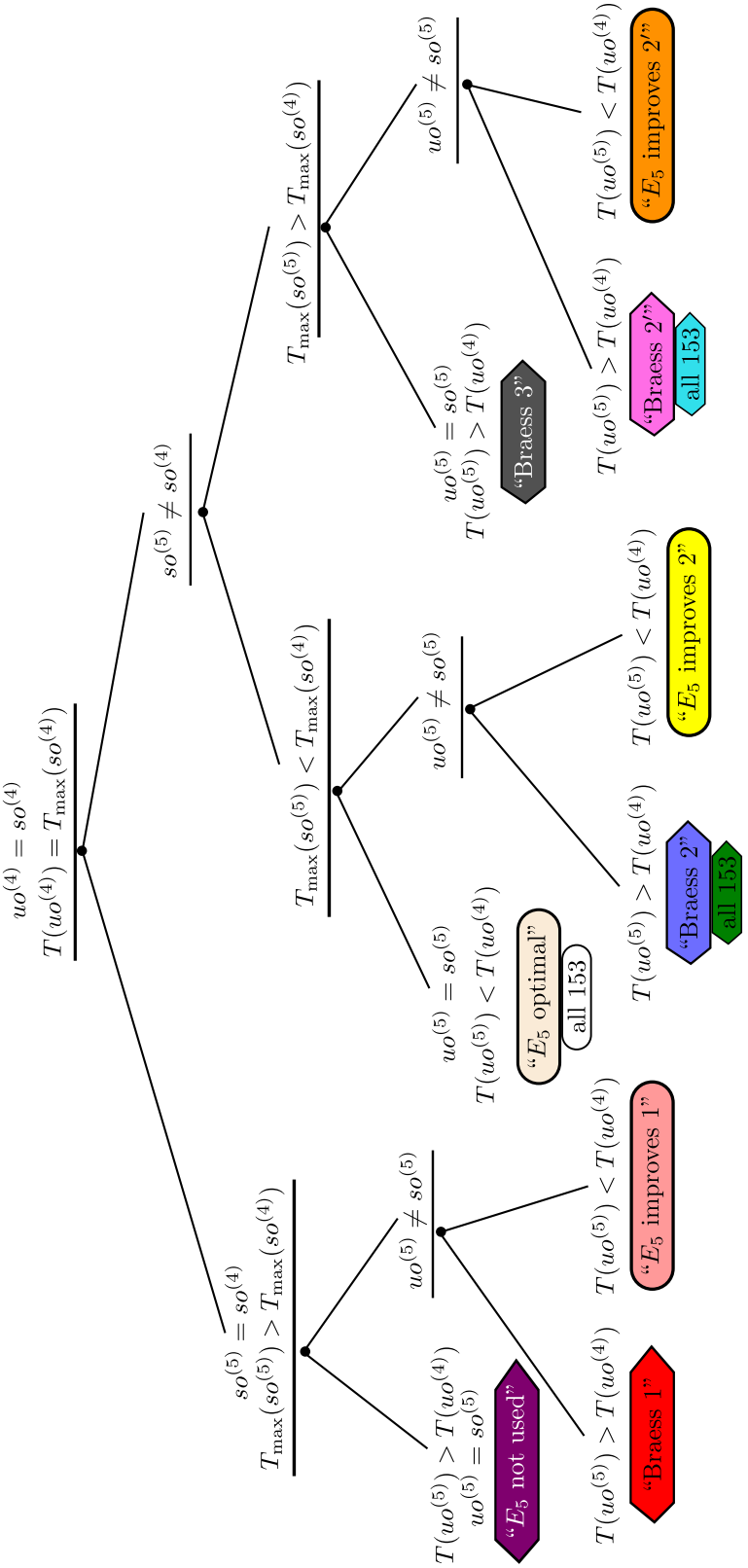

Figure 4.25. The tree of possible phases in the Braess network with parallel updates. Due to the traffic light at junction j_3 the symmetry in the 5link network is broken leading to more possible phases than in the network with random-sequential updates without traffic lights. Names of phases in which the user optimum travel time of the 5link system is higher than that of the 4link system are given inside hexagonally shaped boxes while the names of phases in which E_5 decreases user optimum travel times are given in boxes with rounded edges. For details the reader is referred to [114]. This figure is taken from [114]. The visual appearance has been slightly modified.

4.5.3 Results for Fixed Route Choices

In this section some results on Braess' network with parallel dynamics and fixed route choices are presented. For fixed route choices and the hopping rate $p = 1$ the dynamics is completely deterministic.

As in the the corresponding system with random-sequential dynamics, in the 4link system (short-term) stable travel times can be measured for all densities (cf. Section 4.1.2). This can be seen e.g. in the measured travel times and their associated standard deviations in the 4link system with $n_1^{(j_1)} = 0.5$ for various densities $\rho_{\text{global}}^{(4)} \in [0, 1[$. This is shown in Figure 4.26 for hopping probabilities $p = 1$ and $p = 1/2$. The standard deviation is below 5% throughout most of the density regime. Just for densities $\rho_{\text{global}}^{(4)} > 0.8$ it rises significantly. For $p = 1$ it almost goes up to 30% in some cases while it does not exceed 15% for $p = 1/2$. This indicates that the individual measurement values of the travel times do not stray far from their mean value for densities up to 0.8. The detailed analysis of the 4link system found in [114] is not repeated here.

Artefacts of the deterministic nature in the $p = 1$ case can be seen in the lower part of Figure 4.26 **(a)** for densities $\rho_{\text{global}}^{(4)} > 0.25$.

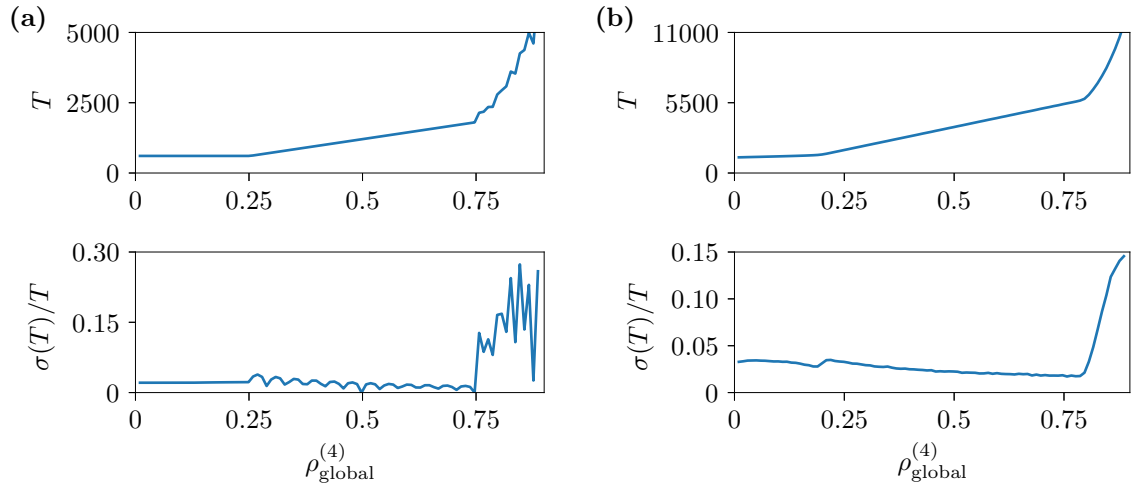

Figure 4.26. The travel time T (the mean value of T_{14} and T_{23}) and its relative standard deviation $\sigma(T)/T$ against the global density $\rho_{\text{global}}^{(4)}$ in the unbiased 4link system with parallel dynamics and fixed route choices for **(a)** $p = 1$ and **(b)** $p = 1/2$. One can see that the relative standard deviation is below 5% for all densities $\rho_{\text{global}}^{(4)} \lesssim 0.75$. For higher densities it grows to approximately 30% for $p = 1$ and up to 15% for $p = 1/2$. This implies that the individual measurements do not deviate strongly from their mean value for global densities lower than approximately 0.75. Short-term stable user/system optimum travel times are found throughout this whole density regime. These figures are taken from [114]. The visual appearances have been slightly modified.

Employing the method of sweeping the $T_{\max}$ and ΔT landscapes as described in Section 3.2.5.1, the user and system optima of the 5link system were found. For parameter sets for which true system and user optima were found their travel time values were compared to those of the 4link's user and system optima. According to the scheme shown in Figure 4.25 the phase diagram could be constructed.

Figure 4.27 shows the phase diagrams. In Figure 4.28, the ratios of the average travel times in the 5link's and 4link's user optimum travel times for hopping probabilities $p = 1$ and $p = 1/2$. These average travel times are given by the weighted averages (wav)

$$T_{\text{wav}}(uo^{(4)}) = \frac{n_{14}(uo^{(4)})}{M} T_{14}(uo^{(4)}) + \frac{n_{23}(uo^{(4)})}{M} T_{23}(uo^{(4)})$$
$$T_{\text{wav}}(uo^{(5)}) = \frac{n_{14}(uo^{(5)})}{M} T_{14}(uo^{(5)}) + \frac{n_{23}(uo^{(5)})}{M} T_{23}(uo^{(5)}) + \frac{n_{153}(uo^{(5)})}{M} T_{153}(uo^{(5)}).$$

The ratios can thus not be directly compared to those for random-sequential updates, as given in Figure 4.9 **(d)**, since in the latter $T_{\max}(uo^{(5)})/T_{\max}(uo^{(4)})$ were shown. This discrepancy is to slightly different approaches of Leonard Fischer's thesis and my thesis.

4.5.3.1 Hopping Probability $p = 1$

Figure 4.27 **(a)** shows the phase diagram for $p = 1$, i.e. for deterministic dynamics. In the region of the phase diagram with a blue background color true user optima, i.e. states with $\Delta T < 300$, were found. This region is present for $\rho^{(5)}_{\text{global}} \lesssim 0.3$ for $\hat{L}_{153}/\hat{L}_{14} \approx 0.4$ and for $\rho^{(5)}_{\text{global}} \lesssim 0.6$ for $\hat{L}_{153}/\hat{L}_{14} > 0.5$. This is very reminiscent of the phase diagram for random-sequential updates and fixed route choices (see Figure 4.8, note that therein the threshold was $\Delta T = 100$). As in the random-sequential case, for high global densities and sufficiently low route length ratios, strategies potentially being a user optimum get gridlocked.

A detailed analysis about which strategies can get gridlocked was not done in [114]. Thus it could be the case that some user optima were identified which have gridlocked stationary states (e.g. if the system was not evolved long enough to reach its stationary state while measuring). This is only expected around the boundary of $\Delta T < 300$.

One can observe that there is no region with clear boundaries and only instances of a single phase. This is why no distinctive phases (or phase-regions) can be deduced. The only clear phase-region that can be observed is the "E_5 optimal, all 153" phase which is present at low densities and low route length ratios. Another phase-like region, which contains some points of different states, is a region that is dominated by "Braess 1" states. This is present for all route length ratios and intermediate densities $0.3 \lesssim \rho^{(5)}_{\text{global}} \lesssim 0.6$.

A more clear understanding of the influence of E_5 on the system's performance when it is used by selfish drivers can be obtained when distinguishing of all the specific phases is omitted and just the ratio of the 5link user optimum travel time and the corresponding 4link user optimum (weighted average) travel times ($T_{\text{wav}}(uo^{(5)})/T_{\text{wav}}(uo^{(4)})$) is shown, as seen in Figure 4.28 **(a)**.

For low global densities and low route length ratios, i.e. in the "E_5 optimal, all 153" phase, the ratio is well below 1, indicating that the new road leads to much lower user optimum travel times here. In a small region $0.4 \lesssim \hat{L}_{153}/\hat{L}_{14} \lesssim 0.6$ and $0.1 \lesssim \rho^{(5)}_{\text{global}} \lesssim 0.3$ the ratio is well above 1 indicating that here a Braess-effect of significant amount is found. In most other parts of the phase diagram in which $\Delta T < 300$ the ratio is very close to 1, indicating that the new road does not significantly influence user optimum travel times.

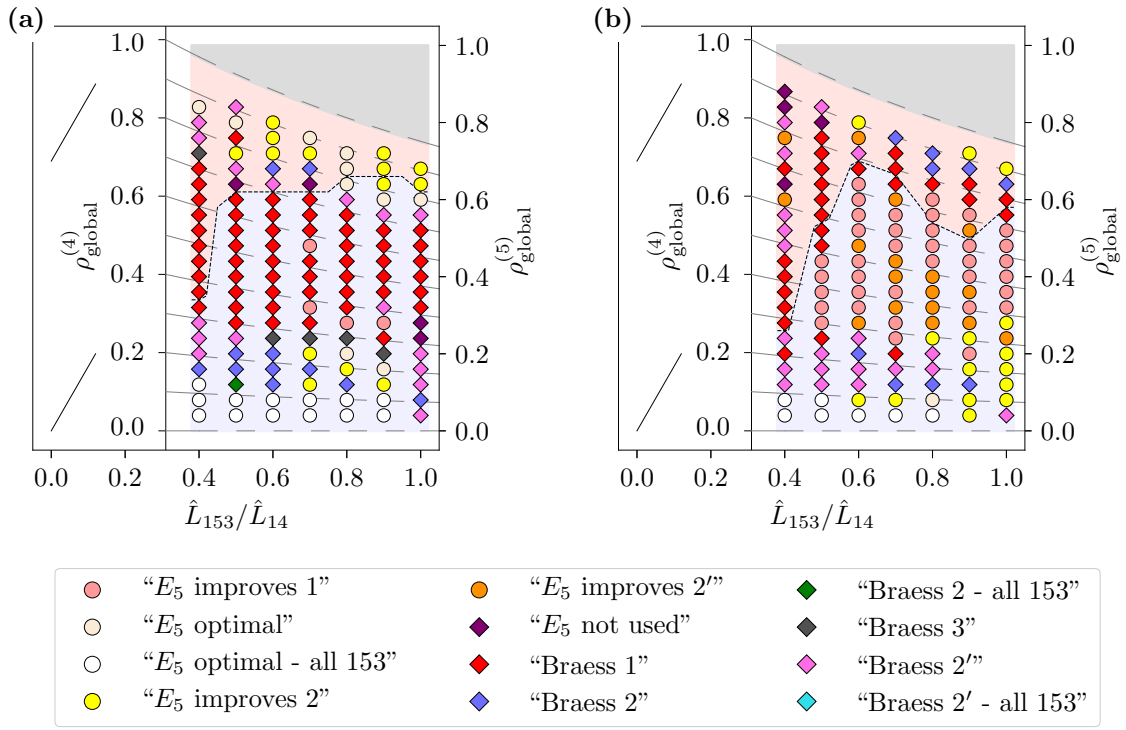

Figure 4.27. The phases diagrams for the Braess network of TASEPs with periodic boundary conditions, parallel updates, fixed route choices and $p = 1$ (Part **(a)**) and $p = 1/2$ (Part **(b)**) according to the classification scheme given in Figure 4.25. The shown results were obtained for $L_1 = L_3 = 100$, $L_2 = L_4 = 500$ and varying lengths of E_5 (resulting in the x-axes $\hat{L}_{153}/\hat{L}_{14}$) and M (resulting in the two y-axes $\rho^{(4)/(5)}_{\text{global}}$). In the parts with blue background real user optima with $\Delta T < 300$ were found. In the parts with red background $\Delta T > 300$ holds. No real phase regions could be identified except for an "E_5 optimal - all 153" phase found at low route length ratios and low densities. Phases in which the 5link's user optimum travel time exceed the 4link's user optimum travel time are marked by quadratic symbols, those in which the opposite is true by circular symbols. These figures are taken from [114]. The visual appearances have been slightly modified.

In the region were no real user optima exist the new road's influence is higher. Note, that in this region, the travel times in the closest candidate for a user optimum of the 5link network were used for the ratio. This means that the values of the ratio are not as meaningful here in the sense that if real drivers were using the system, the system would could end up in other, potentially totally gridlocked, states.

4.5.3.2 Hopping Probability $p = 0.5$

The phase diagram obtained for hopping probability $p = 1/2$, as an example for stochastic bulk dynamics, is shown in Figure 4.27 **(b)**. It shows even less distinct phase-regions than the phase diagram for $p = 1$. Except for the "E_5 optimal, all 153" phase for low route length ratios and low global densities there are no other regions that can be assigned to be of one single phase only.

The influence of E_5 becomes more clear when looking at the user optimum travel time ratio $T_{\text{wav}}(uo^{(5)})/T_{\text{wav}}(uo^{(4)})$, as shown in Figure 4.28 **(b)**.

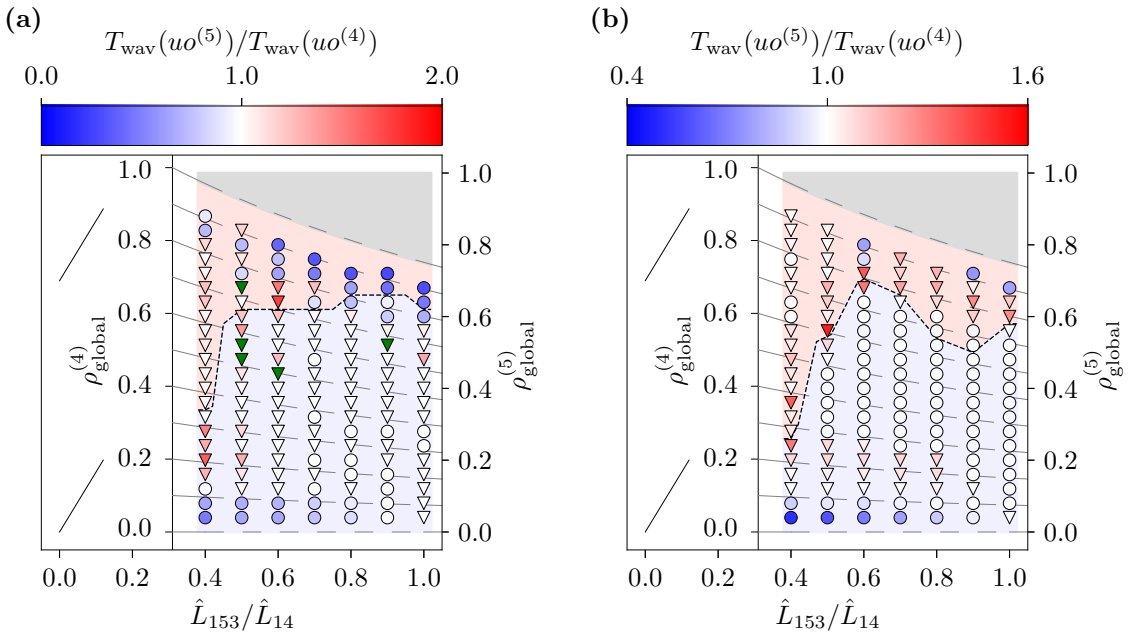

Figure 4.28. The ratio of the weighted averages of the 5link and 4link user optimum travel times for the Braess network of TASEPs with periodic boundary conditions, parallel updates, fixed route choices and $p = 1$ (Part **(a)**) and $p = 1/2$ (Part **(b)**). In the parts with blue background real user optima with $\Delta T < 300$ were found. In the parts with red background $\Delta T > 300$ holds. Circular markers (◯) represent values $T_{\mathrm{wav}}(uo^{(5)})/T_{\mathrm{wav}}(uo^{(4)}) \geq 1$, triangular markers (▽) represent values $T_{\mathrm{wav}}(uo^{(5)})/T_{\mathrm{wav}}(uo^{(4)}) > 1$. One can see that user optimum travel times are significantly lower in the 5link system in the "E_5 optimal - all 153" phase found at low route length ratios and low densities. For $0.4 \lesssim \hat{L}_{153}/\hat{L}_{14} \lesssim 0.6$ and $0.1 \lesssim \rho^{(5)}_{\mathrm{global}} \lesssim 0.3$ the ratio is significantly above 1 indicating that these are connected regions of the phase diagrams in which Braess-like behaviour occurs. In most other parts in which real user optima are found, the influence of the new road is not significant as the ratio is approximately 1. These figures are taken from [114]. The visual appearances have been slightly modified.

One can see that travel times in the 5link's user optimum are reduced significantly in the "E_5 optimal, all 153" phase. As for $p = 1$ there is a region in $0.4 \lesssim \hat{L}_{153}/\hat{L}_{14} \lesssim 0.8$ and $\rho^{(5)}_{\mathrm{global}} \approx 0.2$ in which travel times go up significantly due to the addition of E_5. In the other parts where $\Delta T < 300$ the ratio is approximately 1. It is for $p = 1/2$ in most parts a bit lower than 1 while it is slightly above 1 in most parts for $p = 1$.

4.5.4 Results for Turning Probabilities

Here some results for the system with parallel update scheme and turning probabilities are summarized. With turning probabilities governing the route choice mechanism, in a large intermediate density region ($0.25 \lesssim \rho^{(4)}_{\mathrm{global}}, \lesssim 0.8$) of the symmetric ($\gamma = 0.5$) 4link system fluctuating domain walls form on both routes 14 and 23. This behaviour also occurs for the random-sequential update scheme (cf. Section 4.2.2). Evidence of the domain walls which lead to short-term unstable travel times is found in the standard deviation of the measured travel time values as shown in Figure 4.29. One can see that in the density region $0.25 \lesssim \rho^{(4)}_{\mathrm{global}} \lesssim 0.8$ the standard deviation increases drastically to a maximum of approximately 30% for $p = 1$,

and even 45% for $p = 1/2$. This indicates that the individual measurements of the travel times deviate very strongly from their mean value, hinting at the existence of fluctuating domain walls. Further evidence that indeed domain walls are responsible for the high standard deviations is found in [114]. For our analyses which aim at describing the traffic situation that

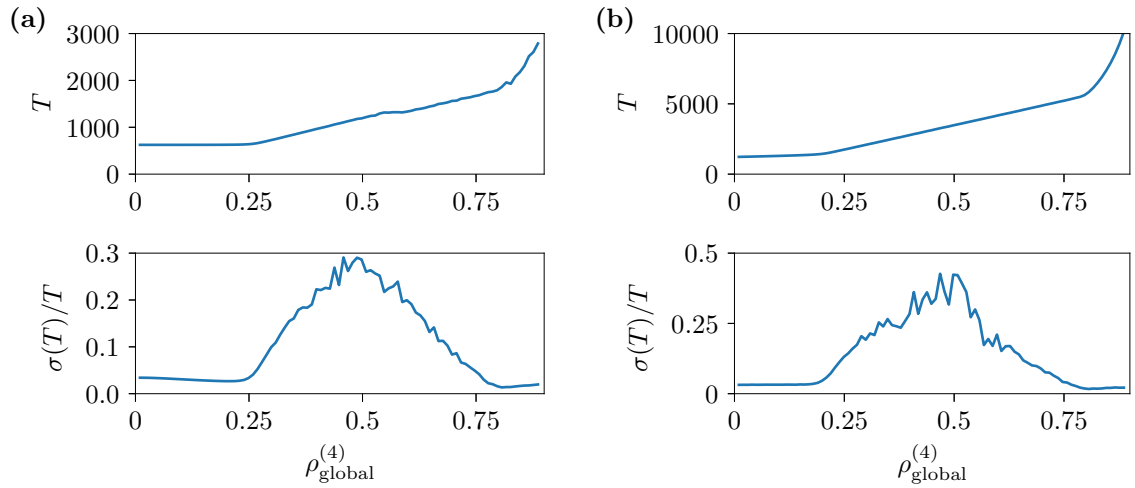

Figure 4.29. The travel time T (the mean value of T_{14} and T_{23}) and its relative standard deviation $\sigma(T)/T$ against the density $\rho^{(4)}_{\text{global}}$ in the unbiased 4link system with parallel dynamics and fixed route choices for **(a)** $p = 1$ and **(b)** $p = 1/2$. One can see that the relative standard deviation grows up to 30% ($p = 1$) and even 45% ($p = 1/2$) in the large intermediate density regime $0.25 \lesssim \rho^{(4)}_{\text{global}} \lesssim 0.8$. In this regime coupled fluctuating domain walls are found on both routes 14 and 23. No (short-term) stable user optimum travel times exist in this regime. These figures are taken from [114]. The visual appearances have been slightly modified.

individual cars would face in the system we conclude that in these density regions there are no stable user optimum travel times in the 4link system and hence they cannot be compared to user optimum travel times in the 5link systems.

4.5.4.1 Hopping Probabilities $p = 1$ and $p = 1/2$

Figures 4.30 **(a)** and **(b)** and Figures 4.31 **(a)** and **(b)** show the obtained phase diagrams and user optimum travel time ratios for $p = 1$ and $p = 1/2$ respectively. In all four figures the region in which no short-term stable 4link user optima exist, i.e. $0.25 \lesssim \rho^{(4)}_{\text{global}}, \lesssim 0.8$, is marked by a hatching in the background. Furthermore, in all four figures the regions in which real 5link user optima exist, i.e. strategies with $\Delta T < 100$, exist are marked by a blue background. Regions in which such real user optima could not be found in the 5link are marked by a red background.

For both jumping probabilities the phase diagrams (Figures 4.30) do not show any distinct phase-regions except for the "E_5 optimal, all 153" phase which is present at route length ratios $\hat{L}_{153}/\hat{L}_{14} \lesssim 0/8$ and low global densities $\rho^{(5)}_{\text{global}} \lesssim 0.1$. Distinct phases could not be identified in any other region.

For the case of turning probabilities the weighted averages of the user optimum travel times

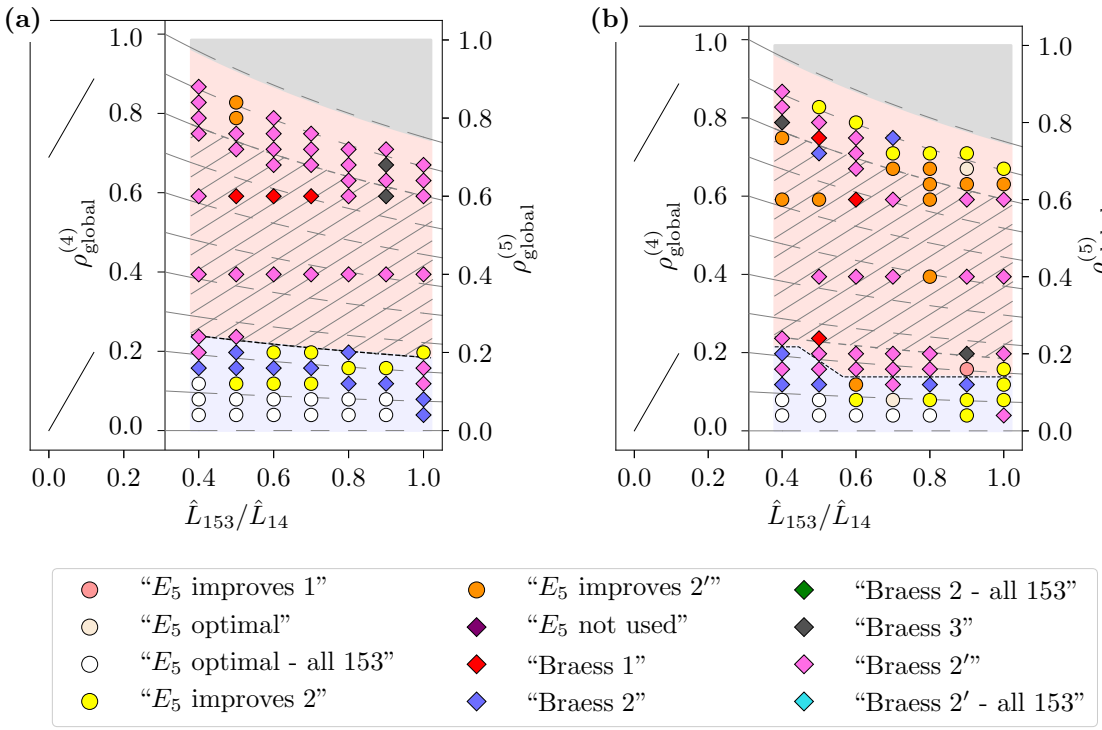

Figure 4.30. The phases diagrams for the Braess network of TASEPs with periodic boundary conditions, parallel updates, turning probabilities and $p = 1$ (Part **(a)**) and $p = 1/2$ (Part **(b)**) according to the classification scheme given in Figure 4.25. The shown results were obtained for $L_1 = L_3 = 100$, $L_2 = L_4 = 500$ and varying lengths of E_5 (resulting in the x-axes $\hat{L}_{153}/\hat{L}_{14}$) and M (resulting in the two y-axes $\rho^{(4)/(5)}_{\text{global}}$). In the parts with blue background real user optima with $\Delta T < 100$ were found. In the parts with red background $\Delta T > 100$ holds. The density regime in which no real user optima exist in the 4link system is marked by a hatching. Except for the "E_5 optimal - all 153" phase at low route length ratios and densities no connected phase regions could be identified. These figures are taken from [114]. The visual appearances have been slightly modified.

are defined as

$$T_{\text{wav}}(uo^{(4)}) = \gamma(uo^{(4)})T_{14}(uo^{(4)}) + (1 - \gamma(uo^{(4)}))T_{23}(uo^{(4)}) \tag{4.48}$$

$$T_{\text{wav}}(uo^{(5)}) = \gamma(uo^{(4)})\delta(uo^{(4)})T_{14}(uo^{(4)}) + (1 - \gamma(uo^{(4)}))T_{23}(uo^{(4)}) \tag{4.49}$$

$$+ \gamma(uo^{(4)})(1 - \delta(uo^{(4)}))T_{153}(uo^{(4)}). \tag{4.50}$$

From the figures showing the user optimum travel time ratio $T_{\text{wav}}(uo^{(5)})/T_{\text{wav}}(uo^{(4)})$ (Figures 4.31), one can obtain some more insights of the new road onto the network's performance inside the regions where real user optima exist. First one can see the user optimum is influenced most significantly – reduced by up to 1/2 – in the "E_5 optimal, all 153" phase. For small route length ratios and global densities in between the aforementioned phase and the region were no 4link optima exist the user optima travel times are increased due to the addition of E_5. In the remaining parts with real user optima the user optimum travel time ratio is approximately 1 which means that the influence of the new road on travel times is negligible.

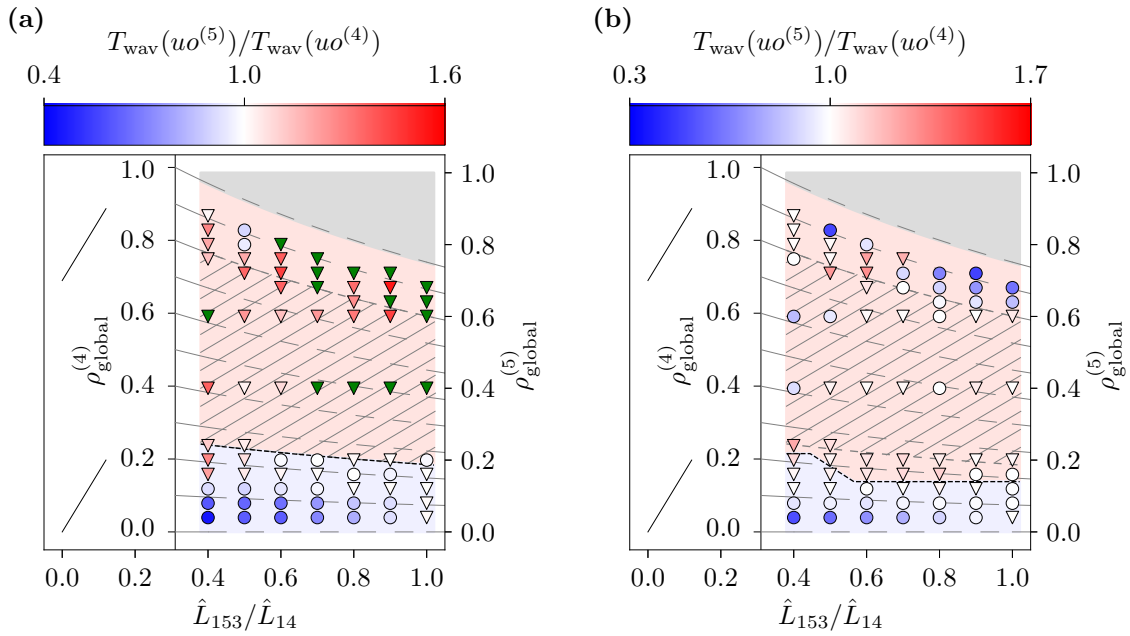

Figure 4.31. The ratio of the weighted averages of the 5link and 4link user optimum travel times for the Braess network of TASEPs with periodic boundary conditions, parallel updates, turning probabilities and $p = 1$ (Part **(a)**) and $p = 1/2$ (Part **(b)**). In the parts with blue background real user optima with $\Delta T < 100$ were found. In the parts with red background $\Delta T > 100$ holds. Circular markers (◯) represent values $T_{\mathrm{wav}}(uo^{(5)})/T_{\mathrm{wav}}(uo^{(4)}) \geq 1$, triangular markers (▽) represent values $T_{\mathrm{wav}}(uo^{(5)})/T_{\mathrm{wav}}(uo^{(4)}) > 1$. The density regime in which no real user optima exist in the 4link system is marked by a hatching. One can see that user optimum are significantly lower in the system with E_5 in the "E_5 optimal - all 153" phase found at low route length ratios and low densities. Well defined phase regions could be identified in any other parts. These figures are taken from [114]. The visual appearances have been slightly modified.

No clear structures in the sense of regions where the ratio is all positive or all negative are found in the regions without real user optima.

4.5.5 Summary of Results

Braess' network with periodic boundary conditions, the edges formed by TASEPs with parallel update scheme and two different route choice mechanisms was examined in Leonard Fischer's Master's thesis [114] and some results were shortly summarized here. The parallel update scheme leads to potential conflicts at the two junctions j_3 and j_4 which are both fed by two incoming TASEP segments. To resolve these conflicts, two traffic lights were introduced. Throughout the analysis the green phases were kept at a constant periodicity.

The traffic light at j_3 is only present in the 5link system. This has the consequence that the 4link system is not anymore exactly included in the 5link system. Thus the tree of possible phases that can arise when comparing the 4link and 5link systems gets more complicated than in the random-sequential update version of the system.

Many characteristics that are present in the random-sequential version are also found in the parallel update version. If route choices are governed by turning probabilities, meaning

that all particles are treated as equal without personal fixed strategies, a large intermediate density region of the 4link network is governed by fluctuating domain walls. If all particles keep their personal fixed route choices, these domain walls are not found. For both route choice processes in the 5link systems real user optima can be detected only in in parts of the phase space. These regions are located at global densities below certain thresholds. Due to the absence of domain walls, for the case of fixed route choices the parts with real user optima are present up to higher densities.

Opposed to the random-sequential update versions, the phase diagrams cannot be divided into phase regions with well defined phase borders. Only the simple "E_5 optimal - all 153" phase can be clearly identified in all examined cases with parallel updates. The fact that no other distinct phase regions could be identified could be caused by the branching of the tree of possible phases being too fine.

The Braess paradox can be observed in the parallely updated versions of the network in a distinct region at intermediate densities and low route length ratios. In this region the travel times in the user optimum increase after the addition of the new road. This phase region is not comprised only of one single phase, but instead different Braess-phases are observed inside that region. Instances of Braess-phases are also found at other positions throughout the phase diagram, though not in other connected regions.

The parallel update version of the Braess' network is more complicated to treat than the random-sequential update versions. If traffic lights are used, as done here, with the traffic light phases two additional parameters are introduced into the system. Those parameters have major influence on travel times measured in the systems. Throughout the analyses presented here these parameters were kept constant. Repeating measurements for different values of these traffic light phases could yield different results.

To get a simpler version of the parallely updated versions one could introduce different rules for the right of way. If at least at junction j_3 a 'right over left' rule was established the 4link system would again be included in the 5link system reducing the number of possible states and thus making the analysis much easier.

In his Master's thesis Leonard Fischer also studied one version of the Braess network with Nagel-Schreckenberg dynamics [106]. These are only first results based on Nage-Schreckenberg dynamics and do not yield any quantifiable information, which is why they not repeated here. An extensive analysis of the network with Nagel-Schreckenberg dynamics could be an interesting future project.

5 The Braess Network of TASEPs with Intelligent Particles

This chapter answers the question if user optima are reached in Braess' network if particles make their own individual route choice decisions based upon different types of information. It thus addresses the second of the two main issues about what can be improved in Braess' model, which were laid out in Section 2.2.5.

In Sections 4.1 to 4.5 it was shown that Braess' paradox occurs in the Braess network of TASEPs (with the exception of the open boundary version of the network in which the paradox is not directly observable, as discussed in Section 4.4). In those analyses the global strategies, i.e. how all particles choose their routes, are tuned externally: either the turning probabilities which are obeyed by all particles, or all individual particles' personal strategies are set to certain values. Then these values are varied to find which specific combinations lead to user optima. By comparing travel times in the obtained user optima of the 4link and corresponding 5link systems it can be inferred if Braess' paradox occurs.

In the present chapter a decision making algorithm which is used by all individual particles is implemented. The particles then choose their routes 'intelligently' instead of being assigned to routes externally. The effects of the intelligent decision makings can be analysed, building on the information about existing user optima that was obtained in the previous chapter.

The individual particles are provided with three different types of information, the definitions of which were given in Section 2.4.1, which are the bases for their decisions: public historical information, public predictive information and personal historical information. It is shown that two types of information drive the networks into their user optima: the Braess paradox occurs in TASEP networks with such intelligent particles.

After analysing the effects of these three different types of information separately, the effects of a combination of personal historical and public predictive information is studied. This combination of information types can also be found in many modern-day real road networks. Braess' paradox is shown to also occur in this setting.

5.1 Decision Making Algorithm with Three Types of Information

The decision making algorithm is implemented to work on the Braess network with periodic boundary conditions as shown in Figure 3.9 **(a)**. The network with periodic boundary conditions is chosen since in this version all individual particles stay in the system. Hence, personal information (i.e. information available to individual particles from their own memories) can

be implemented.

The systems are always initialized by placing a fixed number of particles M randomly on the routes. Each particle is additionally assigned an initial pure strategy (to take either route 14, 23 or 153) randomly. For two types of information the system then has to undergo a relaxation process, which will be explained in the following sections corresponding to these specific types of information.

Independent of the type of information available to the particles, once the system is initialized, route choice decisions are made before beginning each new round[1] and also on junctions j_1 and j_2. Each particle has information about travel times on all three routes denoted as $T_{14,\text{info}}$, $T_{23,\text{info}}$ and $T_{153,\text{info}}$ for routes 14, 23 and 153, respectively.

Between finishing one round and beginning the next round, i.e. after jumping onto E_0 and before jumping to j_1, each particle decides upon the strategy for the next round as described in Algorithm 5.1. Two parameters are introduced.

1. The probability p_{info} with which route choice decisions are made based upon the available information. With probability $1 - p_{\text{info}}$ a random route is chosen.

2. The travel time difference threshold $\Delta T_{\text{thres.}}$. For travel time differences ΔT up to this value it is assumed that particles do not care about potential travel time savings. The particles thus act boundedly rational (see Section 2.1).

Algorithm 5.1: The decision making of each particle before starting a new round, used as soon as values for $T_{i,\text{info}}$ are available for all routes i. The algorithm is shown for the 5link network. In the 4link network route 153 is not available and ΔT is reduced accordingly.

```
if (Random number between 0 and 1 smaller than p_info) then
    Calculate ΔT = |T_14,info − T_23,info| + |T_14,info − T_153,info| + |T_23,info − T_153,info|;
    if (ΔT > ΔT_thres.) then
        Switch to route with smallest T_info;
    end
    else
        Stay on same route;
    end
end
else
    Choose a route randomly with equal probability;
end
```

The strategy of each particle is thus updated *before* beginning each new round according to Algorithm 5.1. *During* one round there can also be individual strategy changes if a particle 'sits' on junction j_1 or j_2 and is not able to jump to its desired target site. This could e.g. be the case if a particle chose to take route 23: if that particle sits on j_1 and the first site on E_2

[1] A "round" refers to one complete trip that starts when a particle sits on j_1 and finishes when the particle jumps out of j_4.

is occupied, after some waiting time the particle will change its strategy in favour of route 14 or route 153. In Algorithm 5.2 it is described how these decisions during individual rounds are implemented.

Algorithm 5.2: The algorithm for decisions made during one round for particles sitting on junction j_1 if their target site is occupied. The algorithm shown here is used in the 4link system.

```
   // (The variable tw is the time the particle has already waited on j_1
      since its first attempt of jumping to its target site.)
 1 if (intended route is route 14) then
 2 |   if (T_14,info < T_23,info) then
 3 |   |   if (tw > (T_23,info − T_14,info) · κ_j1thres.) then
 4 |   |   |   switch to route 23
 5 |   |   end
 6 |   end
 7 |   else
 8 |   |   switch to route 23 immediately
 9 |   end
10 end
11 else if (intended route is route 23) then
12 |   if (T_23,info < T_14,info) then
13 |   |   if (tw > (T_14,info − T_23,info) · κ_j1thres.) then
14 |   |   |   switch to route 14
15 |   |   end
16 |   end
17 |   else
18 |   |   switch to route 14 immediately
19 |   end
20 end
```

The algorithms for decisions on the junctions introduce the following two parameters.

1. The parameter $\kappa_{j_1\text{thres.}}$. If a particle decides to take route i based on the information that it has the lowest travel time ($T_{i,\text{info}}$ is lower than $T_{j,\text{info}}$, with $j \neq i$) and cannot jump immediately onto its desired route i, it waits for $\kappa_{j_1\text{thres.}}$ multiplied by the estimated saved travel time on route i.

2. The parameter $\kappa_{j_2\text{thres.}}$ for decisions on j_2 in the 5link system, which is defined equivalently to $\kappa_{j_1\text{thres.}}$.

Basically, the junction algorithms say that, if before starting the present round, a particle decided *not* to take the route with the lowest expected travel time (due to a random decision that happened with probability $1-p_{\text{info}}$, as in lines 10 to 12 in Algorithm 5.1) and the desired target route's first site is blocked, it will immediately re-decide for another route. If a particle chose the route with the lowest expected travel time and the first site of its target route is blocked it will wait for a certain fraction $\kappa_{j_1\text{thres.}}$ of the estimated saved travel time before switching to a different route.

In the 5link network the algorithm for decisions on j_1 is slightly more complicated: when changing away from route 23, there are two possible alternatives to choose from. The decision making during a round at junction j_2 in the 5link system works analogously to Algorithm 5.2. The two algorithms used in the 5link system are shown in Appendix A.3.

Algorithms 5.1 and 5.2 are implemented for each of the three types of information explained in the following subsections. The types of information determine how the $T_{i,\text{info}}$ are obtained.

5.1.1 Public Historical Information

The first type of available information that is implemented is public historical information: each time any particle finishes a round the travel time of the used route is made available for all particles. These travel time values are used as $T_{14,\text{info}}$, $T_{23,\text{info}}$ and $T_{153,\text{info}}$ for the decision makings of all particles based on Algorithms 5.1 and 5.2.

When using this type of information a short relaxation period is needed. The simulation is started with all particles following randomly assigned strategies. They continue to follow these strategies until each route has been used at least once and thus travel time information is available for all routes. From this point in time onwards particles decide their new strategies based on the available information.

As summarized in Section 2.4 and detailed in the references cited therein, this type of information has been shown to lead to overreactions and thus to oscillations in a symmetric two route network: it is already well established that user optima are not realized by providing this type of information. It was implemented here to confirm these observations in the 4link network (which is also a symmetric two route network) and to test how it influences route choices and resulting travel times in the 5link network.

5.1.2 Public Predictive Information

This type of information provides estimated future travel times[2] of all routes to all particles. The predicted travel times are based on the current state of the network or, more precisely, on the current positions of all particles.

To provide predicted travel times at any point in time, the numbers of particles on each of the five edges E_1 to E_5 (or E_1 to E_4 in the 4link network) are added up[3]. If there are n_i particles on edge E_i, a density $\rho_i = n_i/L_i$ for this edge is calculated. Employing Equation (3.4) for the travel time of a periodic TASEP an approximation of the travel time $T_{i,\text{app}}$ on edge E_i is calculated:

$$T_{i,\text{app}} = \frac{L_i}{1-\rho_i}. \tag{5.1}$$

Even though Equation (3.4) provides fairly accurate approximations of the steady-state travel times of periodic TASEPs, in the present case it is just a rough approximation. This is due

[2]The term "future travel times" refers to the fact that the travel time of a journey starting at any moment in time reaches into the future from this point in time. It could also be called present travel times.

[3]In real networks such data is crowdsourced and used in navigational apps (see Section 2.4).

to the fact that during the systems evolution the density on the edge may keep changing as particles re-decide their strategies. The edge does not reach a steady state with the present density.

From the approximations of the travel times of all edges the estimated route travel times are calculated as

$$T_{14,\text{info}} = T_{1,\text{app}} + T_{4,\text{app}}, \tag{5.2}$$

$$T_{23,\text{info}} = T_{2,\text{app}} + T_{3,\text{app}}, \tag{5.3}$$

$$T_{153,\text{info}} = T_{1,\text{app}} + T_{5,\text{app}} + T_{3,\text{app}}, \tag{5.4}$$

and decision making is then based on Algorithms 5.1 and 5.2, employing this information. Each time any particle finishes one round, the $T_{i,\text{info}}$ are updated based on the network's situation at that point in time. Also, if a particle considers re-deciding for another route when waiting on junction j_1 or j_2 (based on Algorithm 5.2) the latest available $T_{i,\text{info}}$ are used. Thus, when deciding for a route *before* starting a round the predicted travel times are calculated based on the situation in the moment of that decision. When considering re-deciding the strategy *during* the same round, since a junction is blocked, the predicted travel times may be provided according to newer information than that used before starting the round.

For this type of information no relaxation period is needed since the densities of all edges and thus the predicted travel times of all routes are available from the beginning of the simulation.

This type of information is an approximation of the information provided by smartphone routing apps widely used in real road networks nowadays (Section 2.4 and the references therein describe the working principle and some consequences of these apps).

5.1.3 Personal Historical Information

In the scenario with personal historical information, particles decide upon which routes to take based on their own experiences. Each particle is assigned a memory capacity of c_{mem} rounds, i.e. it 'remembers' which routes it took the last c_{mem} rounds and the corresponding travel times it experienced. Additionally, each particle remembers the travel times of all three routes, as experienced when last using them, no matter how much time has passed since. Thus, particles have memories of travel times on all three routes, even if a certain route was not used in the last c_{mem} rounds.

The $T_{i,\text{info}}$ are different for all particles. For each particle the $T_{i,\text{info}}$ for each route i is either given by the mean of all experienced travel times on route i in the last c_{mem} rounds or, if route i was not used in the last c_{mem} rounds, the $T_{i,\text{info}}$ is given by the single latest memory of route i's travel time. The decision making in the network is then based on Algorithms 5.1 and 5.2 with each particle employing its own personal information.

The system subject to this type of information is considered to be relaxed if each particle

has used each route at least once and if each particle has completed at least c_{mem} rounds. To guarantee that the system will relax, particles intentionally try to use each of the routes at least once before starting to rely on the route choice algorithms. That way it can be achieved that each particle has at least one travel time experience for all three routes.

In real networks route choices may be based on such a type of information, e.g. in commuter's scenarios, in which the commuters do not have any external information except their own experiences to rely on.

5.2 The Algorithm Applied on a Potential "Braess 1" State

The implemented decision making algorithm was first tested with all particles relying on only one type of information during one simulation. Furthermore, also a system in which some particles base their decisions on personal historical information and the remaining particles base their decisions on public predictive information was analysed.

The algorithm was tested in a network with random-sequential updates on an example for a "Braess 1" state: the lengths of the TASEPs are chosen to be $L_0 = 1$, $L_1 = L_3 = 100$, $L_2 = L_4 = 500$ and in the 5link system $L_5 = 37$. A total of $M = 248$ particles are in the system. This corresponds to a route length ratio $\hat{L}_{153}/\hat{L}_{14} \approx 0.4$ and global densities $\rho^{(4)}_{\text{global}} \approx 0.21$ and $\rho^{(5)}_{\text{global}} \approx 0.20$. According to the phase diagrams this parameter set leads to a "Braess 1" state both in the network with fixed route choices (see Figure 4.8) and with turning probabilities (see Figure 4.15). The observable landscapes for the cases of fixed route choices and turning probabilities are shown in Appendix A.1 in Figures A.3 and A.12, respectively.

In the 4link system the user optimum (and also the system optimum) is

- for fixed route choices given by a pure user optimum: $n_{14} = n_{23} = 124$ with $T_{\max}(uo^{(4)}) \approx 765$,
- for turning probabilities given by a mixed user optimum: $\gamma = 0.5$ with $T_{\max}(uo^{(4)}) \approx 764$.

In the 5link system the user optimum is

- not unique for fixed route choices: one pure user optimum is given by $n_{14} = n_{153} = 124,\ n_{23} = 0$, another by $n_{14} = n_{23} = 124,\ n_{153} = 0$; both with $T_{\max}(uo^{(5)}) \approx 978$.
- for turning probabilities uniquely given by a mixed user optimum at $\gamma = 0.87$, $\delta = 0.1$ with $T_{\max}(uo^{(5)}) \approx 895$.

In the following two subsections, the question is answered, whether these user optima are reached if particles choose their routes according to the presented Algorithms 5.1 and 5.2. The parameters of the route choice algorithm are in all cases chosen to be:

- $p_{\text{info}} = 0.9$,

- $\Delta T_{\text{thres.}} = 10$,
- $\kappa_{j_1,\text{thres.}} = \kappa_{j_2,\text{thres.}} = 0.1$,
- $c_{\text{mem}} = 30$ (if personal historical information is used).

A detailed analysis of the influence of varying these parameters on the performance of the algorithm is an interesting potential future project.

5.2.1 Systems with Only One Type of Information

Figures 5.1 to 5.6 show the time evolutions of the system with decisions based on the different types of information: Figures 5.1 and 5.2 display the influence of public historical information in the 4link and 5link systems. Figures 5.3 and 5.4 depict what happens if decisions are based on personal historical information in the 4link and 5link systems. Figures 5.5 and 5.6 illustrate the influence of public predictive information in the systems without and with E_5. Individual data points for Parts **(b)** - **(d)** are always obtained when one particle finishes one round. Then this particle's travel time is recorded and the numbers of particles following the different strategies are counted. The "implicit turning probabilities" γ_{imp} and δ_{imp} shown in Parts **(d)** of these figures are obtained from the numbers of particles using the individual routes as $\gamma_{\text{imp}} = n_{14}/M$ in the 4link system and $\gamma_{\text{imp}} = 1 - n_{23}/M$ and $\delta_{\text{imp}} = n_{14}/(n_{14}+n_{153})$ in the 5link. They are presented to check whether the systems reach the mixed user optima.

Public historical information does not lead to user optima neither in the 4link system nor in the 5link system. Due to overreaction the numbers of particles on the roads keep changing in an oscillatory manner (Figures 5.1 **(c)** and 5.2 **(c)**). Accordingly, the measured individual travel times (Parts **(b)** of Figures 5.1 and 5.2) are changing. The averaged travel times equalize in the symmetric 4link system but at a much higher value than the user optimum travel time (Figure 5.1 **(a)**). In the 5link system the average travel times of all three routes stabilize at different values, all larger than the user optimum values. The fact that this type of information does not lead to user optima is well established for two route scenarios (see Section 2.4 and references therein).

The situation changes if *personal historical information* is used. If users rely on their own memories a user optimum is reached in the 4link system, as can be seen in Figure 5.3 **(c)**. After the relaxation process approximately half of the particles choose route 14 and the remaining particles choose route 23. Apart from some minor fluctuations the number of particles on the two routes stays constant. Accordingly, the average travel times of both routes equalize at the travel time expected in the user optimum (Figure 5.3 **(a)**). As can be seen in Figure 5.3 **(e)** most individual particles stick to their routes, i.e. the total number of particles not switching routes is much greater than the number of particles switching routes: particles relying on their own experiences establish a user optimum close to a pure user optimum.

In the 5link system used by particles that base their decisions on their own memories, a user optimum is reached as well. After the relaxation process approximately half of the particles

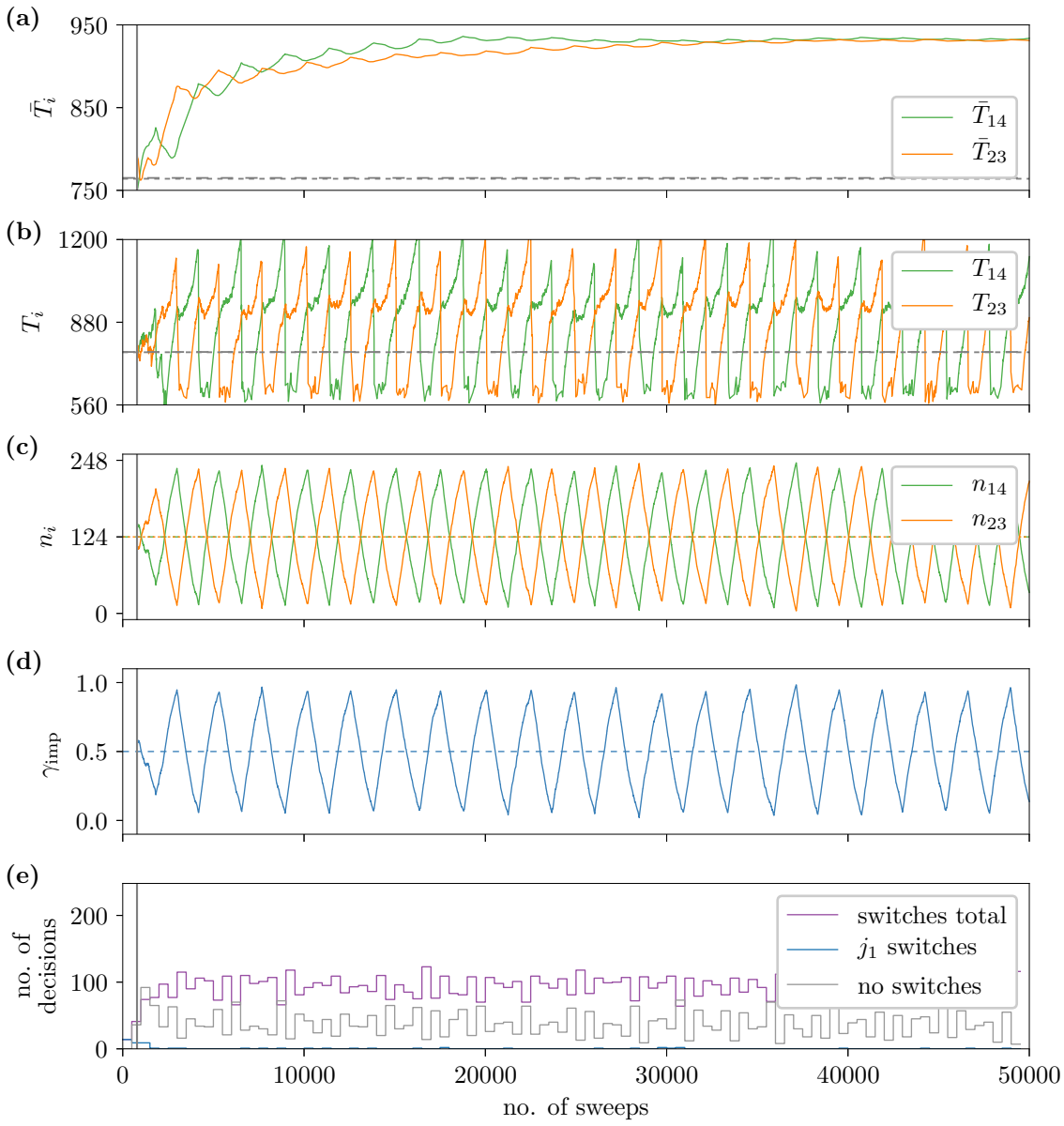

Figure 5.1. The time evolution of observables in the 4link system with particle decisions based on public historical information. All parts share the same x-axis denoting the number of sweeps executed after random initialization. The grey vertical lines show the point in the time evolution when the system was relaxed. Part **(a)** shows the time evolution of the averaged travel times $\bar{T}_i$ of both routes i. Part **(b)** shows the individual measured travel times T_i on both routes i. In Parts **(a)** and **(b)** the dashed grey lines show the average travel times in the pure (longer dashes) and mixed user optima (shorter dashes). Part **(c)** shows the number of particles n_i on the routes i. The according numbers of particles expected in the pure user optimum are also shown as dashed lines. Part **(d)** shows the implicit turning probability γ_{imp} and also the turning probability which leads to the mixed user optimum (dashed line). Part **(e)** shows how many decisions were made. These numbers are collected in bins with a length of 500 sweeps. It is shown how many route switches were made totally ("switches total"), how many of those were done at junction j_1 ("j_1 switches") and how many particles did not change their routes ("no switches").

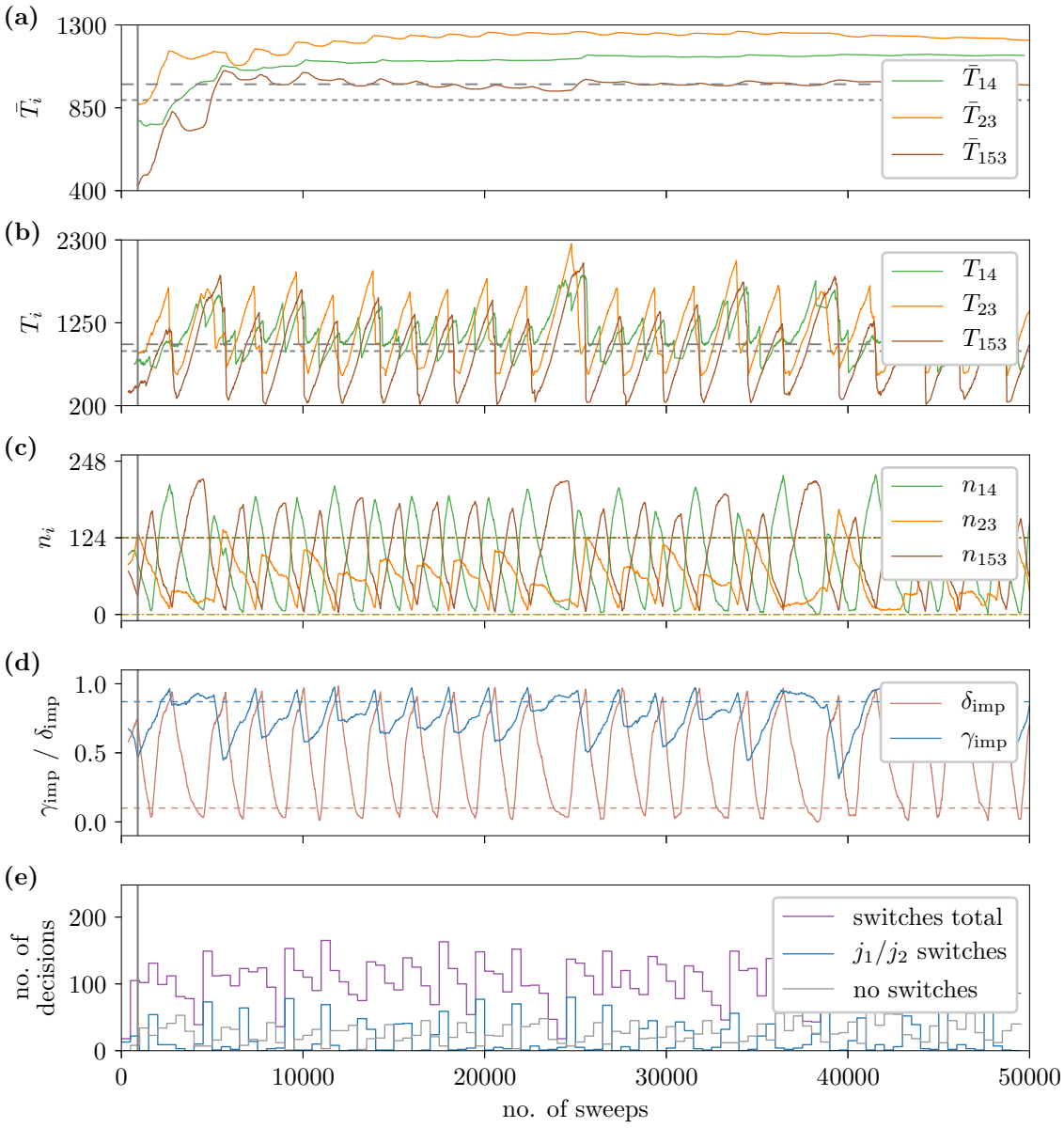

Figure 5.2. The time evolution of observables in the 5link system with particle decisions based on public historical information. All parts share the same x-axis denoting the number of sweeps executed after random initialization. The grey vertical lines show the point in the time evolution when the system was relaxed. Part **(a)** shows the time evolution of the averaged travel times $\bar{T}_i$ of the routes i. Part **(b)** shows the individual measured travel times T_i on the routes i. In Parts **(a)** and **(b)** the dashed grey lines show the average travel times in the pure (longer dashes) and mixed user optima (shorter dashes). Part **(c)** shows the number of particles n_i on the routes i. The according numbers of particles expected in the two pure user optima are also shown as dashed lines. Part **(d)** shows the implicit turning probabilities γ_{imp} and δ_{imp} and also the turning probabilities which lead to the mixed user optimum (dashed lines). Part **(e)** shows how many decisions were made. These numbers are collected in bins with a length of 500 sweeps. It is shown how many route switches were made totally ("switches total"), how many of those were done at the junctions ("j_1/j_2 switches") and how many particles did not change their routes ("no switches").

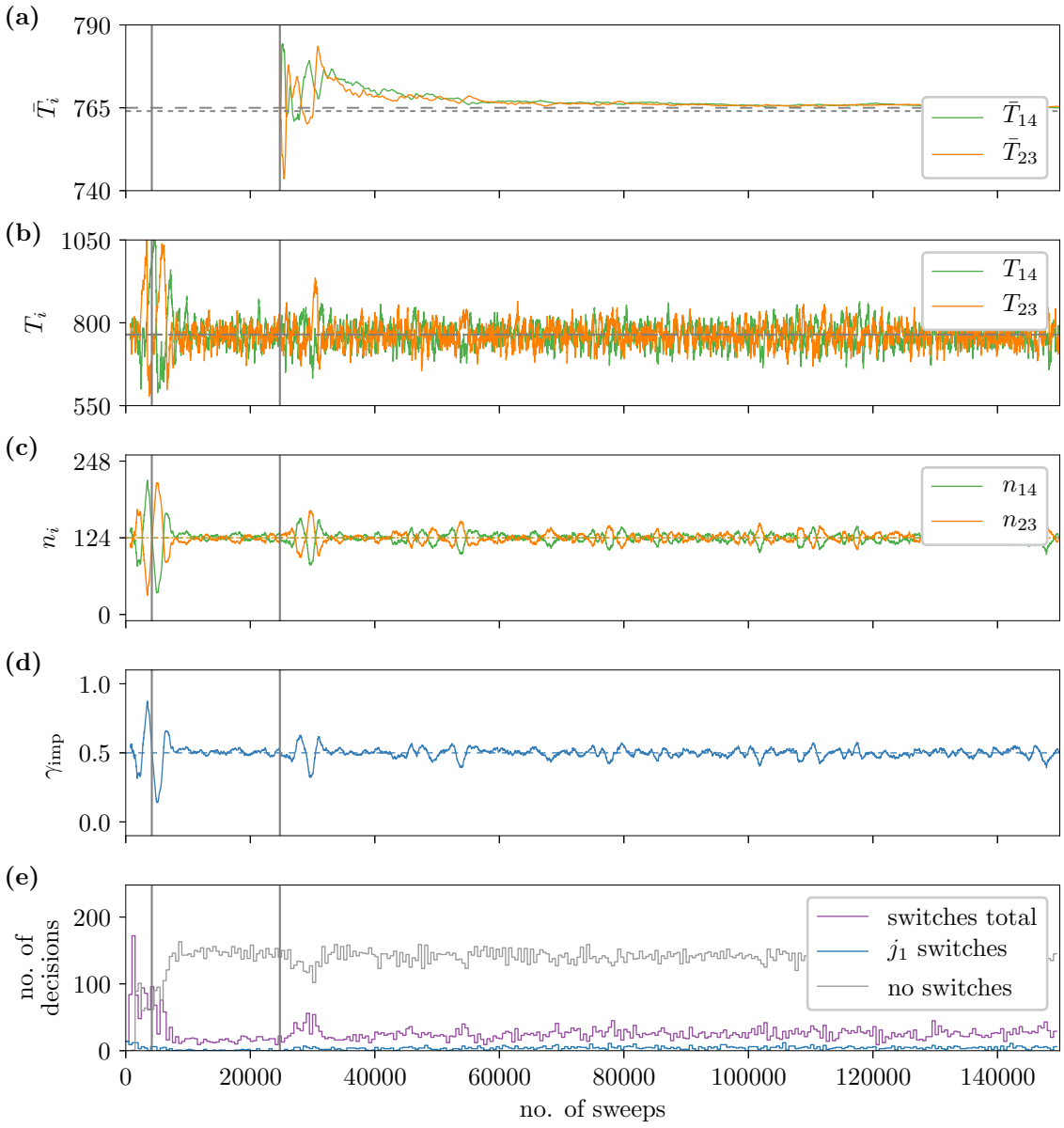

Figure 5.3. The time evolution of observables in the 4link system with particle decisions based on personal historical information, i.e. particles relying on their own memories for route choice decisions. All parts share the same x-axis denoting the number of sweeps executed after random initialization. The grey vertical lines show the points in the time evolution when the system was relaxed: at the first vertical lines each particle used each route once, at the second ones each particle's memory was filled with $c_{\mathrm{mem}} = 30$ travel time values. Part **(a)** shows the time evolution of the averaged travel times $\bar{T}_i$ of both routes i. Part **(b)** shows the individual measured travel times T_i on both routes i. In Parts **(a)** and **(b)** the dashed grey lines show the average travel times in the pure (longer dashes) and mixed user optima (shorter dashes). Part **(c)** shows the number of particles n_i on the routes i. The according numbers of particles expected in the pure user optimum are also shown as dashed lines. Part **(d)** shows the implicit turning probability γ_{imp} and also the turning probability which leads to the mixed user optimum (dashed line). Part **(e)** shows how many decisions were made. These numbers are collected in bins with a length of 500 sweeps. It is shown how many route switches were made totally ("switches total"), how many of those were done at junction j_1 ("j_1 switches") and how many particles did not change their routes ("no switches").

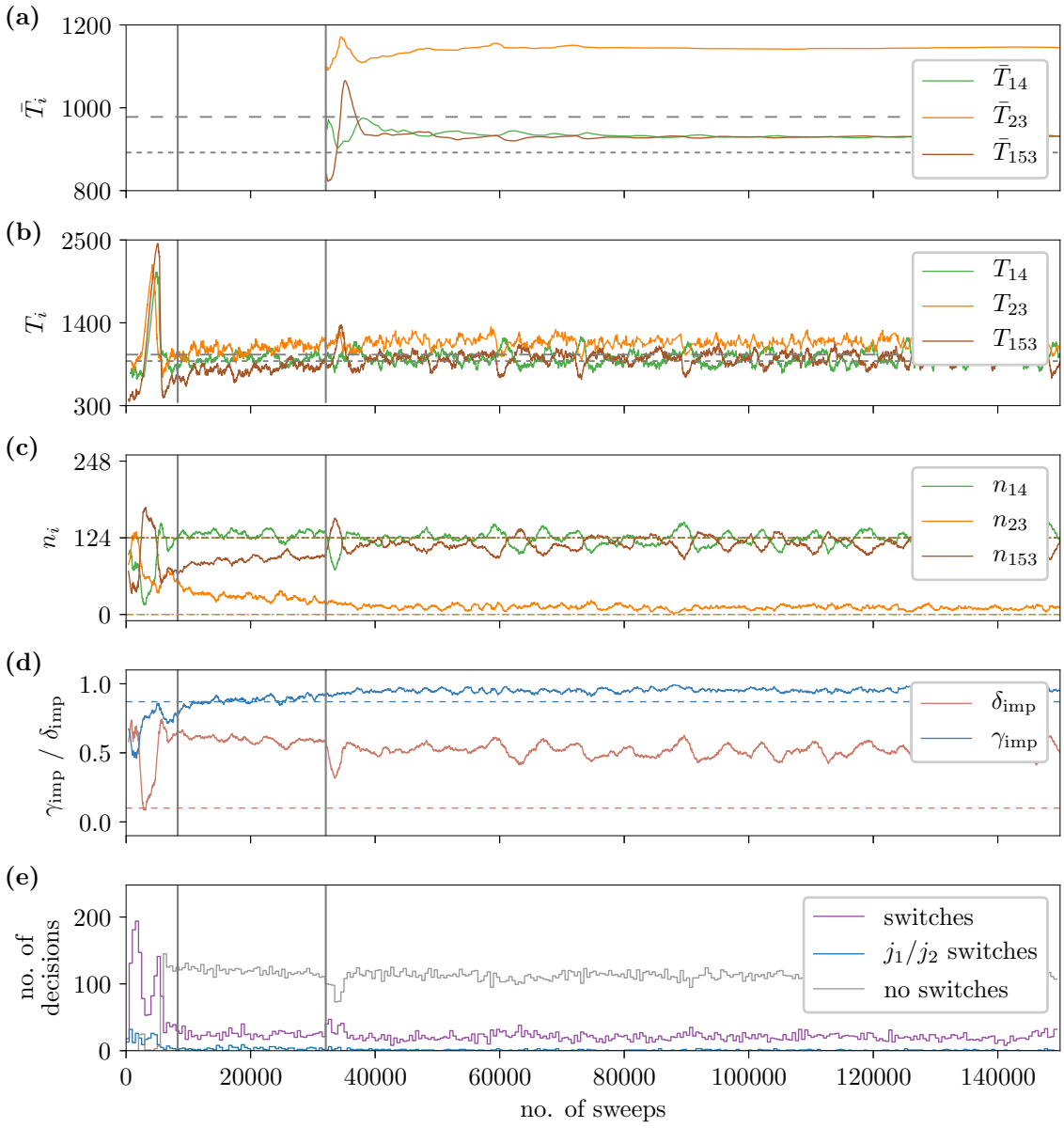

Figure 5.4. The time evolution of observables in the 5link system with particles decisions based on personal historical information, i.e. particles relying on their own memories for route choice decisions. All parts share the same x-axis denoting the number of sweeps executed after random initialization. The grey vertical lines show the points in the time evolution when the system was relaxed: at the first vertical lines each particle used each route once, at the second ones each particle's memory was filled with $c_{\text{mem}} = 30$ travel time values. Part **(a)** shows the time evolution of the averaged travel times $\bar{T}_i$ of the routes i. Part **(b)** shows the individual measured travel times T_i on the routes i. In Parts **(a)** and **(b)** the dashed grey lines show the average travel times in the pure (longer dashes) and mixed user optima (shorter dashes). Part **(c)** shows the number of particles n_i on the routes i. The according numbers of particles expected in the two pure user optima are also shown as dashed lines. Part **(d)** shows the implicit turning probabilities γ_{imp} and δ_{imp} and also the turning probabilities which lead to the mixed user optimum (dashed lines). Part **(e)** shows how many decisions were made. These numbers are collected in bins with a length of 500 sweeps. It is shown how many route switches were made totally ("switches total"), how many of those were done at the junctions ("j_1/j_2 switches") and how many particles did not change their routes ("no switches").

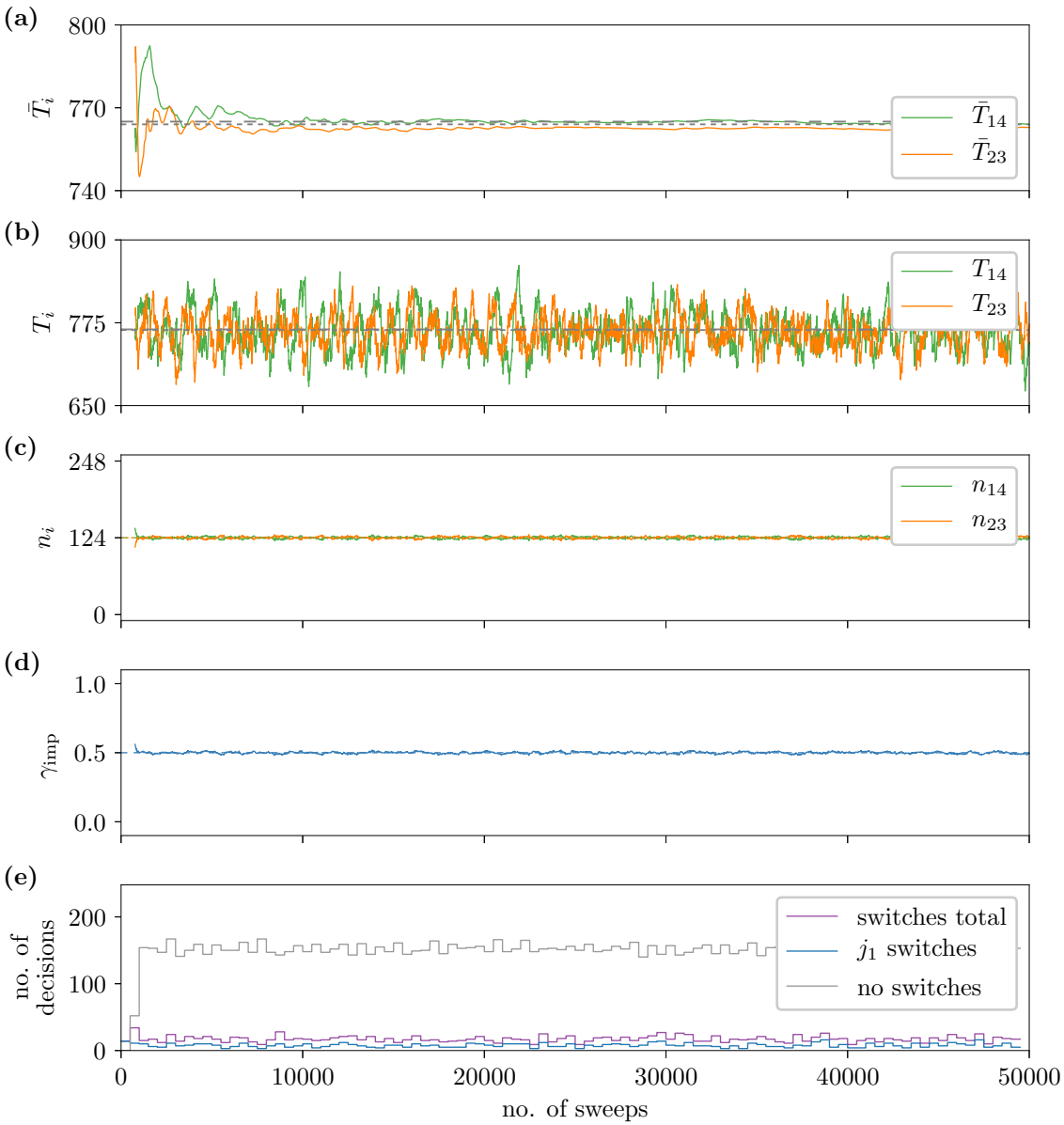

Figure 5.5. The time evolution of observables in the 4link system with particle decisions based on public predictive information. All parts share the same x-axis denoting the number of sweeps executed after random initialization. Part **(a)** shows the time evolution of the averaged travel times $\bar{T}_i$ of both routes i. Part **(b)** shows the individual measured travel times T_i on both routes i. In Parts **(a)** and **(b)** the dashed grey lines show the average travel times in the pure (longer dashes) and mixed user optima (shorter dashes). Part **(c)** shows the number of particles n_i on the routes i. The according numbers of particles expected in the pure user optimum are also shown as dashed lines. Part **(d)** shows the implicit turning probability γ_{imp} and also the turning probability which leads to the mixed user optimum (dashed line). Part **(e)** shows how many decisions were made. These numbers are collected in bins with a length of 500 sweeps. It is shown how many route switches were made totally ("switches total"), how many of those were done at junction j_1 ("j_1 switches") and how many particles did not change their routes ("no switches").

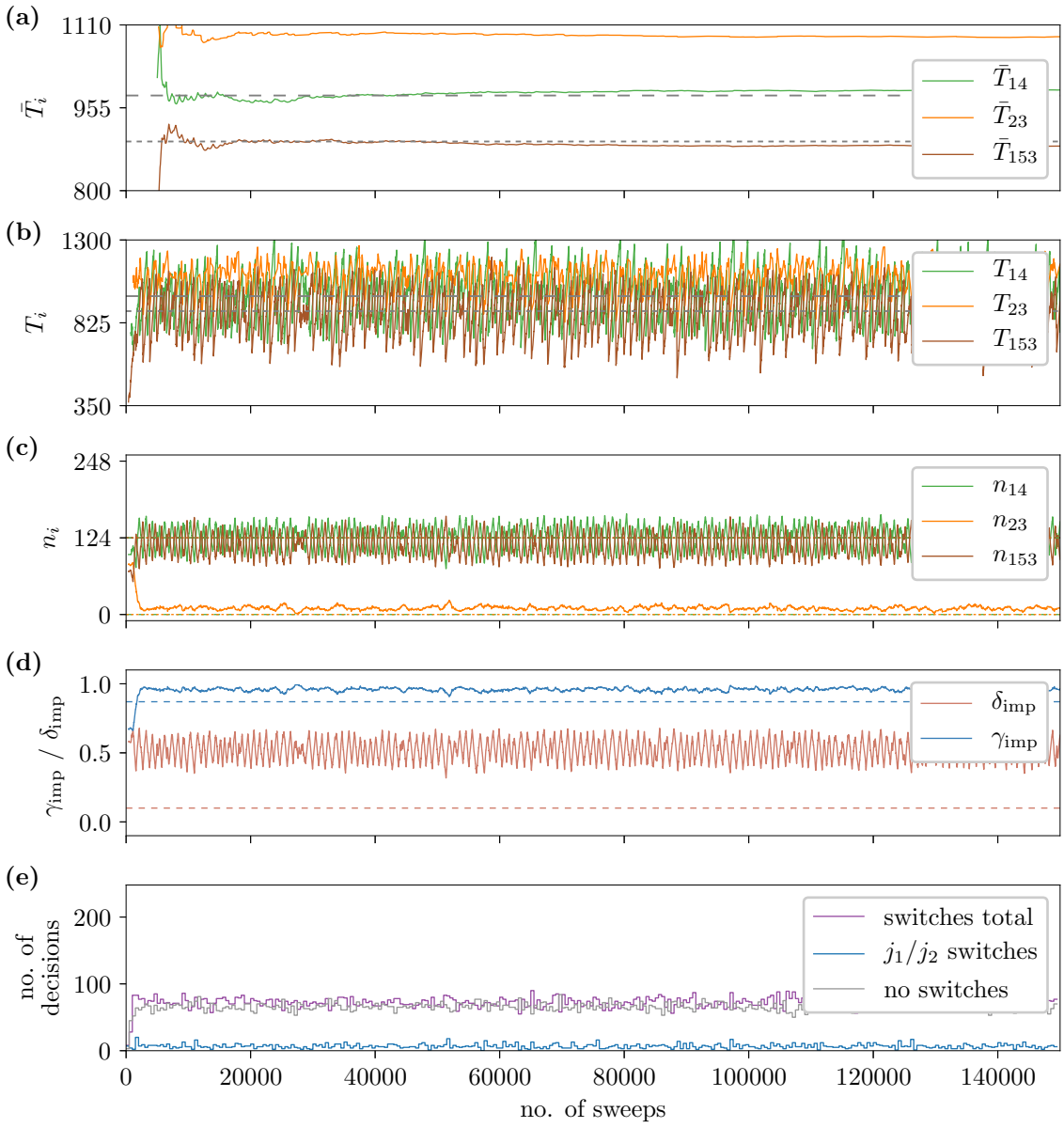

Figure 5.6. The time evolution of observables in the 5link system with particle decisions based on public predictive information. All parts share the same x-axis denoting the number of sweeps executed after random initialization. Part **(a)** shows the time evolution of the averaged travel times $\bar{T}_i$ of the routes i. Part **(b)** shows the individual measured travel times T_i on the routes i. In Parts **(a)** and **(b)** the dashed grey lines show the average travel times in the pure (longer dashes) and mixed user optima (shorter dashes). Part **(c)** shows the number of particles n_i on the routes i. The according numbers of particles expected in the two pure user optima are also shown as dashed lines. Part **(d)** shows the implicit turning probabilities γ_{imp} and δ_{imp} and also the turning probabilities which lead to the mixed user optimum (dashed lines). Part **(e)** shows how many decisions were made. These numbers are collected in bins with a length of 500 sweeps. It is shown how many route switches were made totally ("switches total"), how many of those were done at the junctions ("j_1/j_2 switches") and how many particles did not change their routes ("no switches").

choose route 14 and the remaining particles choose route 153. A small amount of particles chooses route 23 from time to time (Figure 5.4 **(c)**).

The average travel times of routes 14 and 153 equalize at a value between those of the mixed and pure user optima. The travel time on route 23 is significantly longer (Figures 5.4 **(a)** and **(b)**). This can be considered a user optimum because route 23 is rarely used and the other two routes have lower, almost equal travel times. The fact that some particles choose route 23 from time to time could be due to random decisions (occurring with probability $1 - p_{\text{info}}$). The number of particles which stick to their routes is much greater than the number of particles switching their routes (Figure 5.4 **(e)**), leading to the conclusion that the obtained state is close to a pure user optimum.

When particles are provided with *public predictive information*, in the 4link system the user optimum is also reached (see Figure 5.5). Approximately half the particles choose route 14 and the other half route 23. Almost no switches occur (Figure 5.5 **(e)**) and the travel times of both routes equalize (Figure 5.5 **(a)** and **(b)**). This is expected as the 4link system is symmetric and the predictive information is based on Equation (5.1).

In the 5link system public predictive information leads to a situation close to a user optimum. Similar to the case for personal historical information almost no particles choose route 23. In the present case an oscillatory behaviour is observed: while on average half the particles choose routes 14 and the other half route 153, some of them keep switching back and forth between the two routes (see Figure 5.6 **(c)**). One can see that an almost equal amount of particles switches routes and keeps on the same route (Figure 5.6 **(e)**). The oscillating travel times of the used routes are lower than those measured on the almost unused route 23. Nevertheless, their average values are not as close to each other as in the network with personal information. Still, one can conclude that the system is in a stable state with minor oscillations (much lower than for public historical information, see Figure 5.1 and 5.2).

In summary, one can say that providing public historical travel time information is not useful in a road network. However, systems of particles relying on their own memories and systems with public predictive information seem to reach user optimum states. In the 5link system with predictive information a state is obtained which oscillates around a user optimum. In both 5link systems the same pure user optimum is approached. This is interesting because a second pure user optimum and a mixed user optimum exist which were not reached in either of the cases. These other user optima may be reached for different initializations.

Braess' paradox occurs in the two systems with personal historical and public predictive information. In both cases the 5link systems stabilize in states which are close to pure user optima and have higher travel times than the stable states reached in the 4link systems.

Systematic studies of different values for L_5 and M and for the parameters of the decision making algorithm are needed to reach a final conclusion about the overall performance of the algorithm.

5.2.2 Systems with Personal and Public Information

To obtain a better approximation of the situation occurring in present real world commuter scenarios, the network was also studied for the case that some particles rely on their own

memories and the rest relies on public predictive information (e.g. smartphone apps if transferred to the real world). Three different distributions of information types are studied: 75% to 25%, 50% to 50% and 25% to 75% of particles relying on personal to public information. The results are shown in Figures 5.7 and 5.8 for the 4link and 5link networks, respectively.

In the 4link systems the ratio of the two types of information does not seem to have a significant effect on the network's state. The user optima are reached for all different ratios. Only if all users rely on their own memories the fluctuations around the user optimum seem to be a bit higher (see Figure 5.3 **(c)**). If public predictive information is used in the network, these fluctuations get smaller for all saturation levels (25%, 50%, 75% and 100%). While the differences are indeed really small, one could thus conclude that public predictive information is positive with respect to the realization of pure user optima in the 4link network.

In the 5link network the opposite is observed: the pure user optimum is reached with relatively low fluctuations if only personal information is used: Figures 5.4 **(c)** and **(e)** show that the number of particles on the routes stays approximately constant and the number of individual switches is very low. If public predictive information is introduced (from 25% upwards) the systems start to fluctuate around the pure user optimum. While the number of particles on average stays equal on routes 14 and 153, the fluctuations increase with a growing ratio of particles using public information (see Figures 5.8 **(c_1)** – **(c_3)** and Figure 5.6 **(c)**). Also, the number of individual switches grows with the ratio: for only personal information almost no individual switches occur while for only public information as many switches occur as particles sticking to their routes (see Figure 5.4 **(e)**, Figures 5.8 **(d_1)** – **(d_3)** and Figure 5.6 **(e)**). It can be concluded that in the 5link system public information leads to a destabilization on the level of individual particles, while the whole system stays close to a pure user optimum.

These systems with both types of information are approximations of modern real road traffic networks. The fact that Braess' paradox is observed in these systems further stresses its importance for real traffic networks.

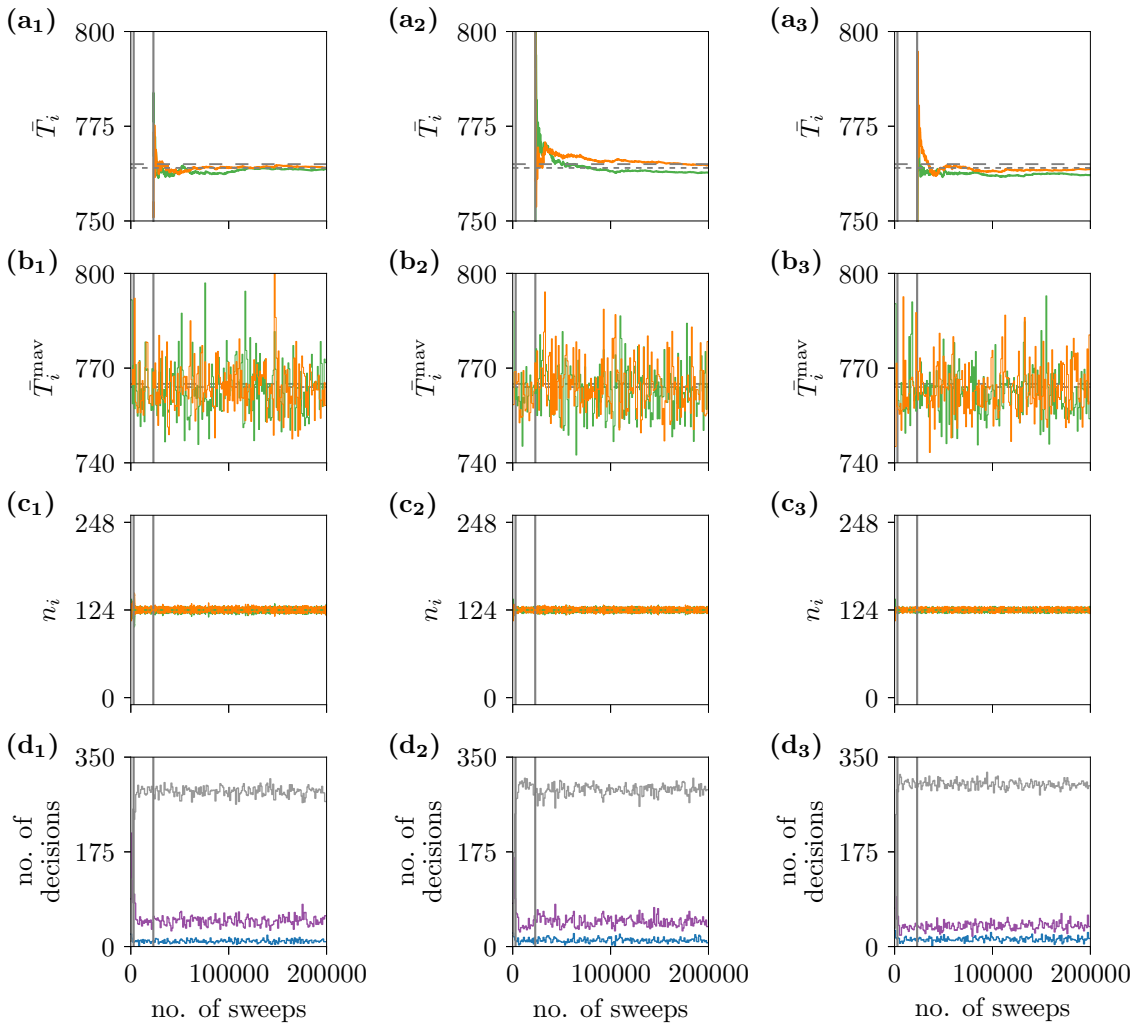

Figure 5.7. Comparison of the effects of different amounts of particles deciding based on either personal historical or public predictive information in the 4link system. Parts **(a$_1$)** to **(d$_1$)** correspond to 75% relying on personal information and 25% on public predictive information. Parts **(a$_2$)** to **(d$_2$)** correspond to 50% relying on personal information and 50% on public predictive information. Parts **(a$_3$)** to **(d$_3$)** correspond to 25% relying on personal information and 75% on public predictive information. All parts share the same x-axis denoting the number of sweeps executed after random initialization. The grey vertical lines show the points in the time evolution when the particles relying on personal information were relaxed: at the first vertical lines each such particle used each route once, at the second ones each of these particles' memories were filled with $c_{\mathrm{mem}} = 30$ travel time values. Parts **(a)** show the time evolutions of the averaged travel times $\bar{T}_i$ of the routes i. Parts **(b)** show moving averages of the travel travel times $\bar{T}_i^{\mathrm{mav}}$ on the routes i. It was averaged over 1000 sweeps for each point. In Parts **(a)** and **(b)** the dashed grey lines show the average travel times in the pure (longer dashes) and mixed user optima (shorter dashes). Parts **(c)** show the number of particles n_i on the routes i. The according numbers of particles expected in the pure user optimum are also shown as dashed lines. Green and orange lines correspond to observables on routes 14 and 23, respectively. Parts **(d)** show how many decisions were made. These numbers are collected in bins with a length of 1000 sweeps. It is shown how many route switches were made totally (purple lines), how many of those were done at junction j_1 (blue lines) and how many particles did not change their routes (grey lines).

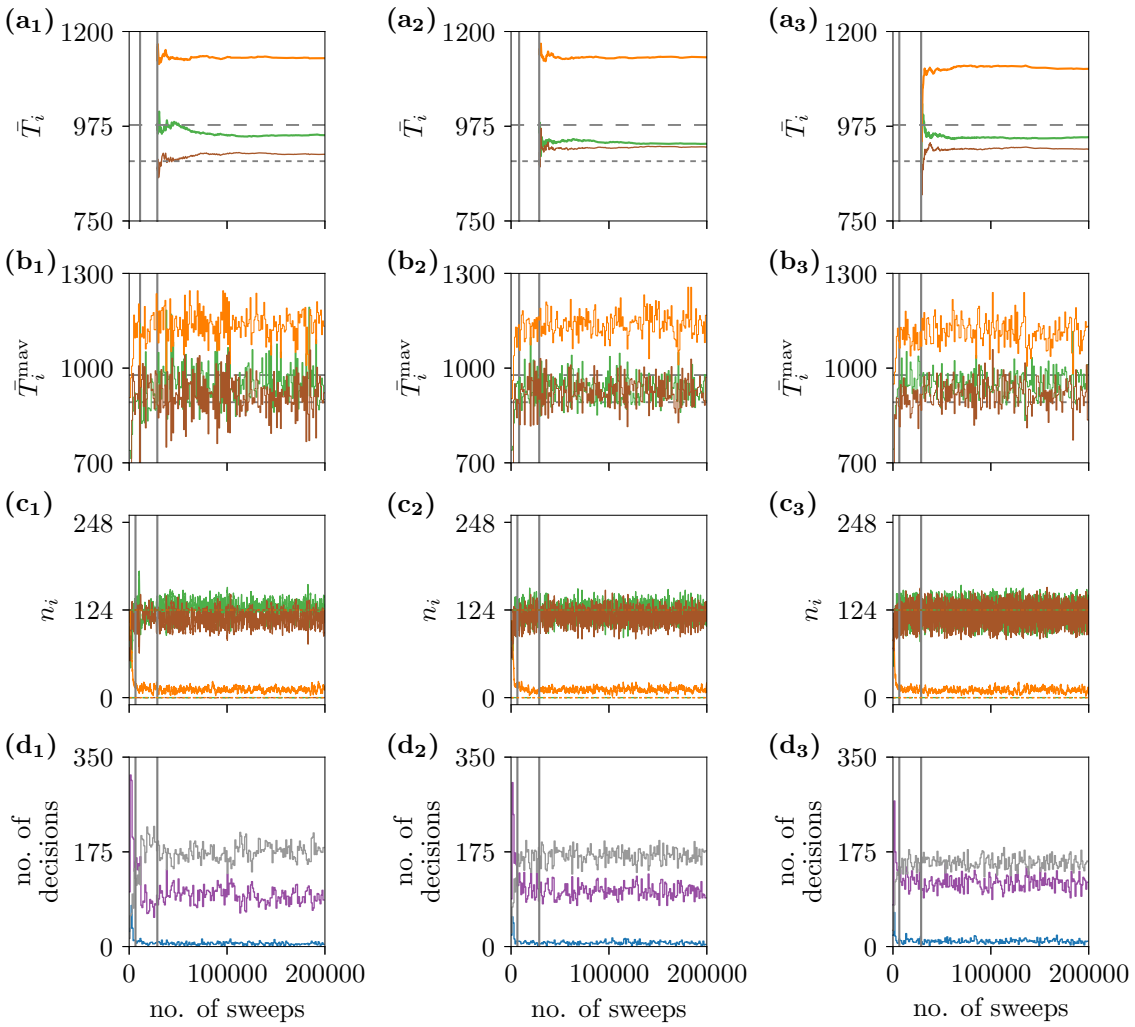

Figure 5.8. Comparison of the effects of different amounts of particles deciding based on either personal historical or public predictive information in the 5link system. Parts **(a$_1$)** to **(d$_1$)** correspond to 75% relying on personal information and 25% on public predictive information. Parts **(a$_2$)** to **(d$_2$)** correspond to 50% relying on personal information and 50% on public predictive information. Parts **(a$_3$)** to **(d$_3$)** correspond to 25% relying on personal information and 75% on public predictive information. All parts share the same x-axis denoting the number of sweeps executed after random initialization. The grey vertical lines show the points in the time evolution when the particles relying on personal information were relaxed: at the first vertical lines each such particle used each route once, at the second ones each of these particle's memories were filled with $c_{\mathrm{mem}} = 30$ travel time values. Parts **(a)** show the time evolutions of the averaged travel times $\bar{T}_i$ of the routes i. Parts **(b)** show moving averages of the travel travel times $\bar{T}_i^{\mathrm{mav}}$ on the routes i. It was averaged over 1000 sweeps for each point. In Parts **(a)** and **(b)** the dashed grey lines show the average travel times in the pure (longer dashes) and mixed user optima (shorter dashes). Parts **(c)** show the number of particles n_i on the routes i. The according numbers of particles expected in the pure user optimum are also shown as dashed lines. Green, orange and brown lines correspond to observables on routes 14, 23 and 153, respectively. Parts **(d)** show how many decisions were made. These numbers are collected in bins with a length of 1000 sweeps. It is shown how many route switches were made totally (purple lines), how many of those were done at junction j_1 (blue lines) and how many particles did not change their routes (grey lines).

6 Summary and Conclusions

In this thesis it was shown that the Braess paradox can be observed in networks of TASEPs. The network structure which was used in the original article on the paradox [10, 11], with TASEP dynamics describing transport in the network was analysed. It was shown that the paradox can be observed in large parts of the phase space when comparing user optima travel times of networks with and without an additional edge. Furthermore, a route choice algorithm was implemented which simulates intelligent route choices for all particles based on various types of information. It was shown that the paradox is realized if particles base their decisions on information similar to that available in real road networks.

In Chapter 2 the main findings of previous research on the paradox were summarized. It was also shown, which assumptions that are made in most of the previous publications, limit the application of the results to real world road networks. The research methodology of this thesis was motivated by recapitulating some important established facts about real road networks, as obtained in various scientific fields. In Chapter 3, the main methods and models used in my research were presented. In particular, the basic model of my reasearch, the Braess network of TASEPs was introduced. Figure 3.11 shows a phase classification scheme which can be used to characterize the influence of the new road on the network. This scheme was used in the following chapters.

In Chapter 4 various variants of the network, differing in boundary conditions, route choice strategies and update types, were analysed with the particles' strategies being tuned externally. The particles do not decide their routes intelligently in this case, but their route choices are set externally. Either fixed amounts of particles choose the exact same routes over and over, a strategy type called "fixed route choices", or all particles decide which routes they take based on fixed probabilities. The latter route choice type is called "turning probabilites". Chapter 4 does not address the question whether the Braess paradox would actually be realized by real drivers. Instead, it answers and affirms the question, whether the paradox is in principal accessible in the networks (Question 1 posed in Chapter 1). Beyond affirming that the paradox can be observed, phase diagrams that characterize the influence of the added road in more detail could be obtained.

Different variants of the network employing random-sequential updates were analysed in Sections 4.1 to 4.4. The cases of periodic boundary conditions with fixed route choices and turning probabilities were studied in Sections 4.1 and 4.2, respectively. In both cases the new road leads to lower user optimum travel times at low global densities. The Braess paradox is observed for intermediate global densities. It is the largest phase in the case of fixed route choices, while the phase is smaller for the case of turning probabilities. Fine tuning is not

required for the phase to be observed in either case.

At intermediate densities, the system with turning probabilities is dominated by fluctuating domain walls. For single open boundary TASEP segments, these domain walls only occur for fine tuned parameters on the phase transition line separating the low density from the high density phase. In the network with turning probabilities, they dominate the largest part of the phase space. In this whole part, travel times are not stable in the short term, the average travel times only stabilize when measuring for a very long time. The system can thus not be classified with regards to the Braess paradox, since fixed travel time values are needed to apply the phase classification scheme presented in Figure 3.11.

In the system with fixed strategies, many states which could potentially be user optima will lead to gridlocks. This is why this system can not be properly classified for high global densities, either. In both systems the new road seems to lead to lowered user optimum travel times at really high densities.

The Braess networks with open boundaries and turning probabilities are analysed in Section 4.4. The Braess paradox is not observed directly in those networks. For low outer exit probabilities, unexpected phases are found in the 5link systems: in these phases no user optima exist. The phases in which the travel times of all three routes are closest to each other, are those phases in which only one route is used. In those phases, the travel times of the used routes are higher than those of unused routes. If the system was used by intelligent particles, they would not stick to such strategies but instead start using the other routes as well. Since the total particle number is not conserved in the network with open boundary conditions, the other routes would then also fill up with particles and the system would end up in states with higher travel times than those of the 4link systems' user optima. The system might also be oscillating between phases in which only one of the three routes is used. In the remaining parts of the phase space, the new road leads to lower travel times in the networks with open boundary conditions.

Braess' paradox can also be observed in TASEP networks with parallel dynamics. The phase diagrams for the network with periodic boundary conditions and fixed route choices as well as turning probabilities are shown in Section 4.5. If parallel dynamics are employed, certain conflicts which cannot occur in TASEP networks with random-sequential updates, are possible. These conflicts occur, if two TASEPs segments merge into one junction. If the last sites of both segments are occupied, two particles try to jump onto the same site at the same time. To avoid such conflicts, traffic lights were implemented at the two junction sites on which such conflicts are potentially possible in Braess' network. This leads to a more complicated classification scheme, as shown in Figure 4.25, than in the case of random-sequential updates. Braess' paradox was also observed in these networks with parallel dynamics. Opposed to those of the networks with random-sequential dynamics, the phase diagrams cannot be divided into distinct phase areas.

In Chapter 5 the question, whether Braess' paradox is realized if the network is used by intelligent users (Question 2 posed in Chapter 1), is addressed. A route choice algorithm, which is used as the basis of all individual particles' route choice decisions, is implemented.

The effects of several types of information on which the algorithm is based are analysed. The most important types are personal historical information and a type of public predictive information. The former is knowledge that individual particles have based on their own experiences of travel times in previous rounds. The latter provides approximations of future travel times in the network, based on the current positions of all particles. It is an approximation of information which is provided by smartphone routing apps in real road networks.

The algorithm is tested in the Braess network with random-sequential updates and periodic boundary conditions. Route lengths and the global density are chosen such that for externally tuned parameters a "Braess 1" state is expected both for fixed route choices and turning probabilities. It turns out that the paradox is realized for only personal historical information, only public predictive information and for various combinations of both types. This confirms that states leading to Braess' paradox are not only in principle accessible, but are actually realized in situations which are very similar to those present in real road networks. Question 2 from Chapter 1 is thus confirmed.

In conclusion, it can be stated that Braess' paradox occurs in networks of stochastic microscopic transport processes. The paradox is observed in large parameter regions for various variants of the network. It is also realized, if particles choose their routes intelligently based on information, similar to information available in real road networks. This emphasizes the importance of the paradox.

Some Ideas for Additional Research. Further research on the paradox in realistic models is needed. Some ideas for possible future research on the topic are given in the following.

- Analysing networks of different topologies can lead to a general understanding about the prerequisites that need to be fulfilled for the paradox to occur.
- Studying the influence of different hopping probabilities on different edges could be used to approximate different maximum speeds. In doing so, different types of roads, e.g. rural roads and freeways, could be approximately distinguished.
- The influence of Langmuir dynamics [133] could be studied: this dynamics could be used to model cars that start at various positions of the roads, which could be regarded as an approximation of traffic in cities.
- Analysing the network employing more realistic traffic models, such as the Nagel-Schreckenberg model [106] or the velocity-dependent randomization model [120], could be a next step to enhance the applicability to reality. First results for the Nagel-Schreckenberg model are presented in [114].
- The influence of the parameters of the route choice algorithm could be studied in greater detail. It would also be interesting to test the algorithm on different states which are expected to lead e.g. to "Braess 2" phases or "E_5 optimal" phases.

Acknowledgements

I want to thank my supervisor Professor Andreas Schadschneider for giving me the opportunity to conduct my doctoral research on the fascinating topics presented in this dissertation. I am very grateful for his friendly guidance and support.

I also want to thank Leonard Fischer for the fruitful discussions during the time he worked on his master's thesis. Furthermore, I want to thank the rest of our group for the nice times spent together. I am very thankful to Sonja Lambertz, Torsten Held, Sebastian Hild, Marcel Usner and Johannes Schmidt for helping me with the proofreading process.

Financial support by Deutsche Forschungsgemeinschaft (DFG) under the grant 636/8-2, as well as support of conference travel expenses by the Bonn-Cologne Graduate School of Physics and Astonomy (BCGS), are gratefully acknowledged.

Monte Carlo simulations were in large parts carried out on the CHEOPS (Cologne High Efficiency Operating Platform for Science) cluster of the RRZK (University of Cologne).

Bibliography

[1] K. Nagel. Particle hopping models and traffic flow theory. *Physical review E*, 53(5): 4655, 1996.

[2] W. Thomson. On a mechanical theory of thermo-electric currents. *Proceedings of the Royal Society of Edinburgh*, 3:91–98, 1857.

[3] A. Hunt, R. Ewing, and B. Ghanbarian. *Percolation theory for flow in porous media*, volume 880. Springer, 2014.

[4] M. Schreckenberg and R. Selten. *Human behaviour and traffic networks*. Springer Science & Business Media, 2013.

[5] I. Neri, N. Kern, and A. Parmeggiani. Exclusion processes on networks as models for cytoskeletal transport. *New Journal of Physics*, 15(8):085005, 2013.

[6] C. Otto, S. N. Willner, L. Wenz, K. Frieler, and A. Levermann. Modeling loss-propagation in the global supply network: The dynamic agent-based model acclimate. *Journal of Economic Dynamics and Control*, 83:232–269, 2017.

[7] M. S. Obaidat, F. Zarai, and P. Nicopolitidis. *Modeling and simulation of computer networks and systems: Methodologies and applications*. Morgan Kaufmann, 2015.

[8] F. Brauer and C. Castillo-Chavez. *Mathematical models in population biology and epidemiology*, volume 40. Springer, 2012.

[9] A. E. Motter and M. Timme. Antagonistic phenomena in network dynamics. *Annual Review of Condensed Matter Physics*, 9:463–484, 2018.

[10] D. Braess. Über ein Paradoxon aus der Verkehrsplanung. *Unternehmensforschung*, 12: 258, 1968.

[11] D. Braess, A. Nagurney, and T. Wakolbinger. On a paradox of traffic planning. *Transportation Science*, 39:446, 2005. *(English translation of [10]).*

[12] J. G. Wardrop. Road Paper. Some Theoretical Aspects Of Road Traffic Research. *Proceedings of the Institution of Civil Engineers*, 1(3):325–362, 1952.

[13] J. F. Nash. Non-cooperative games. *Annals of Mathematics*, pages 286–295, 1951.

[14] United Nations. World Urbanization Prospects: The 2018 Revision. 2018. URL `https://population.un.org/wup/Publications/Files/WUP2018-KeyFacts.pdf`. (Online, accessed 26-September-2018).

[15] M. Barthelemy, P. Bordin, H. Berestycki, and M. Gribaudi. Self-organization versus top-down planning in the evolution of a city. *Scientific Reports*, 3:2153, 2013.

[16] D. Schraenk, B. Eisele, T. Lomax, and J. Bak. 2015 Urban Mobility Scorecard. Technical report, The Texas A&M Transportation Institute and INRIX, 2015.

[17] TomTom International BV. TomTom Traffic Index, 2017. URL `https://www.tomtom.com/en_gb/trafficindex/`. (Online, accessed 26-September-2018).

[18] G. Duranton and M. A. Turner. The fundamental law of road congestion: Evidence from us cities. *American Economic Review*, 101(6):2616–52, 2011.

[19] W. Knödel. *Graphentheoretische Methoden und ihre Anwendungen*, volume 13. Springer-Verlag, 1969.

[20] G. Kolata. What if They Closed 42d Street and Nobody Noticed? *The New York Times*, December 1990.

[21] M. M. Grynbaum. New York Traffic Experiment Gets Permanent Run. *The New York Times*, February 2010.

[22] L. Baker. Removing Roads and Traffic Lights Speeds Urban Travel. *Scientific American*, February 2009.

[23] J. Vidal. Heart and soul of the city. *The Guardian*, November 2006.

[24] K. Schön. Stau? Reißt die Stadtautobahn ab! *Urbanist Magazin*, February 2014.

[25] D. Rißle. Verkehrsausschuss Sperrung der Zülpicher Straße wird wohl verlängert. *Kölner Stadt-Anzeiger*, December 2017.

[26] H. Youn, M. T. Gastner, and H. Jeong. Price of Anarchy in Transportation Networks: Efficiency and Optimality Control. *Physical Review Letters*, 101:128701, 2008.

[27] T. Thunig and K. Nagel. Braess's Paradox in an Agent-based Transport Model. *Procedia Computer Science*, 83:946–951, 2016.

[28] R. Steinberg and W. I. Zangwill. The prevalence of Braess' paradox. *Transportation Science*, 17:301, 1983.

[29] S. Dafermos and A. Nagurney. On some traffic equilibrium theory paradoxes. *Transportation Research Part B: Methodological*, 18(2):101–110, 1984.

[30] E. I. Pas and S. L. Principio. Braess' paradox: Some new insights. *Transportation Research Part B: Methodological*, 31(3):265–276, 1997.

[31] M. Frank. The Braess paradox. *Mathematical Programming*, 20(1):283–302, 1981.

[32] Y. Sheffi. *Urban Transportation Networks: Equilibrium Analysis with Mathematical programming Methods*. Prentice Hall, Inc., 1985.

[33] A. Rapoport, T. Kugler, S. Dugar, and E. Gisches. Choice of routes in congested traffic networks: Experimental tests of the Braess Paradox. *Games and Economic Behavior*, 65(2):538–571, 2009.

[34] A. Nagurney. The negation of the Braess paradox as demand increases: The wisdom of crowds in transportation networks. *EPL (Europhysics Letters)*, 91(4):48002, 2010.

[35] A. Schadschneider, D. Chowdhury, and K. Nishinari. *Stochastic Transport in Complex Systems: from Molecules to Vehicles*. Elsevier, 2010.

[36] F. L. Hall, B. L. Allen, and M. A. Gunter. Empirical analysis of freeway flow-density relationships. *Transportation Research Part A: General*, 20(3):197–210, 1986.

[37] L. Neubert, L. Santen, A. Schadschneider, and M. Schreckenberg. Single-vehicle data of highway traffic: A statistical analysis. *Physical Review E*, 60(6):6480, 1999.

[38] D. Helbing. Empirical traffic data and their implications for traffic modeling. *Physical Review E*, 55(1):R25, 1997.

[39] Y. Sugiyama, M. Fukui, M. Kikuchi, K. Hasebe, A. Nakayama, K. Nishinari, S. Tadaki, and S. Yukawa. Traffic jams without bottlenecks—experimental evidence for the physical mechanism of the formation of a jam. *New Journal of Physics*, 10(3):033001, 2008.

[40] United States, Bureau of Public Roads. *Traffic assignment manual for application with a large, high speed computer*. U.S. Dept. of Commerce, Bureau of Public Roads, Washington, D.C., 1964.

[41] K. B. Davidson. A flow travel time relationship for use in transportation planning. In *Australian Road Research Board (ARRB) Conference, 3rd, 1966, Sydney*, volume 3, 1966.

[42] R. Akcelik. Travel time functions for transport planning purposes: Davidson's function, its time dependent form and alternative travel time function. *Australian Road Research*, 21(3), 1991.

[43] J. E. Cohen and F. P. Kelly. A paradox of congestion in a queuing network. *Journal of Applied Probability*, 27(3):730–734, 1990.

[44] W.-H. Lin and H. K. Lo. Investigating braess' paradox with time-dependent queues. *Transportation Science*, 43(1):117–126, 2009.

[45] M. Ben-Akiva, A. De Palma, and K. Isam. Dynamic network models and driver information systems. *Transportation Research Part A: General*, 25(5):251 – 266, 1991.

[46] E. Ben-Elia and E. Avineri. Response to travel information: a behavioural review. *Transport Reviews*, 35(3):352–377, 2015.

[47] P. Parthasarathi, D. Levinson, and H. Hochmair. Network Structure and Travel Time Perception. *PLOS ONE*, 8(10):1–13, 10 2013.

[48] T.-Y. Chen, H.-L. Chang, and G.-H. Tzeng. Using a weight-assessing model to identify route choice criteria and information effects. *Transportation Research Part A: Policy and Practice*, 35(3):197–224, 2001.

[49] S. Zhu and D. Levinson. Do People Use the Shortest Path? An Empirical Test of Wardrop's First Principle. *PLOS ONE*, 10(8):1–18, 08 2015.

[50] R. Selten, T. Chmura, T. Pitz, S. Kube, and M. Schreckenberg. Commuters route choice behaviour. *Games and Economic Behavior*, 58(2):394 – 406, 2007.

[51] C. F. Daganzo and Y. Sheffi. On stochastic models of traffic assignment. *Transportation Science*, 11(3):253–274, 1977.

[52] H. S. Mahmassani and G.-L. Chang. On boundedly rational user equilibrium in transportation systems. *Transportation Science*, 21(2):89–99, 1987.

[53] T. Cabannes, M. A. S. Vincentelli, A. Sundt, H. Signargout, E. Porter, V. Fighiera, J. Ugirumurera, and A. M. Bayen. The impact of GPS-enabled shortest path routing on mobility: a game theoretic approach. Technical report, Transportation Research Board, 2018.

[54] C. T. MacDonald, J. H. Gibbs, and A. C. Pipkin. Kinetics of biopolymerization on nucleic acid templates. *Biopolymers*, 6(1):1–25, 1968.

[55] J. Krug. Boundary-induced phase transitions in driven diffusive systems. *Physical Review Letters*, 67(14):1882, 1991.

[56] I. Neri, N. Kern, and A. Parmeggiani. Totally Asymmetric Simple Exclusion Process on Networks. *Physical Review Letters*, 107:068702, 2011.

[57] J. Brankov, N. Pesheva, and N. Bunzarova. Totally asymmetric exclusion process on chains with a double-chain section in the middle: Computer simulations and a simple theory. *Physical Review E*, 69:066128, 2004.

[58] E. Pronina and A. B. Kolomeisky. Theoretical investigation of totally asymmetric exclusion processes on lattices with junctions. *Journal of Statistical Mechanics: Theory and Experiment*, 2005(07):P07010, 2005.

[59] B. Embley, A. Parmeggiani, and N. Kern. Understanding totally asymmetric simple-exclusion-process transport on networks: Generic analysis via effective rates and explicit vertices. *Physical Review E*, 80:041128, 2009.

[60] R. Wang, M. Liu, and R. Jiang. Theoretical investigation of synchronous totally asymmetric exclusion processes on lattices with multiple-input–single-output junctions. *Physical Review E*, 77:051108, 2008.

[61] M. Liu and R. Wang. Asymmetric exclusion processes on -input -output junctions with parallel update. *Physica A: Statistical Mechanics and its Applications*, 388(19): 4068–4074, 2009.

[62] X. Song, L. Ming-Zhe, W. Jian-Jun, and W. Hua. Effect of unequal injection rates on asymmetric exclusion processes with junction. *Chinese Physics B*, 20(6):060509, 2011.

[63] P. Jing, M. Zhao, M. He, and L. Chen. Travel Mode and Travel Route Choice Behavior Based on Random Regret Minimization: A Systematic Review. *Sustainability*, 10(4): 1185, 2018.

[64] Car 2 Car Communication Consortium and others. CAR 2 CAR Communication Consortium Manifesto. *DLR Electronic Library*, August 2007. URL `https://elib.dlr.de/48380/1/C2C-CC_manifesto_v1.1.pdf`. (Online, accessed 12-August-2018).

[65] A. C. Pigou. *The economics of welfare, 1920*. Palgrave Macmillan UK, 1932.

[66] F. H. Knight. Some fallacies in the interpretation of social cost. *The Quarterly Journal of Economics*, 38(4):582–606, 1924.

[67] E. Youngblom. Travel time in macroscopic traffic models for origin-destination estimation. *Theses and Dissertations. 185.*, 2013. URL `https://dc.uwm.edu/etd/185`. (Online, accessed 12-August-2018).

[68] J. F. Nash. Equilibrium points in n-person games. *Proceedings of the National Academy of Sciences*, 36(1):48–49, 1950.

[69] M. J. Beckmann, C. B. McGuire, and C. B. Winsten. *Studies in the Economics of Transportation*. Yale University Press, 1956.

[70] N. F. Stewart. Equilibrium vs system-optimal flow: some examples. *Transportation Research Part A: General*, 14(2):81–84, 1980.

[71] T. Roughgarden and É. Tardos. How bad is selfish routing? *Journal of the ACM (JACM)*, 49(2):236–259, 2002.

[72] J. D. Murchland. Braess's paradox of traffic flow. *Transportation Research*, 4(4):391–394, 1970.

[73] Wikipedia contributors. Braess-Paradoxon – Wikipedia. *Wikimedia Foundation Inc.*, 2018. URL `https://de.wikipedia.org/wiki/Braess-Paradoxon`. (Online, accessed 12-September-2018).

[74] Stadt Köln. Tagesordnungspunkt - TOP 7.7: Verkehrsversuch Sperrung Zülpicher Straße. *Stadt Köln*, 2017. URL `https://ratsinformation.stadt-koeln.de/to0050.asp?__ktonr=223562`. (Online, accessed 30-April-2018).

[75] R. Singh and R. Dowling. Improved speed-flow relationships: application to transportation planning models. In *Seventh TRB Conference on the Application of Transportation Planning Methods*, 2002.

[76] T. Roughgarden. On the severity of Braess's paradox: designing networks for selfish users is hard. *Journal of Computer and System Sciences*, 72(5):922–953, 2006.

[77] J. E. Cohen and P. Horowitz. Paradoxical behaviour of mechanical and electrical networks. *Nature*, 352(6337):699, 1991.

[78] C. M. Penchina and L. J. Penchina. The Braess paradox in mechanical, traffic, and other networks. *American Journal of Physics*, 71(5):479–482, 2003.

[79] L. Crociani and G. Lämmel. Multidestination Pedestrian Flows in Equilibrium: A Cellular Automaton-Based Approach. *Computer-Aided Civil and Infrastructure Engineering*, 31(6):432–448, 2016.

[80] D. Witthaut and M. Timme. Braess's paradox in oscillator networks, desynchronization and power outage. *New Journal of Physics*, 14(8):083036, 2012.

[81] E. B. T. Tchuisseu, D. Gomila, P. Colet, D. Witthaut, M. Timme, and B. Schäfer. Curing braess' paradox by secondary control in power grids. *New Journal of Physics*, 20(8):083005, 2018.

[82] K. Bhattacharyya. A thermodynamic parallel of the Braess road-network paradox. *arXiv preprint arXiv:1703.02213*, 2017.

[83] D. Braess. D. Braess, 2018. URL `http://homepage.ruhr-uni-bochum.de/Dietrich.Braess/#paradox`. (Online, accessed 12-September-2018).

[84] G. Rose, M. A. P. Taylor, and P. Tisato. Estimating travel time functions for urban roads: options and issues. *Transportation Planning and Technology*, 14(1):63–82, 1989.

[85] D. Branston. Link capacity functions: A review. *Transportation Research*, 10(4):223 – 236, 1976.

[86] B. D. Greenshields, J. R. Bibbins, W. Channing, and H. Miller. A study of traffic capacity. In *Highway Research Board Proceedings*, volume 1935. National Research Council (USA), Highway Research Board, 1935.

[87] R. D. Kühne. Foundations of Traffic Flow Theory I: Greenshields' Legacy–Highway Traffic. In *Symposium on the Fundamental Diagram: 75 Years (Greenshields 75 Symposium) Transportation Research Board*, 2008.

[88] R. D. Kühne. Das Fundamentaldiagramm – Grundlagen und Anwendungen. *FGSV Merkblatt (Entwurf)*, 59, 2004.

[89] W. Knospe, L. Santen, A. Schadschneider, and M. Schreckenberg. Empirical test for cellular automaton models of traffic flow. *Physical Review E*, 70(1):016115, 2004.

[90] B. S. Kerner. The physics of traffic. *Physics World*, 12(8):25, 1999.

[91] Wikipedia contributors. Advanced traveller information system – Wikipedia. *Wikimedia Foundation Inc.*, 2018. URL `https://en.wikipedia.org/wiki/Advanced_traveller_information_system`. (Online, accessed 10-August-2018).

[92] C. Meneguzzer and A. Olivieri. Day-to-day traffic dynamics: laboratory-like experiment on route choice and route switching in a simple network with limited feedback information. *Procedia-Social and Behavioral Sciences*, 87:44–59, 2013.

[93] J. Wahle, A. L. C. Bazzan, F. Klügl, and M. Schreckenberg. Decision dynamics in a traffic scenario. *Physica A: Statistical Mechanics and its Applications*, 287(3):669 – 681, 2000.

[94] eMarketer. Smartphone penetration rate as share of the population in the United States from 2010 to 2021*. *Statista - The Statistics Portal.*, September 2018. URL `https://www.statista.com/statistics/201183/forecast-of-smartphone-penetration-in-the-us/`. (Online, accessed 11-September-2018).

[95] M. Anderson. More Americans using smartphones for getting directions, streaming TV — Pew Research Center. *Pew Research Center, Washington D.C.*, January 2016. URL `http://www.pewresearch.org/fact-tank/2016/01/29/us-smartphone-use/`. (Online, accessed 12-September-2018).

[96] comScore. Most popular mobile apps in the United States as of December 2016, ranked by average unique monthly visitors (in millions). *Statista – The Statistics Portal*, December 2016. URL `https://www.statista.com/statistics/250862/unique-visitors-to-the-most-popular-mobile-apps-in-the-us/`. (Online, accessed 11-Septmenber-2018).

[97] D. Barth. Official Google Blog: The bright side of sitting in traffic: Crowdsourcing road congestion data. *Google*, August 2009. URL `https://googleblog.blogspot.com/2009/08/bright-side-of-sitting-in-traffic.html`. (Online, accessed 12-September-2018).

[98] B. Brindle. How does Google Maps predict traffic? *HowStuffWorks*, September 2014. URL `https://electronics.howstuffworks.com/how-does-google-maps-predict-traffic.htm`. (Online, accessed 10-September-2018).

[99] A. C. Madrigal. The Perfect Selfishness of Mapping Apps. *The Atlantic*, March 2018. URL `https://www.theatlantic.com/technology/archive/2018/03/mapping-apps-and-the-price-of-anarchy/555551/`. (Online, accessed 11-September-2018).

[100] J. Thai, N. Laurent-Brouty, and A. M. Bayen. Negative externalities of GPS-enabled routing applications: A game theoretical approach. In *19th International Conference on Intelligent Transportation Systems (ITSC)*, pages 595–601. IEEE, 2016.

[101] J. L. Horowitz. The stability of stochastic equilibrium in a two-link transportation network. *Transportation Research Part B: Methodological*, 18(1):13 – 28, 1984.

[102] R. Arnott, A. de Palma, and R. Lindsey. Does providing information to drivers reduce traffic congestion? *Transportation Research Part A: General*, 25(5):309 – 318, 1991.

[103] A. L. C. Bazzan, J. Wahle, and F. Klügl. Agents in traffic modelling-from reactive to social behaviour. *KI*, 99:303–307, 1999.

[104] J. Wahle, A. L. C. Bazzan, F. Klügl, and M. Schreckenberg. Anticipatory traffic forecast using multi-agent techniques. In *Traffic and Granular Flow '99*. Springer, 2000.

[105] R. W. Hall. Route choice and advanced traveler information systems on a capacitated and dynamic network. *Transportation Research Part C: Emerging Technologies*, 4(5): 289 – 306, 1996.

[106] K. Nagel and M. Schreckenberg. A cellular automaton model for freeway traffic. *Journal de Physique I*, 2(12):2221–2229, 1992.

[107] K. Lee, P. M. Hui, B.-H. Wang, and N. F. Johnson. Effects of announcing global information in a two-route traffic flow model. *Journal of the Physical Society of Japan*, 70(12):3507–3510, 2001.

[108] W.-X. Wang, B.-H. Wang, W.-C. Zheng, C.-Y. Yin, and T. Zhou. Advanced information feedback in intelligent traffic systems. *Physical Review E*, 72:066702, 2005.

[109] B. K. Chen, W. Tong, W. Y. Zhang, X. Y. Sun, and B. H. Wang. Flux information feedback strategy in intelligent traffic systems. *EPL (Europhysics Letters)*, 97(1):14001, 2012.

[110] Z. He, B. Chen, N. Jia, W. Guan, B. Lin, and B. Wang. Route guidance strategies revisited: Comparison and evaluation in an asymmetric two-route traffic network. *International Journal of Modern Physics C*, 25(04):1450005, 2014.

[111] N. Levy and E. Ben-Elia. Emergence of system optimum: A fair and altruistic agent-based route-choice model. *Procedia Computer Science*, 83:928–933, 2016.

[112] H. Ye, F. Xiao, and H. Yang. Exploration of day-to-day route choice models by a virtual experiment. *Transportation Research Procedia*, 23:679 – 699, 2017.

[113] V. Mak, D. A. Seale, E. J. Gisches, R. Yang, M. Cheng, M. Moon, and A. Rapoport. The Braess Paradox and Coordination Failure in Directed Networks with Mixed Externalities. *Production and Operations Management*, 27(4):717–733, 2018.

[114] L. Fischer. Das Braess-Paradoxon in TASEP-Netzwerken. Master's thesis, Institut für Theoretische Physik Mathematisch-Naturwissenschaftliche Fakultät Universität zu Köln, 2018.

[115] B. Derrida. An exactly soluble non-equilibrium system: the asymmetric simple exclusion process. *Physics Reports*, 301(1-3):65–83, 1998.

[116] B. Derrida, E. Domany, and D. Mukamel. An exact solution of a one-dimensional asymmetric exclusion model with open boundaries. *Journal of Statistical Physics*, 69 (3):667–687, 1992.

[117] G. Schütz and E. Domany. Phase transitions in an exactly soluble one-dimensional exclusion process. *Journal of Statistical Physics*, 72(1-2):277–296, 1993.

[118] B. Derrida, M. R. Evans, V. Hakim, and V. Pasquier. Exact solution of a 1D asymmetric exclusion model using a matrix formulation. *Journal of Physics A: Mathematical and General*, 26(7):1493, 1993.

[119] A. B. Kolomeisky, G. M. Schütz, E. B. Kolomeisky, and J. P. Straley. Phase diagram of one-dimensional driven lattice gases with open boundaries. *Journal of Physics A: Mathematical and General*, 31(33):6911, 1998.

[120] R. Barlovic, L. Santen, A. Schadschneider, and M. Schreckenberg. Metastable states in cellular automata for traffic flow. *The European Physical Journal B - Condensed Matter and Complex Systems*, 5(3):793–800, 1998.

[121] L. Ming-Zhe, L. Shao-Da, and W. Rui-Li. Asymmetric simple exclusion processes with complex lattice geometries: A review of models and phenomena. *Chinese Physics B*, 21(9):090510, 2012.

[122] A. B. Kolomeisky. Asymmetric simple exclusion model with local inhomogeneity. *Journal of Physics A: Mathematical and General*, 31(4):1153, 1998.

[123] J. Schmidt. Numerische und analytische untersuchung von gekoppelten exklusionsprozessen. Master's thesis, Institut für Theoretische Physik Mathematisch-Naturwissenschaftliche Fakultät Universität zu Köln, 2014.

[124] A. Raguin, A. Parmeggiani, and N. Kern. Role of network junctions for the totally asymmetric simple exclusion process. *Physical Review E*, 88(4):042104, 2013.

[125] Y. Baek, M. Ha, and H. Jeong. Effects of junctional correlations in the totally asymmetric simple exclusion process on random regular networks. *Physical Review E*, 90: 062111, 2014.

[126] S. Bittihn and A. Schadschneider. Braess paradox in a network of totally asymmetric exclusion processes. *Physical Review E*, 94:062312, 2016.

[127] S. Bittihn and A. Schadschneider. Braess paradox in a network with stochastic dynamics and fixed strategies. *Physica A: Statistical Mechanics and its Applications*, 507:133 – 152, 2018.

[128] M. Matsumoto and T. Nishimura. Mersenne twister: a 623-dimensionally equidistributed uniform pseudo-random number generator. *ACM Transactions on Modeling and Computer Simulation (TOMACS)*, 8(1):3–30, 1998.

[129] N. Metropolis, A. W. Rosenbluth, M. N. Rosenbluth, A. H. Teller, and E. Teller. Equation of State Calculations by Fast Computing Machines. *The Journal of Chemical Physics*, 21(6):1087–1092, 1953.

[130] S. Bittihn and A. Schadschneider. Braess Paradox in Networks of Stochastic Microscopic Traffic Models. In *Traffic and Granular Flow '17*. Springer, (to be published in 2019).

[131] J. de Gier and B. Nienhuis. Exact stationary state for an asymmetric exclusion process with fully parallel dynamics. *Physical Review E*, 59:4899–4911, 1999.

[132] M. R. Evans, N. Rajewsky, and E. R. Speer. Exact Solution of a Cellular Automaton for Traffic. *Journal of Statistical Physics*, 95(1):45–96, 1999.

[133] A. Parmeggiani, T. Franosch, and E. Frey. Totally asymmetric simple exclusion process with Langmuir kinetics. *Physical Review E*, 70:046101, 2004.

A Appendix

A.1 Observable Landscapes and Density Profiles

In this section the $T_{\max}$ and ΔT landscapes (and for open boundary conditions also the no. of particles landscapes) for some example states of all the different phases are shown. Furthermore, density profiles of all routes in the system and user optima of the 5link systems are shown.

A.1.1 Periodic Boundary Conditions and Fixed Route Choices

In this section examples of the $T_{\max}$ and ΔT landscapes depending on $\left(n_1^{(j_1)}, n_1^{(j_2)}\right)$ and density profiles and explicit travel times of the system optimum and the (closest candidates for the) user optimum of all phases appearing in the periodic Braess network with random-sequential dynamics and fixed route choices (results are shown in Section 4.1) are shown. Figures A.1 to A.9 show examples of all phases found in the phase diagram shown in Figure 4.8. In all figures presented here the shared parameters are $L_0 = 1$, $L_1 = L_3 = 100$, $L_2 = L_4 = 500$.

In each of the figures, Part **(a)** shows the $T_{\max}$ and ΔT landscapes with a $\left(n_1^{(j_1)}, n_1^{(j_2)}\right)$ discretization resolution of 0.1. The strategies which correspond to the system optimum and the user optimum (in primed phases the closest candidate for a real user optimum) are also indicated. Depending on the specific parameter set, the optima were found by different methods (described in Sections 3.2.5 and 3.3.2) and may actually lie in between the discrete point of the 0.1 grid which is shown. The 0.1 grid is underlayed to give a coarse impression of how the observable landscapes look like.

Parts **(b)** of the figures show the density profiles of the three routes in the optimum states and also provide travel time values with standard deviations of the routes in those states. The exact values of $\left(n_1^{(j_1)}, n_1^{(j_2)}\right)$ of the optima and the corresponding $T_{\max}$ and ΔT values are given in the figure captions as well as the travel times in the corresponding 4link user and system optimum.

From the density profiles one can see that the roads are either all in LD, HD or MC states, or that there are localized domain walls. There is no indication of fluctuating domain walls which would show in parts of the density profiles being linearly ascending. Furthermore, one can see from Parts **(b)** of the figures that the standard deviations of the route's travel times stay well below 10% in all shown user and system optima. This indicates that the travel times are stable in the sense that all individual cars will experience similar travel times in the stationary states.

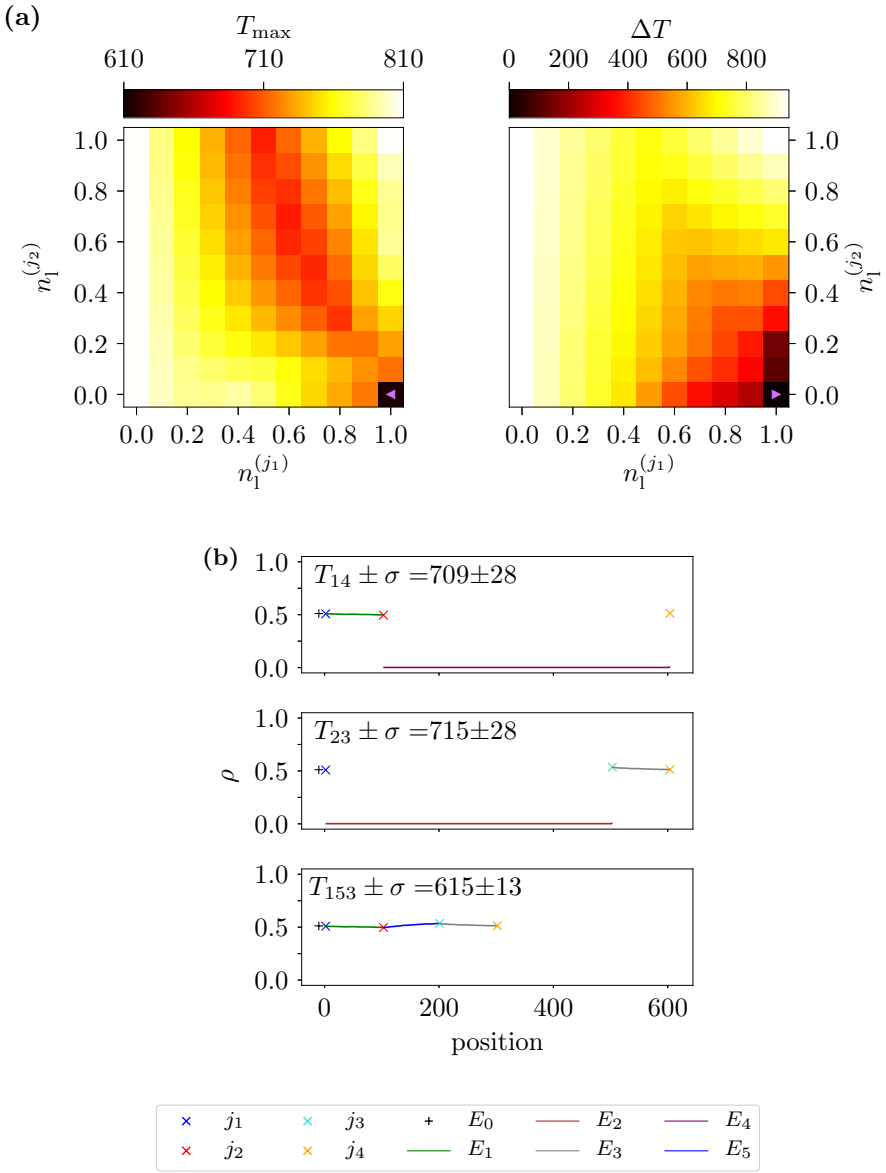

Figure A.1. An example of an "E_5 optimal" ("all 153") state for the case of fixed route choices. Parameters are $L_5 = 97$, $M = 156$. This means $\hat{L}_{153}/\hat{L}_{14} = 0.5$, $\rho^{(5)}_{\text{global}} \approx 0.12$. The travel time in the 4link user and system optimum is $T_{\max}(uo^{(4)}) = T_{\max}(so^{(4)}) \approx 692$.
Part **(a)** shows the $T_{\max}$ (left) and ΔT (right) landscapes. The pink ◀ and ▶ indicate the system and user optimum, respectively.
Part **(b)** shows density profiles and average travel times $T_i \pm$ standard deviation σ of the three paths for $\min(T_{\max})$ and $\min(\Delta T)$ at $so^{(5)} = uo^{(5)} \mathrel{\widehat{=}} \left(n_1^{(j_1)}, n_1^{(j_2)}\right) = (1.0, 0.0)$ with $\Delta T(so^{(5)}) = \Delta T(uo^{(5)}) = 0$, $T_{\max}(so^{(5)}) = T_{\max}(uo^{(5)}) \approx 615$.

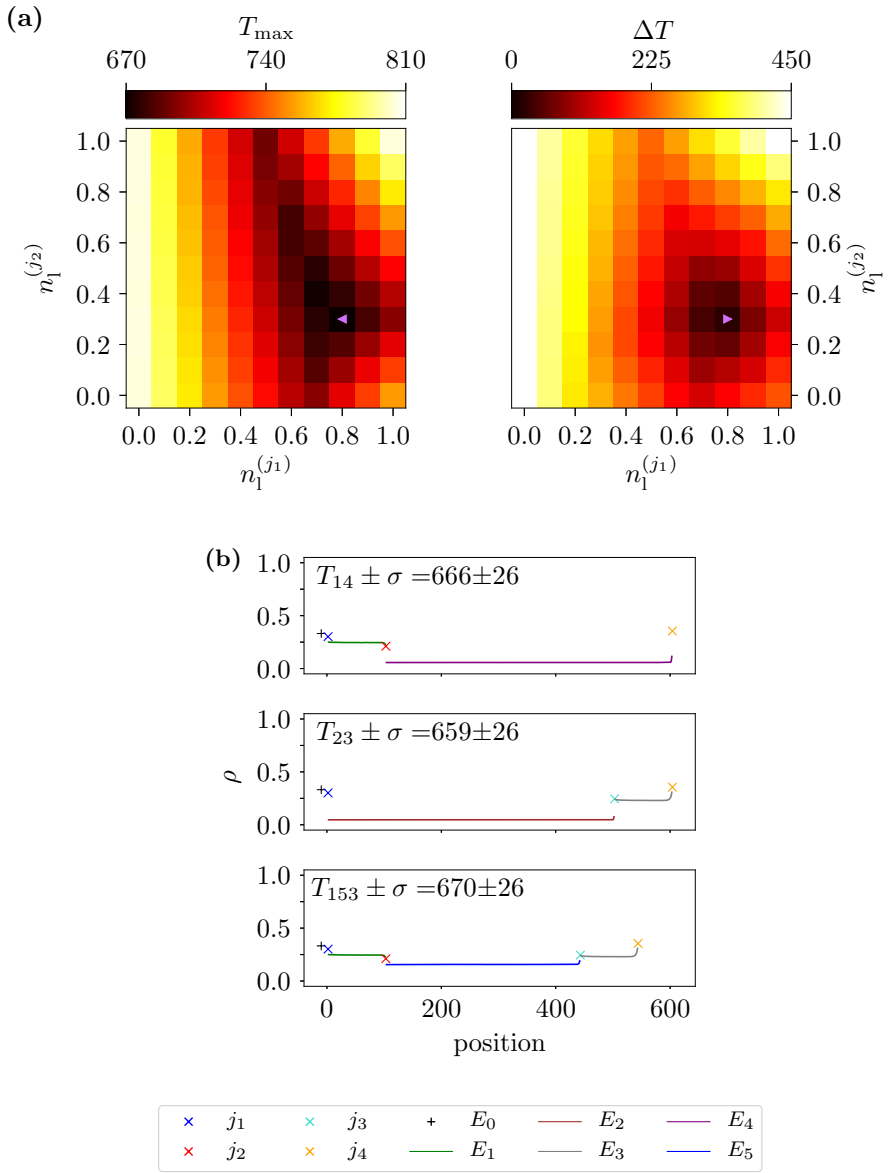

Figure A.2. An example of an "E_5 optimal" state for the case of fixed route choices. Parameters are $L_5 = 339$, $M = 154$. This means $\hat{L}_{153}/\hat{L}_{14} \approx 0.9$, $\rho^{(5)}_{\text{global}} \approx 0.1$. The travel time in the 4link user and system optimum is $T_{\max}(uo^{(4)}) = T_{\max}(so^{(4)}) \approx 691$.
Part **(a)** shows the $T_{\max}$ (left) and ΔT (right) landscapes. The pink ◀ and ▶ indicate the system and user optimum, respectively.
Part **(b)** shows density profiles and average travel times $T_i \pm$ standard deviation σ of the three paths for $\min(T_{\max})$ and $\min(\Delta T)$ at $so^{(5)} = uo^{(5)} \mathrel{\widehat{=}} \left(n_1^{(j_1)}, n_1^{(j_2)}\right) = (0.8, 0.3)$ with $\Delta T(so^{(5)}) = \Delta T(uo^{(5)}) \approx 22$, $T_{\max}(so^{(5)}) = T_{\max}(uo^{(5)}) \approx 670$.

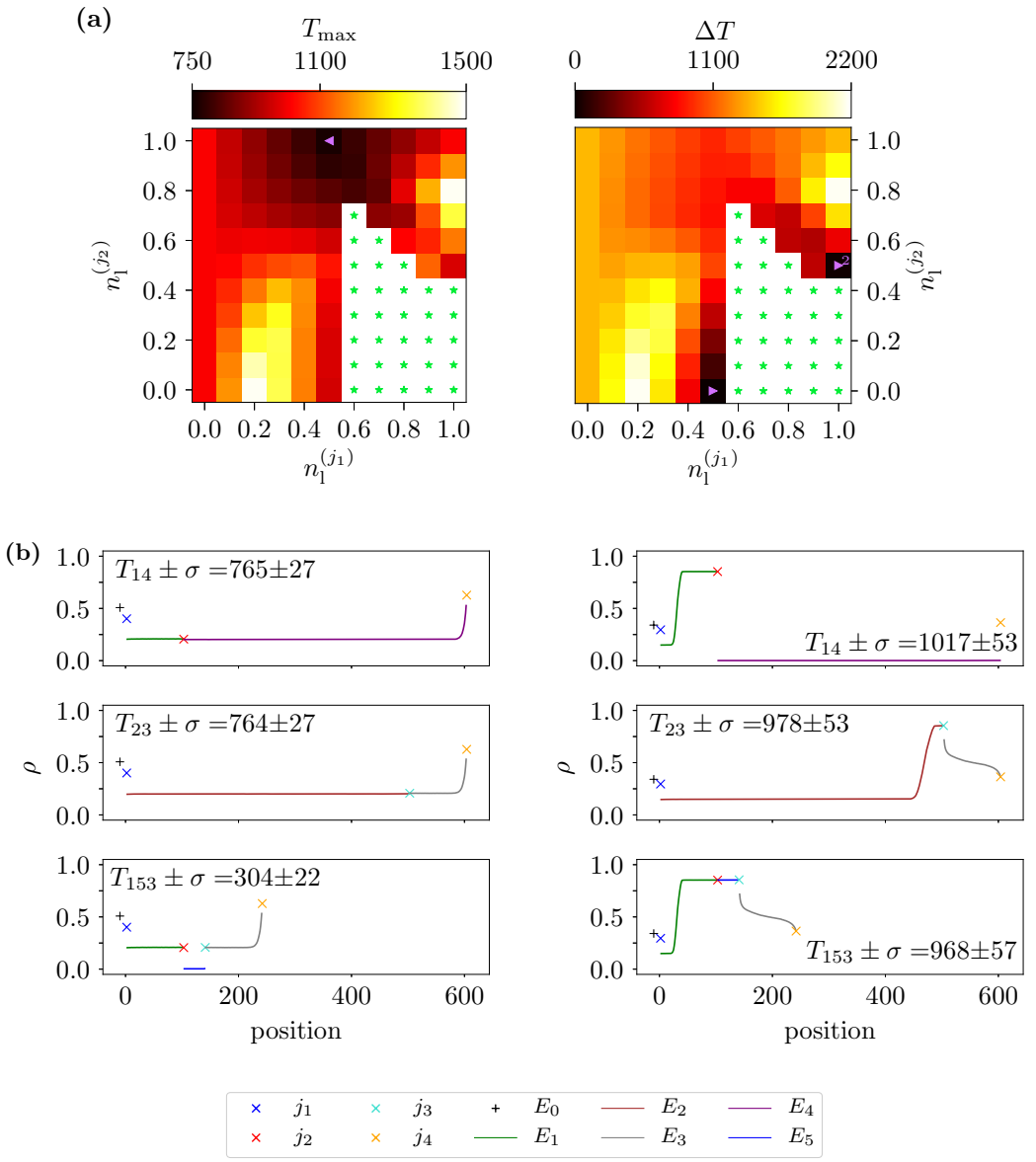

Figure A.3. An example of a "Braess 1" state for the case of fixed route choices. Parameters are $L_5 = 37$, $M = 248$. This means $\hat{L}_{153}/\hat{L}_{14} \approx 0.4$, $\rho^{(5)}_{\text{global}} \approx 0.2$. The travel time in the 4link user and system optimum is $T_{\max}(uo^{(4)}) = T_{\max}(so^{(4)}) \approx 764$.
Part **(a)** shows the $T_{\max}$ (left) and ΔT (right) landscapes. The pink ◀ and ▶ indicate the system and user optimum, respectively. For this parameter set there exist two user optima. The second user optimum is marked by a pink ▶ 2. Strategies with a gridlocked stationary state on route 153 are marked with green ⋆'s.
Part **(b)** shows density profiles and average travel times $T_i \pm$ standard deviation σ of the three paths for (left): $\min(T_{\max})$ at $so^{(5)} \mathrel{\widehat{=}} \left(n_1^{(j_1)}, n_1^{(j_2)}\right) = (0.5, 1.0)$ with $\Delta T(so^{(5)}) \approx 922$, $T_{\max}(so^{(5)}) \approx 765$ and (right): $\min(\Delta T)$ at $uo^{(5)} \mathrel{\widehat{=}} \left(n_1^{(j_1)}, n_1^{(j_2)}\right) = (0.5, 0.0)$ with $\Delta T(uo^{(5)}) \approx 10$, $T_{\max}(uo^{(5)}) \approx 978$.

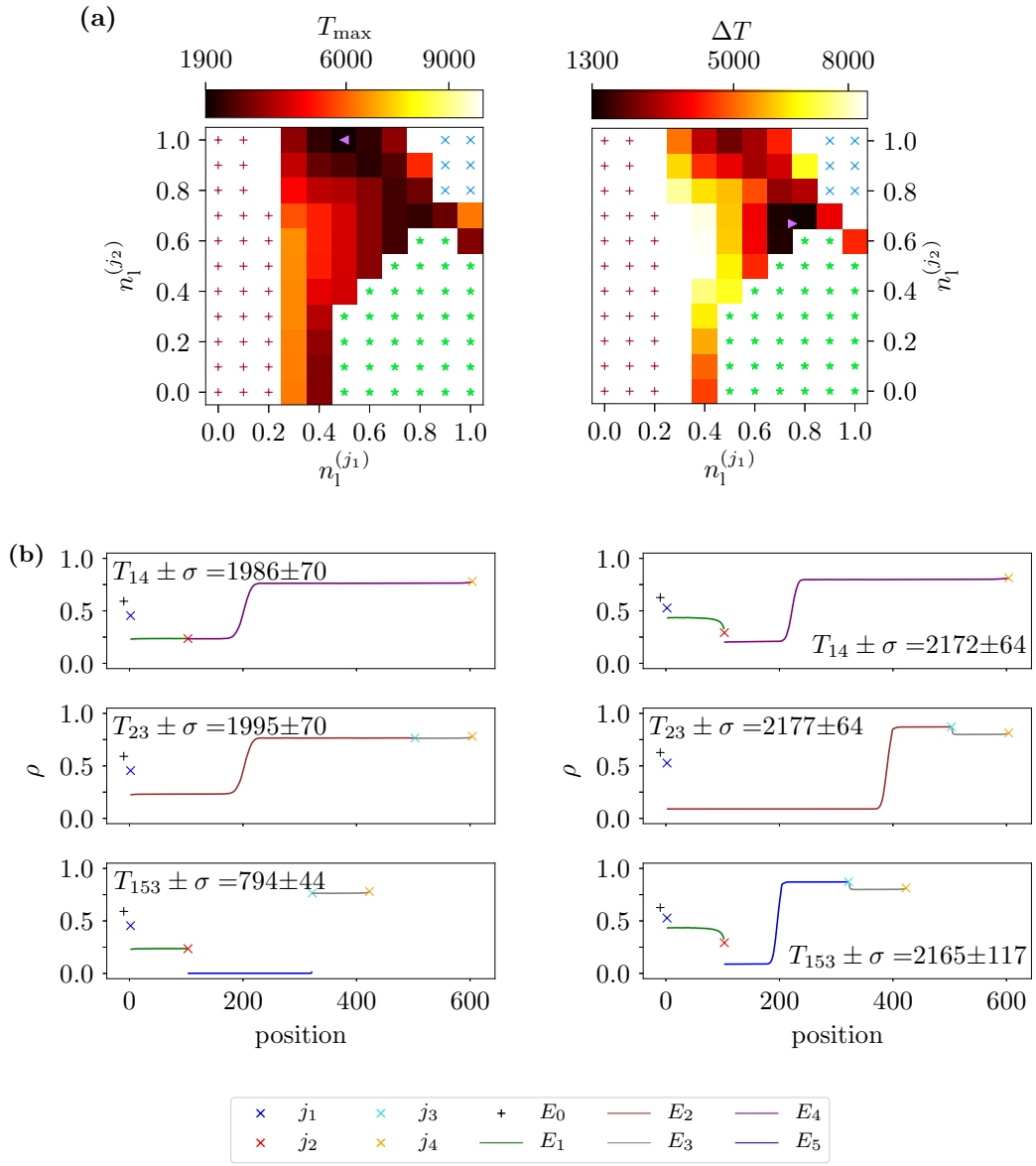

Figure A.4. An example of a "Braess 1" state for the case of fixed route choices. Parameters are $L_5 = 218$, $M = 712$. This means $\hat{L}_{153}/\hat{L}_{14} \approx 0.7$, $\rho^{(5)}_{\text{global}} \approx 0.5$. The travel time in the 4link user and system optimum is $T_{\max}(uo^{(4)}) = T_{\max}(so^{(4)}) \approx 1991$.
Part **(a)** shows the $T_{\max}$ (left) and ΔT (right) landscapes. The pink ◀ and ▶ indicate the system and user optimum, respectively. Strategies with gridlocked stationary states on routes 14, 23 and 153 are marked with blue ×'s, red +'s and green ⋆'s, respectively.
Part **(b)** shows density profiles and average travel times $T_i \pm$ standard deviation σ of the three paths for (left): $\min(T_{\max})$ at $so^{(5)} \mathrel{\widehat{=}} \left(n_1^{(j_1)}, n_1^{(j_2)}\right) = (0.5, 1.0)$ with $\Delta T(so^{(5)}) \approx 2402$, $T_{\max}(so^{(5)}) \approx 1995$ and (right): $\min(\Delta T)$ at $uo^{(5)} \mathrel{\widehat{=}} \left(n_1^{(j_1)}, n_1^{(j_2)}\right) = (0.75, 0.669)$ with $\Delta T(uo^{(5)}) \approx 24$, $T_{\max}(uo^{(5)}) \approx 2177$.

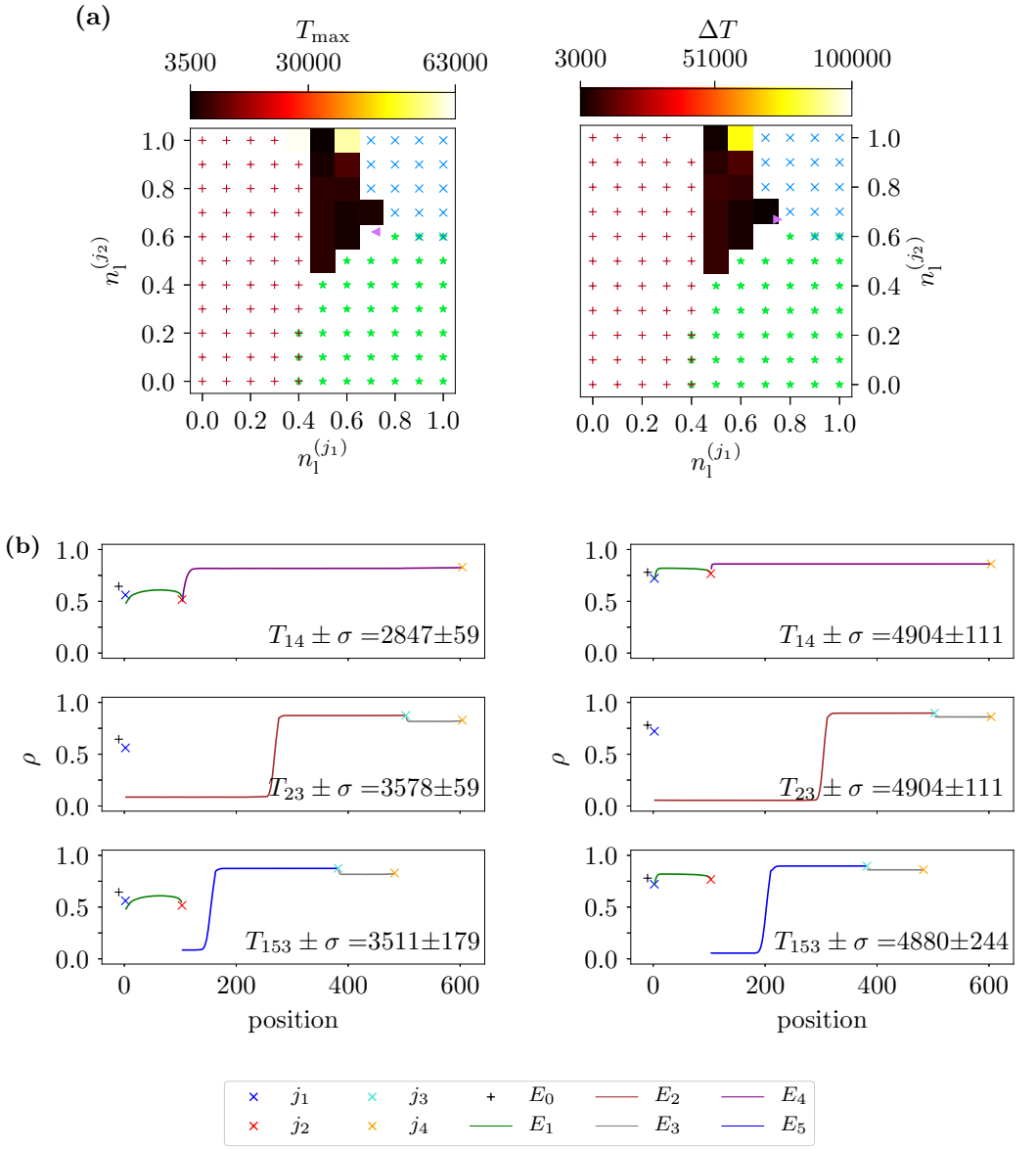

Figure A.5. An example of an "Braess 2" state for the case of fixed route choices. Parameters are $L_5 = 278$, $M = 994$. This means $\hat{L}_{153}/\hat{L}_{14} \approx 0.8$, $\rho^{(5)}_{\text{global}} \approx 0.67$. The travel time in the 4link user and system optimum is $T_{\max}(uo^{(4)}) = T_{\max}(so^{(4)}) \approx 3631$.
Part **(a)** shows the $T_{\max}$ (left) and ΔT (right) landscapes. The pink ◀ and ▶ indicate the system and user optimum, respectively. Strategies with gridlocked stationary states on routes 14, 23 and 153 are marked with blue ×'s, red +'s and green ⋆'s, respectively.
Part **(b)** shows density profiles and average travel times $T_i \pm$ standard deviation σ of the three paths for (left): $\min(T_{\max})$ at $so^{(5)} \widehat{=} \left(n_1^{(j_1)}, n_1^{(j_2)}\right) = (0.72, 0.62)$ with $\Delta T(so^{(5)}) \approx 1462$, $T_{\max}(so^{(5)}) \approx 3578$ and (right): $\min(\Delta T)$ at $uo^{(5)} \widehat{=} \left(n_1^{(j_1)}, n_1^{(j_2)}\right) = (0.749, 0.669)$ with $\Delta T(uo^{(5)}) \approx 48$, $T_{\max}(uo^{(5)}) \approx 4904$.

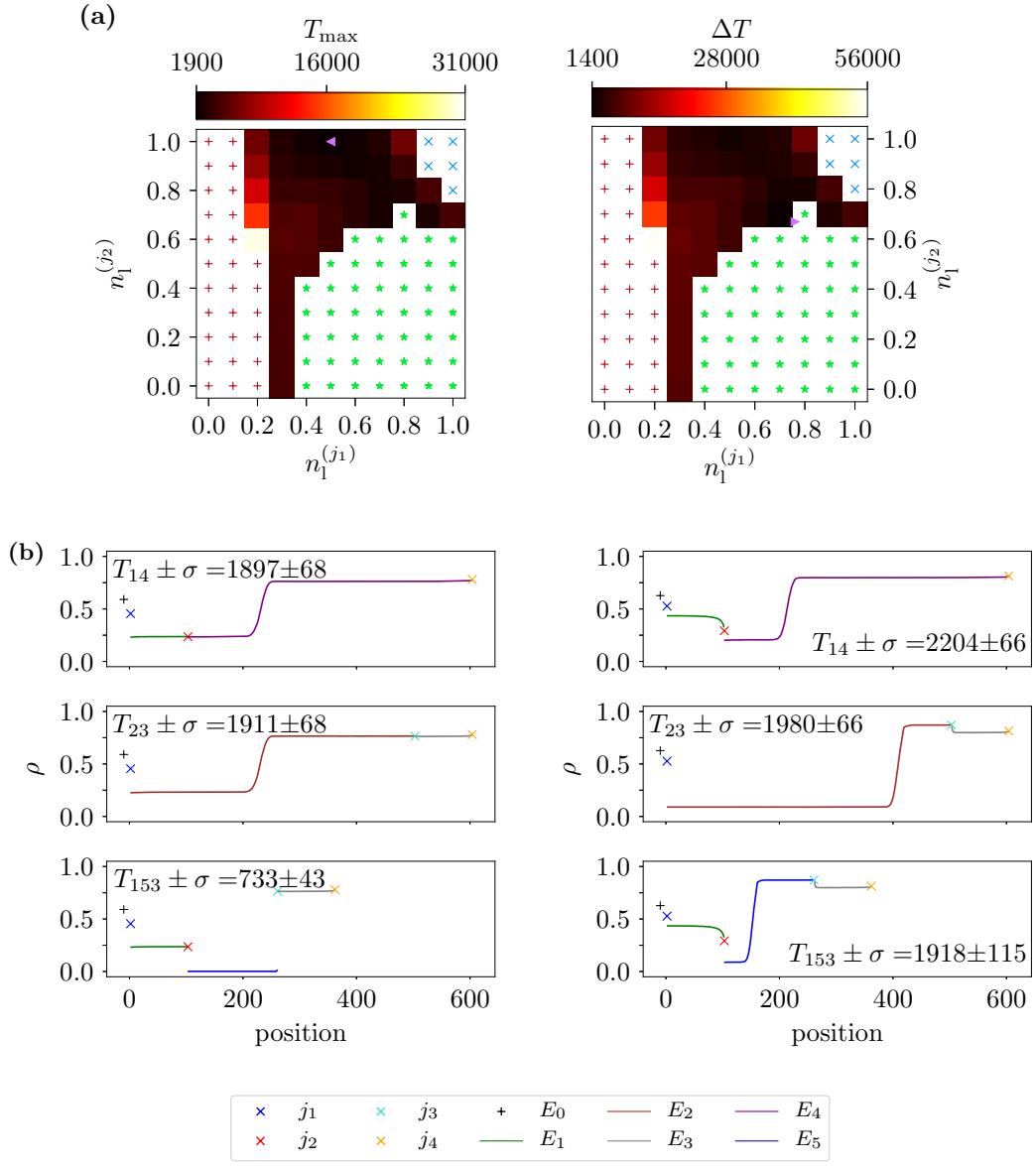

Figure A.6. An example of an "Braess 1 - like" state for the case of fixed route choices. Parameters are $L_5 = 157$, $M = 681$. This means $\hat{L}_{153}/\hat{L}_{14} \approx 0.6$, $\rho^{(5)}_{\text{global}} = 0.5$. The travel time in the 4link user and system optimum is $T^{(4)}_{uo} = T^{(4)}_{so} \approx 1904$.
Part **(a)** shows the $T_{\max}$ (left) and ΔT (right) landscapes. The pink ◀ and ▶ indicate the system optimum and the closest candidate for a user optimum, respectively. Strategies with gridlocked stationary states on routes 14, 23 and 153 are marked with blue ×'s, red +'s and green ⋆'s, respectively.
Part **(b)** shows density profiles and average travel times $T_i \pm$ standard deviation σ of the three paths for (left): $\min(T_{\max})$ at $so^{(5)} \mathrel{\widehat{=}} \left(n_1^{(j_1)}, n_1^{(j_2)}\right) = (0.5, 1.0)$ with $\Delta T(so^{(5)}) \approx 2356$, $T_{\max}(so^{(5)}) \approx 1911$ and (right): $\min(\Delta T)$ at $uo^{(5)} \mathrel{\widehat{=}} \left(n_1^{(j_1)}, n_1^{(j_2)}\right) = (0.761, 0.669)$ with $\Delta T(uo^{(5)}) \approx 572$, $T_{\max}(uo^{(5)}) \approx 2204$.

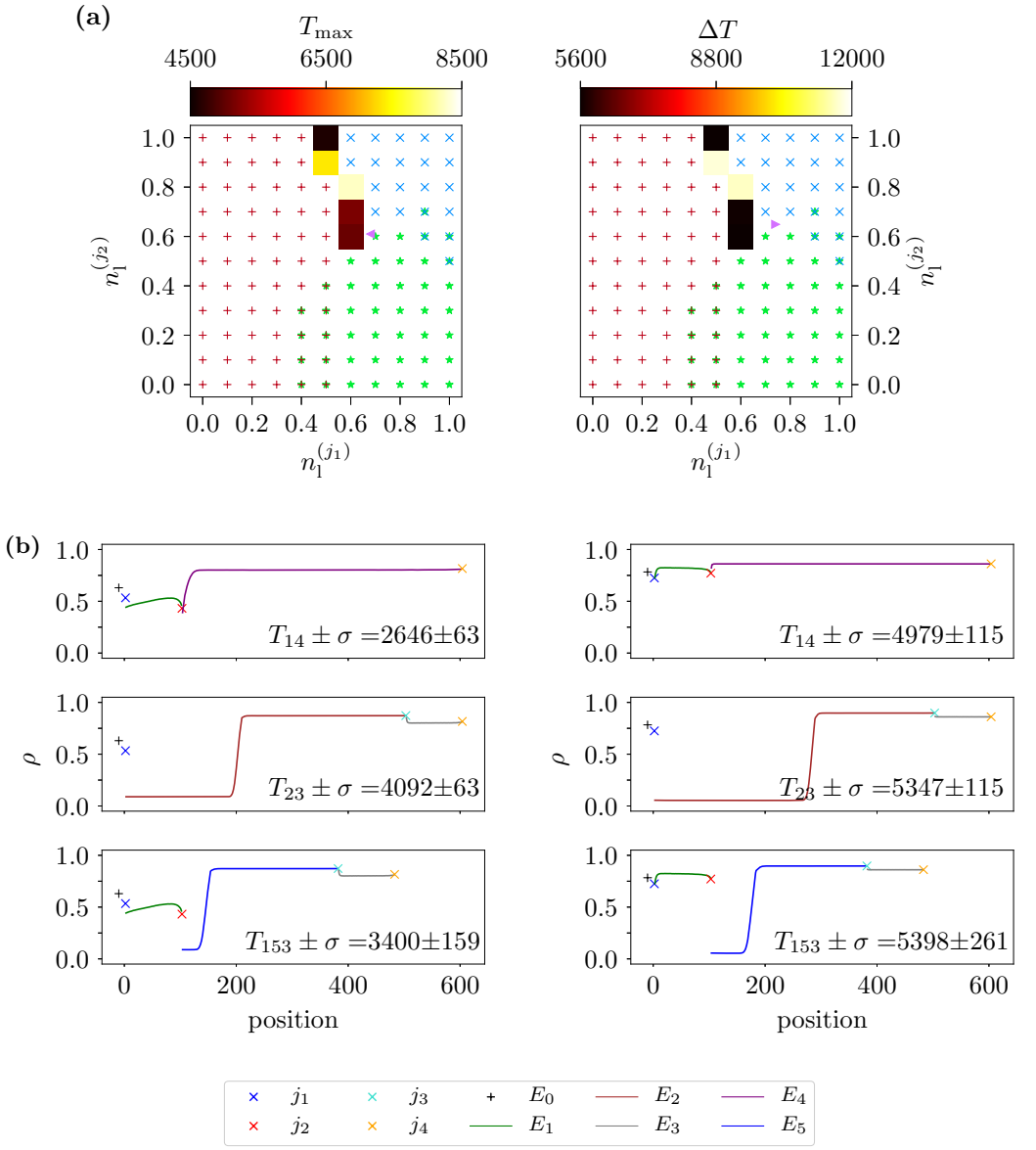

Figure A.7. An example of an "Braess 2 - like" state for the case of fixed route choices. Parameters are $L_5 = 278$, $M = 1038$. This means $\hat{L}_{153}/\hat{L}_{14} \approx 0.8$, $\rho^{(5)}_{\text{global}} \approx 0.7$. The travel time in the 4link user and system optimum is $T_{\max}(uo^{(4)}) = T_{\max}(so^{(4)}) \approx 4615$.
Part **(a)** shows the $T_{\max}$ (left) and ΔT (right) landscapes. The pink ◀ and ▶ indicate the system optimum and the closest candidate for a user optimum, respectively. Strategies with gridlocked stationary states on routes 14, 23 and 153 are marked with blue ×'s, red +'s and green ⋆'s, respectively.
Part **(b)** shows density profiles and average travel times $T_i \pm$ standard deviation σ of the three paths for (left): $\min(T_{\max})$ at $so^{(5)} \mathrel{\widehat{=}} \left(n_1^{(j_1)}, n_1^{(j_2)}\right) = (0.68, 0.61)$ with $\Delta T(so^{(5)}) \approx 2892$, $T_{\max}(so^{(5)}) \approx 4092$ and (right): $\min(\Delta T)$ at $uo^{(5)} \mathrel{\widehat{=}} \left(n_1^{(j_1)}, n_1^{(j_2)}\right) = (0.741, 0.649)$ with $\Delta T(uo^{(5)}) \approx 838$, $T_{\max}(uo^{(5)}) \approx 5398$.

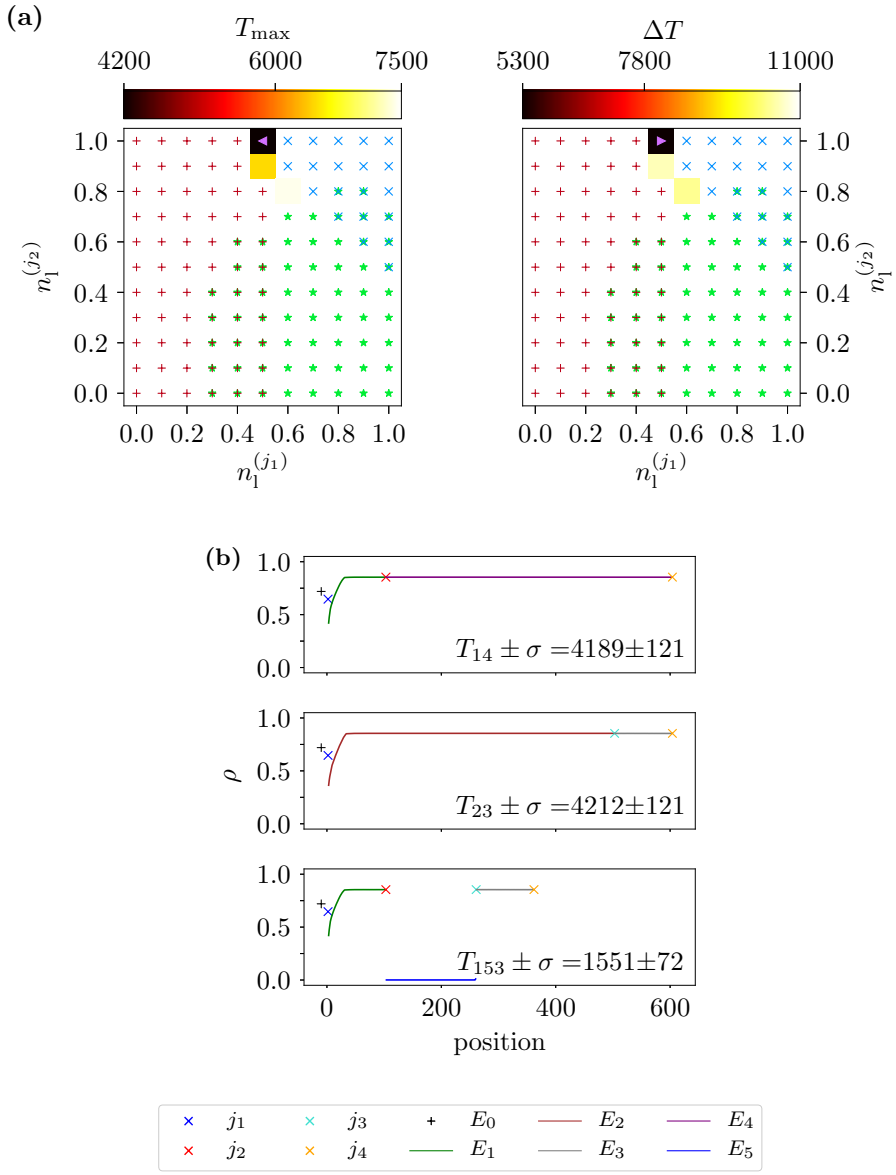

Figure A.8. An example of an "E_5 not used - like" state for the case of fixed route choices. Parameters are $L_5 = 157$, $M = 1022$. This means $\hat{L}_{153}/\hat{L}_{14} \approx 0.6$, $\rho^{(5)}_{\text{global}} \approx 0.75$. The travel time in the 4link user and system optimum is $T_{\max}(uo^{(4)}) = T_{\max}(so^{(4)}) \approx 4201$.
Part **(a)** shows the $T_{\max}$ (left) and ΔT (right) landscapes. The pink ◀ and ▶ indicate the system optimum and the closest candidate for a user optimum, respectively. Strategies with gridlocked stationary states on routes 14, 23 and 153 are marked with blue ×'s, red +'s and green ⋆'s, respectively.
Part **(b)** shows density profiles and average travel times $T_i \pm$ standard deviation σ of the three paths for $\min(T_{\max})$ and $\min(\Delta T)$ at $so^{(5)} = uo^{(5)} \mathrel{\widehat{=}} \left(n_1^{(j_1)}, n_1^{(j_2)}\right) = (0.5, 1.0)$ with $\Delta T(so^{(5)}) = \Delta T(uo^{(5)}) = 5322$, $T_{\max}(so^{(5)}) = T_{\max}(uo^{(5)}) \approx 4212$.

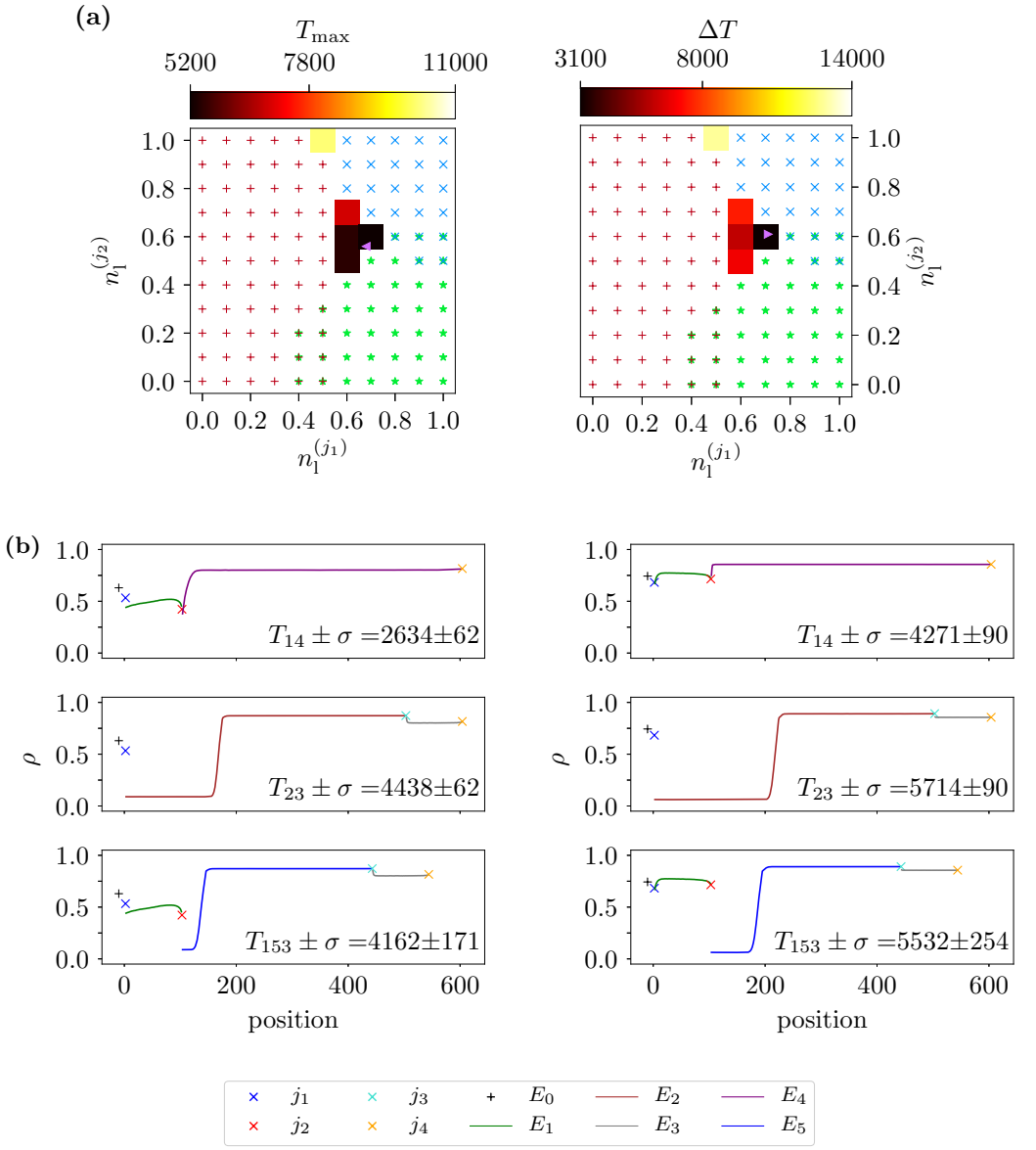

Figure A.9. An example of an "E_5 improves - like" state for the case of fixed route choices. Parameters are $L_5 = 339$, $M = 1127$. This means $\hat{L}_{153}/\hat{L}_{14} \approx 0.9$, $\rho^{(5)}_{\text{global}} \approx 0.73$. The travel time in the 4link user and system optimum is $T_{\max}(uo^{(4)}) = T_{\max}(so^{(4)}) \approx 10152$.
Part **(a)** shows the $T_{\max}$ (left) and ΔT (right) landscapes. The pink ◀ and ▶ indicate system optimum and the closest candidate for a user optimum, respectively. Strategies with gridlocked stationary states on routes 14, 23 and 153 are marked with blue ×'s, red +'s and green ⋆'s, respectively.
Part **(b)** shows density profiles and average travel times $T_i \pm$ standard deviation σ of the three paths for (left): $\min(T_{\max})$ at $so^{(5)} \widehat{=} \left(n_1^{(j_1)}, n_1^{(j_2)}\right) = (0.68, 0.56)$ with $\Delta T(so^{(5)}) \approx 3608$, $T_{\max}(so^{(5)}) \approx 4438$ and (right): $\min(\Delta T)$ at $uo^{(5)} \widehat{=} \left(n_1^{(j_1)}, n_1^{(j_2)}\right) = (0.711, 0.609)$ with $\Delta T(uo^{(5)}) \approx 2886$, $T_{\max}(uo^{(5)}) \approx 5714$.

A.1.2 Periodic Boundary Conditions and Turning Probabilities

This section shows examples of the $T_{\max}$ and ΔT landscapes, depending on (γ, δ), and density profiles and explicit travel times of the system optimum and the (closest candidates for the) user optimum of all phases appearing in the periodic Braess network with random-sequential updates and turning probabilities (results are shown in Section 4.2). Figures A.10 to A.14 show examples of all phases found in the phase diagram shown in Figure 4.15. In all figures presented here the shared parameters are $L_0 = 1$, $L_1 = L_3 = 100$, $L_2 = L_4 = 500$.

In each of the figures Part **(a)** shows the $T_{\max}$ and ΔT landscapes with a (γ, δ) discretization resolution of 0.1. The strategies which correspond to the system optimum and the user optimum (in the domain wall phase and the "E_5 improves - like" phase: the closest candidate for a real user optimum) are also indicated. Depending on the specific parameter set, the optima were found by different methods (compare Sections 3.2.5 and 3.3.2) and may actually lie in between the discrete point of the 0.1 grid which is shown. The 0.1 grid is underlayed to give a coarse impression of how the observable landscapes look like.

Parts **(b)** of the figures show the density profiles of the three routes in the optimum states and also provide travel time values and their standard deviations of the routes in those states. The exact values of (γ, δ) of the optima and the corresponding $T_{\max}$ and ΔT values are given in the figure captions as well as the travel times in the corresponding 4link user and system optimum.

Some of the figures shown in the present subsection have been published in [126].

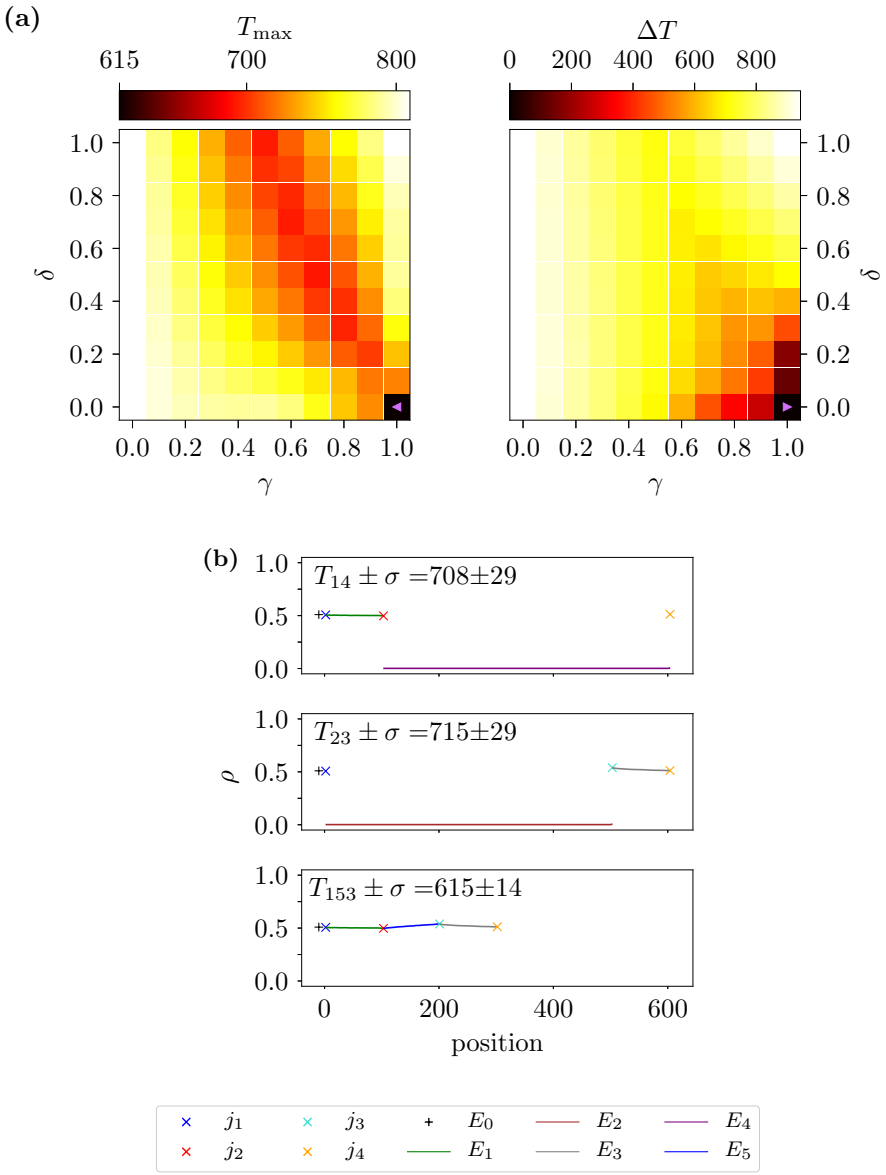

Figure A.10. An example of an "E_5 optimal" ("all 153") state for the case of turning probabilities. Parameters are $L_5 = 97$, $M = 156$. This means $\hat{L}_{153}/\hat{L}_{14} = 0.5$, $\rho^{(5)}_{\text{global}} \approx 0.12$. The travel time in the 4link user and system optimum is $T_{\max}(uo^{(4)}) = T_{\max}(so^{(4)}) \approx 693$.
Part **(a)** shows the $T_{\max}$ (left) and ΔT (right) landscapes. The pink ◀ and ▶ indicate the system and user optimum, respectively.
Part **(b)** shows density profiles and average travel times $T_i \pm$ standard deviation σ of the three paths for $\min(T_{\max})$ and $\min(\Delta T)$ at $so^{(5)} = uo^{(5)} \mathrel{\widehat{=}} (\gamma, \delta) = (1.0, 0.0)$ with $\Delta T(so^{(5)}) = \Delta T(uo^{(5)}) = 0$, $T_{\max}(so^{(5)}) = T_{\max}(uo^{(5)}) \approx 615$.

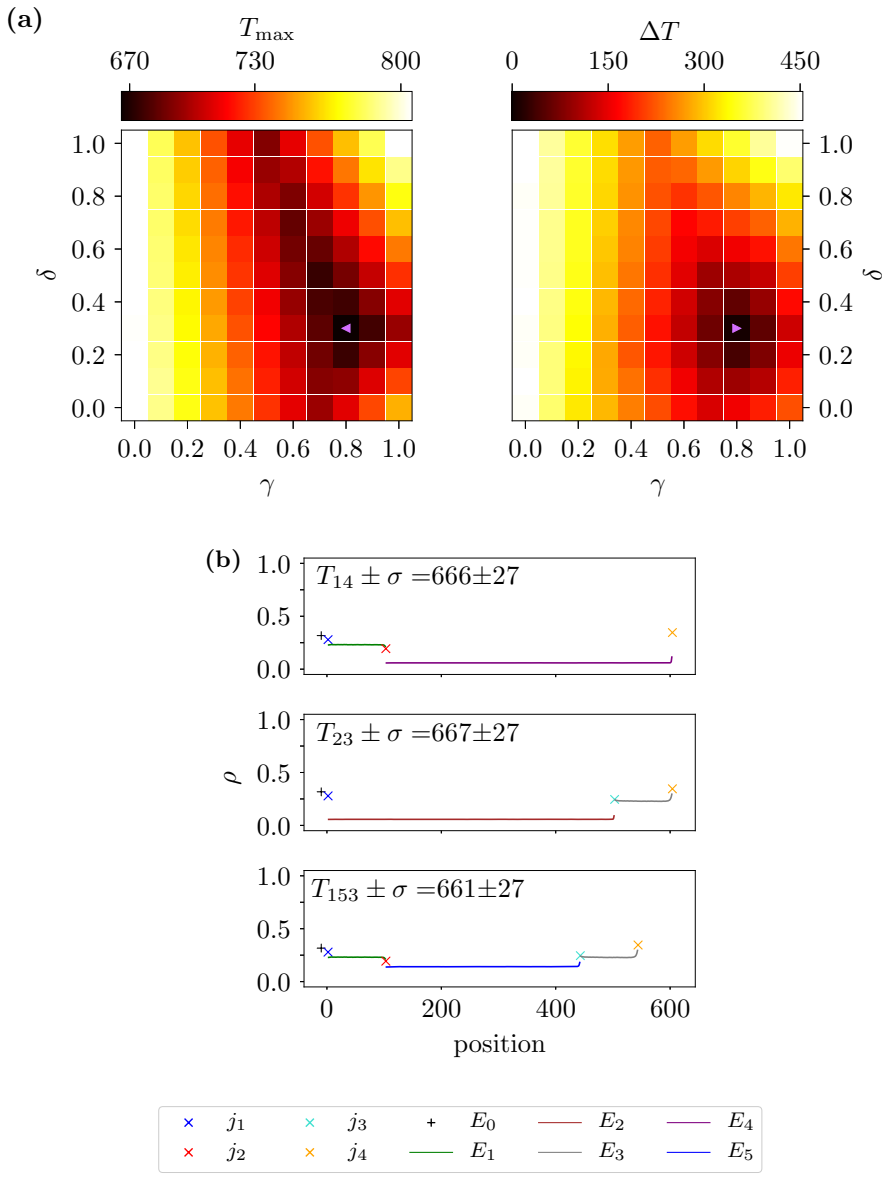

Figure A.11. An example of an "E_5 optimal" state for the case of turning probabilities. Parameters are $L_5 = 339$, $M = 154$. This means $\hat{L}_{153}/\hat{L}_{14} \approx 0.9$, $\rho^{(5)}_{\text{global}} \approx 0.1$. The travel time in the 4link user and system optimum is $T_{\max}(uo^{(4)}) = T_{\max}(so^{(4)}) \approx 692$.
Part **(a)** shows the $T_{\max}$ (left) and ΔT (right) landscapes. The pink ◀ and ▶ indicate the system and user optimum, respectively.
Part **(b)** shows density profiles and average travel times $T_i \pm$ standard deviation σ of the three paths for $\min(T_{\max})$ and $\min(\Delta T)$ at $so^{(5)} = uo^{(5)} \mathrel{\widehat{=}} (\gamma, \delta) = (0.8, 0.3)$ with $\Delta T(so^{(5)}) = \Delta T(uo^{(5)}) = 12$, $T_{\max}(so^{(5)}) = T_{\max}(uo^{(5)}) \approx 667$.

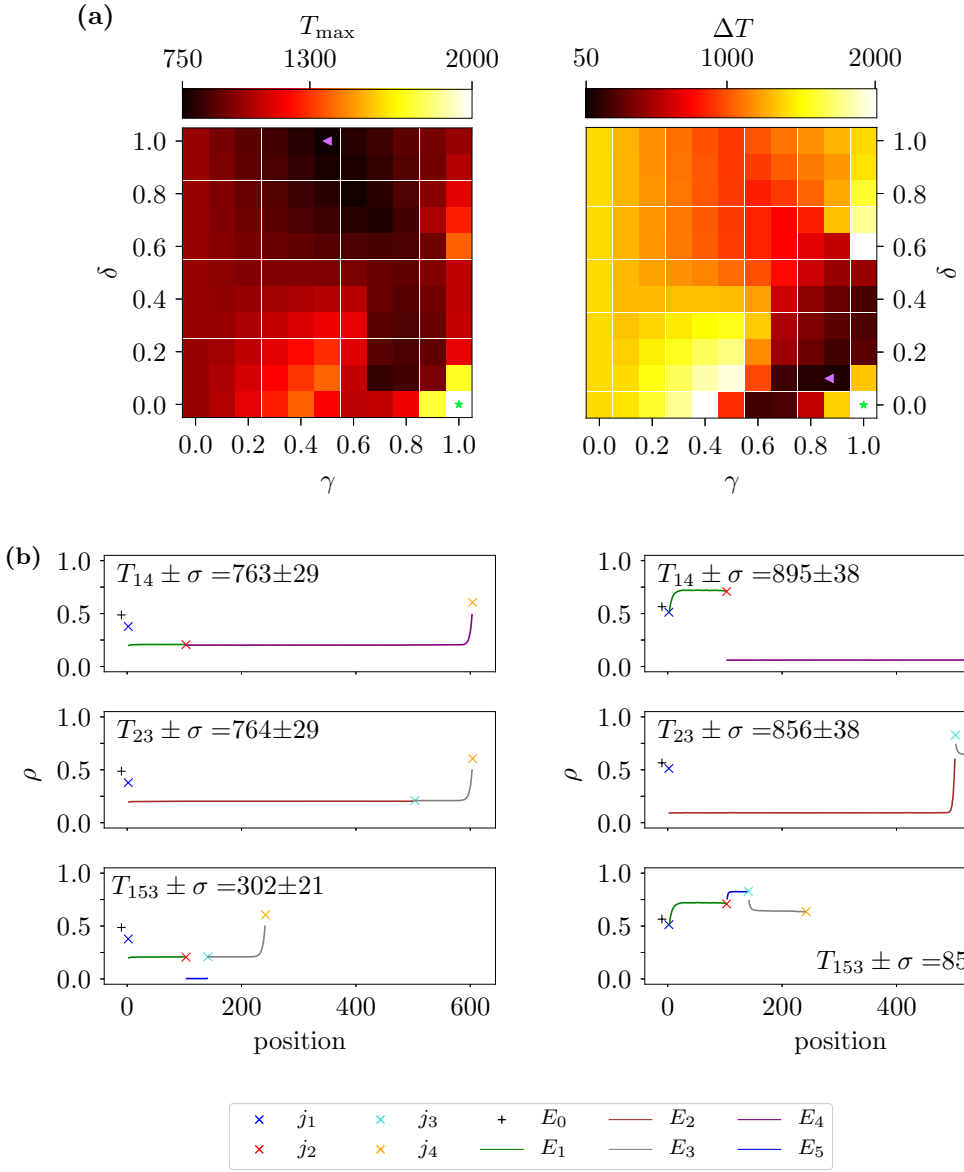

Figure A.12. An example of a "Braess 1" state for the case of turning probabilities. Parameters are $L_5 = 37$, $M = 248$. This means $\hat{L}_{153}/\hat{L}_{14} \approx 0.4$, $\rho^{(5)}_{\text{global}} \approx 0.2$. The travel time in the 4link user and system optimum is $T_{\max}(uo^{(4)}) = T_{\max}(so^{(4)}) \approx 763$.
Part **(a)** shows the $T_{\max}$ (left) and ΔT (right) landscapes. The pink ◀ and ▶ indicate the system and user optimum, respectively. Strategies with a gridlocked stationary state on route 153 are marked with green ⋆'s.
Part **(b)** shows density profiles and average travel times $T_i \pm$ standard deviation σ of the three paths for (left): $\min(T_{\max})$ at $so^{(5)} \mathrel{\widehat{=}} (\gamma, \delta) = (0.5, 1.0)$ with $\Delta T(so^{(5)}) \approx 924$, $T_{\max}(so^{(5)}) \approx 764$ and (right): $\min(\Delta T)$ at $uo^{(5)} \mathrel{\widehat{=}} (\gamma, \delta) = (0.87, 0.1)$ with $\Delta T(uo^{(5)}) \approx 78$, $T_{\max}(uo^{(5)}) \approx 895$.

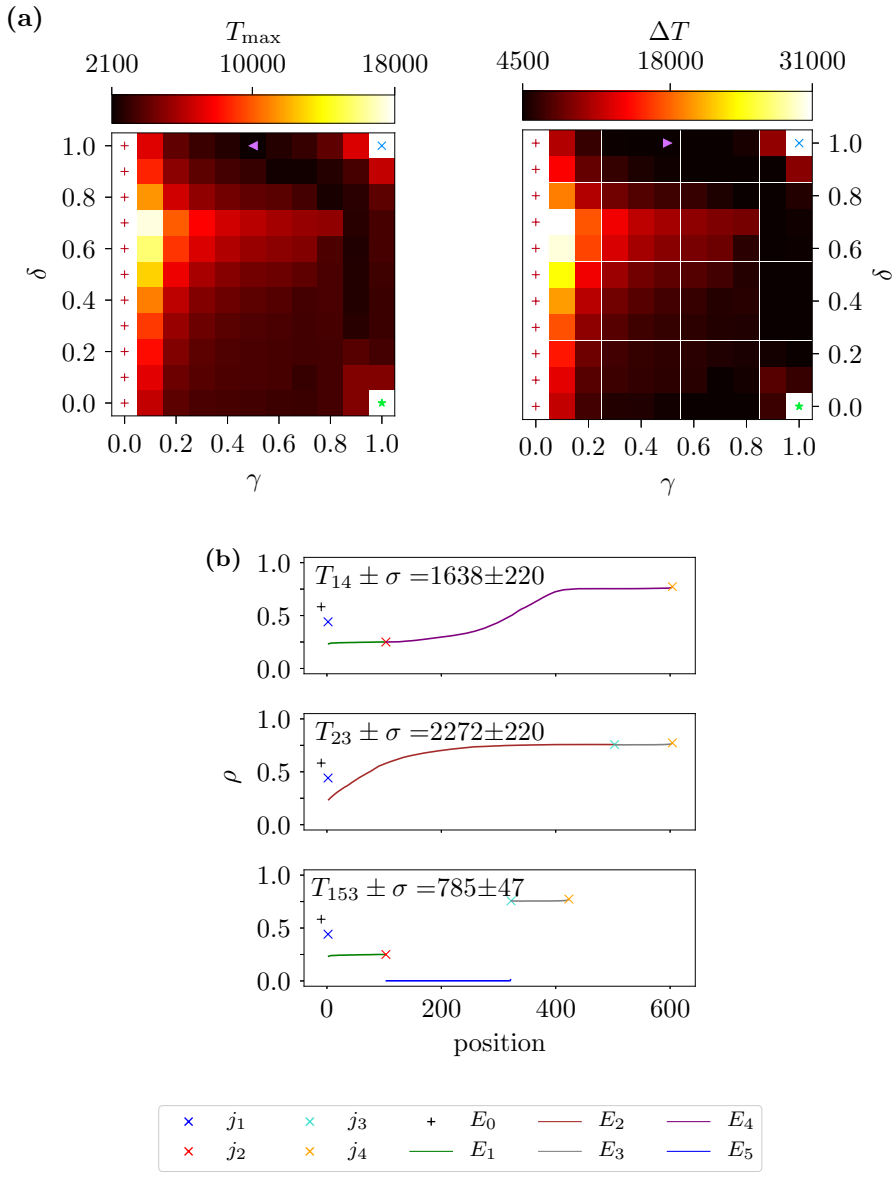

Figure A.13. An example of a "domain wall" state for the case of turning probabilities. Parameters are $L_5 = 218$, $M = 712$. This means $\hat{L}_{153}/\hat{L}_{14} \approx 0.7$, $\rho^{(5)}_{\text{global}} \approx 0.5$. The travel time in the 4link user and system optimum is $T_{\max}(uo^{(4)}) = T_{\max}(so^{(4)}) \approx 1955$.
Part **(a)** shows the $T_{\max}$ (left) and ΔT (right) landscapes. The pink ◀ and ▶ indicate the closest candidates for system and user optimum, respectively. Strategies with gridlocked stationary states on routes 14, 23 and 153 are marked with blue ×'s, red +'s and green ⋆'s, respectively. The travel time in the 4link user and system optimum is $T_{\max}(uo^{(4)}) = T_{\max}(so^{(4)}) \approx 692$.
Part **(b)** shows density profiles and average travel times $T_i \pm$ standard deviation σ of the three paths for $\min(T_{\max})$ and $\min(\Delta T)$ at $so^{(5)} = uo^{(5)} \mathrel{\widehat{=}} (\gamma, \delta) = (0.5, 1.0)$ with $\Delta T(so^{(5)}) = \Delta T(uo^{(5)}) = 2974$, $T_{\max}(so^{(5)}) = T_{\max}(uo^{(5)}) \approx 2272$.

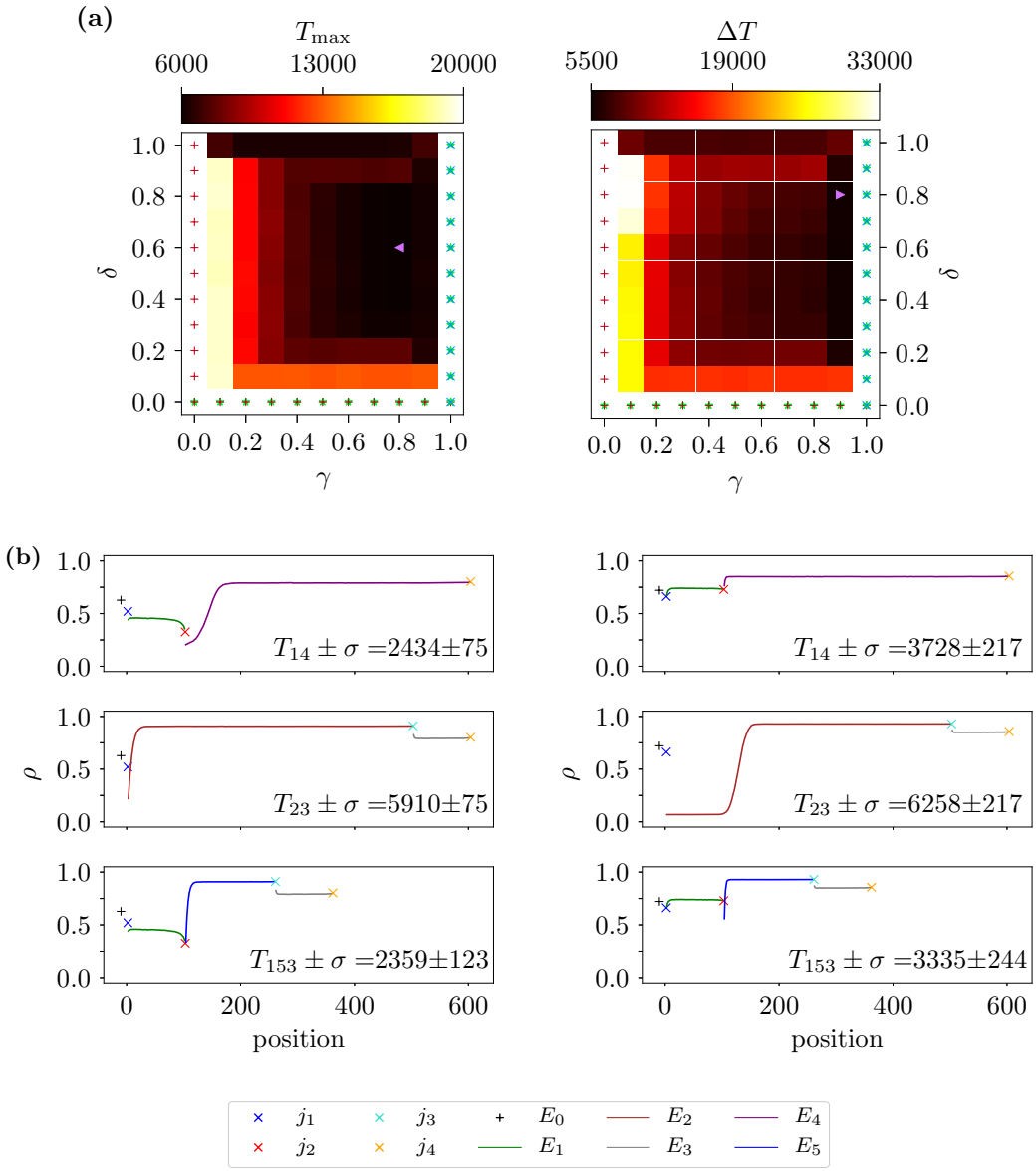

Figure A.14. An example of an "E_5 improves - like" state for the case of turning probabilities. Parameters are $L_5 = 157$, $M = 1090$. This means $\hat{L}_{153}/\hat{L}_{14} \approx 0.6$, $\rho^{(5)}_{\text{global}} \approx 0.8$. The travel time in the 4link user and system optimum is $T_{\max}(uo^{(4)}) = T_{\max}(so^{(4)}) \approx 6329$.
Part **(a)** shows the $T_{\max}$ (left) and ΔT (right) landscapes. The pink ◀ and ▶ indicate the system optimum and the closest candidate for a user optimum, respectively. Strategies with gridlocked stationary states on routes 14, 23 and 153 are marked with blue ×'s, red +'s and green ⋆'s, respectively.
Part **(b)** shows density profiles and average travel times $T_i \pm$ standard deviation σ of the three paths for (left): $\min(T_{\max})$ at $so^{(5)} \mathrel{\widehat{=}} (\gamma, \delta) = (0.8, 0.6)$ with $\Delta T(so^{(5)}) \approx 7102$, $T_{\max}(so^{(5)}) \approx 5910$ and (right): $\min(\Delta T)$ at $uo^{(5)} \mathrel{\widehat{=}} (\gamma, \delta) = (0.9, 0.8)$ with $\Delta T(uo^{(5)}) \approx 5846$, $T_{\max}(uo^{(5)}) \approx 6258$.

A.1.3 Open Boundary Conditions and Turning Probabilities

In this section examples of the $T_{\max}$, ΔT and the number of particles in the system landscapes, depending on $(\gamma,\ \delta)$, and density profiles and explicit travel times of the system optimum and the (closest candidates for the) user optimum of all phases appearing in the open boundary Braess network with random-sequential updates and turning probabilities are shown (results are shown in Section 4.4). Figures A.15 to A.21 show examples of all phases found in the phase diagrams shown in Figures 4.19 and 4.20. In all figures presented here the shared parameters are $L_1 = L_3 = 100$, $L_2 = L_4 = 500$.

In each of the figures Part **(a)** shows the $T_{\max}$ and ΔT and total number of particles in the system landscapes with a (γ, δ) discretization resolution of 0.1. The strategies which correspond to the system optimum and the user optimum (in unstable phases the closest candidate for a real user optimum) are also indicated. Depending on the specific parameter set, the optima were found by different methods (compare Sections 3.2.5 and 3.3.2) and may actually lie in between the discrete point of the 0.1 grid which is shown. The 0.1 grid is underlayed to give a coarse impression of how the observable landscapes look like.

One can see that neither the system optimum nor the user optimum do necessarily have to equal to the strategy with the least number of particles in the system.

Parts **(b)** of the figures show the density profiles of the three routes in the optimum states and also provide travel time values and their standard deviations of the routes in those states. The exact values of (γ, δ) of the optima and the corresponding $T_{\max}$ and ΔT values are given in the figure captions as well as the travel times in the corresponding 4link user and system optimum.

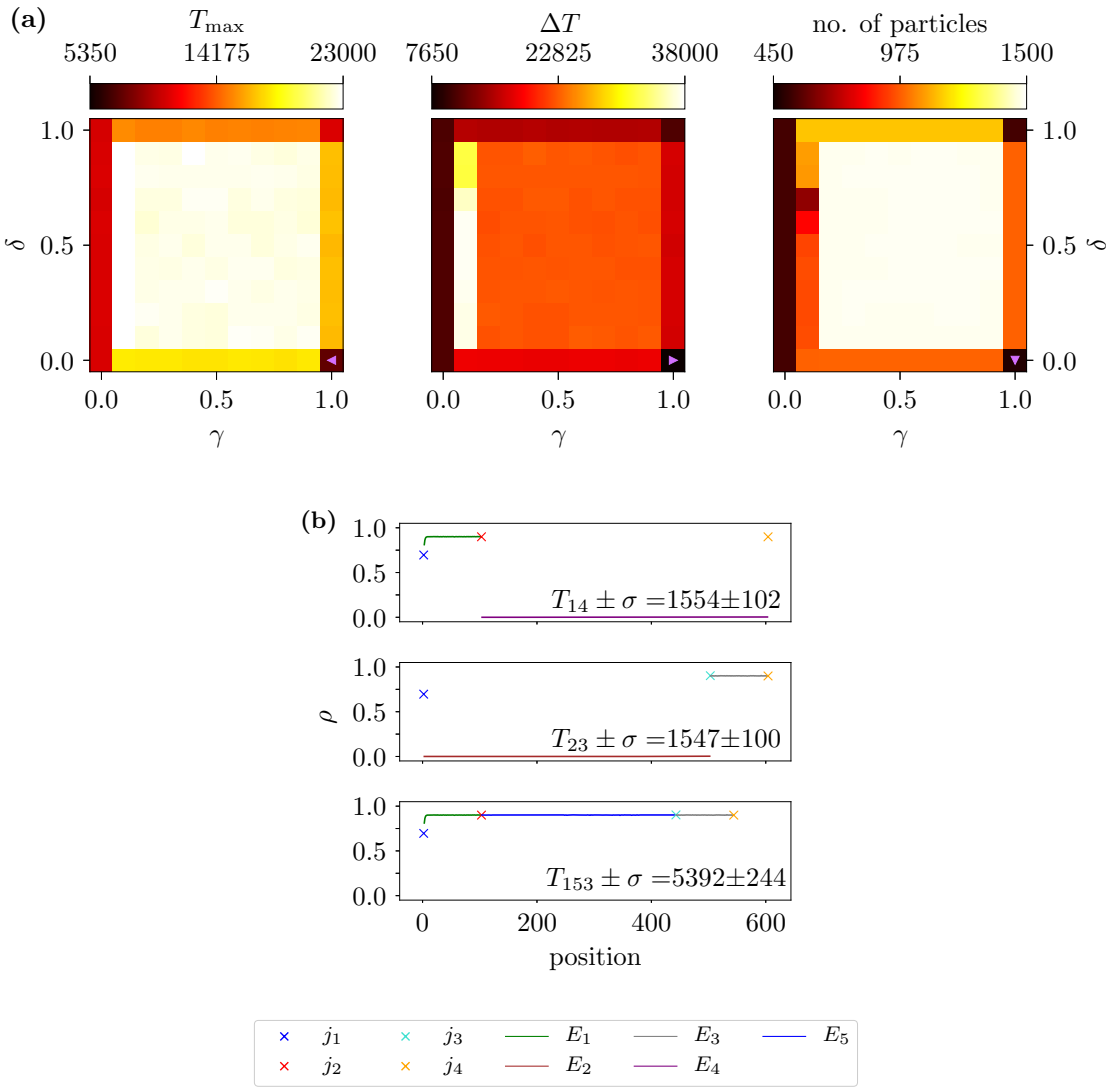

Figure A.15. An example of an "all 153 - unstable" state for the open boundary system. Parameters are $L_5 = 339$, i.e. $\hat{L}_{153}/\hat{L}_{14} = 0.9$, and $\alpha_{\text{in}} = 0.3$, $\beta_{\text{out}} = 0.1$. The travel time in the 4link user and system optimum is $T_{\max}(uo^{(4)}) = T_{\max}(so^{(4)}) \approx 11983$.
Part **(a)** shows the $T_{\max}$ (left) and ΔT (middle) and number of particles in the system (right) landscapes. The pink ◀, ▶ and ▼ indicate the system optimum, user optimum and strategy with the least particles in the system respectively.
Part **(b)** shows density profiles and average travel times $T_i \pm$ standard deviation σ of the three paths for $\min(T_{\max})$ and $\min(\Delta T)$ at $so^{(5)} = uo^{(5)} \mathrel{\widehat{=}} (\gamma, \delta) = (1.0, 0.0)$ with $\Delta T(so^{(5)}) = \Delta T(uo^{(5)}) = 7690$, $T_{\max}(so^{(5)}) = T_{\max}(uo^{(5)}) \approx 5392$.

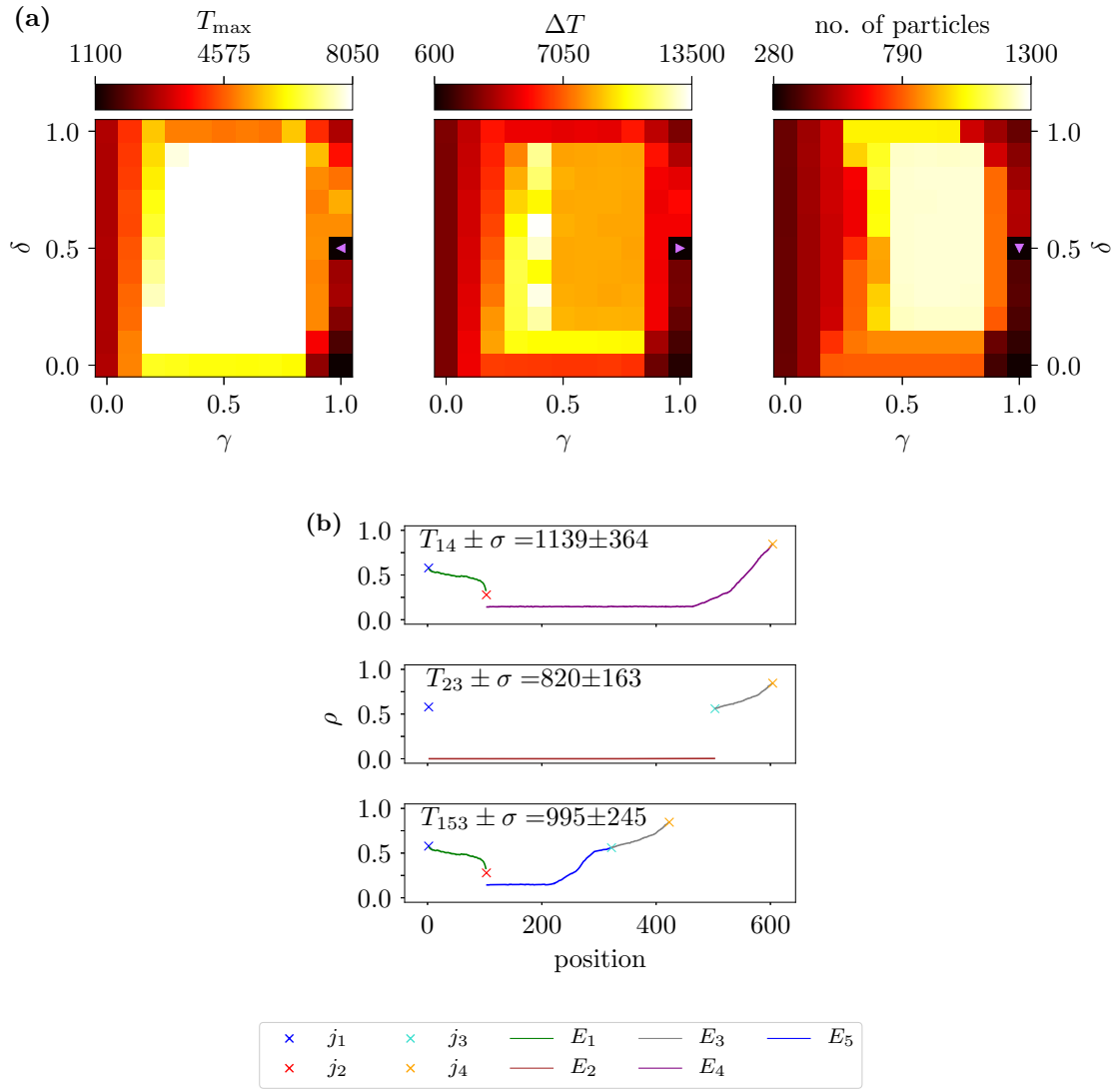

Figure A.16. An example of an "E_5 optimal - unstable" state for the open boundary system. Parameters are $L_5 = 218$, i.e. $\hat{L}_{153}/\hat{L}_{14} = 0.7$, and $\alpha_{\text{in}} = 0.6$, $\beta_{\text{out}} = 0.3$. The travel time in the 4link user and system optimum is $T_{\max}(uo^{(4)}) = T_{\max}(so^{(4)}) \approx 3989$.
Part **(a)** shows the $T_{\max}$ (left) and ΔT (middle) and number of particles in the system (right) landscapes. The pink ◀, ▶ and ▼ indicate the system optimum, user optimum and strategy with the least particles in the system respectively.
Part **(b)** shows density profiles and average travel times $T_i \pm$ standard deviation σ of the three paths for $\min(T_{\max})$ and $\min(\Delta T)$ at $so^{(5)} = uo^{(5)} \mathrel{\widehat{=}} (\gamma, \delta) = (1.0, 0.5)$ with $\Delta T(so^{(5)}) = \Delta T(uo^{(5)}) = 638$, $T_{\max}(so^{(5)}) = T_{\max}(uo^{(5)}) \approx 1139$.

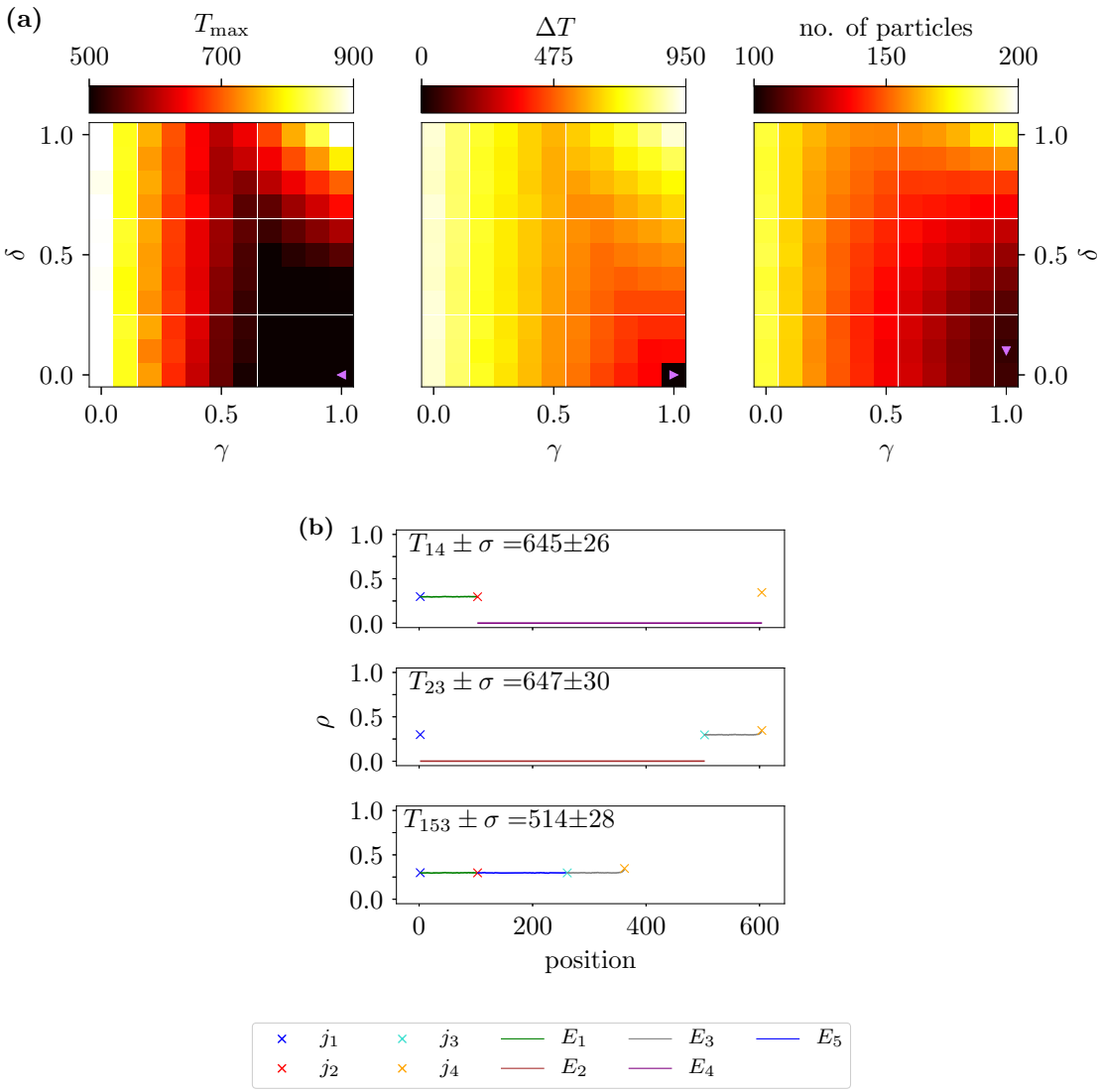

Figure A.17. An example of an "E_5 optimal - all 153" state for the open boundary system. Parameters are $L_5 = 157$, i.e. $\hat{L}_{153}/\hat{L}_{14} = 0.6$, and $\alpha_{\text{in}} = 0.3$, $\beta_{\text{out}} = 0.6$. The travel time in the 4link user and system optimum is $T_{\max}(uo^{(4)}) = T_{\max}(so^{(4)}) \approx 694$.
Part **(a)** shows the $T_{\max}$ (left) and ΔT (middle) and number of particles in the system (right) landscapes. The pink ◀, ▶ and ▼ indicate the system optimum, user optimum and strategy with the least particles in the system respectively.
Part **(b)** shows density profiles and average travel times $T_i \pm$ standard deviation σ of the three paths for $\min(T_{\max})$ and $\min(\Delta T)$ at $so^{(5)} = uo^{(5)} \mathrel{\widehat{=}} (\gamma, \delta) = (1.0, 0.0)$ with $\Delta T(so^{(5)}) = \Delta T(uo^{(5)}) = 0$, $T_{\max}(so^{(5)}) = T_{\max}(uo^{(5)}) \approx 514$.

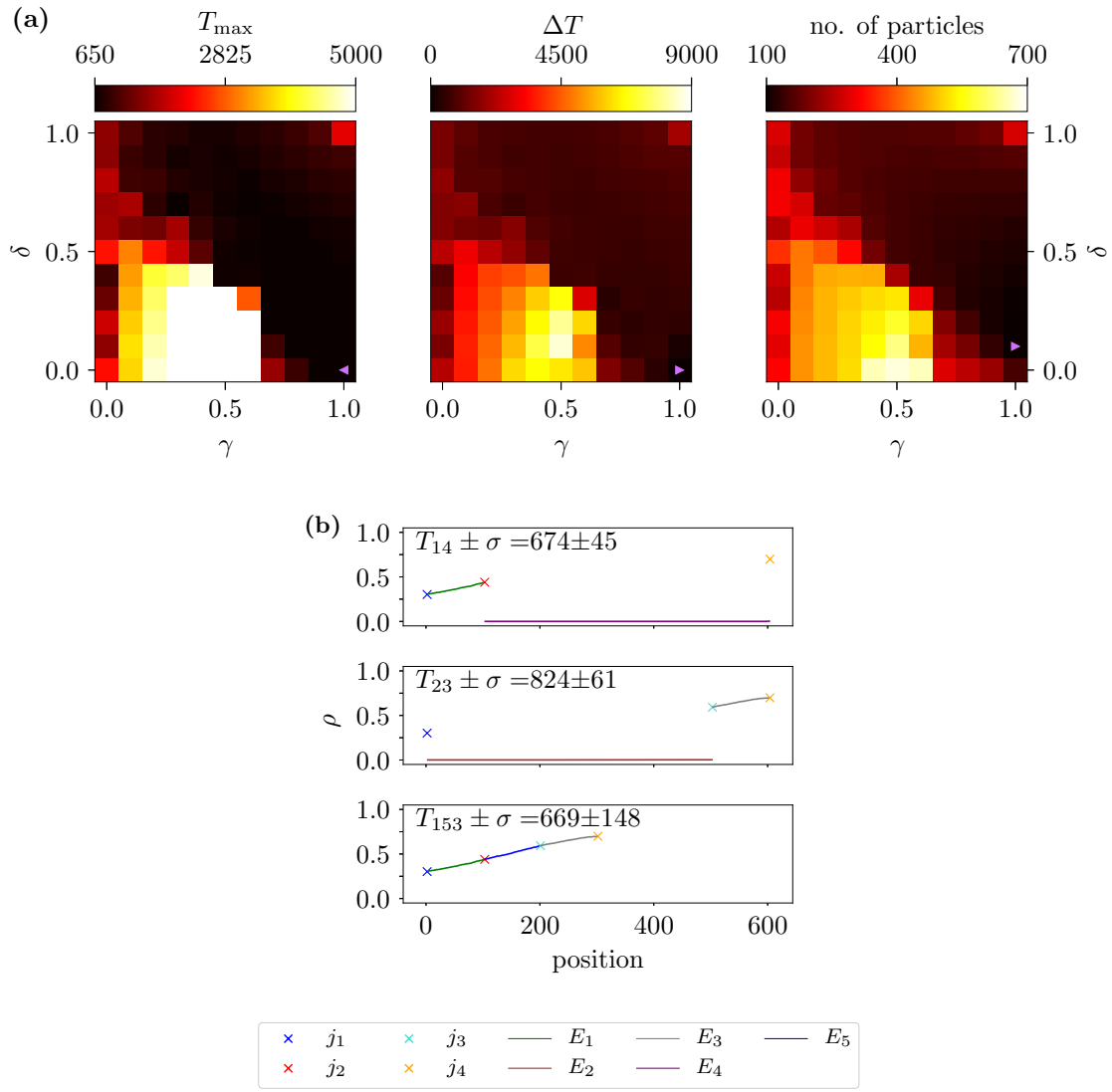

Figure A.18. An example of an "E_5 optimal - all 153" state with domain walls on route 153 for the open boundary system. Parameters are $L_5 = 97$, i.e. $\hat{L}_{153}/\hat{L}_{14} = 0.5$, and $\alpha_{\text{in}} = 0.3$, $\beta_{\text{out}} = 0.3$. The travel time in the 4link user and system optimum is $T_{\max}(uo^{(4)}) = T_{\max}(so^{(4)}) \approx 718$.
Part **(a)** shows the $T_{\max}$ (left) and ΔT (middle) and number of particles in the system (right) landscapes. The pink ◀, ▶ and ▼ indicate the system optimum, user optimum and strategy with the least particles in the system respectively.
Part **(b)** shows density profiles and average travel times $T_i \pm$ standard deviation σ of the three paths for $\min(T_{\max})$ and $\min(\Delta T)$ at $so^{(5)} = uo^{(5)} \mathrel{\widehat{=}} (\gamma, \delta) = (1.0, 0.0)$ with $\Delta T(so^{(5)}) = \Delta T(uo^{(5)}) = 0$, $T_{\max}(so^{(5)}) = T_{\max}(uo^{(5)}) \approx 669$.

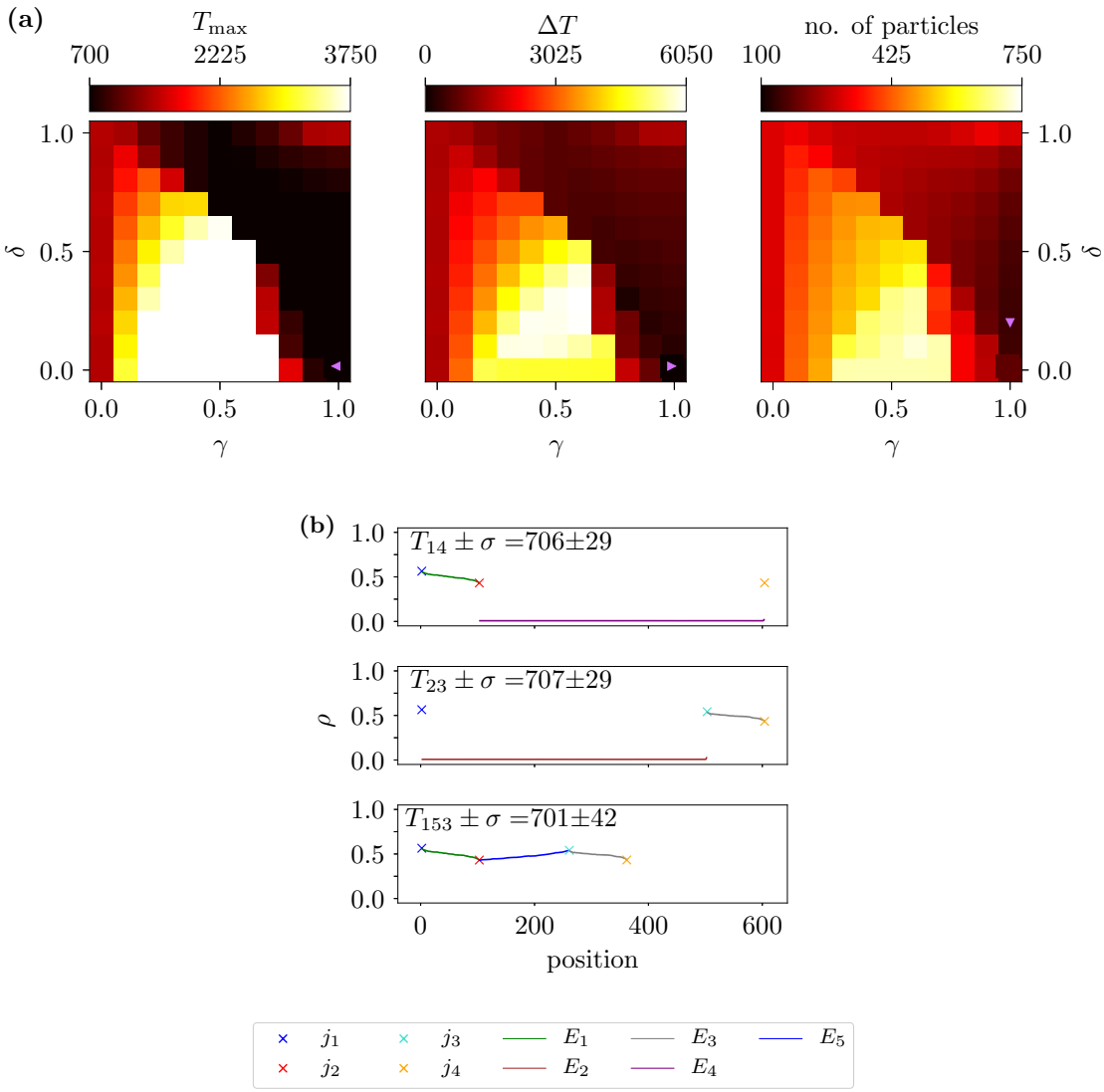

Figure A.19. An example of an "E_5 optimal - almost all 153" state for the open boundary system. Parameters are $L_5 = 157$, i.e. $\hat{L}_{153}/\hat{L}_{14} = 0.6$, and $\alpha_{\text{in}} = 0.6$, $\beta_{\text{out}} = 0.6$. The travel time in the 4link user and system optimum is $T_{\max}(uo^{(4)}) = T_{\max}(so^{(4)}) \approx 782$.
Part **(a)** shows the $T_{\max}$ (left) and ΔT (middle) and number of particles in the system (right) landscapes. The pink ◀, ▶ and ▼ indicate the system optimum, user optimum and strategy with the least particles in the system respectively.
Part **(b)** shows density profiles and average travel times $T_i \pm$ standard deviation σ of the three paths for $\min(T_{\max})$ and $\min(\Delta T)$ at $so^{(5)} = uo^{(5)} \mathrel{\widehat{=}} (\gamma, \delta) = (0.9889, 0.0165)$ with $\Delta T(so^{(5)}) = \Delta T(uo^{(5)}) = 12$, $T_{\max}(so^{(5)}) = T_{\max}(uo^{(5)}) \approx 707$.

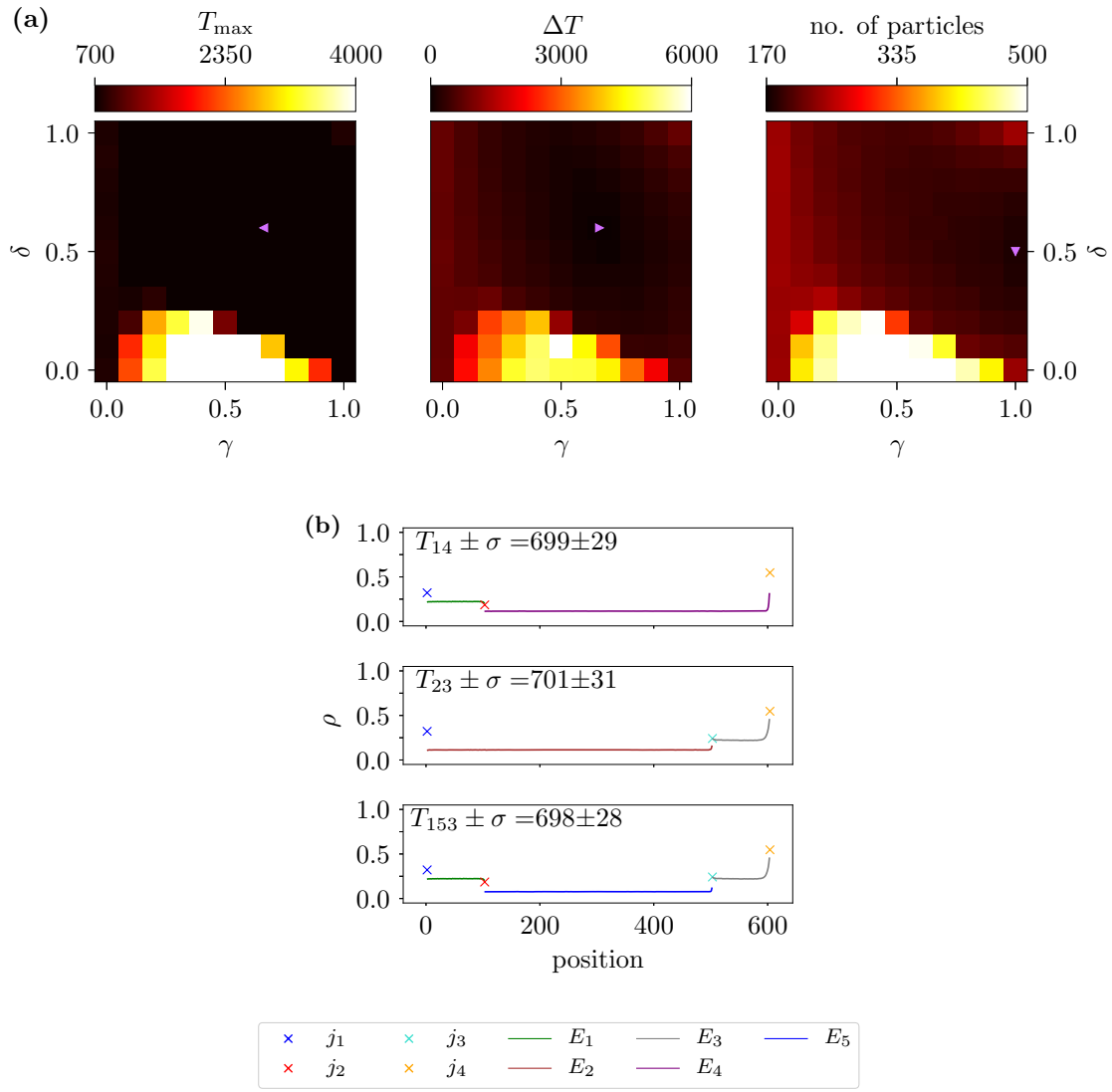

Figure A.20. An example of an "E_5 optimal" state for the open boundary system. Parameters are $L_5 = 399$, i.e. $\hat{L}_{153}/\hat{L}_{14} = 1$, and $\alpha_{\text{in}} = 0.4$, $\beta_{\text{out}} = 0.5$. The travel time in the 4link user and system optimum is $T_{\max}(uo^{(4)}) = T_{\max}(so^{(4)}) \approx 725$.
Part **(a)** shows the $T_{\max}$ (left) and ΔT (middle) and number of particles in the system (right) landscapes. The pink ◀, ▶ and ▼ indicate the system optimum, user optimum and strategy with the least particles in the system respectively.
Part **(b)** shows density profiles and average travel times $T_i \pm$ standard deviation σ of the three paths for $\min(T_{\max})$ and $\min(\Delta T)$ at $so^{(5)} = uo^{(5)} \mathrel{\widehat{=}} (\gamma, \delta) = (0.662, 0.5998)$ with $\Delta T(so^{(5)}) = \Delta T(uo^{(5)}) = 6$, $T_{\max}(so^{(5)}) = T_{\max}(uo^{(5)}) \approx 701$.

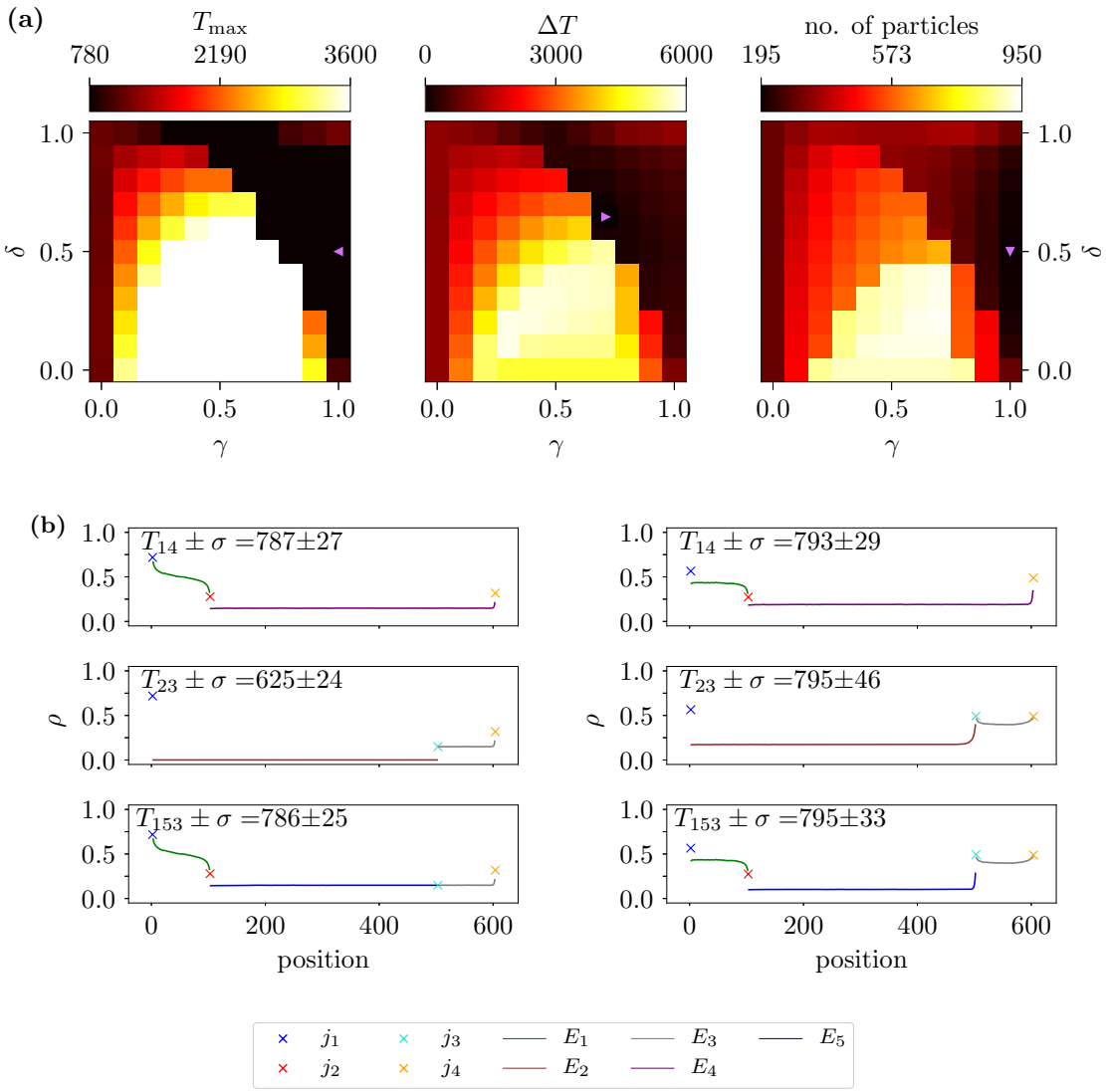

Figure A.21. An example of an "E_5 improves" state for the open boundary system. Parameters are $L_5 = 399$, i.e. $\hat{L}_{153}/\hat{L}_{14} = 1$, and $\alpha_{\text{in}} = 0.9$, $\beta_{\text{out}} = 0.8$. The travel time in the 4link user and system optimum is $T_{\max}(uo^{(4)}) = T_{\max}(so^{(4)}) \approx 854$.
Part **(a)** shows the $T_{\max}$ (left) and ΔT (middle) and number of particles in the system (right) landscapes. The pink ◀, ▶ and ▼ indicate the system optimum, user optimum and strategy with the least particles in the system respectively.
Part **(b)** shows density profiles and average travel times $T_i \pm$ standard deviation σ of the three paths for $\min(T_{\max})$ at $so^{(5)} \mathrel{\widehat{=}} (\gamma, \delta) = (1.0, 0.5)$ with $\Delta T(so^{(5)}) = 333$ and $T_{\max}(so^{(5)}) = 789$ (left), and $\min(\Delta T)$ at $uo^{(5)} \mathrel{\widehat{=}} (\gamma, \delta) = (0.711, 0.646)$ with $\Delta T(uo^{(5)}) = 4$, $T_{\max}(uo^{(5)}) \approx 795$ (right).

A.2 Approximations Used for Open Boundary Conditions

For the analysis of the Braess network of TASEPs with open boundary conditions, random-sequential updates and turning probabilities, as presented in Section 4.4, some approximation techniques were used. Those are examined in some more detail in the present section.

A.2.1 Mean Field Theory for the 4link Network

Here, the predictions from the mean field (MF) theory derived in Section 4.4.1 are compared against Monte Carlo (MC) data. In said section, estimates of the effective entrance and exit rates of routes 14 and 23 for the symmetrically fed open boundary 4link system were derived. Figure A.22 shows the mean field predictions (Parts **(a)** to **(c)**), simulated Monte Carlo data (Parts **(d)** to **(f)**) and their relative differences (Parts **(g)** to **(i)**) of the effective entrance rate α^{eff}, the effective exit rate β^{eff} and their difference $\alpha^{\text{eff}} - \beta^{\text{eff}}$. The predicted phase diagram is underlayed in all parts of the Figure. One can see that the mean field predictions are very accurate, the simulated data confirms the predictions and the relative difference between the two is smaller or equal to 20% for all α_{in} and β_{out}. The predicted LD and HD phases and the phase border on which DWs are expected to occur also seem valid as seen from Parts **(c)** (and **(f)**) of the Figure. The effective entrance rate is smaller/larger than the effective exit rate in the LD/Hd phases and the two rates are equal on the phase border.

Figure A.23 shows the average Monte Carlo travel time $T_{\text{av}}^{\text{MC}} = (T_{14}^{\text{MC}} + T_{23}^{\text{MC}})/2$ of the open boundary 4link user/system optimum. Mean field predictions for this travel time where given in Equations (4.33) to 4.35) and visualized in Figure 4.17 **(b)**. Figure A.23 **(a)** shows the simulation results for the travel times. Part **(b)** of the figure shows the relative difference between the travel times on the routes 14 and 23. They are all below 1% except for some points on the phase border where there are fluctuating domain walls on both paths leading to the different travel times. Those differences could be eradicated by simulating and measuring for a really long time. This part of the figure confirms the assumption that $\gamma = 0.5$ is indeed the user and system optimum of the 4link system.

Part **(c)** of Figure A.23 shows the difference between the mean field predictions and the Monte Carlo measurements of the travel times. It turns out that the predictions are very accurate since the relative differences are below 10% except for the region close to the phase boundary which is as expected.

To further test the validity of the phase diagram predicted by mean field theory one can look at density profiles of the two routes in all of the three phases LD, HD and DW. This is done here for eight exemplary points. Figures A.22 **(d)** and **(f)** already showed that the general prediction of the LD and HD phases is correct. In Figure A.24 eight points on, or close to, the phase border are marked and the density profiles of the two routes for these parameter sets are shown in Figure A.25.

One can see, that for the points below the phase border HD phases are observed and for the points above the phase border LD phases are observed. This is as expected. The points that lie directly on the phase border are given in Figure A.25 **(c)** and **(d)**. One can see that

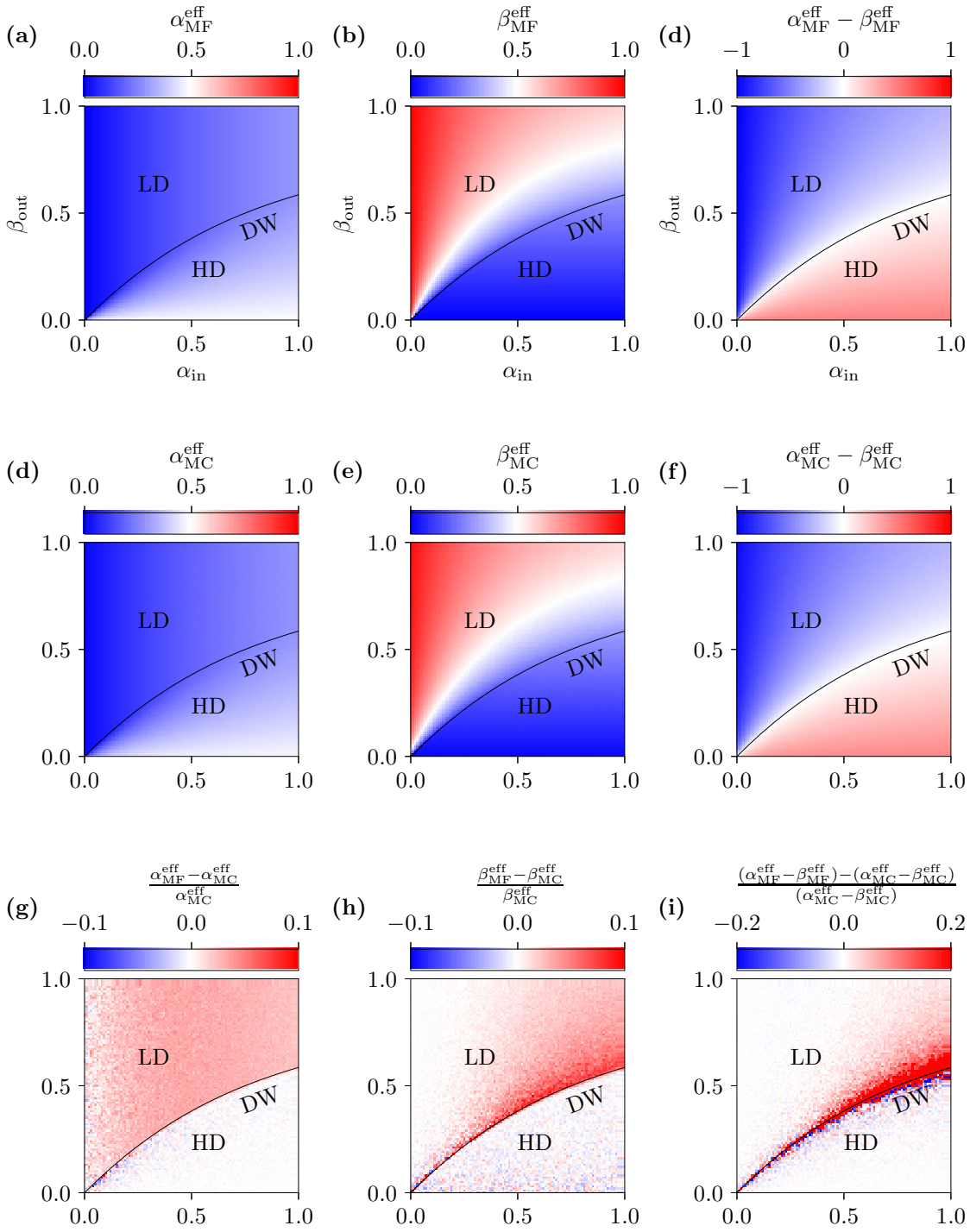

Figure A.22. The effective entrance and exit rates of routes 14 and 23 for the symmetrically fed open boundary 4link system: mean field predictions (Parts **(a)** to **(c)**), simulated Monte Carlo data (Parts **(d)** to **(f)**) and their difference (Parts **(g)** to **(i)**) of the effective entrance rate α^{eff}, the effective exit rate β^{eff} and their difference $\alpha^{\text{eff}} - \beta^{\text{eff}}$. One can see that the Monte Carlo data agrees very well with the mean field predictions. The lengths of the simulated system were $L_1 = L_3 = 100$ and $L_2 = L_4 = 500$.

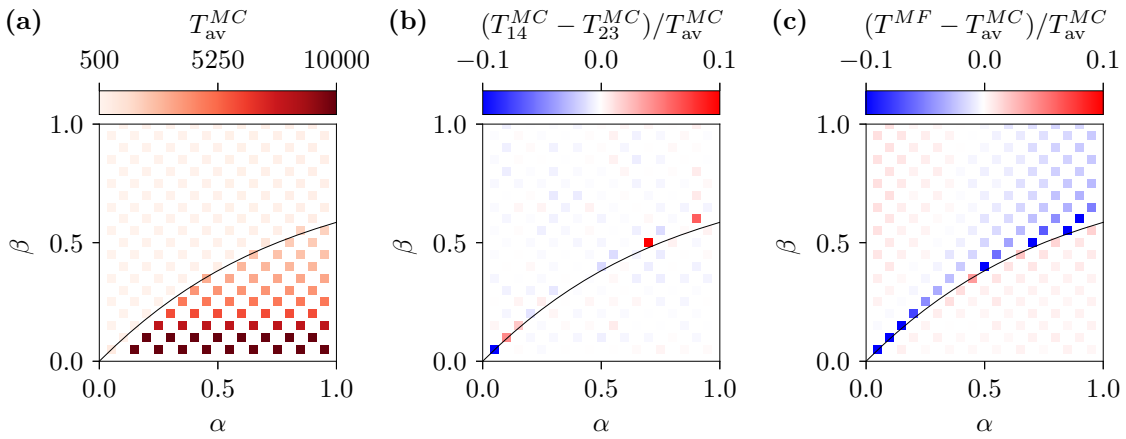

Figure A.23. Travel time values of the 4link open boundary system/user optimum (results of the mean field predictions for this can be found in Figure 4.17 **(b)**). Part **(a)** shows the average Monte Carlo travel time $T_{\text{av}}^{\text{MC}} = (T_{14}^{\text{MC}} + T_{23}^{\text{MC}})/2$. Part **(b)** shows the difference of the travel times on both routes 14 and 23. It can be seen that the travel times on both routes are almost equal which confirms the assumption that this state is the user optimum of the system. Part **(c)** shows the relative difference of the mean field predictions to the Monte Carlo data. It shows that the predictions are correct since the deviations are smaller than 10% almost everywhere but on the DW line (the phase border). Monte Carlo simulations were performed for $L_1 = L_3 = 100$ and $L_2 = L_4 = 500$.

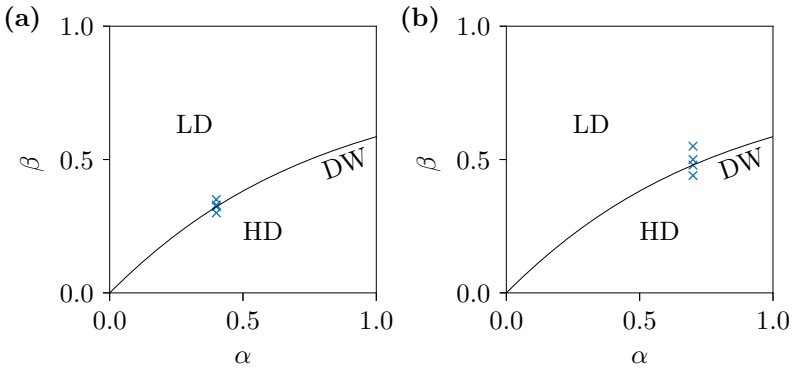

Figure A.24. The four points are marked in Part **(a)**/**(b)** show the parameter sets for which the density profiles are shown in the left/right parts of Figure A.25. For the entrance rates $\alpha_{\text{in}} = 0.4$ and $\alpha_{\text{in}} = 0.7$ for four different values of β_{out} close to (including one point directly on) the phase border were picked and the corresponding density profiles are shown in Figure A.25.

the density profiles in both cases still look roughly like HD phases while for both α_{in} the density profiles for β_{out} slightly above the phase border (Parts **(e)** and **(f)**) look like domain walls are present. This indicates that the position of the phase border derived by mean field theory is not taken to be a hundred percent exact. This could e.g. be an effect of the finite edge lengths shown here and it has to be noted that the points showing domain wall - like density profiles are really close to the phase border.

Summarized one can conclude that the mean field theory derived in Section 4.4.1 describes the 4link system very well.

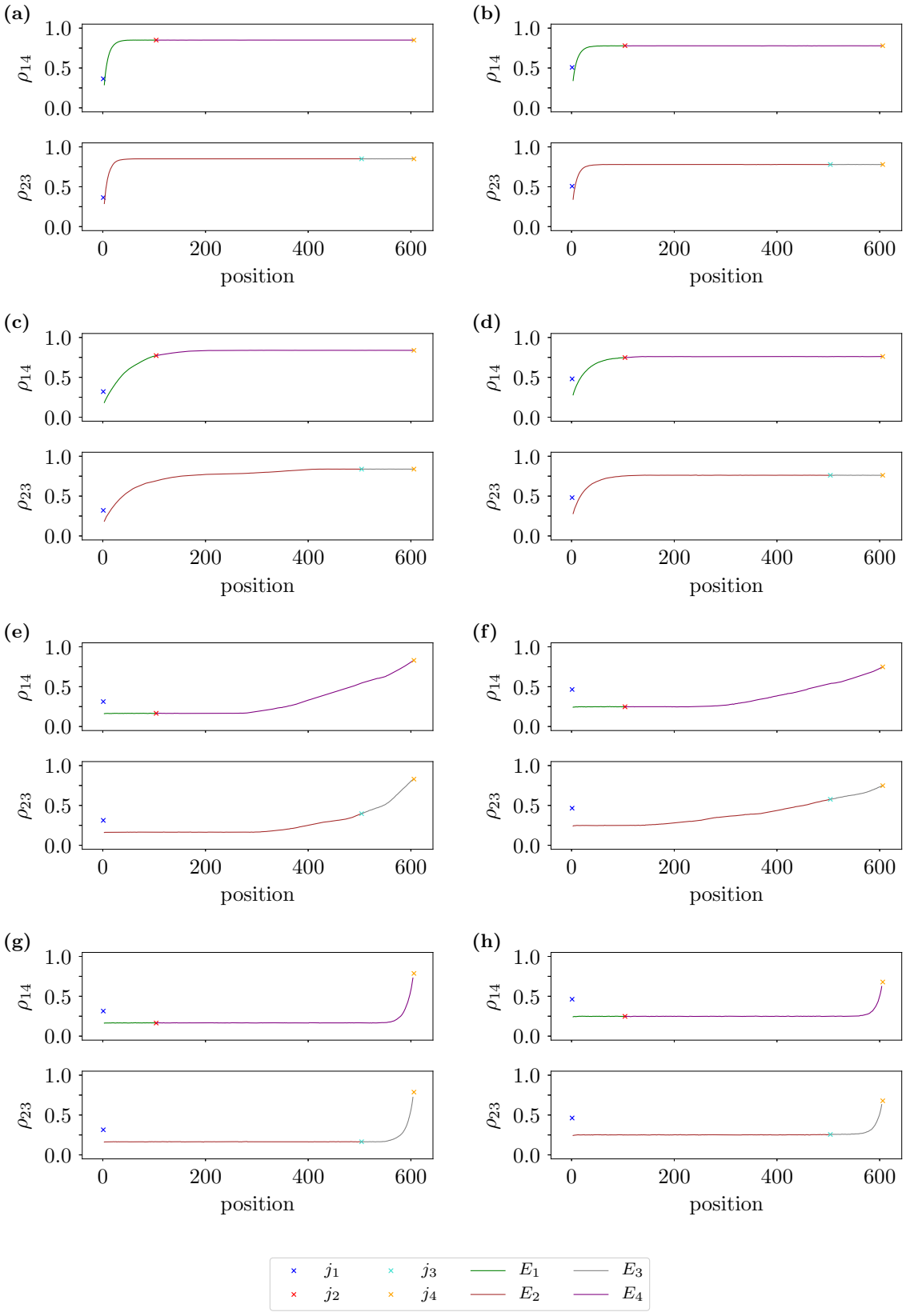

Figure A.25. Density profiles of the routes 14 and 23 for the parameter sets shown in Figure A.24. Left parts (corresponding to the points in Figure A.24 **(a)**): Part **(a)**: $\alpha_{\text{in}} = 0.4$, $\beta_{\text{out}} = 0.3$, Part **(c)**: $\alpha_{\text{in}} = 0.4$, $\beta_{\text{out}} = 0.323$, Part **(e)**: $\alpha_{\text{in}} = 0.4$, $\beta_{\text{out}} = 0.33$, Part **(g)**: $\alpha_{\text{in}} = 0.4$, $\beta_{\text{out}} = 0.35$. Right parts (corresponding to the points in Figure A.24 **(b)**): Part **(b)**: $\alpha_{\text{in}} = 0.7$, $\beta_{\text{out}} = 0.44$, Part **(d)**: $\alpha_{\text{in}} = 0.7$, $\beta_{\text{out}} = 0.479$, Part **(f)**: $\alpha_{\text{in}} = 0.7$, $\beta_{\text{out}} = 0.5$, Part **(h)**: $\alpha_{\text{in}} = 0.7$, $\beta_{\text{out}} = 0.55$

A.2.2 Approximative Border of the "E_5 optimal / all 153" Phase

Here the procedure for approximating the "E_5 optimal / all 153" phase border based on the MFT derived in Section 4.4.1 is described in some detail. In Section 3.2.4.1 it was established that for the all 153 phase to be present two conditions have to be met. Firstly in the 5link system the travel time on route 153 has to be lower than on the two other routes in the case that all particles choose route 153. Secondly if in the 5link system all particles choose route 153, the travel time on that route has to be lower than the (equal) travel times on both routes in the user optimum of the 4link system.

The first condition is met if Equation (3.28) is met:

$$\rho_{L/2,153} < \frac{1}{L_2}(L_2 - L_3 - L_5 - 1),$$

i.e. the bulk density on route 153, which is determined by the entrance and exit rates (as given in Table 3.1) to be α_{in} (LD), $1 - \beta_{\text{out}}$ (HD) or 1/2 (MC), has to be below the given threshold.

The second is met if Equation (3.29),

$$\frac{\hat{L}_{153}}{1 - \rho_{L/2,153}} < T_{14}\left(uo^{(4)}\right) = T_{23}\left(uo^{(4)}\right),$$

holds. In the open boundary case this condition takes five different forms, depending on the entrance and exit rates.

The MFT for the user optimum of the 4link system revealed that the phase border between LD and HD phases in the 4link user optimum is given by Equation (4.32):

$$\beta_{\text{out}} = 1 + \alpha_{\text{in}} - \sqrt{1 + \alpha_{\text{in}}^2}.$$

For smaller β_{out} the two routes of the 4link system are in HD phases, For larger β_{out} They are in LD phases.

This means that route 153 can be in three different phases, according to the phase diagram of an ordinary single TASEP, and the two routes of the 4link system in either HD or LD phases according to Equation (4.32). Superimposing the two phase diagrams results in five distinct regions shown in Figure A.26. Each of the regions leads to different explicit realizations of condition (3.29).

In regions I and II, the 4link system's user optimum is given by a state in which both routes are in HD phases. Their travel times are according to Equation (4.34) given by $T_{\text{HD}} = \frac{2\hat{L}_{14}}{\beta_{\text{out}}}$. The second all153 condition (3.29) becomes

$$\rho_{L/2,153} < \frac{\beta}{2\hat{L}_{14}}\left(\frac{2\hat{L}_{14}}{\beta} - \hat{L}_{153}\right). \tag{A.1}$$

In region I if all particles choose route 153, that route is in an HD state thus $\rho_{L/2,153} =$

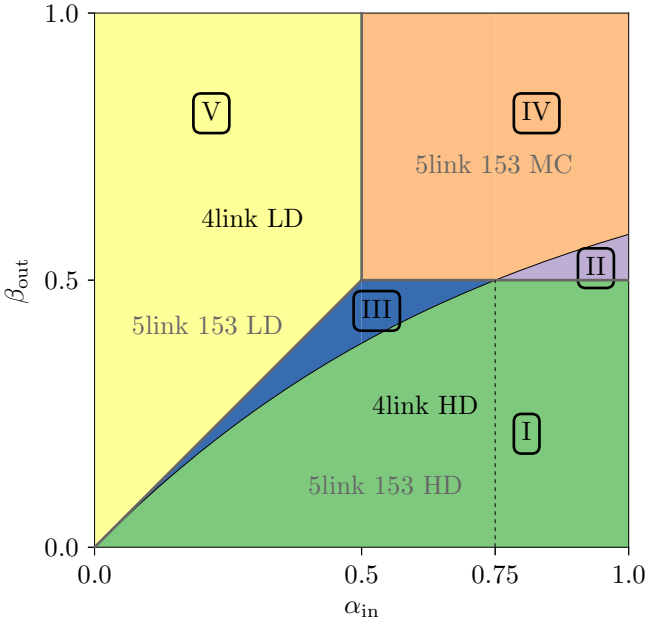

Figure A.26. For the "E_5 optimal / all 153" phase to be present in the open boundary system Equation (3.29) has to be valid. Depending on the entrance and exit rates α_{in} and β_{out} this condition can take a different form. Superimposing the phase diagram of a single TASEP (shown by black lines) and the phase diagram of the open boundary 4link system, shown by the MFT phase border (grey line according to Equation (4.32)) reveals the five regions leading to different realizations of Equation (3.29).

$1 - \beta_{\text{out}}$. Equation (3.29) becomes

$$L_5 < 2\hat{L}_{14} - 2L_1 - 4 \tag{A.2}$$

which is to be expected since if this Equation becomes an equality, $\hat{L}_{153} = 2\hat{L}_{14}$ and the travel time of the routes in the 4link is just twice the travel time of a single TASEP in an HD state. For the system analysed in this thesis ($L_1 = L_3 = 100$, $L_2 = L_4 = 500$) it becomes:

$$L_5 < 1002. \tag{A.3}$$

In region II if all particles choose route 153 that route is in an MC state, thus $\rho_{L/2,153} = 1/2$. Equation (3.29) becomes

$$L_5 < \frac{\hat{L}_{14}}{\beta} - 2L_1 - 4. \tag{A.4}$$

Opposed to the condition of region I it depends on β_{out}. For region II $1/2 < \beta_{\text{out}} < 2 - \sqrt{2}$

holds ($2-\sqrt{2}$ being the value of β_{out} on the phase border if $\alpha_{\text{in}} = 1.0$). For the system analysed in this thesis ($L_1 = L_3 = 100$, $L_2 = L_4 = 500$) it becomes:

$$\beta_{\text{out}} = 1/2: \qquad L_5 < 1002 \tag{A.5}$$

$$\beta_{\text{out}} = 2+\sqrt{2}: \qquad L_5 < 825.385. \tag{A.6}$$

The maximum length of L_5 considered in this thesis is 399 (leading to $\hat{L}_{153} = \hat{L}_{14}$ ($= \hat{L}_{23}$).

This means that in our systems in regions I and II condition (3.29) is always met: if the 4link system is in an HD state, the travel time of route 153 in the 5link system (if all particles choose that route) is always smaller than that in the 4link system[1]. Note that this does not mean that there is always an "E_5 optimal / all 153" phase in regions I and II since the first condition (3.28) is not always fulfilled.

In regions III, IV and V the user optimum of the 4link system is given by both routes being in LD states and according to the derived MFT their travel times are (Equation (4.33)):

$$T_{\text{LD}} = \frac{\hat{L}_{14}}{1-\alpha^{\text{eff}}} = \frac{2\hat{L}_{14}}{\sqrt{\alpha_{\text{in}}^2+1}-\alpha_{\text{in}}+1}.$$

In region III route 153 in the 5link is in an HD state if all particles choose that route, thus $\rho_{L/2,153} = 1-\beta_{\text{out}}$. Equation (3.29) then becomes

$$\frac{\hat{L}_{153}}{\beta_{\text{out}}} < 2\frac{\hat{L}_{14}}{1-\alpha_{\text{in}}+\sqrt{\alpha_{\text{in}}+1}} \tag{A.7}$$

which leads to

$$\begin{aligned}\beta_{\text{out}} > \quad & \tfrac{1}{2}\sqrt{\tfrac{\alpha_{\text{in}}^2(2L_1+L_5+4)^2+(2L_1+L_5+4)^2}{(L_1+L_2+3)^2}} \\ & +\tfrac{-\alpha_{\text{in}}(2L_1+L_5+4)+2L_1+L_5+4}{2(L_1+L_2+3)}.\end{aligned} \tag{A.8}$$

In region IV route 153 in the 5link is in an MC state if all particles choose that route, thus $\rho_{L/2,153} = 1/2$. Equation (3.29) then becomes

$$2\hat{L}_{153} < 2\frac{\hat{L}_{14}}{1-\alpha_{\text{in}}+\sqrt{\alpha_{\text{in}}+1}} \tag{A.9}$$

which leads to

$$\alpha_{\text{in}} > \frac{2(L_1+L_2+3)(2L_1+L_5+4)-(L_1+L_2+3)^2}{2(L_1+L_2+3)(2L_1+L_5+4)-2(2L_1+L_5+4)^2} \tag{A.10}$$

a lengthy equation for α_{in} that is easily evaluated numerically for given set of L_i.

[1] Please note that this is also true for 5link states with all particles choosing route 14 or route 23, as can also be seen in the example landscapes of the "all 153 - unstable" states (Figure 4.18). Still since in this thesis $\hat{L}_{153} \leq \hat{L}_{14}$ the travel time on route 153 will always be smaller than on the other routes if only one route is chosen by all particles.

In region V route 153 in the 5link is in an LD state if all particles choose that route, thus $\rho_{L/2,153} = \alpha_{\text{in}}$. Equation (3.29) then becomes

$$\alpha_{\text{in}} < \frac{1}{2\hat{L}_{14}} \left(2L_2 - L_5 + 2 + (2L_1 + L_5 + 4) \left(\alpha_{\text{in}} - \sqrt{1 + \alpha_{\text{in}}^2} \right) \right) \tag{A.11}$$

which leads to a

$$\alpha_{\text{in}} < \frac{-4(L_1+L_2+3)(2L_1+L_5+4)+4(L_1+L_2+3)^2+(2L_1+L_5+4)^2}{4(L_1+L_2+3)(-L_1+L_2-L_5-1)} - \frac{1}{4}\sqrt{\frac{-8(L_1+L_2+3)(2L_1+L_5+4)^3+8(L_1+L_2+3)^2(2L_1+L_5+4)^2+(2L_1+L_5+4)^4}{(L_1+L_2+3)^2(-L_1+L_2-L_5-1)^2}}, \tag{A.12}$$

a lengthy equation for α_{in} that is easily evaluated numerically for a given set of L_i.

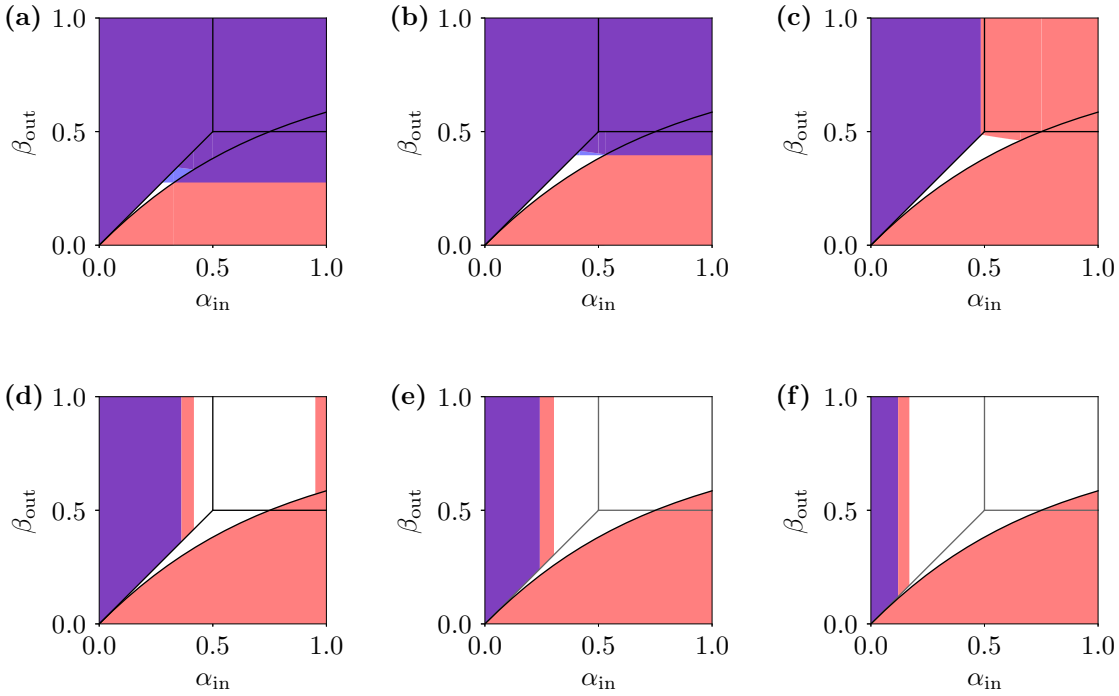

Figure A.27. The regions of the phase spaces of $L_1 = L_3 = 100$, $L_2 = L_4 = 500$ and **(a)** $L_5 = 37$, $\hat{L}_{153} = 0.4$, **(b)** $L_5 = 97$, $\hat{L}_{153}/\hat{L}_{14} = 0.5$, **(c)** $L_5 = 157$, $\hat{L}_{153}/\hat{L}_{14} = 0.6$, **(d)** $L_5 = 218$, $\hat{L}_{153}/\hat{L}_{14} = 0.7$, **(e)** $L_5 = 278$, $\hat{L}_{153}/\hat{L}_{14} = 0.8$ and **(f)** $L_5 = 339$, $\hat{L}_{153}/\hat{L}_{14} = 0.9$, where the MFT conditions for the "E_5 optimal / all 153" phase hold.
The first condition (Equation (3.28)) holds in the regions marked in blue color and the second condition (the five forms of Equation (3.29)) holds in the regions marked in red color. Where both conditions are fulfilled, the overlayed color becomes purple.
For $L_5 = 399$, $\hat{L}_{153}/\hat{L}_{14} = 1.0$ no region of the phase space shows "E_5 optimal / all 153" behaviour which is why the landscape of this parameter-set is not shown.

Figure A.27 shows the resulting regions of the phase spaces in which the two conditions Equation (3.28) and Equation (3.29) are valid for the parameter sets examined in this thesis (see Section 4.4.2.2). One can see that only for the small route length ratios $\hat{L}_{153}/\hat{L}_{14} = 0.4$ (Part **(a)**) and $\hat{L}_{153}/\hat{L}_{14} = 0.5$ (**(b)**) there are small parts of region III in which the first

condition holds while the second one does not. In all other parts where the first condition holds, the second one holds as well. This is not the case vice versa: there are many regions in which the second conditon holds (especially in regions I and II) and the first one does not.

Only the parts where both conditions hold (resulting in a purple coloration in Figure A.27) are assumed to lead to the "E_5 optimal / all 153" phase and thus they are shown in the obtained phase diagrams in the main part of the thesis (Section 4.4.2.2).

A.3 Route Choice Algorithms

In Section 5.1 the decision making algorithms for the implementation of intelligent particles were presented. Concerning the strategy changes which can occur during one round, if a particle sits on junction j_1 or j_2 and the desired target site is occupied, only the algorithm for the 4link system was presented.

In the present section the algorithms for decision makings on junctions j_1 and j_2 in the 5link system are shown explicitly in Algorithms A.1 and A.2, respectively.

Algorithm A.1: Decision makings on junction j_2, as used in the 5link system.

```
   // (The variable tw is the time the particle has already waited on j2
      since its first attempt of jumping to its target site.)
 1 if (intended route is route 14) then
 2 |   if (T_14,info < T_153,info) then
 3 |   |   if (tw > (T_153,info − T_14,info) · κ_j2thres.) then
 4 |   |   |   switch to route 153
 5 |   |   end
 6 |   end
 7 |   else
 8 |   |   switch to route 153 immediately
 9 |   end
10 end
11 else if (intended route is route 153) then
12 |   if (T_153,info < T_14,info) then
13 |   |   if (tw > (T_14,info − T_14,info) · κ_j2thres.) then
14 |   |   |   switch to route 14
15 |   |   end
16 |   end
17 |   else
18 |   |   switch to route 14 immediately
19 |   end
20 end
```

Algorithm A.2: Decision makings on junction j_1, as used in the 5link system.

```
// (The variable tw is the time the particle has already waited on j1
   since its first attempt of jumping to its target site.)
if (intended route is route 14 or route 153) then
    if (intended route is route 14 then
        if (T14,info < T23,info) then
            if (tw > (T23,info − T14,info) · κj1thres.) then
                switch to route 23
            end
        end
        else
            switch to route 23 immediately
        end
    if (intended route is route 153 then
        if (T153,info < T23,info) then
            if (tw > (T23,info − T153,info) · κj1thres.) then
                switch to route 23
            end
        end
        else
            switch to route 23 immediately
        end
    end
end
else if (intended route is route 23) then
    if (T23,info < T14,info) and (T23,info < T153,info) then
        if (T14,info < T153,info) then
            if (tw > (T14,info − T23,info) · κj1thres.) then
                switch to route 14
            end
        else if (T153,info < T14,info) then
            if (tw > (T153,info − T23,info) · κj1thres.) then
                switch to route 153
            end
    end
    else
        if (T14,info < T153,info) then
            switch to route 14
        else if (T153,info < T14,info) then
            switch to route 153
        else
            switch to route 14 or route 153 with equal probabilities.
        end
    end
```

Erklärung

Ich versichere, dass ich die von mir vorgelegte Dissertation selbständig angefertigt, die benutzten Quellen und Hilfsmittel vollständig angegeben und die Stellen der Arbeit – einschließlich Tabellen, Karten und Abbildungen –, die anderen Werken im Wortlaut oder dem Sinn nach entnommen sind, in jedem Einzelfall als Entlehnung kenntlich gemacht habe; dass diese Dissertation noch keiner anderen Fakultät oder Universität zur Prüfung vorgelegen hat; dass sie – abgesehen von unten angegebenen Teilpublikationen – noch nicht veröffentlicht worden ist, sowie, dass ich eine solche Veröffentlichung vor Abschluss des Promotionsverfahrens nicht vornehmen werde. Die Bestimmungen der Promotionsordnung sind mir bekannt. Die von mir vorgelegte Dissertation ist von Prof. Dr. Andreas Schadschneider betreut worden.

Nachfolgend genannte **Teilpublikationen** liegen vor:

1. S. Bittihn and A. Schadschneider. Braess paradox in a network of totally asymmetric exclusion processes. *Physical Review E*, 94:062312, 2016.

2. S. Bittihn and A. Schadschneider. Braess paradox in a network with stochastic dynamics and fixed strategies. *Physica A: Statistical Mechanics and its Applications*, 507:133 – 152, 2018.

3. S. Bittihn and A. Schadschneider. Braess Paradox in Networks of Stochastic Microscopic Traffic Models. In *Traffic and Granular Flow '17*. Springer, (to be published in 2019).

Köln, den 30.09.2018

(Stefan Bittihn)